UNIVERSITY OF ALBERTA

SAND FLOW MECHANISMS AT WELL CASING PERFORATIONS

BY

WARREN GREGORY MILLER ©

A THESIS

SUBMITTED TO THE FACULTY OF GRADUATE STUDIES AND RESEARCH IN
PARTIAL FULFILLMENT OF THE REQUIREMENTS FOR THE DEGREE OF
MASTER OF SCIENCE

DEPARTMENT OF CIVIL ENGINEERING
EDMONTON, ALBERTA
FALL 1994

National Library
of Canada

Acquisitions and
Bibliographic Services Branch

395 Wellington Street
Ottawa, Ontario
K1A 0N4

Bibliothèque nationale
du Canada

Direction des acquisitions et
des services bibliographiques

395, rue Wellington
Ottawa (Ontario)
K1A 0N4

Your file Votre référence

Our file Notre référence

The author has granted an irrevocable non-exclusive licence allowing the National Library of Canada to reproduce, loan, distribute or sell copies of his/her thesis by any means and in any form or format, making this thesis available to interested persons.

L'auteur a accordé une licence irrévocable et non exclusive permettant à la Bibliothèque nationale du Canada de reproduire, prêter, distribuer ou vendre des copies de sa thèse de quelque manière et sous quelque forme que ce soit pour mettre des exemplaires de cette thèse à la disposition des personnes intéressées.

The author retains ownership of the copyright in his/her thesis. Neither the thesis nor substantial extracts from it may be printed or otherwise reproduced without his/her permission.

L'auteur conserve la propriété du droit d'auteur qui protège sa thèse. Ni la thèse ni des extraits substantiels de celle-ci ne doivent être imprimés ou autrement reproduits sans son autorisation.

ISBN 0-315-95078-1

Canada

Name Warren Gregory Miller

Dissertation Abstracts International is arranged by broad, general subject categories. Please select the one subject which most nearly describes the content of your dissertation. Enter the corresponding four-digit code in the spaces provided.

Civil Engineering
SUBJECT TERM

0 5 4 3
SUBJECT CODE

UMI

Subject Categories

THE HUMANITIES AND SOCIAL SCIENCES

COMMUNICATIONS AND THE ARTS

Architecture	0729
Art History	0377
Cinema	0900
Dance	0378
Fine Arts	0357
Information Science	0723
Journalism	0391
Library Science	0399
Mass Communications	0708
Music	0413
Speech Communication	0459
Theater	0465

EDUCATION

General	0515
Administration	0514
Adult and Continuing	0516
Agricultural	0517
Art	0273
Bilingual and Multicultural	0282
Business	0688
Community College	0275
Curriculum and Instruction	0727
Early Childhood	0518
Elementary	0524
Finance	0277
Guidance and Counseling	0519
Health	0680
Higher	0745
History of	0520
Home Economics	0278
Industrial	0521
Language and Literature	0279
Mathematics	0280
Music	0522
Philosophy of	0998
Physical	0523
Psychology	0525
Reading	0535
Religious	0527
Sciences	0714
Secondary	0533
Social Sciences	0534
Sociology of	0340
Special	0529
Teacher Training	0530
Technology	0710
Tests and Measurements	0288
Vocational	0747

LANGUAGE, LITERATURE AND LINGUISTICS

Language	
General	0679
Ancient	0289
Linguistics	0290
Modern	0291
Literature	
General	0401
Classical	0294
Comparative	0295
Medieval	0297
Modern	0298
African	0316
American	0591
Asian	0305
Canadian (English)	0352
Canadian (French)	0355
English	0593
Germanic	0311
Latin American	0312
Middle Eastern	0315
Romance	0313
Slavic and East European	0314

PHILOSOPHY, RELIGION AND THEOLOGY

Philosophy	0422
Religion	
General	0318
Biblical Studies	0321
Clergy	0319
History of	0320
Philosophy of	0322
Theology	0469

SOCIAL SCIENCES

American Studies	0323
Anthropology	
Archaeology	0324
Cultural	0326
Physical	0327
Business Administration	
General	0310
Accounting	0272
Banking	0770
Management	0454
Marketing	0338
Canadian Studies	0385
Economics	
General	0501
Agricultural	0503
Commerce-Business	0505
Finance	0508
History	0509
Labor	0510
Theory	0511
Folklore	0358
Geography	0366
Gerontology	0351
History	
General	0578
Ancient	0579
Medieval	0581
Modern	0582
Black	0328
African	0331
Asia, Australia and Oceania	0332
Canadian	0334
European	0335
Latin American	0336
Middle Eastern	0333
United States	0337
History of Science	0585
Law	0398
Political Science	
General	0615
International Law and Relations	0616
Public Administration	0617
Recreation	0814
Social Work	0452
Sociology	
General	0626
Criminology and Penology	0627
Demography	0938
Ethnic and Racial Studies	0631
Individual and Family Studies	0628
Industrial and Labor Relations	0629
Public and Social Welfare	0630
Social Structure and Development	0700
Theory and Methods	0344
Transportation	0709
Urban and Regional Planning	0999
Women's Studies	0453

THE SCIENCES AND ENGINEERING

BIOLOGICAL SCIENCES

Agriculture	
General	0473
Agronomy	0285
Animal Culture and Nutrition	0475
Animal Pathology	0476
Food Science and Technology	0359
Forestry and Wildlife	0478
Plant Culture	0479
Plant Pathology	0480
Plant Physiology	0817
Range Management	0777
Wood Technology	0746
Biology	
General	0306
Anatomy	0287
Biostatistics	0308
Botany	0309
Cell	0379
Ecology	0329
Entomology	0353
Genetics	0369
Limnology	0793
Microbiology	0410
Molecular	0307
Neuroscience	0317
Oceanography	0416
Physiology	0433
Radiation	0821
Veterinary Science	0778
Zoology	0472
Biophysics	
General	0786
Medical	0760

EARTH SCIENCES

Biogeochemistry	0425
Geochemistry	0996
Geodesy	0370
Geology	0372
Geophysics	0373
Hydrology	0388
Mineralogy	0411
Paleobotany	0345
Paleoecology	0426
Paleontology	0418
Paleozoology	0985
Palynology	0427
Physical Geography	0368
Physical Oceanography	0415

HEALTH AND ENVIRONMENTAL SCIENCES

Environmental Sciences	0768
Health Sciences	
General	0566
Audiology	0300
Chemotherapy	0992
Dentistry	0567
Education	0350
Hospital Management	0769
Human Development	0758
Immunology	0982
Medicine and Surgery	0564
Mental Health	0347
Nursing	0569
Nutrition	0570
Obstetrics and Gynecology	0380
Occupational Health and Therapy	0354
Ophthalmology	0381
Pathology	0571
Pharmacology	0419
Pharmacy	0572
Physical Therapy	0382
Public Health	0573
Radiology	0574
Recreation	0575
Speech Pathology	0460
Toxicology	0383
Home Economics	0386

PHYSICAL SCIENCES

Pure Sciences

Chemistry	
General	0485
Agricultural	0749
Analytical	0486
Biochemistry	0487
Inorganic	0488
Nuclear	0738
Organic	0490
Pharmaceutical	0491
Physical	0494
Polymer	0495
Radiation	0754
Mathematics	0405
Physics	
General	0605
Acoustics	0986
Astronomy and Astrophysics	0606
Atmospheric Science	0608
Atomic	0748
Electronics and Electricity	0607
Elementary Particles and High Energy	0798
Fluid and Plasma	0759
Molecular	0609
Nuclear	0610
Optics	0752
Radiation	0756
Solid State	0611
Statistics	0463

Applied Sciences

Applied Mechanics	0346
Computer Science	0984
Engineering	
General	0537
Aerospace	0538
Agricultural	0539
Automotive	0540
Biomedical	0541
Chemical	0542
Civil	0543
Electronics and Electrical	0544
Heat and Thermodynamics	0348
Hydraulic	0545
Industrial	0546
Marine	0547
Materials Science	0794
Mechanical	0548
Metallurgy	0743
Mining	0551
Nuclear	0552
Packaging	0549
Petroleum	0765
Sanitary and Municipal	0554
System Science	0790
Geotechnology	0428
Operations Research	0796
Plastics Technology	0795
Textile Technology	0994

PSYCHOLOGY

General	0621
Behavioral	0384
Clinical	0622
Developmental	0620
Experimental	0623
Industrial	0624
Personality	0625
Physiological	0989
Psychobiology	0349
Psychometrics	0632
Social	0451

UNIVERSITY OF ALBERTA

RELEASE FORM

NAME OF AUTHOR: WARREN GREGORY MILLER

TITLE OF THESIS: SAND FLOW MECHANISMS AT WELL CASING PERFORATIONS

DEGREE: MASTER OF SCIENCE

YEAR THIS DEGREE GRANTED: FALL 1994

Permission is hereby granted to the University of Alberta Library to reproduce single copies of this thesis and to lend or sell such copies for private, scholarly or scientific research purposes only.

The author reserves all other publication and other rights in association with the copyright in the thesis, and except as hereinbefore provided neither the thesis nor any substantial portion thereof may be printed or otherwise reproduced in any material form whatever without the author's prior written permission.

Warren Miller

Permanent Address
#606 10883 Saskatchewan Drive
Edmonton, Alberta
T6E 4S6

September 27, 1994

UNIVERSITY OF ALBERTA

FACULTY OF GRADUATE STUDIES AND RESEARCH

The undersigned certify that they have read, and recommend to the Faculty of Graduate Studies and Research for acceptance, a thesis entitled Sand Flow Mechanisms At Well Casing Perforations submitted by WARREN GREGORY MILLER in partial fulfillment of the requirements for the degree of MASTER OF SCIENCE.

J.D. Scott

Dr. J.D. Scott
Supervisor

D C Sego

Dr. D.C. Sego
Committee Chairman

Dr. N. Rajaratnam

Dr. S.M. Farouq Ali

September 14, 1994

ABSTRACT

Sand production in oil wells in high porosity, poorly consolidated heavy oil reservoirs is a multimillion dollar problem. The consequences of sand production result in several deleterious effects on well operation and in increased operating costs. The wide range of geologic formation and well operation factors influencing sand production has caused difficulty in identifying the critical mechanisms of sand production and their influences. Fundamental knowledge of the mechanisms of sand production at well casing perforations is necessary to optimize heavy oil production strategies.

A laboratory testing program utilizing a visualization model was conducted to provide a better understanding of the processes occurring at the perforation during sand flow or nonflow. The objectives of the testing program were to determine the mechanisms of sand flow into and through well-casing perforations and to evaluate the processes which govern sand arching or plugging at the perforations. The effects of sand particle size, casing perforation diameter, shape and roughness of perforation opening, sand porosity, sand confining stress, flow conditions through sand and perforations and capillary cohesion between two fluids in a sand were examined experimentally.

The results of this testing program were analyzed to determine the relative significance of the various variables that affect sand production. It was found that heavy oil formation sand, with only one fluid present, would not arch over or plug field size perforation openings. However, increased confining stress results in decreased sand flow rates and the presence of a high enough confining stress may be able to prevent sand flow. Furthermore, capillary cohesion between two fluids in a sand, such as gas and water, gas and oil or oil and water results in the formation of sand arches over perforation openings. The capillary cohesion at various saturations was quantified using fall-cone and direct shear tests. The fall-cone provided relative measures of capillary cohesion while the direct shear tests provided absolute measurements. The other variables investigated had no or small effects on sand arching compared to the effect of capillary cohesion and confining stress.

ACKNOWLEDGMENTS

The research work performed in this thesis was performed over the period of 1991 to 1994. I would like to acknowledge the financial support provided by the Mechanisms and Management of Sand Production Research Group managed by the Center For Frontier Engineering Research (C-FER). Funding was used to develop and machine the visualization models used during this research project.

The guidance and advice provided by Dr. J.D. Scott throughout the course of this study was much appreciated. The learning experience resulting from this research was greatly enhanced because of the maturity and wisdom of Dr. Scott who willingly provided key advice at critical stages yet encouraged independent research and personal development.

The technical assistance and suggestions provided by G. Cyre, S. Gamble and other staff members was greatly appreciated. I am grateful to the entire Civil Engineering support staff for their unwavering and cheerful assistance during periods of need. The contribution of Theresa Cloake during the visualization model testing portion of the research program was invaluable and I am thankful of her efforts.

The learning experience at the University of Alberta was enriched by many friends among staff and students in both civil and petroleum engineering. Particular thanks to Tim Pitman whose example proved an inspiration and whose friendship I greatly appreciate.

The patience and moral support provided by my family during the research years merits great appreciation. Their understanding, encouragement and irrepressible willingness to help in all situations and under any conditions is deeply cherished and certainly helped in setting my goal towards attaining my master's degree.

Table of Contents

Page
1. Introduction 1
    1.1 Statement of Problem 1
    1.2 Objectives and Scope of Research 2
    1.3 Organization of Thesis 4

2. Literature Review 8
    2.1 Fundamentals of Arching 8
    2.2 Influence of Sand Particle Size and Perforation Diameter 11
    2.3 Influence of Confining Stress 13
    2.4 Influence of Flow Conditions Through Sand and Perforations 16
    2.5 Influence of Capillary Cohesion 22
    2.6 Summary of Findings 27

3. Laboratory Testing 43
    3.1 Properties of Sands Used In Testing Program 43
        3.1.1 Grain Size Analysis 43
        3.1.2 Specific Gravity 45
        3.1.3 Maximum and Minimum Dry Density 46
        3.1.4 Hydraulic Conductivity 48
        3.1.5 Dry Sand Direct Shear Tests 49
        3.1.6 Wall Friction Direct Shear Tests 52
    3.2 Design of Visualization Model 55
        3.2.1 First Visualization Model Design 56
        3.2.2 Second Visualization Model Design 57
        3.2.3 Third Visualization Model Design 58
    3.3 Laboratory Procedures 60
        3.3.1 Dry Sand Without Confining Stress Applied 60
            3.3.1.1 First Visualization Model 60
            3.3.1.2 Second Visualization Model 62
        3.3.2 Dry Sand With Confining Stress Applied 63

Page
3.3.3 Fully Water Saturated Flow Tests.................................. 65
  3.3.3.1 First Visualization Model.................................... 66
  3.3.3.2 Third Visualization Model.................................... 67
3.3.4 Upward Air Flow Tests... 67
3.3.5 Partial Saturation Arching Tests.................................... 68
  3.3.5.1 Gas-Water Saturation Tests................................... 68
  3.3.5.2 Oil-Water Saturation Tests................................... 70
3.3.6 Index Capillary Cohesion Tests..................................... 71
3.3.7 Capillary Cohesion Direct Shear Tests............................ 74

4. Experimental Results.. 89
  4.1 Scope of Experimental Program.. 89
  4.2 First Visualization Model Design Tests............................. 90
    4.2.1 Horizontal Orientation.. 91
    4.2.2 Vertical Orientation.. 94
      4.2.2.1 Dry Conditions.. 95
        4.2.2.1.1 Fine Sand... 95
        4.2.2.1.2 Medium Sand... 96
        4.2.2.1.3 Coarse Sand.. 98
      4.2.2.2 Water Saturated Conditions.................................. 98
        4.2.2.2.1 Fine Sand... 99
        4.2.2.2.2 Medium Sand... 99
        4.2.2.2.3 Coarse Sand.. 100
  4.3 Second Visualization Model Design Tests............................ 101
    4.3.1 Dry Sand Without Confining Stress Applied..................... 102
      4.3.1.1 Fine Sand.. 102
      4.3.1.2 Medium Sand... 103
      4.3.1.3 Coarse Sand.. 104
    4.3.2 Dry Sand With Confining Stress Applied......................... 107

Page

4.4 Third Visualization Model Design Tests 107
  4.4.1 Dry Sand With Confining Stress Applied Results 108
    4.4.1.1 Fine Sand 108
    4.4.1.2 Medium Sand 109
    4.4.1.3 Coarse Sand 113
  4.4.2 Fully Saturated Water Flow Test Results 115
  4.4.3 Upward Air Flow Test Results 119
  4.4.4 Partial Saturation Arching Test Results 119
    4.4.4.1 Gas-Water Saturation Tests 119
    4.4.4.2 Oil-Water Saturation Tests 123
      4.4.4.2.1 Water-Oil Capillary Results (Non-saline Water, No Flow) 124
      4.4.4.2.2 Water-Oil Capillary Results (Saline Water, No Flow) 126
      4.4.4.2.3 Water-Oil Capillary Results (Non-saline Water, Flow Applied) 127
4.5 Index Capillary Cohesion Between Two Fluids In a Sand 130
  4.5.1 Index Capillary Cohesion Between Gas and Water in Fine Sand 130
  4.5.2 Index Capillary Cohesion Between Gas and Heavy Oil in Fine Sand 130
  4.5.3 Index Capillary Cohesion Between Gas and Medium Oil in Fine Sand 131
  4.5.4 Index Capillary Cohesion Between Heavy Oil and Water in Fine Sand 131
4.6 Capillary Cohesion Direct Shear Tests 133

5. Analysis of Experimental Results 166
  5.1 Sand Particle Size and Perforation Diameter 166
  5.2 Shape and Roughness of Perforation Opening 168
  5.3 Sand Porosity 169
  5.4 Confining Stress 170

Page
5.5 Flow Conditions Through Sand and Perforations....176
    5.5.1 Fully Water Saturated flow Conditions....176
    5.5.2 Upward Air Flow Conditions....180
5.6 Capillary Cohesion Between Two Fluids in a Sand....180
    5.6.1 Capillary Cohesion Between Gas and Water in Fine Sand....180
    5.6.2 Capillary Cohesion Between Gas and Heavy Oil in Fine Sand....183
    5.6.3 Capillary Cohesion Between Gas and Medium Oil in Fine Sand....183
    5.6.4 Capillary Cohesion Between Heavy Oil and Water in Fine Sand....184

6. Conclusions and Recommendations....200
    6.1 Summary....200
    6.2 Conclusions....204
    6.3 Recommendations for Further Research....206

References....208

Appendix A: Dry Sand Direct Shear Tests and Wall Friction Direct Shear Tests...211

Appendix B: Capillary Cohesion Direct Shear Tests....224

Appendix C: Upward Air Flow Tests....231

List of Tables

Page

Table 2-1: Results of Hall and Harrisberger Arching Tests........................ 32

Table 2-2: Experimental Conditions and Results of Bratli and Risnes............ 33

Table 2-3: Summary of Direct Shear Tests on Laboratory Compacted........... 34
Oil Sand Performed by Golder Associates Ltd.

Table 3-1: Sieve Opening Sizes.. 76

Table 3-2: Specific Gravity of Test Sands.. 76

Table 3-3: Maximum Dry Density of Test Sands.................................... 77

Table 3-4: Minimum Dry Density of Test Sands.................................... 77

Table 4-1: Summary of Results From First Visualization Model:.................138
Horizontal Orientation

Table 4-2: Summary of Results From First Visualization Model:.................139
Vertical Orientation - Dry Conditions

Table 4-3: Summary of Results From First Visualization Model:.................140
Vertical Orientation - Water Saturated Conditions

Table 4-4: Summary of Results From Second Visualization Model:..............141
Dry Sand Without Confining Stress Applied

Table 4-5: Summary of Results From Third Visualization Model:................142
Dry Sand With Confining Stress Applied

Table 4-6: Summary of Gas-Water Low Saturation Tests Results................143

Table 4-7: Summary of Heavy Oil-Water Low Saturation Tests Results.........144

Table 4-8: Dry Densities and Relative Densities of Gas-Water Index.............145
Capillary Cohesion Tests

Table 4-9: Dry Densities and Relative Densities of Gas-Heavy Oil Index........145
Capillary Cohesion Tests

Table 4-10: Dry Densities and Relative Densities of Gas-Medium Oil Index......146
Capillary Cohesion Tests

Table 4-11: Dry Densities and Relative Densities of Heavy Oil-Water Index..... 146
Capillary Cohesion Tests

Table 4-12: Index Capillary Cohesion Magnitude Comparison.....................147

Table 4-13: Capillary Cohesion Direct Shear Tests...................................148

Page

Table 5-1: Effect of Sand Particle Size and Perforation Diameter................ 191
Table 5-2: Effect of Shape and Roughness of Perforation......................... 192
Table 5-3: Effect of Confining Stress..193
Table 5-4: Gas-Water Low Saturation Tests..194
Table 5-5: Heavy Oil-Water Low Saturation Tests..................................195

Table C-1: Summary of Results From Third Visualization Model.................247
Table C-2: Upward Air Flow Velocity and Minimum Fluidization Velocity..... 248 of Test #87 (30 cm^2 Air Flow Area Assumption)
Table C-3: Upward Air Flow Velocity and Minimum Fluidization Velocity..... 249 of Test #87 (7.2 cm^2 Air Flow Area Assumption)
Table C-4: Upward Air Flow Velocity and Minimum Fluidization Velocity..... 250 of Test #90 (16.2 cm^2 Air Flow Area Assumption)

List of Figures

Page

Figure 1-1: Major Lower Cretaceous Oil Sands and Heavy Oil Deposits of Western Canada 5
Figure 1-2: General Lithologic Cross Section of Northeastern Alberta Heavy Oil Deposits 6
Figure 1-3: Cross Sectional View of Typical Heavy Oil Well 7

Figure 2-1: Arching Test Cell Used by Hall and Harrisberger 35
Figure 2-2: Coulomb Line of Failure 36
Figure 2-3: Cohesive Strength of Simulated Formation at Various Levels of Air-Water Saturation 37
Figure 2-4: Cohesive Strength For Oil-Water System 38
Figure 2-5: Drag Force Acting Though a Clean Sand Versus a Pseudo-Reynolds Number 38
Figure 2-6: Critical velocity For Fluid Transport 39
Figure 2-7: Apparent Fluid Velocity at Sand-Gravel Interface 39
Figure 2-8: Peak and Residual Shear Strength of First Set of Tests by Golder Associates Ltd. 40
Figure 2-9: Peak and Residual Shear Strength of Second Set of Tests by Golder Associates Ltd. 41
Figure 2-10: Peak and Residual Shear Strength of Third Set of Tests by Golder Associates Ltd. 42

Figure 3-1: Grain Size Distribution for Test Sands and Typical Formation Sand 78
Figure 3-2: Hydraulic Conductivity of Test Sands 79
Figure 3-3: Peak Shear Stress Versus Normal Stress - Dry Sand Direct Shear Tests 80
Figure 3-4: Residual Shear Stress Versus Normal Stress - Dry Sand Direct Shear Tests 81
Figure 3-5: Peak Shear Stress Versus Normal Stress - Wall Friction Direct Shear Tests 82
Figure 3-6: Residual Shear Stress Versus Normal Stress - Wall Friction Direct Shear Tests 83

Page
Figure 3-7: Inside Dimensions of Third Visualization Model........................ 84
Figure 3-8: Schematic Drawing of Third Visualization Model....................... 85

Figure 4-1: Sketch of Semispherical Cavity Formed in Fine Sand During........149
Water Flow With First Visualization Model in Horizontal Orientation
Figure 4-2: Typical Parabolic Sand Flow Pattern in Fine and Medium Sand..... 150
Figure 4-3: Typical Arch Formed By Dry Coarse Sand Over a 5 mm Wide...... 151
Slot Perforation
Figure 4-4: Typical Dome Shaped Sand Flow Pattern in Fine and Medium...... 152
Sand
Figure 4-5: Apparent Water Velocities of Fully Saturated Water Flow Test...... 153
and Durrett et al. (1976) Fluidization and Critical Transport
Velocities
Figure 4-6: Typical Growth of an Arch Formed By Partially Gas-Water......... 154
Saturated Fine Sand at Low Gas Saturations Due to Vibration
Figure 4-7: Typical Arch Formed By Partially Oil-Water Saturated Fine Sand...155
at Low Water Saturations
Figure 4-8: Gas-Water Index Capillary Cohesion....................................156
Figure 4-9: Gas-Heavy Oil Index Capillary Cohesion...............................157
Figure 4-10: Gas-Medium Oil Index Capillary Cohesion.............................158
Figure 4-11: Heavy Oil-Water Index Capillary Cohesion.............................159
Figure 4-12: Peak Shear Stress vs. Normal Stress - Direct Shear Tests............ 160
Figure 4-13: Residual Shear Stress vs. Normal Stress - Direct Shear Tests........161

Figure 5-1: Effect of Sand Porosity on Dry Fine Sand..............................196
Figure 5-2: Effect of Sand Porosity on Partially Saturated Fine Sand............. 197
Figure 5-3: Comparison of Capillary Cohesions Measured on..................... 198
Gas-Water Systems
Figure 5-4: Comparison of Capillary Cohesions Measured on..................... 199
Gas-Water Systems

Page

Figure A-1: Shear Stress vs. Horizontal Displacement - Dry Fine Sand...........212
Figure A-2: Vertical Displacement vs. Horizontal Displacement - Dry Fine Sand.............213
Figure A-3: Shear Stress vs. Horizontal Displacement - Dry Medium Sand...... 214
Figure A-4: Vertical Displacement vs. Horizontal Displacement - Dry Medium Sand.............215
Figure A-5: Shear Stress vs. Horizontal Displacement - Dry Coarse Sand........216
Figure A-6: Vertical Displacement vs. Horizontal Displacement - Dry Coarse Sand.............217
Figure A-7: Shear Stress vs. Horizontal Displacement - Dry Fine Sand/Plexiglass Interface..................218
Figure A-8: Vertical Displacement vs. Horizontal Displacement - Dry Fine Sand/Plexiglass Interface.............219
Figure A-9: Shear Stress vs. Horizontal Displacement - Dry Medium Sand/Plexiglass Interface............. 220
Figure A-10: Vertical Displacement vs. Horizontal Displacement - Dry Medium Sand/Plexiglass Interface.............221
Figure A-11: Shear Stress vs. Horizontal Displacement - Dry Coarse Sand/Plexiglass Interface...............222
Figure A-12: Vertical Displacement vs. Horizontal Displacement - Dry Coarse Sand/Plexiglass Interface.............223

Figure B-1: Shear Stress vs. Horizontal Displacement - Dry Fine Sand...........225
Figure B-2: Vertical Displacement vs. Horizontal Displacement - Dry Fine Sand.............226
Figure B-3: Shear Stress vs. Horizontal Displacement - 40% Gas/60% Water Saturated Fine Sand... 227
Figure B-4: Vertical Displacement vs. Horizontal Displacement - 40% Gas/60% Water Saturated Fine Sand...........228
Figure B-5: Shear Stress vs. Horizontal Displacement - 20% Gas/80% Water Saturated Fine Sand... 229
Figure B-6: Vertical Displacement vs. Horizontal Displacement - 20% Gas/80% Water Saturated Fine Sand...........230

List of Plates

Page

Plate 3-1: Third Visualization Model 86

Plate 3-2: Side View of Third Visualization Model 87

Plate 3-3: Overall Setup Of Third Visualization Model 88

Plate 4-1: First Visualization Model - Horizontal Orientation 162

Plate 4-2: Dry Fine Sand Without Confining Stress Applied Flowing Through 5 mm Wide Slot Perforation 163

Plate 4-3: Stable Arches Formed By Dry Coarse Sand Over 5 mm Wide Slot Perforation 164

Plate 4-4: Stable Arch Formed By Partially Gas/Water Saturated Fine Sand at a Gas Saturation of 98.8% over 12.7 mm Wide Slot Perforation 165

1. Introduction

1.1 Statement of Problem

The majority of heavy oil reservoirs in Alberta and Saskatchewan are in high porosity, poorly consolidated formations. A plan view of Alberta and Saskatchewan indicating the location of heavy oil reservoirs is provided in Figure 1-1. A multimillion dollar problem and a seemingly unavoidable consequence of oil production in these reservoirs is sand production. Sand production results in lost production, workovers, cleaning and disposal of waste solids, accelerated equipment wear and damage, flow line erosion, formation disturbance and casing damage. These occurrences result in significantly increased operating costs. Factors influencing sand production include virgin formation characteristics, production effects, drilling effects, completion effects, bottomhole effects and production systems and practices. The wide range of possible factors influencing sand production has caused difficulty in identifying the critical factors and their influence.

The heavy oil deposits of Alberta and Saskatchewan can be classified as (1) reservoirs capable of primary production for a 2 to 3 year period before enhanced oil recovery methods are necessary and (2) reservoirs which require enhanced oil recovery from the outset (Chalaturnyk et al., 1992). Figure 1-2 shows the geologic formations of these reservoirs in northeastern Alberta. It has been observed that primary heavy oil wells are often more prolific sand producers than their thermal counterparts. Primary heavy oil wells average 2% to 3% sand by bulk volume (including voids in settled sand) with a maximum of up to 60%. Thermal wells average less than 1% sand. Typical wells, over their primary production life, can produce on the order of 500 to 600 m^3 of sand, with some wells producing in excess of 1000 m^3 (McCaffrey, 1990).

It has been shown (McCaffrey, 1990) that sand production enhances reservoir oil productivity. Sand production is now viewed as an additional drive mechanism and encouragement of sand production is looked upon positively. This production, however, leads to issues regarding sand disposal and casing integrity. Thus, fundamental knowledge of the mechanisms of sand production is necessary to design an "optimized" production strategy which "manages" sand production (Chalaturnyk et al., 1992).

1.2 Objectives and Scope of Research

This study was undertaken to investigate the mechanisms of sand flow at well casing perforations. Communication between the interior of a well casing and a reservoir is established by forming holes through the well casing and surrounding cement. These holes are referred to as well casing perforations. This can be done with shaped charges which perforate the casing and cement or with abrasive fluid jets which cut slots through the casing and cement. With both methods, discrete horizons within the formation can be selectively accessed to produce the richest pay or to avoid water saturated zones. A cross sectional view of a typical well is provided in Figure 1-3. The well casing is placed into the hole drilled in the formation and is surrounded by cement which provides intimate contact between the casing and formation. The production tubing in placed inside the well casing. Well casing perforations pass through the casing, cement and into the formation in order to allow flow into the well casing.

The major part of this testing program utilized a visualization model to provide a better understanding of the processes occurring at the perforation during sand flow or nonflow. Such a laboratory model provides a small scale simulation of flow through a perforation with controlled stress and pressure boundary conditions and a simple geometry which accommodates interpretation of the laboratory experiments. Similar but less ideal conditions may occur under actual wellbore conditions. At the perforation, the sand may either arch or bridge over the opening, plug in the hole through the cement and casing, or flow through the perforation. The purpose of the study can be summarized into the objectives listed below:

- Determine the mechanisms of sand flow into and through well casing perforations using laboratory models

- Evaluation of the processes which govern sand arching or plugging at well casing perforations

The research concentrated on the development of a laboratory visualization model which was used to investigate the mechanisms of sand flow at well casing perforations. A lengthy and complex testing program was required to study all the factors related to formation and reservoir characteristics and completion and production practices. The scope of this study was limited to the examination of the variables considered to be the most prominently involved in the mechanisms of sand flow or nonflow at well casing perforations. The effects of the following variables were examined:

- Sand particle size and perforation diameter
- Shape and roughness of perforation opening
- Sand porosity
- Confining stress
- Flow conditions through sand and perforations
- Capillary cohesion between two fluids in a sand:
    - gas and water
    - gas and oil
    - oil and water

Over 120 tests were performed using the visualization models. These and other related tests allowed qualitative and quantitative measurements that have led to the evaluation of the effect of the variables listed above.

1.3 Organization of Thesis

A literature review of work done previously by other researchers regarding sand production at well casing perforations is presented in Chapter 2. Provided is a brief review of previous laboratory apparatus used to investigate sand production. As well, theories and analytical methods employed during previous research regarding sand production are explored.

Chapter 3 details the laboratory apparatus and procedures used during this research program. Firstly, a description of the sands used in the testing program is presented. The procedures used during geotechnical characterization tests performed on these sands are specified. The results of these tests are summarized and the use of these values later in the thesis are identified. Next, detailed descriptions regarding the components of the visualization models are provided along with the reasons governing the design of the three visualization models used in this study. As well, the preparation and testing procedures adhered to when using the visualization models and for the capillary cohesion tests are described.

The results of the laboratory tests using the visualization models and the tests for capillary cohesion are summarized in Chapter 4. Chapter 5 includes a discussion of the experimental results as well as comparisons of the results with previous data. The relative significance of the variables that affect sand production studied in this project are assessed. Conclusions, based on the experimental findings, are drawn and presented in Chapter 6. This final chapter of this thesis also includes recommendations for future research.

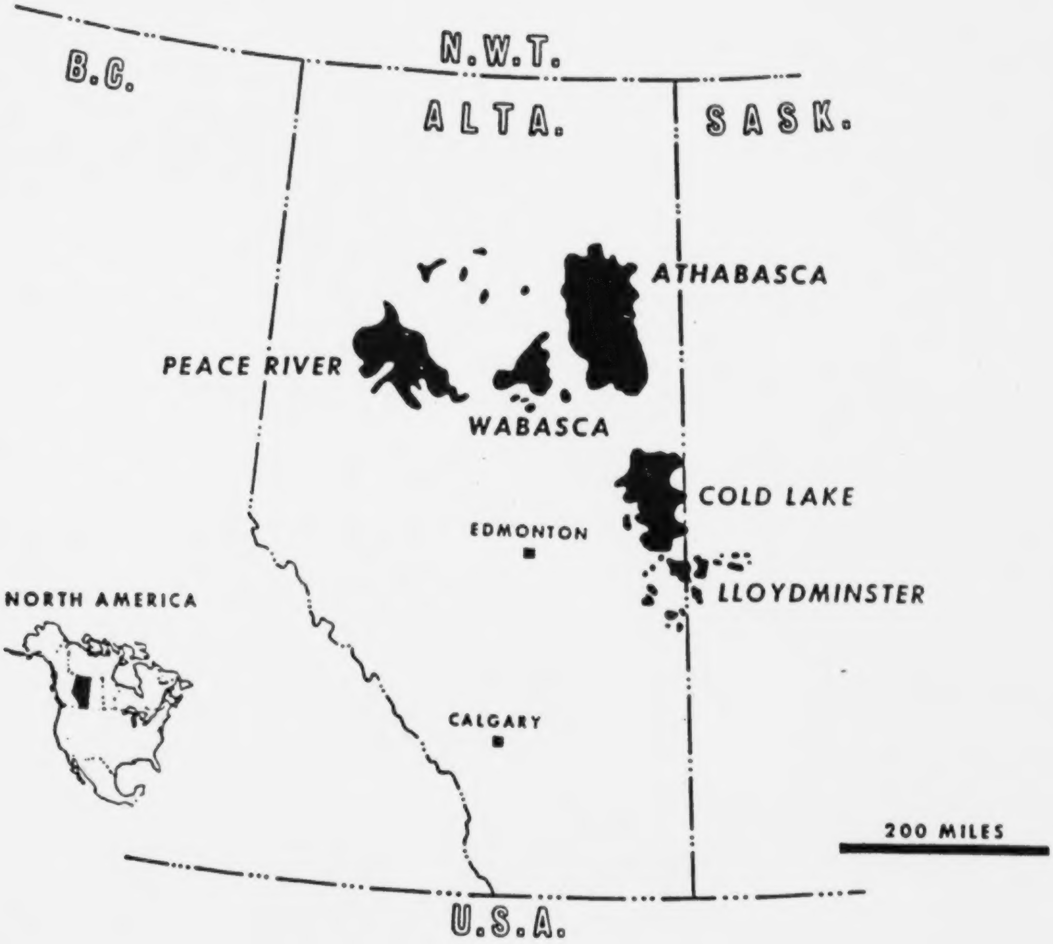
N.W.T.
B.C.
ALTA.
SASK.
ATHABASCA
PEACE RIVER
WABASCA
COLD LAKE
EDMONTON
LLOYDMINSTER
NORTH AMERICA
CALGARY
200 MILES
U.S.A.

Figure 1-1: Major Lower Cretaceous Oil Sands and Heavy Oil Deposits of Western Canada (after Jardine, 1974)

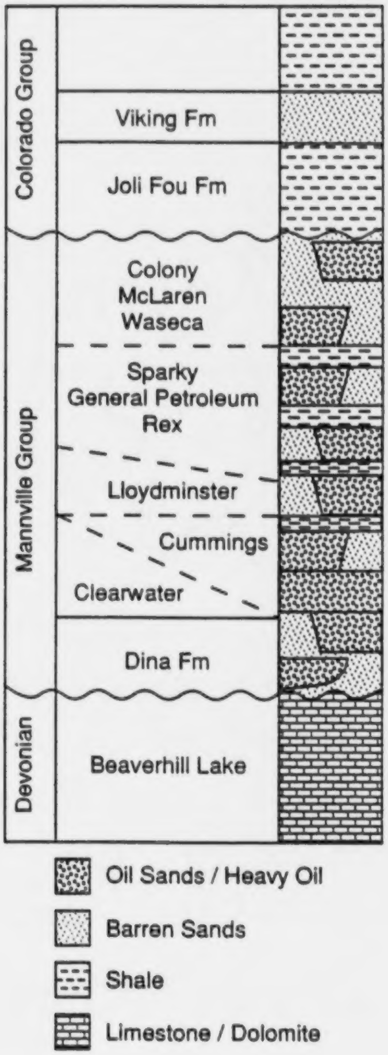
Colorado Group
Viking Fm
Joli Fou Fm
Mannville Group
Colony
McLaren
Waseca
Sparky
General Petroleum
Rex
Lloydminster
Cummings
Clearwater
Dina Fm
Devonian
Beaverhill Lake
Oil Sands / Heavy Oil
Barren Sands
Shale
Limestone / Dolomite

Figure 1-2: **General lithologic cross section of northeastern Alberta heavy-oil deposits (after Chalaturnyk et al., 1992)**

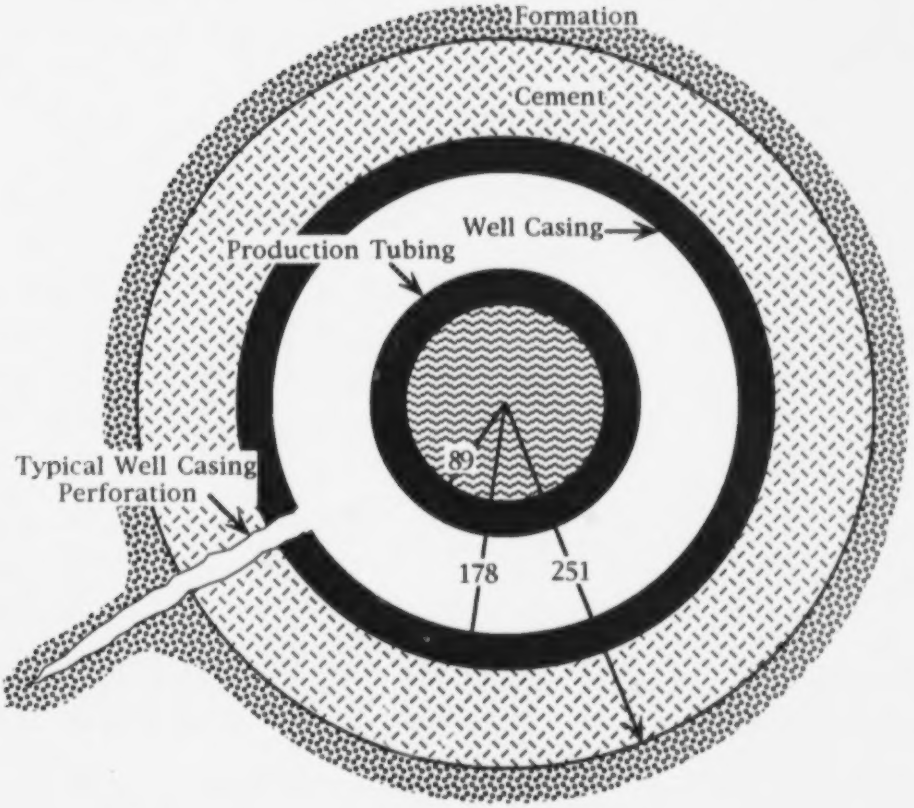
Formation
Cement
Well Casing
Production Tubing
Typical Well Casing Perforation
89
178
251

All dimensions in millimeters

Figure 1-3: Cross Sectional View of Typical Heavy Oil Well

2. Literature Review

2.1 Fundamentals of Arching

Several studies of sand control for oil wells have been performed and documented in the literature. A review and summary of the work done previously concerning sand flow mechanisms at well casing perforations and related subjects was compiled. In order to explain what a well casing perforation is and how it is created, a brief description of the procedures followed during drilling of a well, subsequent well completion and creation of well casing perforations is provided below. The hole is drilled with a drilling fluid, usually composed of a slurry of fresh water and bentonite clay. These are generally termed gel chem drilling systems. The density of the drilling mud is adjusted by adding more or less clay to balance the formation fluid pressure to ensure that gas does not escape from the reservoir and flow to the surface. The mud also serves to clean the drill cuttings from the well. Drilling mud forms a filter cake on the borehole wall which acts as a low permeability membrane between the drilling mud and the formation fluid. The drilling mud pressure acting on this membrane tends to support the borehole wall, thus reducing borehole yielding.

Following drilling, steel casing is run in the hole to provide long term support for the borehole wall. Cement is injected behind the casing to ensure intimate contact between the casing and formation. This serves two purposes: (1) it provides better support for the formation, and (2) it creates a seal between the formation and the casing to prevent communication along the wellbore to formations uphole. Care must be taken that the wellbore does not provide a pathway for hydrocarbons and saline reservoir fluids to migrate up into potable water aquifers or to the surface.

Communication between the interior of the casing and the reservoir is established by forming holes through the casing and cement. These holes are referred to as well casing perforations. This can be done with shaped charges which perforate the casing and cement or with abrasive fluid jets which cut slots through the casing and cement. With both methods, discrete horizons within the formation can be selectively accessed to produce the richest pay or to avoid water saturated zones. A cross sectional view of a typical well is provided in Figure 1-3.

Research performed by others on the subject of sand control for oil wells has been approached from several different aspects. The fundamentals of arching behavior, which is a key component in behavior of sand over a perforation was first described by Terzaghi (1943).

Terzaghi provides definitions of arching in ideal soils. He states that if part of the support of a soil mass yields, the soil on the yielding support moves between adjacent stationary masses of the soil. There is a shearing resistance between the yielding and stationary masses of soil which opposes the relative movement within the soil mass. The shearing resistance tends to keep the yielding mass in its original position. Thus, it reduces the pressure on the yielding part of the support and increases the pressure on the adjoining stationary part. Transfer of pressure from a yielding mass of soil onto adjoining stationary parts is called the arching effect. Soil is said to arch over the yielding part of the support. Terzaghi further states that arching is maintained solely by shearing stresses in the soil and that it is no less permanent than any other state of stress in the soil which depends on the existence of shearing stresses. As well, external influences can be expected to reduce the intensity of existing arching effects. The most important influence of this type are vibrations.

Terzaghi (op cit) describes the state of stress in the zone of arching for the case of arching in an ideal sand due to the local yield of a horizontal support. The lowering of a horizontal support (in Terzaghi's work a plane strain strip was used) from a bed of sand causes the sand located above the strip to follow. Frictional resistance along the boundaries between the moving and the stationary mass of sand opposes this movement. Terzaghi states that, as a consequence, the total stress on the yielding strip decreases by an amount equal to the vertical component of the shearing resistance which acts on the boundaries and the stress on the adjoining stationary parts of the support increases by the same amount. The transfer of part of the weight of the sand located above the yielding strip onto the adjoining masses of sand constitutes the arching effect.

Terzaghi provides a detailed explanation of a theory of arching that assumes surfaces of sliding normal to and at the outer edges of the strip and that the pressure on the yielding strip is equal to the difference between the stress of the sand normal to the strip and the full frictional resistance along the surfaces of sliding. From this explanation and other investigations, he concludes that the stress on a yielding strip is almost independent of the state of stress which exists in the sand normal to the strip at a distance of more than two or three times the width of the strip.

He also provides detailed definitions of arching and descriptions of the state of stress of an arch within a soil mass. However, these explanations deal with ideal soils which are assumed to arch over a yielding support. Terzaghi does not include the conditions necessary to initiate arching in a soil over an opening such as grain size to width of opening ratio, cohesive and frictional shear strength of the soil mass or confining stress. As well, the influence of fluid flow conditions through the soil and the opening is not discussed. To address the influence of these and other variables on the conditions required to initiate arching and on arch stability requires further investigation.

The work of Hall and Harrisberger (1970) is an in-depth look at the mechanical processes of failure of the sand structure around a perforated well casing and the factors that affect the stability of the formation sand. This work proved to be a sound basic study that provided direction to subsequent research projects. The field of powder mechanics also provides valuable insights (Brown and Richards, 1970). The results and conclusions from the various literature sources have been summarized with respect to the influence of the variables which affect sand production in oil wells. These variables include sand particle size and perforation diameter, confining stress, flow conditions through sand and perforations and capillary cohesion. Descriptions of experimental apparatus and testing procedures are also included in the literature review.

2.2 Influence of Sand Particle Size and Perforation Diameter

Hall and Harrisberger (1970) provided an explanation of the mechanisms of unconsolidated sand failure and studied the arching behavior of sand. They attempted to qualitatively determine the conditions required to form and maintain an arch over an opening at stresses greater than 760 kPa (110 psi) using their arching apparatus. A schematic drawing of their arching test apparatus is presented in Figure 2-1. A cylindrical chamber having 95.25 mm (3.75 inch) inside diameter, was used to confine the sand sample. A hydraulic jack was used to vertically load a piston fitted into the cylindrical chamber. The perforation or "trap door" was 11.1 mm (7/16 inch) in diameter and was located in the center of the chamber floor. Fluid could flow upward or downward through the chamber. The arching test apparatus was designed so that the sand depth was less than half of the chamber diameter. These dimensions were to ensure that almost the entire axial stress applied by the piston was applied to the chamber floor and trap door. They felt that little or no stress would be transferred to the side walls by friction using this configuration. A sand depth of 44.5 mm (1.75 inch) was used. With the sand depth four times the trap door diameter, it was felt that the full arching effect should be developed. The purpose of the arching test apparatus used by Hall and Harrisberger was to qualitatively observe arch formation by the sand when the trap door is removed and evaluate arch stability to fluid flow or changed loading.

They describe general test procedures using their arching test apparatus. The sand was compacted by holding a vibrating-tool against the side of the cylinder, while the sand was loaded under the weight of the piston. They assumed a medium-dense packing as the sand porosity was not measured. The hydraulic jack was used to apply the axial stress and the trap door was lowered carefully and removed. The result was observed to be either the formation of an arch or the production of sand. One limitation of their arching test apparatus is that it was not possible to visually examine the sand inside the arching test apparatus. Thus, the nonflow of sand out of the apparatus was considered to show the formation of an arch and the flow of sand was considered to be production of sand. Some tests involved load increases to cause arch failure, while other tests were subjected to a fluid or fluids flowing in or out to determine the stability of an established arch.

Hall and Harrisberger (op cit) performed arching tests using angular and round sand under dry conditions. They observed that a 10-20 mesh angular sand, under no confining stress, formed arches of slight stability or not at all at a grain diameter to width of opening ratio of 1:9.4. They also observed that rounded, 20-40 mesh and 80-100 mesh sand, under no confining stress, would not arch at grain diameter to width of opening ratios of 1:20 and 1:68, respectively. The results of Hall and Harrisberger are provided in Table 2-1.

Selby and Farouq Ali (1988) discuss the results of laboratory experiments investigating the mechanics of the movement of fines and sand flow into the wellbore. Experiments were performed in a radial flow model simulating a wellbore and the surrounding formation. They determined that sand production is affected by the overburden pressure applied, the flow rate and the size and shape of sand grains.

The model used by Selby and Farouq Ali was designed to simulate a wellbore and the surrounding formation under various overburden loads. The model consisted of a stainless steel cylindrical cell, with a height of 17.7 cm and a diameter of 20 cm. A perforated tubing 1.3 cm in diameter was fitted in a hole drilled in the center of the cell bottom. Two flow inlets were located at the outer walls of the cell, and the inner cell walls were lined with a sintered sheet to allow radial flow into the tubing. Overburden pressure was applied using a Enerpac hydraulic press. Overburden pressures were kept constant by adjusting the load with a manual air pump. Distilled water was used as the saturation and flowing fluid. Ottawa sand with a nominal grain size range of 111 to 187 μm (70 to 140 mesh), silica 187 to 369 μm (40 to 70 mesh), and glass beads 119 to 175 μm (80 to 120 mesh) or 44 to 99 μm (170 to 325 mesh) were used to pack the cell.

Regarding sand grain size, when no overburden stress was applied, sand arches formed using both the fine and medium sand, although sand production was higher when smaller sand grains were employed. Experimental results also show that no sand arches were formed in experiments conducted using spherical glass beads. They concluded that more sand is produced from spherical, small-grained packs than from angular, large-grained packs.

2.3 Influence of Confining Stress

Hall and Harrisberger also investigated the influence of confining stress on sand production using the equipment described in Section 2.2. They observed that a confining stress of 3500 kPa applied to fully gas saturated, 10-20 mesh angular sand improved arch stability at a grain diameter to width of opening ratio of 1:9.4. They presumed the increase in arch stability was due to better interlocking of the surface grains. However, a confining stress of 14 MPa caused failure of the angular sand due to grain crushing. They also observed confining stresses of up to 14 MPa could not induce arching in fully gas saturated, rounded 20-40 mesh and 80-100 mesh sand at grain diameter to width of opening ratios of 1:20 and 1:136, respectively.

They also looked at the effects of very high confining stress. Water moistened 20-40 mesh rounded sand formed an arch that remained stable to the maximum loading capacity of the apparatus, 23 800 kPa. However, dry and water moistened 8-12 mesh angular sand failed due to grain crushing at confining stresses of 13 500 kPa and 14 500 kPa, respectively. A wider particle range, 30-250 mesh angular sand failed by crushing at

11 700 kPa. The same sand under water moistened conditions did not fall through the perforation as the maximum confining stress of 23 800 kPa was applied. Hall and Harrisberger state that the sand did crush, but the crushed material remained in the apparatus.

Suman (1975) presents two methods for controlling wellbore stress state in order to stabilize unconsolidated sands. The first is the application of elevated drilling fluid weight to prevent dilation or crushing of sand grains surrounding the wellbore. Instabilities resulting from such formation failure would be expected to increase the likelihood for sand production. The second method suggests that there is an elevated range in stress state in which stable sand arches will form over perforations and permit unrestricted production flow rates from many wells without sand production. This method uses one or more inflatable external packer(s) opposite the interval(s) to be perforated, for establishing and maintaining the proper stress state for stable sand arches. Suman found support for these concepts is provided through interpretation of sand arch experimentation, considerations of the state of stress at the wellbore face and general field observations. Suman used the results of Hall and Harrisberger (1970) to extract all possible indicators regarding arch stability as a function of load.

Suman goes on to describe the effect of well depth on arch load. The following would be expected as a general function of well depth: (1) formation sands surrounding boreholes drilled to an extremely shallow depth would either not arch over the perforations or would form tenuous arches. Sand could readily flow (roll and slide) through the perforation, (2) at intermediate depths, flow rate sensitive arches would form. Sand production would depend on rate of flow and restraint provided by interfacial tension and sand angularity. Arch failure would result in rolling and sliding of sand through the perforation, (3) somewhat deeper, the arch load may be sufficient to provide for high rates of fluid flow without failure, and (4) for a given sand quality, arch load may reach the level where arch failure through grain crushing will occur. However, due to the reservoir of formation material, arch loading may be self-adjusting shifting to a lower but stable arch load. This type of situation could account for trace sand production noted in wells. Suman notes that the above descriptions correspond in general with field experience.

Cleary et al. (1979) investigated the effect of confining stress and fluid properties on arch stability in unconsolidated sands. They state that the mechanism of sand stabilization around a wellbore is the formation of sand arches across a perforation opening. Hence, they recorded sand instability at the moment of failure of sand arches. Overburden stresses of 1.7, 5.2, 10.4, 15.5 and 20.7 MPa were used. Fluid saturations consisted of an irreducible water phase and liquid hydrocarbons. The hydrocarbon fluids were kerosene and mineral spirits. The sand used was Gopher State 20-40 frac sand.

Cleary et al. thought that sand flow into a wellbore is generally a function of one or more of the following factors: (1) fluid drag associated with high oil viscosities, (2) fluid drag due to high fluid velocity, (3) skin buildup (reduction of permeability due to fines buildup) around the wellbore, (4) rate surges, (5) changing loading conditions around the wellbore due to pore pressure changes, and (6) the destruction of cohesive forces between the sand grains due to phase changes or changing saturations around the wellbore.

The apparatus used by Cleary et al. as a sand cell was a pressure vessel 221 cm long and 76 cm in diameter. The sand pack was 134 cm long and 41 cm in diameter. The pressure vessel contained two plexiglass viewing ports. Within the cell, a length of semicircular 10.2 cm casing was machined through the ports. The perforation was drilled through the viewing port and was 27.9 cm long. The cell had 5 oil inlets and a maximum 34.5 MPa (5000 psi) grain to grain stress in the sand pack. However, the large side friction developed by the stressing of a long cylindrical sand pack diminishes the magnitude of applied stress at the center of the sand pack. Strain gauges were placed opposite the perforation and flow rate was measured with a differential pressure transducer. Stresses, inlet and outlet pressures, flow rate, cavity size, arch restabilization and water production were continually monitored and observed.

They concluded that arch structure is a function of the stress distribution of the sand pack. Also, maximum arch size and stability are found to be a function of confining stress. Arch size decreases with increasing confining stress. They also observed that arch stability increases with increasing horizontal and vertical stress. As well, the most stable vertical arches form when horizontal stress is at a maximum and vertical stress is a minimum.

Selby and Farouq Ali (1988) investigated the influence of confining stress using the experimental setup described in Section 2.2. They determined that when no overburden stress was applied, sand forms arches for both the fine and medium sand, although sand production was higher when smaller sand grains were employed. At low overburden loads, arches occurred in all tests conducted using angular sand. At high loads, no arching was noted using fine sand and unstable arches were formed using the larger sand. They concluded that sand production increases as the overburden pressure increases and that arching of the sand occurs at low overburden stresses.

2.4 Influence of Flow Conditions Through Sand and Perforations

Hall and Harrisberger (1970) performed tests which used air as a flowing fluid through dry sand. They found that 10-20 mesh dry angular sand under a load of 3500 kPa formed an arch over a 11.1 mm diameter perforation. The arch remained stable when a slow outward air flow was applied, but failed when a faster flow was used. Outward air flow is defined as flow downwards through the sand and out the perforation. They also observed that 20-40 mesh and 80-100 mesh rounded sand that previously did not exhibit arching, was able to form arches when air was drawn in against the falling sand grains. Arches would fail and reform as air flow was decreased and increased. The confining stress was increased to 13 800 kPa without causing arch failure. Hall and Harrisberger concluded that the drag force on the surface of the grains gave enough restraint to initiate arching.

Stein and Hilchie (1972) presented a method to estimate critical fluid production rates possible without using sand control techniques. Critical flow rates are defined as limiting flow rates above which troublesome sand production is expected. Stein and Hilchie state that the strength of a hydrocarbon bearing sand can be represented by a Coulomb line of failure as shown in Figure 2-2. The two contributions to the strength of the material are friction between sand grains and cohesion between adjoining grains. Cohesion is made up of mineral cementation between adjoining sand grains and capillary forces generated by interstitial water in hydrocarbon producing formations. It has been shown that interstitial water can generate tensile strength in uncemented granular material (Rumpf, 1961).

Stein and Hilchie provide an explanation for arch formation over a single perforation. Production through a perforation can exert a high enough total force on the sand adjacent to the perforation to cause some sand production. The cavity will grow spherically until the arch has a sand face with an area sufficient to resist the fluid generated force with enough cohesion remaining to stabilize the arch under formation load conditions. Mineral cementation would allow for a smaller arch to be formed. Stein et al. (1974) present theoretical techniques utilizing sonic and density logs for estimates of maximum sand free production rates from friable formation sands. They feel these techniques would be a good estimate to determine if sand control is required in a well.

Tippie and Kohlhaas (1973) conducted an investigation of fluid flow rate effect on arch formation and stability. They point out that in a well completion, sand at a perforation is unstressed and most of the reservoir is stressed due to overburden load. Sand production is prevented by arches that form over each perforation and stabilize the sand. The failure of these arches results in sand production and therefore conditions necessary for formation, stability and failure of these arches are of great interest.

They modeled the region near a perforation in a well completed in an unconsolidated sand reservoir with a semi-cylindrical sand pack confined in a test cell. The cell was designed with a screen inlet for radial fluid flow at the outer radius and with a hole (perforation) at the inner radius wall (casing) for a fluid outlet. Overburden load was applied with a diaphragm on top of the pack. The flat front face of the cell could be removed for visual examination through the lucite casing of the sand pack in the vicinity of the perforation. A well sorted, medium grain, clean Gopher State 20-40 mesh frac sand was used. Tippie and Kohlhaas flowed fluid radially through a sand pack which was loaded vertically to simulate overburden pressure. Flow rates were increased gradually until sand flowed. The arch was then observed. The flow was restarted at a low rate and gradually increased until sand production occurred. They observed arches that were approximately ellipsoidal in shape and in most tests an irregular cavity containing loose sand was observed. In all tests, the perforation was located at the bottom of the cavity and arch. The growth of the arch was vertically upward along the casing.

Tippie and Kohlhaas report that in most cases, arches fail when the pressure drop across the sand suddenly increases. This results in the production of large amounts of sand. Eventually, sand free production would return. They note that the pressure drop at this time would be less than before the sand is produced even though a constant rate is maintained. They state that flow rate influences arch size and stability. As well, the producing characteristics of unconsolidated sand reservoirs can be significantly affected by flow rates. They also observed that smaller arches are more stable and allow a high fluid viscosity to be reached before failure. Gradual rate increases result in higher sand free production when compared to sudden increases to full rate. As well, fines migration contributes to instability and failure of arches.

Tippie and Kohlhaas (1974) also examined variation of skin damage with flow rate associated with sand flow or stability in unconsolidated sand reservoirs. The same equipment referred to above in Tippie and Kohlhaas (1973) was used. Tippie and Kohlhaas (1974) determined an association between fines migration and skin effect change with sand instability.

Bratli and Risnes (1981) analyzed the stress due to fluid flow in the sand arches formed behind perforation openings on the basis of a theoretical model. Their examination of the effect of flowing fluids through sand arches resulted in a criteria describing the stability and failure of the sand. They also studied the arching phenomena in the laboratory. They found that the laboratory experiments qualitatively reproduced the theoretical results.

The laboratory model used by Bratli and Risnes (1981) consisted of a steel cylinder with a central hole in the bottom to simulate a perforation. The inside diameter and height of the cell were 19 and 38 cm, respectively. The wall thickness was 2 cm. The cylinder was filled with unconsolidated sand and compressed vertically by a piston to simulate overburden. Four fluid inlets were spaced equally around the circumference, 22 cm above the bottom of the cell. Fluid was introduced at the top beneath the piston, through the fluid inlets, spread over the total area by a multi-wrapped wire screen, and forced through the sand pack. Bratli and Risnes used air as the flowing fluid during their experiments. The flow rate was varied with a standard pressure regulator. The sand was filled in the cell in layers 2 to 3 cm thick. Each layer was worked thoroughly to get a good packing. During the filling operation, excess water was used to ensure that the sand pack was 100% water saturated. Before performing an arching experiment, the water saturation was reduced by applying a small pressure differential and draining the fluid through a permeable bottom plug. It was assumed that water saturation was near the irreducible water content. Porosity and water saturation were calculated from water volumes used during filling and measured when draining.

In an arching experiment, the flow rate was increased steadily until a small amount of sand was produced suddenly. Further increase of the flow rate could be made without incident before a new lump of sand blew out. This repeated itself several times (5 to 10) until the rest of the sand in the cylinder suddenly flowed out. During an arching experiment, the flow rate was increased and upstream fluid pressure observed. The outlet pressure was kept at atmospheric pressure. At each increase in flow rate, the sand weight, if there was any sand production, was measured. The two sands used in experiments were 20-40 mesh Ottawa sand and 80-100 mesh crushed quartz.

Initial experimental conditions are summarized in Table 2-2. The basic pattern of arching was always the same. The flow rate could be increased steadily until a small amount of sand was produced suddenly. The flow could be increased further without incident until a new amount of sand broke loose. This repeated itself several times until the sand pack broke down suddenly and the sand came pouring out of the opening.

The arches formed were stable in the sense that the flow rate could be reduced to zero and increased to its former value several times without affecting the arch stability. The flow rate could also be held constant for hours without causing significant changes. To find the shape of the cavities formed, experiments with the 80-100 mesh sand were repeated and stopped before the total collapse was reached. Gypsum was then injected through the opening. The cavity profiles obtained show that the cavity grows behind the opening, both in width and depth. The flowlines in the sand will converge into the upper part of the cavity, while there will be no fluid flow in the sand around the lower part of the cavity. The cavity, therefore, may be regarded as consisting of two parts. The upper part which is subjected to the fluid drag forces forms an approximately hemispherical arch, while the lower part acts as a conduit to the opening.

Bratli and Risnes presented a theoretical model concerning the stability of sand arches. To deal with the stability of sand arches, the stress distribution in the sand must be known. These stresses will depend on the principal stresses in the material, the fluid pressure and flow rate, the geometry of the arch, and the stress strain relations in the material. A detailed explanation of the theoretical model is provided by Bratli and Risnes (1981).

They established theoretically that two different modes of failure with increasing flow rate exist: collapses of thin inner shells and total collapse of the material. Initially, a stable arch is formed. Then, thin inner shells collapse to form stable new arches. This takes place several times before total collapse occurs and massive sand production ensues.

Risnes, Bratli and Horsrud (1982) applied the Bratli and Risnes (op cit) theory for stability and failure of sand arches to actual well test data. The formation tested was a poorly consolidated oil bearing sand. No special sand control was installed in the well. The test procedure consisted in measuring simultaneously sand and oil production as the choke size was stepwise increased. In this way the maximum sand free production rate was established.

The theory investigated by Risnes, Bratli and Horsrud states that the formation of sand arches behind perforation openings is a mechanism that can stabilize a poorly consolidated sand and prevent it from flowing into the well. There is however a limit to the load imposed by the fluid drag forces that a given arch can sustain. Therefore the corresponding sand control method essentially consists in keeping the production rates lower than a critical flow rate that will cause continuous sand influx. They concluded that the field results can consistently be described by their arch theory.

Selby and Farouq Ali (1988) reached conclusions regarding the influence of flow rate. Sand production rates were carried out under three different flow rates: 2, 8 and 13.3 mL/min. Tests were run at different flow rates with no overburden stress and one run at a low flow rate and an overburden stress present. In the absence of overburden load, the sand formed arches regardless of the flow rate employed. The sand arched rapidly at higher flow rates. However, the initial sand production was higher at higher flow rates. At high overburden loads, arching occurred when a low flow rate of 2 mL/min was employed, but not at higher flow rates. Sand production increased at higher rates. They concluded that sand production increases as the fluid flow rate is increased and that arching of the sand occurs at low overburden loads and at low flow rates.

Veeken et al. (1991) classified field measurements of sand production. They defined transient sand production as a sand concentration declining with time under constant well production conditions. Continuous sand production is defined as a sand production level which remains relatively constant with the acceptable sand concentration depending on several operating variables. They define catastrophic sand production as a high rate of sand influx that causes the well to suddenly choke and die.

They point out that in previous laboratory tests performed using unconsolidated material, the dominating factors were flow rate and capillary forces. They report that several references report a flow rate of about 5-10 bpd as the flow rate corresponding to cavity failure. This critical flow rate was found to be independent of sand mixture, cavity size, boundary stress and pore pressure.

2.5 Influence of Capillary Cohesion

Hall and Harrisberger (1970) considered two suppositions with regard to the mechanisms of arching. The first was that arch stability requires a small degree of restraint on the grains forming the inner free surface of the arch. The second was that the stabilized surface permits the remainder of the arch structure to distribute and support a large load over the opening. They felt that their results, provided in Table 2-1, confirm these two suppositions. They found that applied loads of any magnitude could not induce arching in round grains until some type of cohesion was applied to the sand. The cohesion took the form of moistening the sand or flowing air upwards into the sand. Numerous tests were performed by Hall and Harrisberger to examine the influence of saturation conditions. They observed that under stress conditions where arches were unstable in dry or saturated sand, arches were stable if immiscible liquid phases were present and the wetting phase saturation was less than funicular, that is, the wetting phase is not continuous (Islam and George, 1991). Arches would fail when the wetting phase saturation reached a funicular state. They concluded that a cohesive force, supplied by interfacial tension within the sand structure, was necessary for arch stability.

Previously, Hall and Harrisberger (op cit) found that dry 20-40 mesh rounded sand would not arch over a 11.1 mm diameter perforation. However, when water moistened, the 20-40 mesh rounded sand formed stable arches at confining stresses up to 13 800 kPa. They also observed that the same sand would not form an arch when saturated with kerosene, but did form an arch after the kerosene was reduced to residual saturation by flowing air upward into the sand. These tests showed that capillary cohesion created by the interfacial tension between two immiscible fluids was sufficient to cause arching.

Hall and Harrisberger also examined the effects of the flow of the wetting and nonwetting fluids through a sand pack. Arches remained stable to the outward flow of the nonwetting fluid with the wetting fluid at residual saturation. However, arches failed when subjected to outward flow of the wetting fluid. They point out that the outward flow of the wetting fluid fills the pores of the sand leaving the nonwetting phase as separated globules existing in the voids. The arch fails as the cohesion created by the interfacial tension between the two fluids is decreased, because there are fewer nonwetting fluid-wetting fluid-sand contacts.

Durrett et al. (1976) conducted a research program to improve understanding of the causes and mechanisms of sand production. The investigation focused on: (1) a study of the static forces tending to hold sand in place, (2) a study of the dynamic and static forces that counteracted these static-holding forces, and (3) a study of the sand transport phenomenon. They also provide insights into formation strength, formation stresses and sand transport. According to these authors, the strength of a formation is derived from cementation material, interlocking of grains under confinement loads and cohesive strength resulting from interfacial tension forces between reservoir fluids. However, mineral cementation is absent in unconsolidated formations and grain interlocking is absent in sand at void ratios larger than the steady state void ratio.

Durrett et al. point out that the cohesive strength derived from reservoir fluids is a function of interfacial tension forces and wetting-phase saturation. They performed static tensile tests on a simulated formation sand at various levels of air-water saturation to determine cohesive strength. Their results are shown in Figure 2-3 and indicate increasing cohesive strength with augmented wetting-phase saturation nearing the pore entry pressure indicated by the drainage capillary pressure curve. They concluded that cohesive strength does not reach the pore entry pressure because of variations in capillary size that cause some capillaries to become fully saturated, while other capillaries still contain mixed-fluid saturation.

They used the cohesive strength measured on the air-water system to calculate cohesive strength for a similar oil-water system having 35 dynes/cm interfacial tension. As shown in Figure 2-4, they calculated a maximum cohesive strength for the oil-water system of approximately 2.4 kPa (0.35 psi) at 20 percent water saturation. Durrett et al. (1976) concluded that although this strength is low, it is significant when compared with the fluid drag forces that cause sand migration near the wellbore. They also calculated the drag force acting through a clean sand vs a pseudo-Reynolds number (N_{Re}) based on medium sand grain diameter, as shown in Figure 2-5. This plot assumes a clean sand (one-fluid phase), but by inspecting and comparing Figures 2-6 and 2-7 it shows that significant producing rates can be achieved in open-hole completions before critical drag forces are reached.

Durrett et al. (op cit) looked at critical fluid velocity. It is described by Stokes' law (settling of particles) that gives critical transport velocity for sand transport in an open channel, that is, unhindered flow. Figure 2-6 shows fluidization and critical transport velocities for water flow plotted against grain size. They also presented Figure 2-7 which describes apparent velocities of produced fluids in clean sands as a function of producing rate. By comparing allowable fluidization velocities (Figure 2-6) with calculated producing velocities (Figure 2-7), it can be seen that most formation size grains are transported readily by typical producing rates, unless they are held in place by some force.

Durrett et al. were unable to measure cohesive tension under dynamic flow conditions. They did make an attempt, but fluid flow through the sand pack with mixed saturation caused the pack to separate. Rather than sloughing individual grains from the free surface, separated sand plugs extruded through the open perforations. This occurred at insufficient flow rates, producing drag forces that exceed the predicted cohesive strength and although the sand pack separated, the plugs still exhibited cohesiveness. They proposed the concept of channel flow as a possible explanation for pack failure. That is, certain permeability channels become nearly saturated with one or another of the fluids. This reduces cohesive strength to low values found at either end of the wetting-phase saturation.

Durrett et al. performed another test using a 20-40 mesh sand with mixed oil and water saturation, placed in a Hassler sleeve cell under a confining load of 8.3 MPa (1200 psi). They measured flow rates up to 7 BOPD per perforation before sand production occurred through the perforation opening at the downstream end of the cell. The test was repeated with only one fluid phase present and sand production occurred at a 0.5 BOPD per perforation flow rate.

These preliminary tests by Durrett et al. indicate that interfacial tension forces could be significant in controlling sand production. These findings also concurred with field observations that sand production usually increases when water production increases, changing fluid saturation distribution around the wellbore.

The effect of cohesion on arch stability was measured relatively by the comparison of the sand pack behavior with two different hydrocarbon fluids by Cleary et al. (1979), namely kerosene and mineral spirits. Kerosene provided stronger cohesive forces, resulting in arches with greater stability than those formed with mineral spirits. They found that although mineral spirits have a higher interfacial tension with water than kerosene does, the pendular volume in a kerosene/water system is more cohesive than in a mineral spirits/water system. The magnitude of the cohesive forces is not very high. However, they have a significant effect on restabilization of arches.

Islam and George (1991) modeled the top one-eighth of a horizontal well. They used this model to test the performance of wire-wrapped screens and flexible tubings. They state that sand production occurs when the formation stresses exceed the strength of the formation. Formation strength is due mainly to natural cementation of sand grains but also from cohesive forces resulting from immobile formation water. Stress on formation sand grains is due mainly to tectonic actions, overburden pressures, pore pressures, stress changes from drilling and drag forces on the producing fluids.

Islam and George point out several reasons why sand production has been related to water production: (1) increased total fluid production needed to maintain oil production rates increases the drag forces on the sand, (2) the forces that make the sand cohere are disturbed as the water phase becomes mobile, (3) two phase flow and mobility of the wetting phase cause drag forces to increase and (4) the natural cementing material is dissolved or softened.

A laboratory testing program was undertaken by Golder Associates Ltd. (Weaver, 1994) with the purpose of measuring apparent cohesion induced by multi-phase pore fluid capillary in a sand matrix. As well, the influence of porosity and oil-water ratio on the magnitude of apparent cohesion was investigated. They chose direct shear tests at normal stresses from 0 to 20 kPa to measure the apparent cohesion. A clean tailings sand with a D_{50} of approximately 0.2 mm was used along with a mineral oil having a viscosity similar to water for the test specimens. Reagent grade deionized water (pH=7) was used in the testing program. Specimens were water-wet, oil saturated and compacted to a desired porosity. The samples were prepared by placing the water-wet sand in the oil and subjecting it to a vacuum for a minimum of two hours to deair them. The specimens were then compacted. It was reported that samples were uniform and most were at or near full saturation.

The first set of tests was on specimens at a dry density of 15.3 kN/m^3 (porosity = 43%) and at 70% oil saturation and 30% water saturation. These tests resulted in an apparent cohesion of 4.5 kPa and a curved peak shear strength envelope. The slope of the peak shear strength envelope decreased with increasing normal effective stress. The constant volume (residual) shear strength envelope had a friction angle of 43° and zero cohesion. The details of the first set of tests are summarized in Table 2-3 and Figure 2-8 presents the peak and residual strength envelopes.

The second set of tests at dry densities of 16.0 kN/m^3 (porosity = 40%) and an oil/water ratio of 70:30 were sheared at normal stresses of 0, 5 and 10 kPa. Similar to the first set of tests, a curved peak shear strength envelope was obtained and the peak apparent cohesion was measured as 4.5 kPa. The residual shear strength had a friction angle of 39° and zero cohesion. These results led Golder Associates Ltd. to conclude that porosity of the sand appeared to not have a major influence on apparent cohesion, in the porosity range used in their testing program. The details of the second set of tests are summarized in Table 2-3 and Figure 2-9 presents the peak and residual strength envelopes.

The third set of tests investigated the influence of the oil/water ratio. Samples had an oil/water ratio of 50:50 and a dry density of 15.3 kN/m^3 (porosity = 43%) and were sheared at normal effective stresses of 0, 5 and 10 kPa. As in the other sets of tests, a curved peak shear strength envelope was measured. However, the peak apparent cohesion had a value of 2.7 kPa. The residual shear strength had a friction angle of 42° and cohesion of zero. Thus, the reduced oil saturation resulted in a decrease in the apparent cohesion. The details of the third set of tests are summarized in Table 2-3 and Figure 2-10 presents the peak and residual strength envelopes.

2.6 Summary of Findings

The most relevant and important findings of the literature review with regard to the objectives of this research project are summarized below. A 10-20 mesh angular sand (D_{50} = 1.4 mm) formed highly unstable arches or did not form arches at all at a grain diameter/opening width ratio of 1:9.4. Likewise, a 20-40 mesh rounded sand (D_{50} = 0.63 mm) also did not exhibit arching behavior at a grain diameter/opening width ratio of 1:20. Most importantly due to its similarity to actual formation sand, a 80-100 mesh rounded sand (D_{50} = 0.17 mm) would not arch at a grain diameter/opening width ratio of 1:68. The average size of formation sand is 0.2 mm and perforations typically have widths of 12.7 mm (1/2 inch) and 19.1 mm (3/4 inch). This results in grain diameter/opening width ratios of 1:64 and 1:96, respectively. Based on the results presented above, at the large width of opening to grain diameter ratios found in the field, arching of dry sand over perforations is highly unlikely.

The results mentioned above also point out a difference in behavior between angular and rounded sand and coarse and fine sand. The uniform, coarser, angular sand arched when the perforation diameter was 9.4 times larger than the sand. Whereas the uniform finer, rounded sand did not exhibit arching at any grain diameter/opening width ratios. Increased angularity and coarseness of sand grains increases the shear strength of sand. This allows angular and coarse sand to form arches at larger grain diameter to width of opening ratios than rounded and fine sand. This supports the conclusion of Selby and Farouq Ali (1988) that more sand is produced from spherical, small-grained packs than from angular, large-grained packs.

The influence of confining stress was also investigated. A confining stress of 3500 kPa applied to dry 10-20 mesh angular sand improved arch stability at a grain diameter/opening width ratio of 1:9.4. This was felt to be due to better interlocking of sand grains resulting in higher shear strength. A confining stress of 13.8 MPa applied to the same sand could cause failure by grain crushing. However, a confining stress of 13.8 MPa could not induce arching in dry rounded sand that previously did not exhibit arching under conditions of no confining stress. Cleary et al. (1979) supports this conclusion stating that arch stability increases with increasing horizontal and vertical stress. As well, arch structure is a function of the stress distribution of the sand pack and arch size decreases with increasing confining stress.

A water moistened 20-40 mesh rounded sand formed an arch at a grain diameter/opening width ratio of 1:20 and remained stable at a confining stress of 23.8 MPa. Dry and water moistened 8-12 mesh angular sand formed arches that failed due to grain crushing at confining stresses of 13.5 MPa and 14.5 MPa, respectively. As well, a 30-250 mesh angular sand having a much wider grain size range, formed arches that failed due to grain crushing under dry and water moistened conditions at confining stresses of 11.7 MPa and 23.8 MPa, respectively. These results indicate that arch failure due to confining stress occurs at lower stresses for angular sands than rounded sands and grain crushing usually accompanies the failure of the angular sand. The relative influence of capillary cohesion on the stability of arches should also be noted. All of the tests performed using water moistened sands where capillary cohesion was present, required higher confining stresses to cause arch failure, compared to similar tests using dry sand. This shows how capillary cohesion plays a significant part in forming and maintaining stable arches which will be discussed later.

The effect of well depth on arch load was well described by Suman (1975). He described four regions of sand behavior as a function of well depth. At shallow depths, sand would either not arch over perforations or form tenuous arches and sand could flow readily through the perforation. At intermediate depths, arches sensitive to flow rate would form. At deeper depths, arches would be sufficiently stable to allow high fluid flow rates without failure. Finally, at somewhat deeper depths and a given sand quality, arch failure through grain crushing may occur. These regions of sand behavior may be compared to the behavior of sand in laboratory tests in order to determine which region of well depth is being modeled.

It was found by Hall and Harrisberger (1970) that a slow flow of air downwards through sand and out a perforation had no effect on the stability of an arch. However, a faster flow was able to destroy the arch. Selby and Farouq Ali (1988) observed that when no confining stress was applied, sand formed arches regardless of different flow rates of 2, 8 and 13.3 mL/min. Sand arched rapidly at higher flow rates and initial sand production was higher at higher flow rates. At high confining stress, arching occurred at a low flow rate of 2 mL/min but not at higher flow rates. As well, sand production increased at higher flow rates. It may be concluded that sand production increases as fluid flow rate is increased. As well, arching of the sand occurs at low and high flow rates under low confining stress and only at low flow rates under high confining stress.

In general, it has been concluded that flow rate has an influence on arch size and stability. Smaller arches are more stable and allow a high fluid viscosity to be reached before failure. As well, gradual rate increases result in stable sand arches while sudden increases cause arch failure. In some cases, arches that were formed were stable in the sense that flow rate could be reduced to zero and increased to its former value several times without affecting the arch stability. It was also possible to hold flow rate constant for several hours without causing significant changes There is a limit to the load imposed by the fluid drag forces that a given arch can sustain. Suggested sand control methods consist of keeping production rates below the critical flow rate. Thus, a certain level of fluid flow rate is capable of destroying an arch. However, arches appear to remain stable below this critical flow rate. As well, fluid flow rate may be manipulated below the critical flow rate without affecting arch stability if sudden increases in flow rate are avoided.

Capillary cohesion has been identified as an important factor with regard to sand arching. It was found that sand grains that would not previously exhibit arching, would do so when capillary cohesion was present in the sand. It was observed that applied loads of up to 13.8 MPa could not induce arching in round sand grains until some type of cohesion was applied to the sand. The cohesion generally took the form of two immiscible fluids in the sand pores. Under stress conditions where arches were unstable in dry or saturated sand, arches were stable if immiscible fluid phases were present and the wetting phase saturation was less than funicular. That is, the wetting phase was not continuous. When the wetting phase saturation did reach a funicular state, arches would fail. A cohesive force, supplied by interfacial tension within the sand structure is necessary for arch stability.

Furthermore, the effects of the flow of the wetting and nonwetting fluids through a sand pack were examined. Flow of the wetting fluid into a partially saturated sand causes sand arch failure by decreasing the nonwetting fluid saturation and thereby decreasing the capillary cohesion present in the sand. Arches remained stable when subjected to flow of the nonwetting fluid. This conclusion agrees with field observations that sand production usually increases when water production increases, which changes fluid saturation distribution around the perforation.

Generally, arches were stable if two immiscible fluids were present in the sand pores. The cohesive strength derived from reservoir fluids is a function of interfacial tension forces and wetting phase saturation. Durrett et al. (1976) measured the cohesive strength of an air-water saturated simulated formation sand and found a peak cohesive strength of 4.8 kPa at 80 percent water saturation. These cohesive strength measurements were used to calculate the cohesive strength of a similar oil-water system having 35 dynes/cm interfacial tension. The maximum cohesive strength was 2.4 kPa at 80 percent water saturation. Even though capillary cohesion strength is generally low, it is significant when compared to fluid drag forces. Examining fluidization and critical transport velocities for typical formation size sand grains led to the conclusion that most formation size grains are transported readily by typical producing rates, unless they are held in place by some force. The strength provided by capillary cohesion in the pores of the sand structure is significant with regard to the formation and stability of sand arches over well casing perforations.

Table 2-1: Results of Hall and Harrisberger (1970) Arching Tests

Test No.	Sand	Step	Initial Saturation	Flow	Load*	Results
1	10-20 Tex. C.Co. loose**		Air	None	0	No arch
2	10-20 Tex. C.Co.		Air	None	0	Arched; failed when tapped
3	10-20 Tex. C.Co.	a.	Air	None	500	Arched
		b.		Air out[◊]	500	Held
		c.		Air out faster	500	Failed
4	10-20 Tex. C.Co.		Air	None	2000	Failed; crushed
5	20-40 Ottawa loose**		Air	None	0	No arch
6	20-40 Ottawa		Air	None	0	No arch
7	20-40 Ottawa	a.	Air	None	500	No arch
8	80-100 Ottawa	b.		Air in[◊◊]	500	Arch formed
	(Same steps)	c.		Air in slower	500	Failed
		d.		Air in faster	500	Reformed
		e.		Same	2000	Held
		f.		Air in slower	2000	Failed
9	20-40 Ottawa		Water-moistened	None	2000	Arched
10	20-40 Ottawa	a.	Kerosene	None	1000	No arch
	Oil-wettable[†]	b.		Air in	1000	Arch formed
		c.		None	1000	Held
11	20-40 Ottawa	a.	Kerosene at residual water	None	1000	Arched
		b.		Kerosene out	1000	Held
		c.		Water out	1000	Failed
12	20-40 Ottawa Oil-wettable[†]	a.	Water at residual mineral oil	None	1000	Arched
		b.		Water out	1000	Held
		c.		Mineral oil out	1000	Failed
13	20-40 Ottawa		Water-moistened	None	3450[††]	Arch held
14	8-12 Tex. C.Co.		Air	None	1950[††]	Failed; crushed suddenly
15	8-12 Tex. C.Co.		Water-moistened	None	2100[††]	Failed; stepwise
16	30-250 Miocene		Air	None	1700[††]	Failed, slow fall-out
17	30-250 Miocene		Water-moistened	None	3450[††]	Failed, no fall-out

*Average vertical stress, psi

**Poured in with no tamping; all other tests were compacted by vibrator

[◊] Flow out define as flow downwards through sand

[◊◊] Flow in defined as flow upwards into sand

[†] Sand treated to be preferentially oil-wettable; all other tests used naturally water-wettable sands

[††] Arch formed at 500 psi; load increased to failure or to apparatus limit of 3450 psi

(after Hall and Harrisberger, 1970)

Table 2-2: Experimental Conditions and Results of Bratli and Risnes (1981)

Experiment Number	Porosity Ø	Water Saturation S_w	Maximum Arch Radius* r_1 (cm)	Maximum Flow Rate q (cm^3/s)	Maximum Upstream Pressure p_u (bar)
Sand: 20-40 U.S. mesh, pore-fluid wetting/flowing: water/air, simulated overburden: 50 bar					
1	0.39	0.15	1.82	2439	1.98
2	0.38	0.19	2.46	2248	1.79
3	0.38	0.14	2.26	2970	2.53
4	0.39	0.15	1.57	2564	2.15
Sand: 80-100 U.S. mesh, pore-fluid wetting/flowing: water/air, simulated overburden: 50 bar					
1	0.42	0.18	2.10	2441	2.34
2	0.41	0.17	1.65	3305	3.16
3	0.42	0.17	2.16	2536	2.26
4	0.41	0.17	1.55	1941	2.33

*Calculated assuming spherical cavity

(after Bratli and Risnes, 1981)

Table 2-3: Summary of Direct Shear Tests on Laboratory Compacted Oil Sand Performed by Golder Associates Ltd.

Test Set	Test No.	Dry Density (kN/m^3)	Porosity (%)	Oil/Water Ratio	Saturation (%)	Normal Stress (kPa)	Shear Stress Peak (kPa)	Shear Stress Constant Volume* (kPa)
First	1	15.3	43	70/30	96	0	4.7	0.3
	2	15.3	43	65/35	96	0	4.3	0.4
	3	15.3	43	67/33	96	5	12.1	4.7
	4	15.3	43	72/28	100	5	11	4.6
	5	15.3	43	63/37	100	10	18	8.5
	6	15.3	43	73/27	100	20	26	19
Second	7	16.0	41	69/31	99	0	4.5	0.5
	8	16.0	41	73/27	100	5	15	4
	9	16.0	41	73/27	100	10	19	8
Third	10	15.3	43	50/50	100	0	2.7	0.5
	11	15.3	43	53/47	100	5	11	4.5
	12	15.3	43	52/48	100	10	17.3	9.2

*Constant volume = residual shear stress

Figure 2-1: Arching Test Cell Used by Hall and Harrisberger (1970)

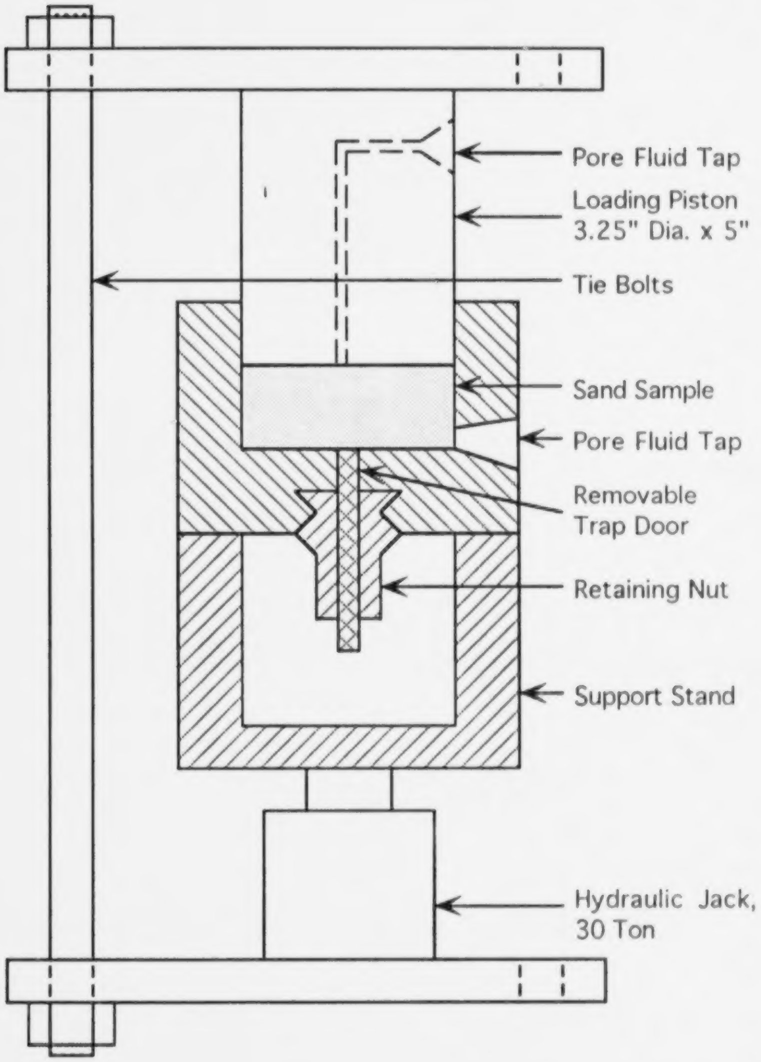
Pore Fluid Tap
Loading Piston
3.25" Dia. x 5"
Tie Bolts
Sand Sample
Pore Fluid Tap
Removable
Trap Door
Retaining Nut
Support Stand
Hydraulic Jack,
30 Ton

(after Hall and Harrisberger, 1970)

Figure 2-2: Coulomb Line of Failure

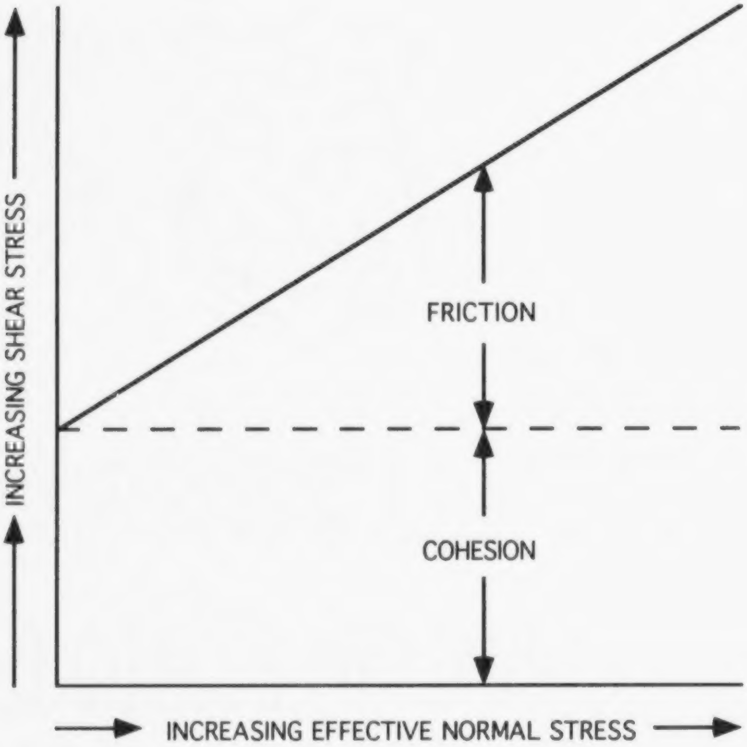
INCREASING SHEAR STRESS
FRICTION
COHESION
INCREASING EFFECTIVE NORMAL STRESS

(after Stein and Hilchie, 1972)

Figure 2-3: Cohesive Strength of Simulated Formation at
Various Levels of Air-Water Saturation
(after Durrett et al., 1976)

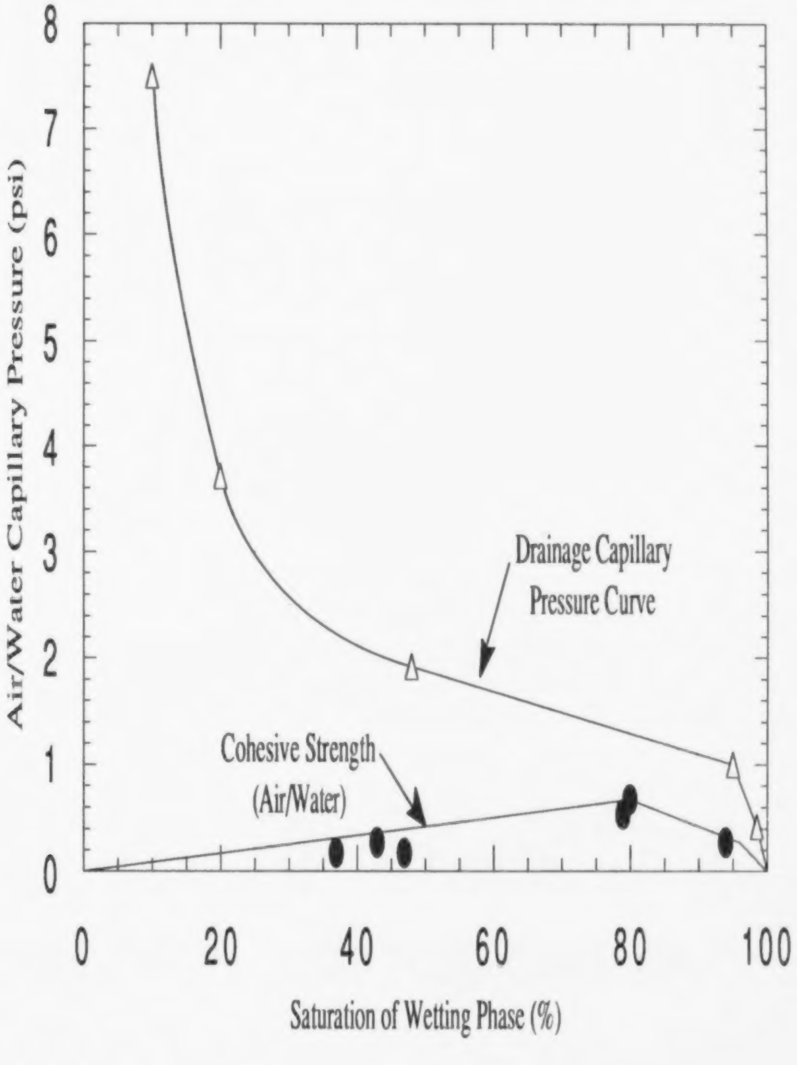

Figure 2-4: Cohesive Strength For Oil-Water System
(after Durrett et al., 1976)

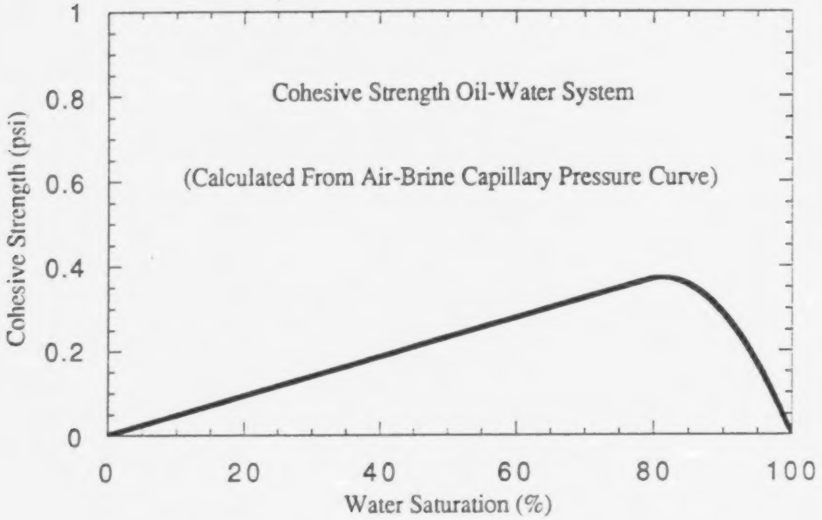

Figure 2-5: Drag Force Acting Through a Clean Sand
versus a Pseudo-Reynolds Number
(after Durrett et al., 1976)

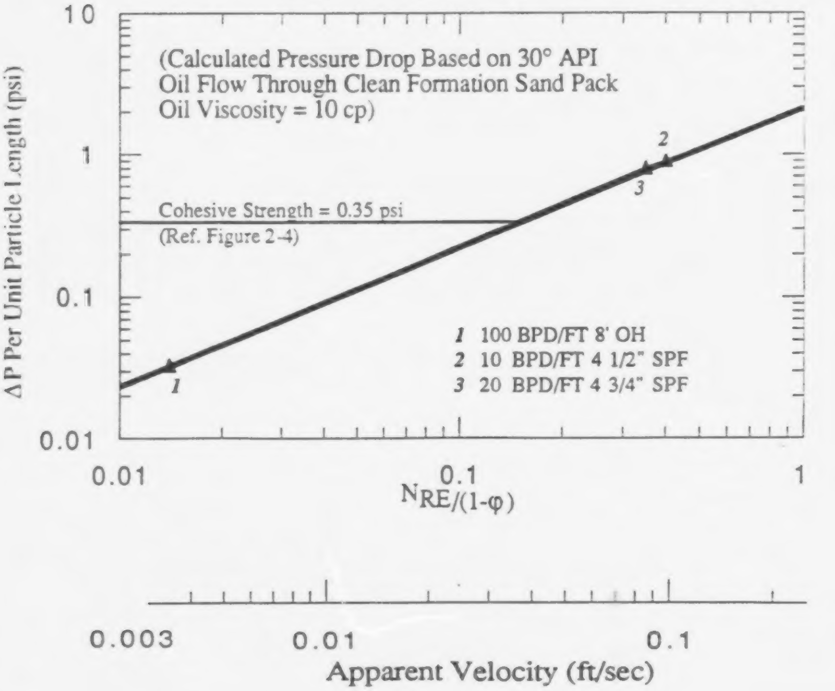

Figure 2-6: Critical Velocity For Fluid Transport (after Durrett et al., 1976)

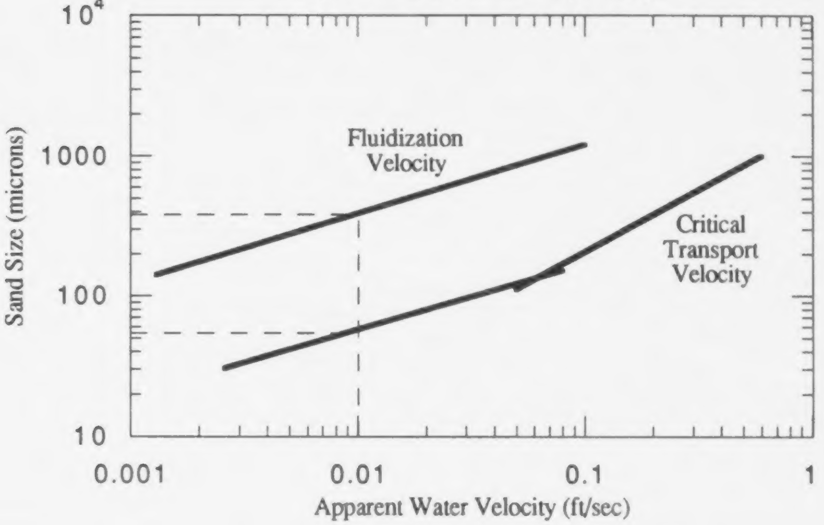

Figure 2-7: Apparent Fluid Velocity at Sand-Gravel Interface (after Durrett et al., 1976)

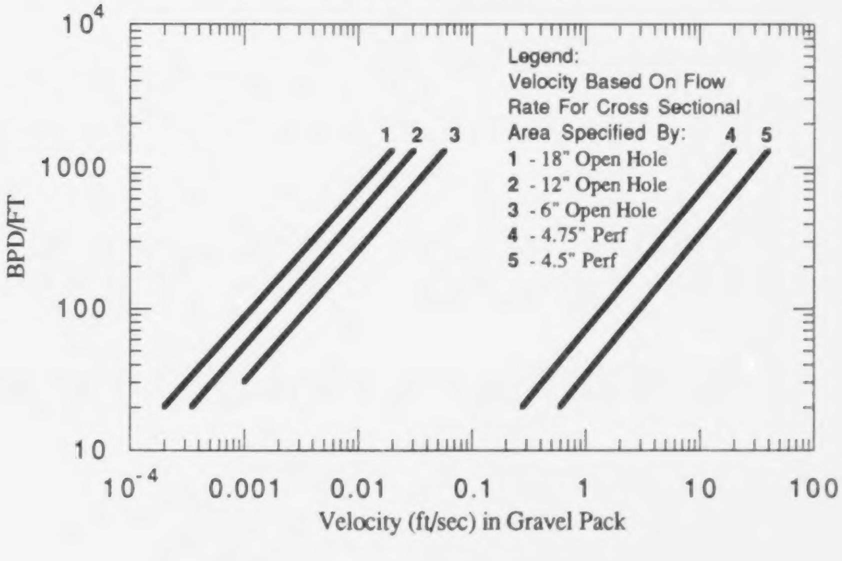

Figure 2-8: Peak and Residual Shear Strength of First Set of Tests by Golder Associates Ltd.

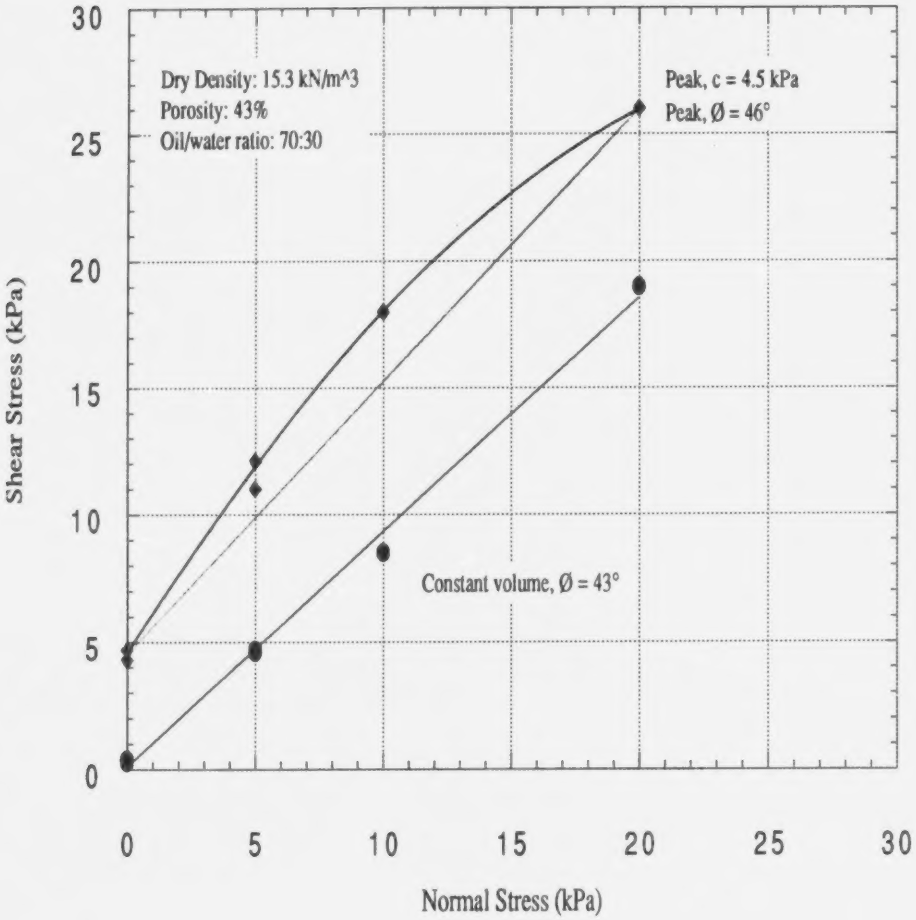

Figure 2-9: Peak and Residual Shear Strength of Second Set of Tests by Golder Associates Ltd.

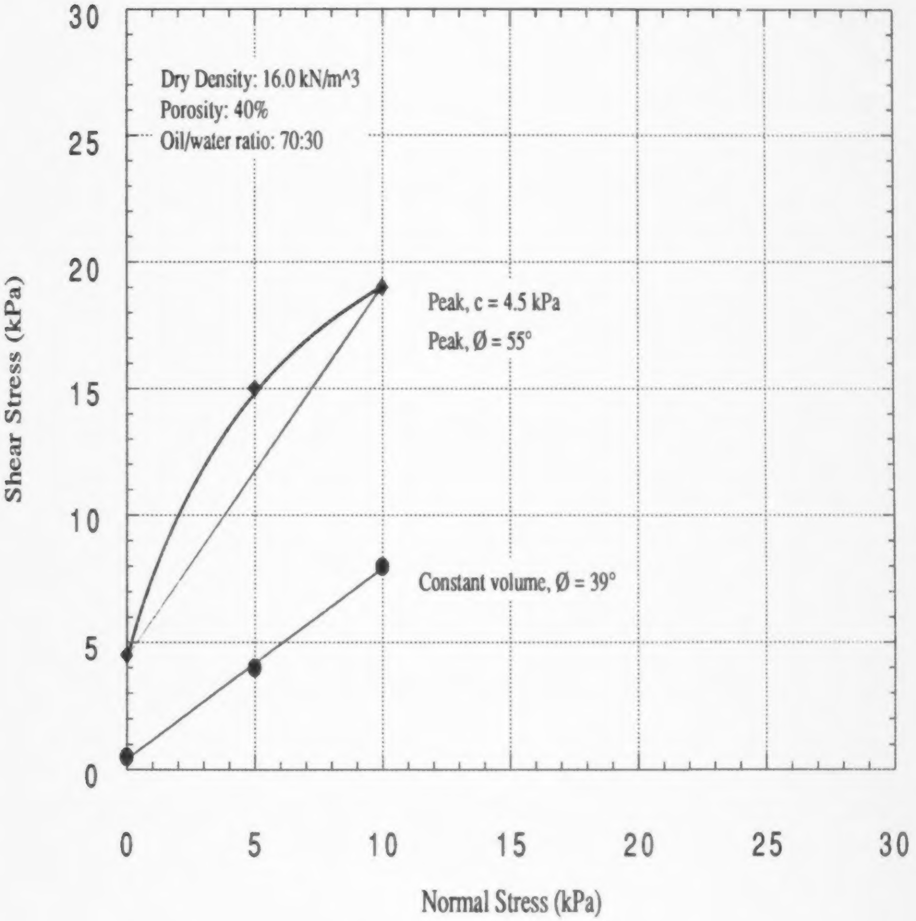

Figure 2-10: Peak and Residual Shear Strength of Third Set of Tests by Golder Associates Ltd.

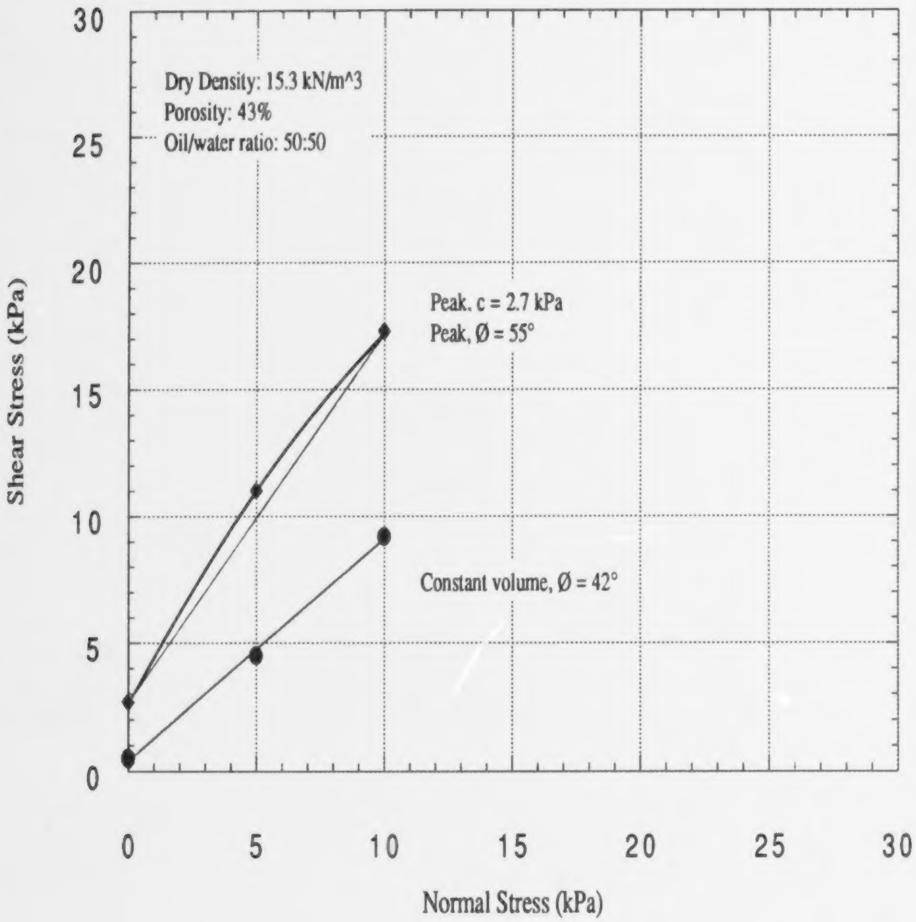

3. Laboratory Testing

3.1 Properties of Sands Used In Testing Program

Three sizes of uniform quartz sand were used in the first part of the testing program. The finest sand was medium to fine grain, clean 40-70 mesh with an average grain size (D_{50}) of 0.30 mm and a coefficient of uniformity (D_{60}/D_{10}) of 1.39. The medium sized sand was coarse grained, clean 12-20 mesh with an average grain size of 1.2 mm and a coefficient of uniformity of 1.36. The largest sand was coarse, clean 8-16 mesh with an average grain size of 1.6 mm and a coefficient of uniformity of 1.40. These three sands will be referred to as fine, medium and coarse sand in the following discussion. The grain size distribution curves for these sands are presented in Figure 3-1. The fine sand is representative of sand found in the heavy oil formations and most of the experimental work used only this sand. The grain size distribution for a typical formation sand is also shown in Figure 3-1 displaying its similarity to the fine sand. The medium and coarse sands were used only to determine the effect of sand particle size on arching behavior. All sands have a particle shape classified as subrounded.

3.1.1 Grain Size Analysis

The purpose of the grain size analyses was to determine the average grain size and the degree of uniformity of the fine, medium and coarse sands. This allowed the fine sand to be compared to the actual formation sand, which it was intended to represent. Grain size analyses were performed on the fine, medium and coarse sands. Dry, 200 gram samples of each sand were accurately weighed and sieved through a set of sieves containing sieve numbers 4, 10, 20, 40, 60, 80, 100, 200 and a pan. The size of opening for each sieve used is provided in Table 3-1. The procedure outlined by ASTM Standard Test Method for

Particle-Size Analysis of Soils (ASTM Designation: D 422-63) was followed when performing the grain size analysis for each sand. Grain size distribution curves were constructed for each sand based on the results of the grain size analysis outlined above. The fine, medium and coarse sands were frac sands composed almost entirely of quartz. The sands had been previously sieved by the distributor and grouped together based on a range of mesh sizes resulting in the highly uniform distribution.

The results of the grain size analysis for each sand is summarized below. The fine sand is a uniform, medium to fine grain, clean 40-70 mesh quartz sand with a range of grain sizes from 0.43 to 0.21 mm. It has a D_{50} of 0.30 mm and a coefficient of uniformity, C_u, equal to 1.39. The D_{50} is the grain diameter corresponding to 50% passing, by weight. The coefficient of uniformity, C_u, is defined as:

$$C_u = \frac{D_{60}}{D_{10}}$$

where: D_{60} = grain diameter (in mm) corresponding to 60% passing, and

D_{10} = grain diameter (in mm) corresponding to 10% passing, by weight.

The medium sand is a uniform, coarse grained, clean 12-20 mesh quartz sand with a range of grain sizes from 1.7 to 0.85 mm. It has a D_{50} of 1.2 mm and a coefficient of uniformity equal to 1.36. The coarse sand is a uniform, coarse, clean 8-16 mesh quartz sand with a range of grain sizes of 2.4 to 1.2 mm. It has a D_{50} of 1.6 mm and a coefficient of uniformity equal to 1.40. Grain size distribution curves, grain size ranges, D_{50} values and coefficient of uniformities for the coarse, medium, and fine sands and a typical formation sand are presented in Figure 3-1. The average grain size of each sand was taken as the D_{50} value obtained from the grain size analysis. The average grain size was used to calculate slot width to grain diameter ratios later in the thesis.

3.1.2 Specific Gravity

In order to have accurate specific gravities for the sands that would be used in the visualization model and capillary cohesion tests, tests to determine the specific gravity of the fine, medium and coarse sands were performed. The procedure used to determine the specific gravity of the sands was the ASTM Standard Test Method for Specific Gravity of Soils (ASTM Designation: D 854-92). The test utilizes a pycnometer to determine the specific gravity of soils. The pycnometer may be either a volumetric flask having a capacity of a least 100 mL or a stoppered bottle having a capacity of at least 50 mL. In determining the specific gravity of the three test sands, a 100 mL volumetric flask was used. The ASTM procedure recommends that the weight of the test sample on an oven-dry basis shall be at least 25 grams when the volumetric flask is used. The weight of the test sample used for each of the three test sands was 60 grams. The ASTM procedure provides two methods for the removal of entrapped air. The first method is to subject the contents to a partial vacuum (air pressure not exceeding 100 mm Hg). The second method is to boil gently for at least 10 minutes while occasionally rolling the pycnometer to assist in the removal of air. The contents are then subjected to reduced air pressure by connecting the pycnometer directly to a vacuum pump. In determining the specific gravity of the three test sands, the boiling method was used to remove entrapped air. For a detailed description of the specific gravity testing method, please refer to the ASTM standard listed above.

In accordance with the ASTM Standard Test Method for Specific Gravity of Soils (ASTM Designation: D 854-92), the specific gravity of the test sands was calculated, based on water at a temperature T_x, as follows:

$$G_s = \frac{W_o}{W_o + W_a - W_b}$$

where: G_s = specific gravity of soil particles

W_o = weight of sample of oven-dry soil, g,

W_a = weight of pycnometer filled with water at temperature T_x, g,

W_b = weight of pycnometer filled with water and soil at temperature T_x, g, and

T_x = temperature of the contents of the pycnometer when weight W_b was determined, °C.

Two tests to determine specific gravity were performed for each sand. The average of the specific gravity tests for each respective sand were taken as the specific gravity for that sand in all future calculations. The fine, medium and coarse sands had specific gravities of 2.72, 2.71 and 2.71, respectively. The results of these tests are summarized in Table 3-2. Specific gravities were used in calculations to determine void ratio and dry density of the sand during visualization model and capillary cohesion tests.

3.1.3 Maximum and Minimum Dry Density

In order to have an accurate range of dry densities for the sand that would be used in the visualization model and capillary cohesion tests, maximum and minimum dry density tests were performed on the fine, medium and coarse sands. The procedure used to determine the maximum dry density of the test sands was the ASTM Standard Test Method for Maximum Index Density of Soils Using a Vibratory Table (ASTM Designation: D 4253-93). The ASTM test method provides four alternative procedures to determine the maximum index density. It was decided that Method 1A, using oven-dried soil and an electromagnetic, vertically vibrating table, would be utilized. A detailed description of terms, apparatus, procedure and calculations associated with the maximum dry density test may be found in the ASTM standard referred to above. All tests were vibrated for 8 minutes at a frequency of 60 hertz. Two maximum density tests were performed on the coarse sand and three maximum density tests were performed on the medium and fine sand. Test results proved to be very similar and the results of the tests were averaged together to determine a maximum dry density value for each sand.

The maximum dry density was calculated in accordance with the ASTM Standard Test Method for Maximum Index Density of Soils Using a Vibratory Table (ASTM Designation: D 4253-93), as follows:

$$\rho_{dmax} = \frac{M_s}{V}$$

where: ρ_{dmax} = maximum dry density, kg/m^3,

M_s = mass of dry specimen, kg, and

V = volume of densified specimen, m^3.

The fine, medium and coarse sands had maximum dry densities of 1.80, 1.84 and 1.76 g/cm^3, respectively. The results of the maximum dry density tests are summarized in Table 3-3. It should be noted that at the completion of the tests using the fine sand, small amounts of fine sand were observed on the top plate of the maximum dry density apparatus. It was decided that the presence of this material did not significantly affect the results obtained for the fine sand. All maximum dry density tests performed met the criteria for judging the acceptability of maximum dry density test results set out in the ASTM standard listed above. The average of the maximum dry density tests for each respective sand was taken as the maximum dry density for that sand in all future calculations.

The procedure used to determine the minimum dry density of the test sands was the ASTM Standard Test Method for Minimum Index Density of Soils and Calculation of Relative Density (ASTM Designation: D 4254-91). The ASTM method provides three alternative procedures to determine the minimum index density. Method A which utilizes a funnel pouring device or a hand scoop to place material in a mold was used for all three test sands. A detailed description of terms, apparatus, procedure and calculations associated with the minimum dry density test may be found in the ASTM standard referred to above.

Two minimum dry density tests were performed on each sand. The minimum dry density was calculated in accordance with ASTM Standard Test Method for Minimum

Index Density of Soils and Calculation of Relative Density (ASTM Designation: D 4254-91) as follows:

$$\rho_{dmin} = \frac{M_S}{V}$$

where: ρ_{dmin} = minimum dry density, kg/m^3,

M_S = mass of dry soil, kg, and

V = volume of soil, m^3.

The fine, medium and coarse sands had minimum dry densities of 1.56, 1.62 and 1.56 g/cm^3, respectively. Results of the minimum dry density tests are summarized in Table 3-4. All minimum dry density tests performed met the criteria for judging the acceptability of minimum dry density test results set out in the ASTM standard listed above. The average of the minimum dry density tests for each respective sand was taken as the minimum dry density for that sand in all future calculations. The maximum and minimum dry densities were used in calculations to determine relative density of the sand during the visualization model and capillary cohesion tests.

3.1.4 Hydraulic Conductivity

The purpose of the hydraulic conductivity tests was to determine the hydraulic conductivity of the fine, medium and coarse sands in order to estimate flow rates and head loss in the visualization model. As well, the hydraulic conductivity tests provided an opportunity to evaluate water flow through the sands. The hydraulic conductivity of the fine, medium and coarse sands was determined using the ASTM Standard Test Method for Permeability of Granular Soils (Constant Head) (ASTM Designation: D 2434-68). The apparatus, sample preparations, procedure and calculations associated with the hydraulic conductivity test of granular soils using a constant head is detailed in the ASTM standard listed above. Each test sand was tested using water as the test fluid under hydraulic gradients of approximately 1.0, 2.0, 3.0 and 4.0. Hydraulic gradient is defined as the head loss due to liquid flowing through the soil divided by the length of the soil. Manometer readings from the manometer ports located at the highest and lowest points within the sand were used to determine the hydraulic conductivity of each sand. These manometer readings were used in order to reduce the effects of fines movement at the top and bottom of the sand inside the permeameter. During the hydraulic conductivity tests, the top of the sand becomes less permeable as fines form a blinding layer and the bottom of the sand becomes more permeable as fines move out of the sand forming a filter layer. The use of overall head measurements does not exclude the influence of these effects as reliably as using the manometers located in the sand mass referred to above. The results from these tests were used to determine the hydraulic conductivity of each soil by constructing a plot of hydraulic gradient versus velocity for each sand. The fine, medium and coarse sands were found to have permeabilities of 0.045, 0.30 and 0.89 cm/sec, respectively. The hydraulic gradients of each soil and the plot mentioned above are presented in Figure 3-2. The permeabilities derived from these tests were used to determine the equivalent sand permeabilities to air flow. These air permeabilities were used in calculations regarding upward air flow through the fine and medium sands.

3.1.5 Dry Sand Direct Shear Tests

Direct shear tests were performed to evaluate the peak and residual angles of internal friction for each sand under dry conditions. The fine, medium and coarse sands could then be compared with similar sands used in other research projects. The ASTM Standard Test Method for Direct Shear Test of Soil Under Consolidated Drained Conditions (ASTM Designation: D 3080-90) was performed on each soil under normal stresses of 50, 150 and 250 kPa. A square shear box with side dimensions of 60 mm and a sand thickness of 40 mm was used and sheared at a height of 26 mm. All tests were conducted using dry, compacted sand. Sand was placed in the shear box in four lifts of approximately 10 mm and compacted until the desired density was achieved. Controlled-displacement tests were performed in order to determine the ultimate stress as well as the maximum stress. Samples were tested under single shear conditions. The fine, medium and coarse sand were all sheared at a rate of 0.61 mm/min.

The dry density of the fine sand under normal stresses of 50, 150 and 250 kPa were 1.70, 1.72 and 1.75 g/cm^3, respectively. These dry densities correspond to relative densities of 62, 70 and 81%, respectively. The dry density of the medium sand under normal stresses of 50, 150 and 250 kPa were 1.76, 1.76 and 1.77 g/cm^3, respectively. These dry densities correspond to relative densities of 67, 67 and 71%, respectively. The dry density of the coarse sand under normal stresses of 50, 150 and 250 kPa were 1.68, 1.67 and 1.70 g/cm^3, respectively. These dry densities correspond to relative densities of 63, 58 and 72%, respectively.

The peak and residual angles of friction of the fine sand (void ratio, $e = 0.58$) were found to be 35° and 33°, respectively. The peak and residual angles of friction of the medium sand ($e = 0.53$) were determined to be 45° and 34°, respectively. Finally, the peak and residual angles of friction of the coarse sand ($e = 0.61$) were found to be 50° and 42°, respectively. A plot of peak shear stress versus normal stress and residual shear stress versus normal stress for the fine, medium and coarse sands are presented in Figures 3-3 and 3-4, respectively. Porosities in the range of 35% to 38% were used in the dry sand direct shear tests. This range of porosities was used as it reflects actual field porosity conditions fairly well. Plots of shear stress versus shear displacement and specimen thickness change versus shear displacement for the fine, medium and coarse sands are presented in Appendix A.

Triaxial tests performed by Hall and Harrisberger (1970) on 20-40 mesh ($e = 0.53$) and 80-100 mesh ($e = 0.58$) Ottawa sand resulted in internal angles of friction on 34° and 36°, respectively. These tests were performed at confining stresses up to 550 kPa. Tippie and Kohlhaas (1973) obtained an angle of internal friction of 30° for a 20-40 mesh Gopher State frac sand (e = 0.44) using triaxial tests at confining stresses up to 550 kPa. Bratli and Risnes (1981) used triaxial tests to obtain friction angles of 38° for a 20-40 mesh Ottawa sand (e = 0.61) and 36° for a 80-100 mesh crushed quartz sand (e = 0.69). As there are no sands fitting the exact mesh sizes used in this project, it is necessary to qualitatively compare sands with as similar mesh sizes as possible.

When comparing the internal angles of friction of the various sands, it is important to note the effect of initial void ratio on friction angle. The relationship between friction angle and the initial void ratio for a given sand is that denser sand will result in higher friction angles. Energy put into a soil by external loads is expended in two ways: (1) overcoming the frictional resistance between particles and (2) to expand the soil against the confining stress. The denser the sand, the greater the expansion which takes place during shear. More energy (hence more force and a higher friction angle) must be expended to shear the soil (Lambe and Whitman, 1969).

To summarize, the friction angles of 80-100 mesh sands were found to be 36° by other researchers cited above, while the fine sand (40-70 mesh) used in this project had a peak friction angle of 35°. The fine sand friction angle agrees well with published friction angles of similar sands and the void ratios are sufficiently similar to allow a reasonable comparison between the sands. The 20-40 mesh sands had friction angles in the range of 30° to 38° as determined by other researchers. The 20-40 mesh sands show an opposite trend of increasing friction angle with increasing void ratio (decreasing density). Differences in the gradation of the sands may account for this trend reversal. That is, well graded sands would have higher friction angles than more uniform sands. The medium sand (12-20 mesh) used in this project had a peak friction angle of 45° and the coarse sand (8-16 mesh) had a peak friction angle of 50°. The friction angles of the medium and coarse sands appear to be slightly higher than expected. The coarse and medium sands had dilation angles of 52° and 43°, respectively, compared to the fine sand which had a dilation angle of 23°. The higher dilation angles indicate that extra work must be done in order to shear the coarser sands. This results in greater strength of the sands which is reflected in the increasing friction angles for increasingly coarser sands. Reasons for this variation are the influence of void ratio, angularity and surface roughness.

The fine sand required only 1.0 mm to 3.0 mm to reach peak shear stress. The medium and coarse sands reached peak shear stress with horizontal displacements in the range of 1.0 mm to 2.0 mm. In all cases, only a small degree of horizontal displacement was required to reach peak shear stress. Thus, relatively small amounts of sand movement will generate peak shear stresses within the sand inside the visualization model.

The specimen thickness change versus horizontal displacement plots for the fine, medium and coarse sand all indicate dilation during shearing. The dilation characteristic of these sands may assist in the formation of arches. This is because the sand grains must ride up and over each other during shearing providing an opportunity for arches to form during this increase in volume due to sand grain movement. It should also be noted that the volume change behavior and stress-deformation behavior of the fine, medium and coarse sands presented in Appendix A may also be of use as input data for future numerical modeling.

3.1.6 Wall Friction Direct Shear Tests

Initial test results using the second visualization model and dry sand with a confining stress applied suggested that because of friction between the sand and the walls of the box, a large portion of the confining stress applied to the sand was lost in the form of wall friction. To determine the amount of confining stress converted to wall friction, direct shear tests were performed on each of the test sands and a smooth piece of plexiglass to determine the angle of wall friction between the test sands and a sheet of plexiglass. These tests provided the degree of wall friction generated by the test sands against the walls of the visualization model. The ASTM Standard Test Method for Direct Shear Test of Soil Under Consolidated Drained Conditions (ASTM Designation: D 3080-90) was performed using the interface between the plexiglass and the sand as the shear plane. Similar to the direct shear tests performed to investigate the peak and residual angles of friction of the tests sands, the direct shear tests performed using plexiglass were conducted using dry, compacted sand in a square shear box with side dimensions of 60 mm. Plexiglass was placed in the bottom shear box so that the plexiglass was flush with the top of the bottom shear box. The sand was placed in the shear box on top of the plexiglass to an average sand thickness of 18 mm. Each sand tested with plexiglass was tested at five different normal stresses (50, 100, 150, 200 and 250 kPa). Controlled-displacement tests were conducted using the interface between the plexiglass and the sand as the shear plane.

The fine sand was sheared at a rate of 1.22 mm/min during tests under normal stresses of 50 and 100 kPa. All other tests were sheared at a rate of 0.61 mm/min. The dry densities of the fine sand under normal stresses of 50, 100, 150, 200 and 250 kPa were 1.56, 1.60, 1.57, 1.61 and 1.64 g/cm^3. These dry densities correspond to relative densities of 0, 19, 5, 23 and 37%, respectively.

The medium sand was sheared at a rate of 1.22 mm/min during tests under normal stresses of 100 and 200 kPa. A shear rate of 0.61 mm/min was used for tests under normal stresses of 150 and 250 kPa. Tests were performed under 50 kPa normal stress at both 1.22 mm/min and 0.61 mm/min. Calculations to determine dry density of the medium sand resulted in dry density values less than the minimum dry density. It was assumed that the density of the medium sand in the direct shear tests was miscalculated and a dry density of 1.62 g/cm^3 was assumed for all tests. This dry density corresponds to a relative density of 0%.

The coarse sand was sheared at a rate of 1.22 mm/min during tests under normal stresses of 50 and 200 kPa. All other tests were sheared at a rate of 0.61 mm/min. Similar to tests using medium sand, calculations to determine dry density of the coarse sand resulted in dry density values less than the minimum dry density. It was assumed that the density of the coarse sand in the direct shear tests was miscalculated and a dry density of 1.62 g/cm^3 was assumed for all tests. This dry density corresponds to a relative density of 0%.

The peak and residual angles of wall friction between the fine sand and plexiglass were found to be 21° and 19°, respectively. The peak and residual angles of wall friction between the medium sand and plexiglass were found to be 23° and 20°, respectively. Finally, the peak and residual angles of wall friction between the coarse sand and plexiglass were found to be 30° and 28°, respectively. A plot of peak shear stress versus normal stress and residual shear stress versus normal stress for the fine, medium and coarse sands and plexiglass are presented in Figures 3-5 and 3-6, respectively. Porosities resulting in relative densities in a very low range were used during the wall friction direct shear tests because this would result in measurement of the lowest friction created by the sand grains against the plexiglass walls. Thus, if this minimum friction proved to cause an unacceptable amount of friction, then all other cases would also prove unacceptable. Plots of shear stress versus shear displacement and specimen thickness change versus shear displacement for the fine, medium and coarse sand and plexiglass are presented in Appendix A.

At a confining stress of 300 kPa and using the peak angles of wall friction, the wall friction between the walls of the visualization model and the fine, medium and coarse sands was 115, 127 and 173 kPa, respectively. The resulting percent of confining stress lost in the form of wall friction was 38, 42 and 58%, respectively. These relatively high values of wall friction confirmed the hypothesis that the second visualization model design was not providing sufficient stress to the sand immediately above the slot perforation area because of friction between the sand and the walls of the box. This conclusion led to the modification in the design of the visualization model which removed the effects of wall friction. The design modifications are discussed in detail in Section 3.2.3 Third Visualization Model Design.

The fine sand/plexiglass and medium sand/plexiglass samples required only small displacements, 0.1 mm to 0.5 mm, to reach peak shear stress. This indicates that the full effects of wall friction would be felt with only a small amount of sand movement. The coarse sand/plexiglass samples reach peak shear stress at horizontal displacements of 0.2 mm to 2 mm. However, the shear stress rises rapidly with only small horizontal displacements. Thus, the majority of wall friction would be present with only small sand movements.

The specimen thickness change versus horizontal displacement plots for the fine sand/plexiglass and medium sand/plexiglass samples show contraction throughout the direct shear test. This is reasonable considering the low relative densities of the samples. The coarse sand/plexiglass samples contracted slightly at first and then proceeded to dilate. This behavior is typical of a dense sand and is surprising because the coarse sand was initially at relatively low relative densities. The application of the confining stress must have caused the coarse sand to compress to a dense state.

3.2 Design of Visualization Model

The purpose of the visualization model was to qualitatively and quantitatively evaluate sand movement at a perforation. To achieve this goal, plexiglass was used to fabricate the visualization model. Plexiglass was chosen because it is transparent, machinable and reasonably safe with regard to breakage. It was also important that the visualization model be a two dimensional model, so that the mechanisms of sand movement could be clearly seen. The visualization model design incorporated a single perforation in the shape of a rectangular slot. The perforation built into the visualization model will be referred to as a slot perforation in the following discussion. The visualization model was designed to allow the effect of the following variables to be examined: sand particle size and perforation size, shape and roughness of perforation opening, sand porosity, confining stress, flow conditions through sand and perforations and capillary cohesion between two fluids in a sand such as gas and water, gas and oil, and oil and water. The original design of the visualization model was modified twice during work on this project. These modifications resulted in three different visualization model designs. Each visualization model design will be explained in detail in the following sections.

3.2.1 First Visualization Model Design

The purpose of the first visualization model design was to examine the effect of the boundary conditions on the visualization model concept and give direction towards designing a more refined visualization model. The first visualization model consisted of a long plexiglass box with a slot perforation and removable plug permanently attached to one end of the box and a fluid injection system connected to the other end. The end of the plexiglass box containing the fluid injection system was removable to allow for the placement of sand inside the visualization model. The sides of the slot perforation were roughened to simulate conditions of completed perforations found in the field. The visualization model was used in both horizontal and vertical orientations. However, since most of the tests performed using the visualization model were performed in the vertical orientation, the thickness, width and height of the model were designated with respect to a vertical orientation. The inside dimensions of the first visualization model are presented in Figure 3-7 and are used consistently when describing the visualization model dimensions regardless of orientation. This dimension reference system applies to the second and third visualization model designs as well. The inside dimensions of the first visualization model were 24 mm thick by 150 mm wide by 700 mm high. The plexiglass was 10 mm thick. This model was designed for use in a horizontal or vertical orientation. A slot perforation 5 mm wide and 10 mm high was initially used with the first visualization model. The slot perforation had the same thickness, 24 mm, as the inside of the visualization model. The slot perforation width of 5 mm was chosen in order to examine grain diameter to width of opening ratios in a range of approximately 1:20 to 1:3. The fine, medium and coarse sands tested using the first visualization model design resulted in grain diameter to width of opening ratios of 1:16.7, 1:4.2 and 1:3.1, respectively. The slot perforation height was later increased to 50 mm to examine the effect of slot perforation height on sand behavior. The test results obtained from the first visualization model resulted in the fabrication of a smaller model which would be used in a vertical orientation only.

3.2.2 Second Visualization Model Design

The purpose of the second visualization model design was to construct a more refined and adapted visualization model based on the knowledge and experience gained from the first visualization model. The second visualization model was approximately half the length of the first visualization model. The model included a plexiglass box with inside dimensions of 20 mm thick by 150 mm wide by 300 mm high. The plexiglass was 12.7 mm thick. An aluminum plate which included attachments for fluid flow, an air vent and a bushing for a piston rod was attached to the top of the plexiglass box by four screws. The aluminum plate will be referred to as the top plate in the following sections. The bottom of the box contained two 50 mm high polyvinyl chloride (PVC) blocks which were rigidly fastened inside the box. The PVC blocks were 50 mm high in order to model the length of actual field perforations through casing and cement which are typically 50 mm to 90 mm long. Different size PVC blocks could be fastened inside the box to allow slot perforation widths of 5.0 mm, 12.7 mm (1/2 inch) and 19.1 mm (3/4 inch) to be tested. The 5 mm wide slot perforation was chosen in order to repeat and check the results obtained using the first visualization model. The 12.7 mm and 19.1 mm wide slot perforations were chosen because these are the sizes most commonly used in the field. The slot perforation had the same thickness, 20 mm, as the inside of the visualization model. In the following sections, the PVC blocks described above will be referred to as the slot perforation blocks. The sides of the slot perforation blocks were roughened to simulate conditions of completed perforations found in the field. A removable PVC plug was inserted between the blocks.

The plexiglass box rested on an aluminum stand which had a hole in the center to allow plug removal and sand flow out of the model. The confining stress loading system consisted of a teflon sweeper, piston plate, piston rod, guide plates and a loading platform. The teflon sweeper rested on top of the sand and prevented sand from binding the piston plate against the sides of the plexiglass box. The piston plate was perforated to allow fluid to flow through unhindered. Dead weights were used to supply the necessary confining stress on the sand. Test results suggested that this design may not provide sufficient stress to the sand immediately above the slot perforation area because of friction between the sand and the walls of the box. Direct shear tests using sand-plexiglass interfaces confirmed this hypothesis.

3.2.3 Third Visualization Model Design

The purpose of the third visualization model design was to modify the previous design in order to ensure that the stress was applied to the sand at the slot perforation opening. The design is essentially the same as the second visualization model with one exception. The slot perforation blocks were 120 mm high and were not fastened to the plexiglass box. Instead, the plexiglass box was allowed to slide smoothly over the slot perforation blocks. The slot perforation blocks were 120 mm high because initially the plexiglass box would be placed on 70 mm high blocks, resulting in an initial slot height of 50 mm which is similar to typical field perforation lengths through casing and cement of 50 mm to 90 mm. Thus, the plexiglass box had a maximum travel of 70 mm before the effects of wall friction would be present. Geotextile sweepers were fixed to the top of the slot perforation blocks to ensure smooth sliding of the plexiglass box. The geotextile sweepers also imitate the roughness of the cement-sand interface around the well casing. This design eliminated the problem of stress transfer from the sand to the plexiglass box. Since the plexiglass box was free to slide over the slot perforation blocks, stress transferred by the sand under the piston to the plexiglass box was returned to the sand above the PVC slot perforation blocks as the plexiglass box slid down. One further modification was made to the second visualization model design. The teflon sweeper was replaced by a three layer sweeper system. Attached to the piston plate was a geotextile, a geonet and finally another geotextile. All three of these materials were cut to fit exactly inside the plexiglass box. This three layer sweeper system prevented sand from binding the piston plate against the sides of the plexiglass box, as well as allowing fluid to easily flow through the sweeper system without disturbing the sand below. At the same time, the three layer sweeper system permitted fluid flow to be redistributed across the entire cross section of the visualization model due to the high in-plane permeability characteristics of the sweeper system materials. Eventually, four manometer ports were installed into the back face of the third visualization model. The manometer ports were located directly over the slot perforation at a spacing of 0, 2.5, 8 and 16 cm above the top of the slot perforation. A drawing of the third visualization model is presented in Figure 3-8. A picture of the third visualization model is presented in Plate 3-1. A side view of the third visualization model which provides a view of the manometer ports and model thickness is provided in Plate 3-2. The overall setup of the visualization model is presented in Plate 3-3.

3.3 Laboratory Procedures

The laboratory procedures followed during tests using the different visualization models and other related tests are described below. Laboratory procedures are separated into sections with respect to conditions imposed on the sand.

3.3.1 Dry Sand Without Confining Stress Applied

Tests involving dry sand without confining stress applied were performed using the first visualization model and the second visualization model. The purpose of these tests was to examine the effect of the following variables: sand particle size and perforation diameter and shape and roughness of perforation opening. The laboratory procedure followed using each model design will be described below.

3.3.1.1 First Visualization Model

Tests on dry sand without confining stress applied using the first visualization model were performed in a vertical orientation. The bottom of the visualization model was placed on two blocks of wood to allow removal of the plug from the slot perforation and unobstructed sand flow out of the model. Two sets of clamps attached to a vertical stand were used to secure the visualization model in a vertical position. A level was used to confirm that the model remained vertical throughout the test.

A cork plug was inserted into the slot perforation and sealed with a thin film of silicon grease to allow easy and quick removal. At no time during testing did the presence of the silicon grease cause problems regarding sand movement into, through and out of the slot perforation. The sand to be tested was poured into the visualization model with a small plastic scoop. After the addition of each scoop of sand, each side of the plexiglass box was vigorously tapped five times with a rubber hammer. Sand was placed into the model using this method until the sand reached a height of 66 cm above the top of the slot perforation. The mass and height of sand inside the visualization model was measured and used to calculate void ratio, dry density and relative density of the sand.

During tests using dry sand without confining stress applied, the top end of the plexiglass box containing the fluid injection system remained open to the atmosphere. Before the test was begun, a video recorder was set up to record the events of the test for later review. This was felt to be an important part of the observational procedure because of the high visual emphasis of these types of tests. The practice of using a video recorder to record the events of a test was continued for all subsequent visualization model tests.

In order to start the test, the plug was removed from the slot perforation in one quick movement. When the plug had been removed, observations were made regarding behavior of the sand. If the sand flowed continuously out of the model, observations were made concerning sand flow pattern and elapsed time of sand flow. If the sand did not continuously flow out of the model, observations were made regarding arching, bridging, the presence of sand blockages in the slot perforation, arch size and shape, arch stability and sand flow pattern. If the sand formed an arch or bridge across the slot perforation, the model was left undisturbed for a reasonable amount of time to assess the stability of the sand arch. If the arch remained stable, the model would be tapped with a rubber hammer to determine the arch's stability when subjected to a vibration. At the completion of a test, all remaining sand would be removed and the visualization model would be washed to clean off any residual sand in the model and thoroughly dried . When performing tests using dry sand, it was essential that the visualization model be completely dry. The presence of water inside the model could lead to capillary forces affecting the behavior of the sand. Dryness of the model was assured by passing air through the model followed by extensive drying of the model using water absorbent towels.

3.3.1.2 Second Visualization Model

As was the case with the first visualization model, it was essential that the second visualization model be completely dry when performing tests using dry sand. It was possible to disassemble all components of the second visualization model and completely dry each component using water absorbent towels after washing the model.

The procedure for running a test using dry sand without confining stress began with the assembly of the visualization model. The appropriate slot perforation blocks were fastened inside the plexiglass box to form a slot perforation of the desired width. Before the plug was put into the slot perforation, a thin film of silicon grease was applied to the sides of the plug to ensure easy removal. The model was placed on an aluminum stand with a hole in the center large enough to allow plug removal and unobstructed sand flow. The test sand was placed into the model with a small plastic scoop. After the addition of each scoop of sand, the sand was rodded 25 times with a 10 mm metal rod and vigorously tapped five times with a rubber hammer on each side of the model. Sand was placed into the model in this manner until the sand reached a height of approximately 20 cm. The mass and height of sand above the top of the slot perforation was measured and used to calculate void ratio, dry density and relative density of the sand in the model. The top of the second visualization model was left open to the atmosphere during these tests. Before the test was begun, a video recorder was set up to record the events of the test for later review.

To start the test, the plug was removed from the slot perforation by applying a sharp pull on a string attached to the plug. After the plug was removed, the same observations and procedure, depending on sand flow or nonflow, that was described in the previous section regarding the first visualization model, was performed for tests using the second visualization model and will not be repeated here.

3.3.2 Dry Sand With Confining Stress Applied

The purpose of these tests was to examine the effect of confining stress. Tests involving dry sand with confining stress applied were performed using only the third visualization model. Initially, the second visualization model design was used in tests of dry sand with confining stress applied. However, the second visualization model design required modifications because it was not providing sufficient stress to the sand immediately above the slot perforation due to high frictional forces between the sand and the walls of the plexiglass box. Thus, the design was modified, resulting in the third visualization model design which corrected this problem.

As was the case with the tests using dry sand without confining stress applied, it was essential that the model be completely dry when performing tests using dry sand with a confining stress applied. It was possible to disassemble all components of the third visualization model and completely dry each component using water absorbent towels after washing the model.

Tests of dry sand with a confining stress applied were only performed with the model in a vertical orientation. After the visualization model was thoroughly dried, the plexiglass components of the model were assembled. Appropriate slot perforation blocks were fastened to an aluminum stand. The slot perforation formed by the slot perforation blocks was centered over a hole in the aluminum stand large enough to allow plug removal and unobstructed sand flow. Three different sets of slot perforation blocks were available to allow slot widths of 5 mm, 12.7 mm (1/2 inch) and 19.1 mm (3/4 inch) to be used. The sides of the plug were coated with a thin film of silicon grease to ensure easy removal. The plug was then inserted into the slot perforation. The assembled plexiglass box was placed over the two slot perforation blocks. After the plexiglass box was in place over the slot perforation blocks, it was slid up and down to assure unrestricted vertical movement. The sides of the plexiglass box were rested on two supports 70 mm in height. In this configuration, the initial slot height was 50 mm. The initial slot perforation height of 50 mm is typical of field perforations lengths ranging from 50 mm to 90 mm. During the test, slot height would increase as sand flowed out through the slot perforation and the plexiglass box moved down over the slot perforation blocks.

Calculations of desired relative density were used to determine required sand masses to be placed into the model. Sand was placed in four lifts of 5 cm in height. A 1.5 cm by 15 cm tamping plate was used to compact the sand to the desired density. The mass of sand placed in the model was recorded and the height of sand inside the model was measured in order to calculate actual density before the test was begun. Void ratio, dry density and relative density of the sand in the model was also calculated.

At this time, the visualization model was positioned directly under the piston in the loading frame. The piston was lowered into the visualization model until it came into contact with the sand, then slid up and down to assure unrestricted vertical movement during the test. The piston was rested on top of the sand and the top plate was fastened to the top of the visualization model. The openings in the top plate were left open to the atmosphere during these tests. A small coating of silicon grease was applied to the piston rod, the bushing in the top plate and the vertical alignment openings in the guide plates to ensure smooth movement of the piston.

The appropriate dead weights for the confining stress desired were placed on the loading plate. Once the dead weights were in place, the supports originally holding the visualization model in place were removed. The plexiglass box was now free to slide down the slot perforation blocks if sand flowed out through the slot perforation. The height of the sand was measured again and a level was used to check that both the visualization model and the loading frame were level. Before the test was begun, a video recorder was set up to record the events of the test for later review.

To start the test, the plug was removed from the slot perforation by applying a sharp pull on a string attached to the plug. When the plug had been removed, observations were made regarding behavior of the test sand. If the sand flowed continuously out of the model, observations were made of sand flow pattern and elapsed time of sand flow. If the sand did not continuously flow out of the model, observations regarding arching, bridging, the presence of sand blockages in the slot perforation, arch size and shape, arch stability and sand flow pattern were made. If the test sand formed an arch or bridge across the slot perforation, the model was left undisturbed for a reasonable amount of time to assess the stability of the sand arch. If the arch remained stable, the model would be tapped with a rubber hammer to determine the arch's stability when subjected to a vibration. Stable sand arches were also subjected to increased confining stresses up to a maximum of 300 kPa in order to observe the effect of increased confining stress on the stability of the sand arch. At the completion of a test, all sand would be removed from the model. The model was washed and carefully dried to remove all remaining moisture.

3.3.3 Fully Water Saturated Flow Tests

Tests involving water flow through fully water saturated sand were performed using the first and third visualization model designs. Tests using the first visualization model were performed in the horizontal and vertical orientations. Tests using the third visualization model were performed in the vertical orientation only. The purpose of the tests performed using the first visualization model was to examine the effect of the boundary conditions of the visualization model concept in both the vertical and horizontal orientations, as well as to provide direction for later tests. The purpose of the tests performed using the third visualization model was to examine the effect of flow conditions through sand and perforations. The laboratory procedure followed with each visualization model will be discussed in detail in the following sections.

3.3.3.1 First Visualization Model

The initial procedure followed during these types of tests was the same for both the horizontal and vertical orientations. A cork plug was inserted into the slot perforation. The visualization model was then put in a vertical position to allow placement of the sand and water. The visualization model was filled with water to approximately half its height. Sand was poured into the model using a small plastic scoop. Care was taken to ensure no air remained entrained in the sand as it entered the model. After the addition of each scoop of sand, the sides of the visualization model were vigorously tapped five times in order to obtain a consistent packing. This procedure of sand placement was repeated until the sand inside the visualization model reached a height of 66 cm above the top of the slot perforation. Water was added until the visualization model was completely full. The end plate was attached and any air remaining in the model was removed. A constant head apparatus was used to provide water flow through the model. The constant head tank was attached to a fitting on the top plate and the visualization model was placed in either a horizontal or vertical orientation.

In the horizontal orientation, the constant head tank was set to the appropriate hydraulic gradient and the plug was removed from the slot perforation. Water and sand were allowed to flow out of the visualization model through the slot perforation. After steady state conditions were reached, the flow rate was measured using a graduated cylinder. If a cavity formed in the sand, the width and height of the cavity was measured and recorded. Elapsed time of flow at a particular hydraulic gradient was recorded and the mass of sand expelled at each hydraulic gradient was measured. A range of hydraulic gradients approximately equal to 0.1, 0.2, 0.4, 0.6, 0.8 and 1.0 were applied to the visualization model. Normally, flow would be initiated at the lowest hydraulic gradient and later increased to the next hydraulic gradient after the flow inside the visualization model had reached a steady state condition.

With the visualization model in the vertical orientation, only a hydraulic gradient equal to 1.1 was applied. After the constant head tank was set to the appropriate height, the plug was removed. Sand and water were now free to flow out of the visualization model through the slot perforation. The formation of an arch or bridge over the slot perforation was recorded as well as the stability of the arch with respect to water flow and vibration.

3.3.3.2 Third Visualization Model

Tests using the third visualization model that incorporated water flow through fully water saturated sand, were done only in a vertical orientation using coarse sand and a 5 mm wide slot perforation with no confining stress applied. The sand was placed into the visualization model following the same procedure outlined in Section 3.3.2 Dry Sand With Confining Stress Applied. The sand inside the visualization model was then fully saturated with water. The plug was removed from the slot perforation and, simultaneously, a water flow was applied to the visualization model. Water flow was controlled using a flow meter connected in-line between the water source and the visualization model. The formation of an arch or bridge over the slot perforation was recorded as well as the stability of the arch with respect to water flow and vibration.

3.3.4 Upward Air Flow Tests

The laboratory procedure followed and related analysis and discussion of the results of the upward air flow tests are described in detail in Appendix C.

3.3.5 Partial Saturation Arching Tests

The ability of fine sand to arch over a 12.7 mm wide slot perforation under gas-water and oil-water saturations was studied using the third visualization model. No confining stress was applied during these tests. Also, the sides of the plexiglass box were permanently rested on two supports to prevent the plexiglass box from sliding down the slot perforation blocks.

3.3.5.1 Gas-Water Saturation Tests

The initial procedure followed during the assembly and preparation of the visualization model is the same as the procedure outlined in Section 3.3.2 Dry Sand With Confining Stress Applied. The model was dried and assembled. The slot perforation blocks were fastened to the aluminum stand and the plug inserted into the slot. The plexiglass box was placed over the slot perforation blocks and rested on two support blocks. In these tests involving gas-water saturation, the plexiglass box was not allowed to move down over the slot perforation blocks. It was not necessary to allow for plexiglass box movement since no confining stress was to be applied.

Calculations were made to determine the required amounts of sand and water that were to be placed within the visualization model to achieve desired saturations. The appropriate amount of sand was weighed and placed in the bowl of a mechanical mixer. The required amount of water was added to the sand. The sand and water were then mixed together until a uniform combination was obtained. Moisture contents were taken from this mixture. Before the sand-water mixture was placed inside the visualization model, the visualization model was weighed to determine its weight when empty. The sand-water mixture was placed in the visualization model in four lifts of approximately 4 cm each. Each lift was tamped into place using a tamping plate. At the conclusion of sand placement, the visualization model was weighed again. The difference in the weights of the visualization model before and after sand placement was taken as the total mass of sand-water mixture placed inside the visualization model. Moisture contents were taken of the remaining sand-water mixture not placed inside the visualization model. The height of sand above the top of the slot perforation was measured and recorded.

Two different procedures were followed from this point. In the first procedure, the application of an air flow was made possible through the top of the visualization model. Opening the valve resulted in an air flow moving through the sand-water mixture from top to bottom and finally out the slot perforation. In order to accommodate the air flow, the piston assembly was inserted into the visualization model but was not allowed to come in contact with the sand-water mixture. The purpose of the piston assembly was to distribute evenly the air flowing into the visualization model across the top of the sand-water mixture. The top plate was attached to the visualization model and an air line was attached to the fitting in the top plate. The manometers in the back face of the visualization model were connected to the manometer board. The visualization model was now ready to start the test.

The plug was removed from the slot perforation in one quick motion. Movement or nonmovement of the sand-water mixture was recorded. If the sand-water mixture formed a stable arch over the slot perforation an air flow was applied. Observations were made regarding the effect of the air flow on arch stability, water migration and arch size and shape. If stable arches were formed, the face of the visualization model was tapped with a rubber hammer in order to observe the arch's stability when subjected to vibration. At the completion of the test, moisture contents were taken of the sand-water mixture that had flowed out the slot perforation and at several locations of sand-water mixture remaining within the visualization model. The second procedure was identical to the first procedure described above with the exception that no air flow was applied to the visualization model. The second procedure was employed when very high gas saturations were used.

3.3.5.2 Oil-Water Saturation Tests

The third visualization model was used for tests investigating the interfacial tension effects of water and oil on sand behavior. The initial procedure followed during the assembly and preparation of the visualization model was the same as the procedure outlined in Section 3.3.2 Dry Sand With Confining Stress Applied. The model was dried and assembled. The slot perforation blocks were fastened to the aluminum stand and the plug inserted into the slot. The plexiglass box was placed over the slot perforation blocks and rested on two support blocks. In these tests involving oil-water saturation, the plexiglass box was not allowed to move down over the slot perforation blocks. It was not necessary to allow movement of the plexiglass box since no confining stress was to be applied during tests involving oil-water saturation.

Calculations were made to determine the required amounts of sand, water and oil that were to be placed within the visualization model to achieve desired saturations. The appropriate amount of sand was weighed and placed in a metal pan. Enough water was added to the sand to ensure that the surface of all sand particles were water wet. The appropriate quantity of oil was added to the sand-water mixture. The sand-water-oil mixture was thoroughly mixed by hand for approximately ten minutes. Mixing time was determined by a trial and error process. Ten minutes proved to be a long enough time to ensure uniformity in the mixture.

At the completion of mixing, the sand-water-oil mixture was ready to be placed in the visualization model. Approximately 2 cm of water was placed in the visualization model to ensure that the sand-water-oil mixture remained saturated when being placed and reducing the possibility of air entrainment. The sand-water-oil mixture was placed inside the model in 3 lifts. Each lift was compacted using a tamping rod. The height of sand above the top of the slot perforation was measured and recorded. The visualization model was then placed inside a plexiglass containment tank in order to keep the slot perforation submerged under water throughout the test. The containment tank was filled with water to a height equal to the height of water inside the visualization model so that no hydraulic gradient would be applied to the sand-water-oil mixture. All air trapped under the model was removed. The visualization model was now ready to begin the testing. The plug was removed in one quick movement. Observations were made regarding flow or nonflow of the sand-water-oil mixture. If there was no sand flow out of the slot perforation, observations were made regarding arch type and shape. Stable sand arches were subjected to vibration by tapping the face of the visualization model with a rubber hammer. During the test, the water levels in the containment tank and visualization model were kept equal by manually adding water to the visualization model. At the completion of the test, samples were taken from inside the visualization model for moisture content and extraction tests. Moisture content and extraction tests were used to determine water and oil saturations of the sample based on calculated void volume. If the water and oil saturations failed to combine to a value of 100% saturation, it was possible to determine the degree of gas saturation caused by air entrainment in the sample.

3.3.6 Index Capillary Cohesion Tests

The Swedish fall-cone test (SFC) is a quick laboratory test used to provide estimates of undrained shear strength of fine grained soils. It is best suited for very soft to cohesive soils. Additional details concerning the fall-cone test and its interpretation is provided by Hansbo (1957). In this study, the fall-cone test was used as a strength index test to provide an estimate of undrained shear strength of the fine sand at varying degrees of gas-water, gas-oil and oil-water saturations, which will be called the index capillary cohesion. It was felt that the results of the fall-cone tests could be used as an index capillary cohesion because the presence of interfacial tension between the fluids in the cohesionless soil would result in a material somewhat similar to a cohesive soil.

Tests were conducted under four different sets of conditions: (1) dry, (2) gas-water, (3) gas-oil and (4) oil-water. The procedures followed during each set of test conditions will be explained in detail below.

Fall-cone tests using dry sand were very simple. Dry fine sand was placed in the fall-cone mold in four lifts of 7.5 mm and tamped using a PVC block until the desired density was achieved. Measurements of mass and volume were recorded for later calculations. Five readings were taken using the 10g/60° cone and/or the 60g/60° cone depending on the strength range of the fine sand. The 10g/60° cone is a metal cone weighing 10 g in the shape of a 60° cone. Likewise, the 60g/60° cone is a metal cone weighing 60 g in the shape of a 60° cone used for samples with higher strengths due to its larger weight. Tests were performed on dry fine sand at porosities ranging from 35% to 43%. These readings were transformed into index capillary cohesion values using the fall-cone calibration for fine grained soils.

The second set of test conditions were gas-water tests. Under these conditions, water was the wetting fluid and air was the non-wetting fluid. The wetting fluid is defined as the fluid which exists as a thin film around the sand grains. The non-wetting fluid is not in direct contact with the sand grains and exists in the voids created by the sand grains. Based on the mass and volume measurements taken during the dry sand tests, void volume within the fall-cone mold was calculated. Based on these values, the appropriate amounts of sand and water were mixed together to achieve the desired degree of water saturation. The water and sand were manually mixed until a uniform distribution of the water was obtained. Two moisture contents were taken immediately after the sand and water were mixed. The water-sand mixture was placed in the fall-cone mold in four lifts of 7.5 mm and tamped with a PVC block until the desired compaction was achieved. The low viscosity of the water allowed the water-sand mixture to be compacted with relative ease.

Five readings were taken with the 10g/60° cone and/or 60g/60° cone depending on the strength range of the water-sand mixture. Immediately after testing was completed, two more moisture contents were taken. This procedure was repeated at degrees of gas saturations of 10, 20, 30, 40, 50, 60, 70, 80, 90 and 100 percent and at ±5 percent of the peak measured strength. Measured index capillary cohesion was plotted against calculated degree of gas saturation.

The third set of test conditions were gas-oil tests. Under these conditions, oil was the wetting fluid and air was the non-wetting fluid. The mixing process and testing procedure for the gas-oil tests was essentially the same as what was described for the gas-water tests. One exception was that the degree of oil saturation was determined by an extraction test. The gas-oil mixture was placed in the fall-cone mold in four 10 mm lifts. Each lift was tamped using a PVC block to achieve the desired density. The gas-oil mixture proved to be more difficult to compact to the desired density at low gas saturations. This was due to air entrainment in the gas-oil mixture caused by the high viscosity of the oil. It was exceedingly difficult to remove the required amounts of air out of the gas-oil mixture by tamping with a PVC block at low gas saturations. Due to these difficulties, the very low gas saturation gas-oil mixtures were not attainable at the desired density. The procedure was repeated at degrees of oil saturation of 30, 40, 50, 60, 70, 80, 90 and 100 percent. Two oils with viscosities of 3600 mPa*s and 1300 mPa*s at 25 °C were tested under these conditions. Measured index capillary cohesion was plotted against calculated degree of gas saturation.

The fourth set of conditions were oil-water tests. Under these conditions, water was the wetting fluid and oil was the non-wetting fluid. The oil used in these tests had a viscosity of 3600 mPa*s at 25 °C. Before any oil was added to the sand, enough water was added to the sand to ensure all the sand particles were water-wet. The appropriate amount of oil was added to the water-sand mixture and mixed until a uniform mixture was attained. It was assumed from the observations that the oil would displace the excess water in the sand. This was visually confirmed during mixing as some water was observed to separate from the mixture. It was assumed that all of the oil remained mixed in the oil-water-sand mixture and only the excess water separated from the mixture. The oil-water-sand mixture was placed in the fall-cone mold in four 1 cm lifts. Each lift was tamped using a PVC block to achieve the desired density. The same problem regarding air entrainment described in the gas-oil tests was also present in the oil-water tests. Air entrainment in the oil-water-sand mixture, which proved to be very difficult to remove by compaction, due to the high viscosity of the oil, made the low water saturation oil-water mixtures unattainable at the desired density. Five readings were taken with the 10g/60° cone and/or the 10g/60° cone depending on the strength range of the oil-water-sand mixture. The entire sample was removed from the mold and sealed in a container for extraction testing to determine degree of oil and water saturation of the oil-water-sand mixture. Extraction tests were used to determine water and oil saturations of the sample based on calculated void volume. If the water and oil saturations failed to combine to a value of 100% saturation, it was possible to determine the degree of gas saturation caused by air entrainment in the sample. This procedure was repeated at degrees of water saturation of 50, 60, 70, 80, 90 and 100 percent. Measured index capillary cohesion was plotted against calculated degree of water saturation.

3.3.7 Capillary Cohesion Direct Shear Tests

Direct shear tests were used to provide a direct measurement of capillary cohesion of fine sand at varying gas-water saturations. The fine sand was subjected to direct shear tests and the peak and residual shear stresses were measured under confining stresses of 0, 5, 10 and 15 kPa at gas saturations of 100, 40 and 20%. The sand was placed in the shear box in four lifts of approximately 10 mm. Each lift was compacted in order to achieve the desired density. A porosity of 35% was used for all these direct shear tests. A square shear box with side dimensions of 60 mm and a total sand height of 38 mm with the shear plane at a height of 26 cm was used. The ASTM Standard Test Method for Direct Shear Test of Soil Under Consolidated Drained Conditions (ASTM Designation: D 3080-90) was followed during these tests with one important exception. When the shear box was assembled, teflon strips were placed between the top and bottom shear boxes. The purpose of the teflon strips was to provide a surface that would generate the least amount of friction as the top shear box moved across during shearing. Trial direct shear tests indicated that the confining stresses that were to be used did not provide enough side wall friction between the sand and the walls of the top shear box to keep the top and bottom shear boxes separated after the top box had been raised prior to shearing. This would result in the top shear box dropping down and riding on the surface of the bottom shear box instead of remaining separated throughout the test. Thus, it was important to reduce friction as much as possible because of the small confining stresses that were used in these tests.

The frictional shear stress generated by the top shear box sliding over the teflon strips was calibrated. A direct shear test was performed with no sand present and the top box under no confining stress riding over the teflon strips. This test resulted in a consistent shear stress reading of 0.6 kPa. This was taken as the frictional shear stress caused by the presence of the teflon strips and all capillary cohesion shear stress measurements were reduced by 0.6 kPa.

Table 3-1: Sieve Opening Sizes

Sieve No.	Size of Opening	
	(mm)	(inches)
4	4.75	0.187
10	2.00	0.079
20	0.850	0.033
40	0.425	0.017
60	0.250	0.0098
80	0.180	0.0071
100	0.150	0.0059
200	0.075	0.0030

Table 3-2: Specific Gravity of Test Sands

Sand Type	Specific Gravity		
	Trial 1	Trial 2	Average
Fine	2.72	2.72	2.72
Medium	2.70	2.71	2.71
Coarse	2.71	2.70	2.71

Table 3-3: Maximum Dry Density of Test Sands

Sand Type	Maximum Dry Density (kg/m^3*10^3)			
	Trial 1	Trial 2	Trial 3	Average
Fine	1.81	1.77	1.83	1.80
Medium	1.84	1.86	1.84	1.84
Coarse	1.75	1.76	-	1.76

Table 3-4: Minimum Dry Density of Tests Sands

Sand Type	Minimum Dry Density (kg/m^3*10^3)		
	Trial 1	Trial 2	Average
Fine	1.55	1.56	1.56
Medium	1.62	1.63	1.62
Coarse	1.56	1.56	1.56

Figure 3-1: Grain Size Distribution for Test Sands and Typical Formation Sand

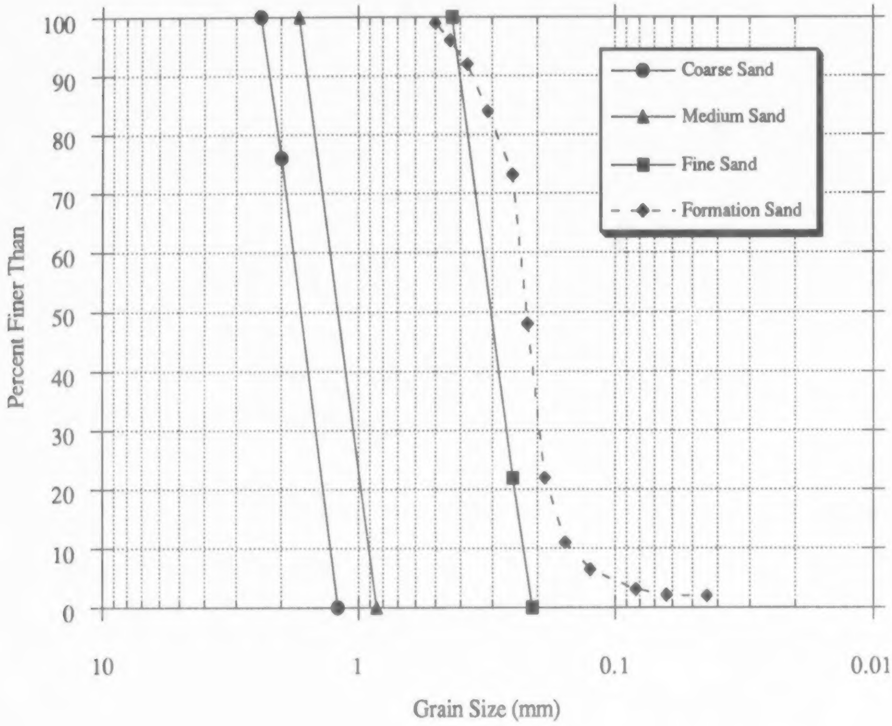

Sand Type	Mesh Size	Grain Size (mm)	D_{50} (mm)	D_{60}/D_{10}
Coarse	8-16	2.4 to 1.2	1.6	1.40
Medium	12-20	1.7 to 0.85	1.2	1.36
Fine	40-70	0.43 to 0.21	0.30	1.39
Formation*		0.63 to 0.04	0.22	1.56

*Typical formation sand from Frog Lake area, Alberta

Figure 3-2: Hydraulic Conductivity of Test Sands

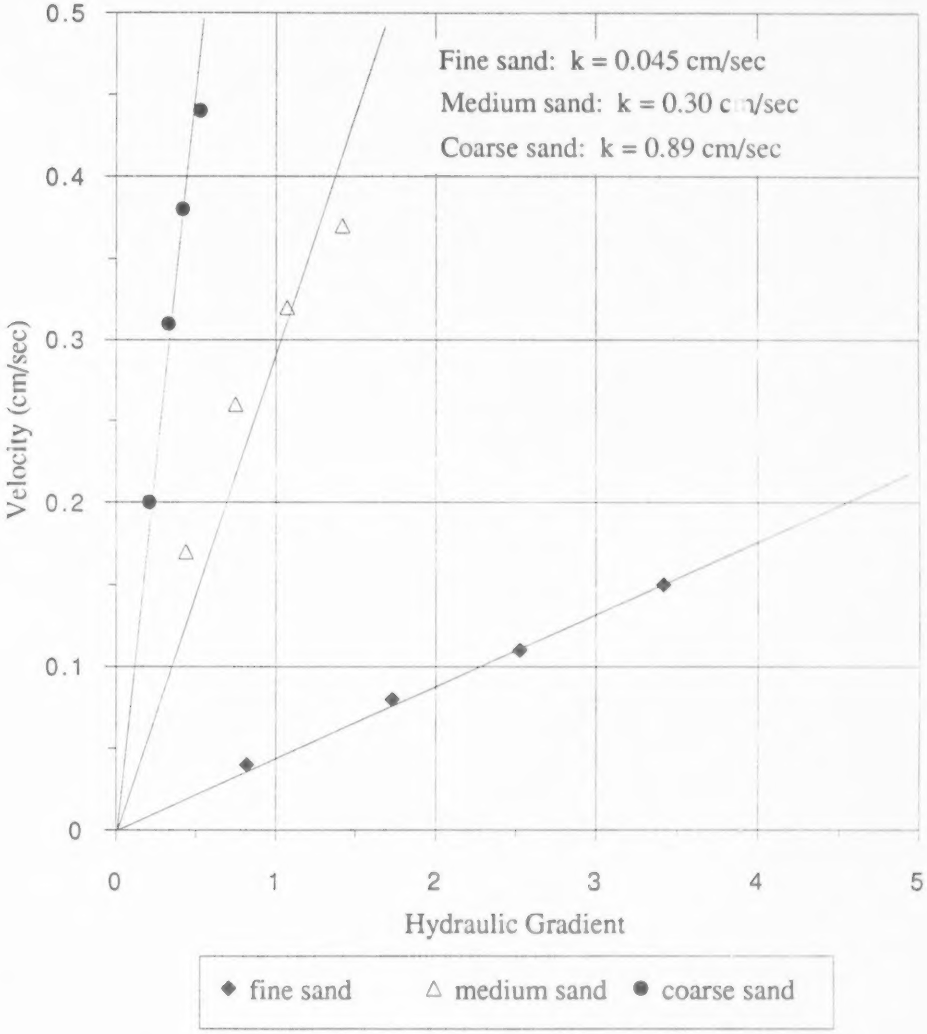

Figure 3-3: Peak Shear Stress Versus Normal Stress - Dry Sand Direct Shear Tests

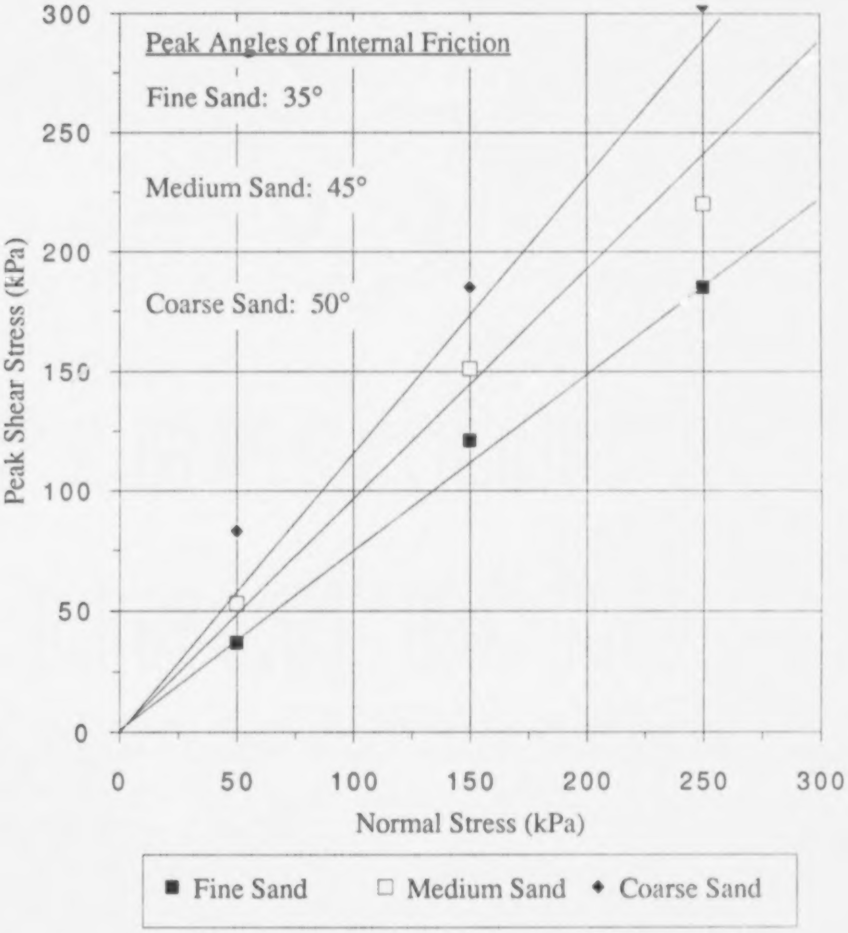

Figure 3-4: Residual Shear Stress Versus Normal Stress - Dry Sand Direct Shear Tests

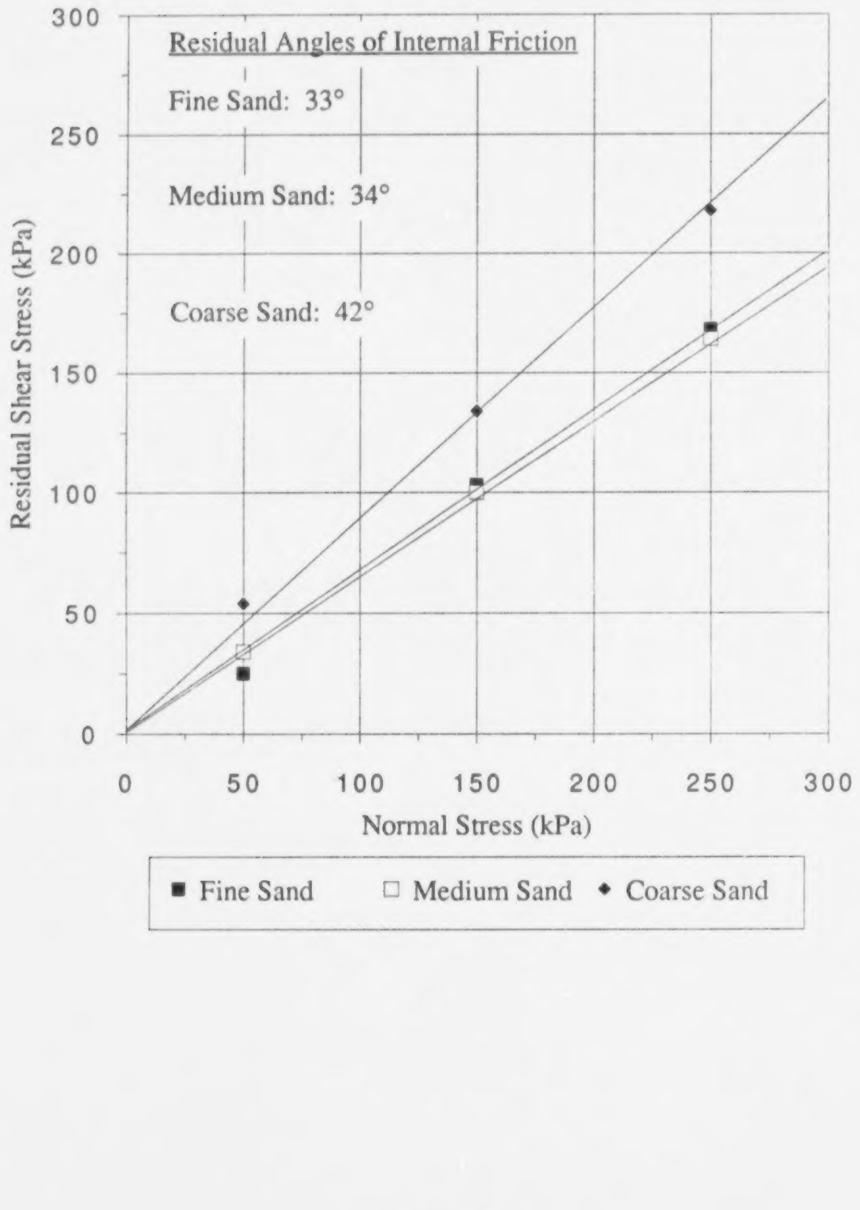

Figure 3-5: Peak Shear Stress Versus Normal Stress - Wall Friction Direct Shear Tests

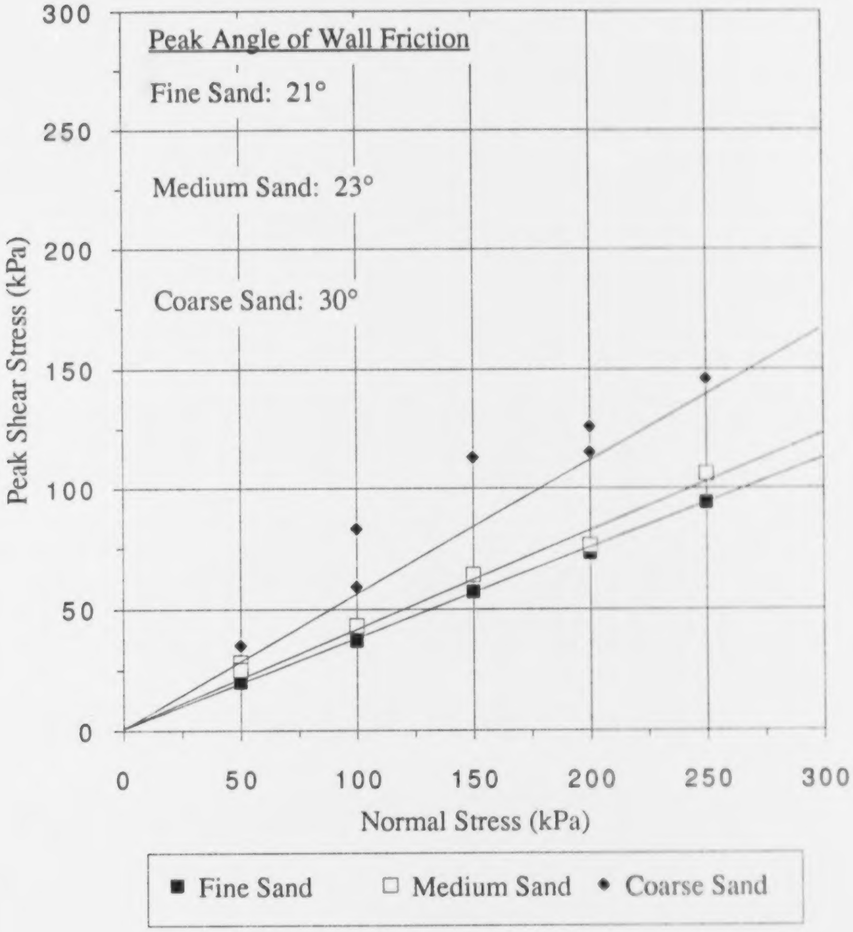

Figure 3-6: Residual Shear Stress Versus Normal Stress - Wall Friction Direct Shear Tests

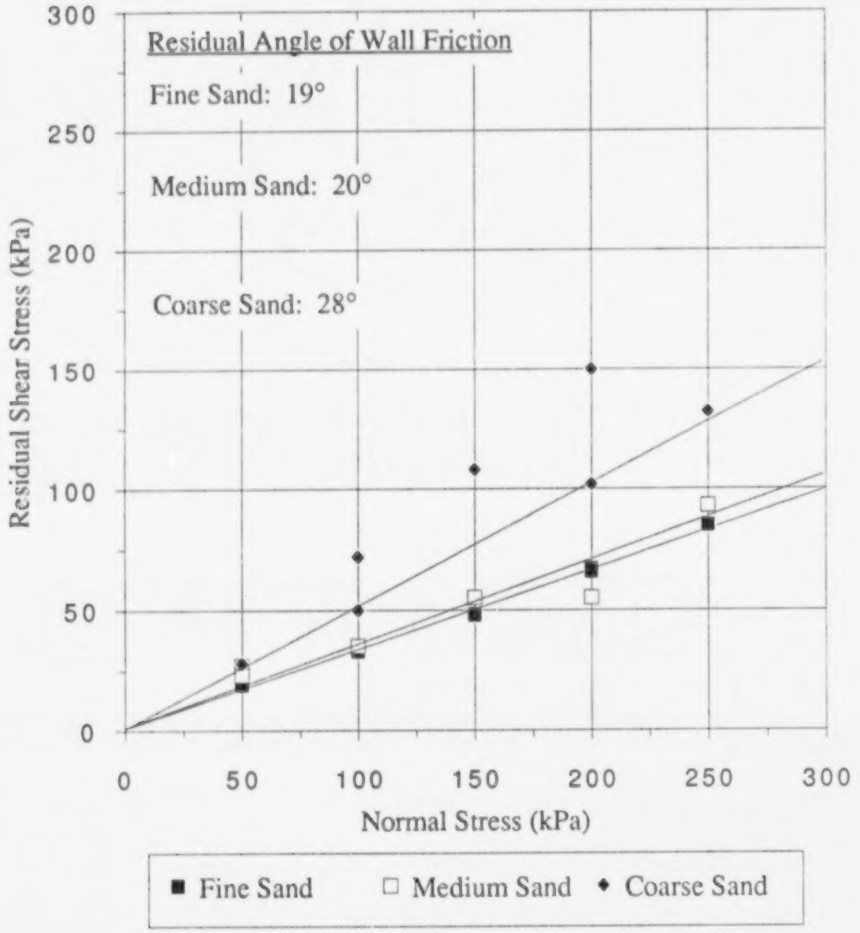

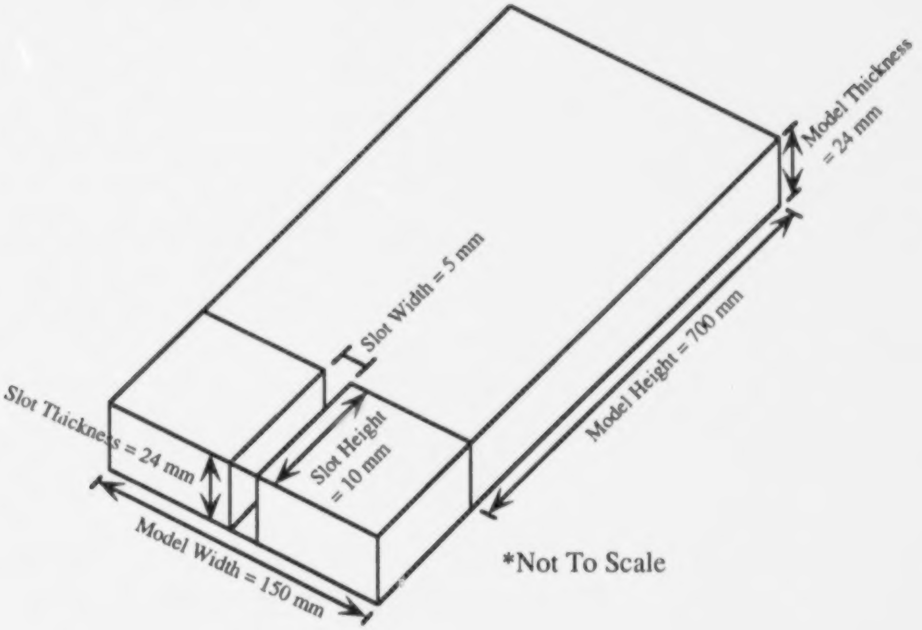
Model Thickness = 24 mm
Slot Width = 5 mm
Model Height = 700 mm
Slot Thickness = 24 mm
Slot Height = 10 mm
Model Width = 150 mm
*Not To Scale

Figure 3-7: Inside Dimensions of the First Visualization Model

Figure 3-8: Third Visualization Model

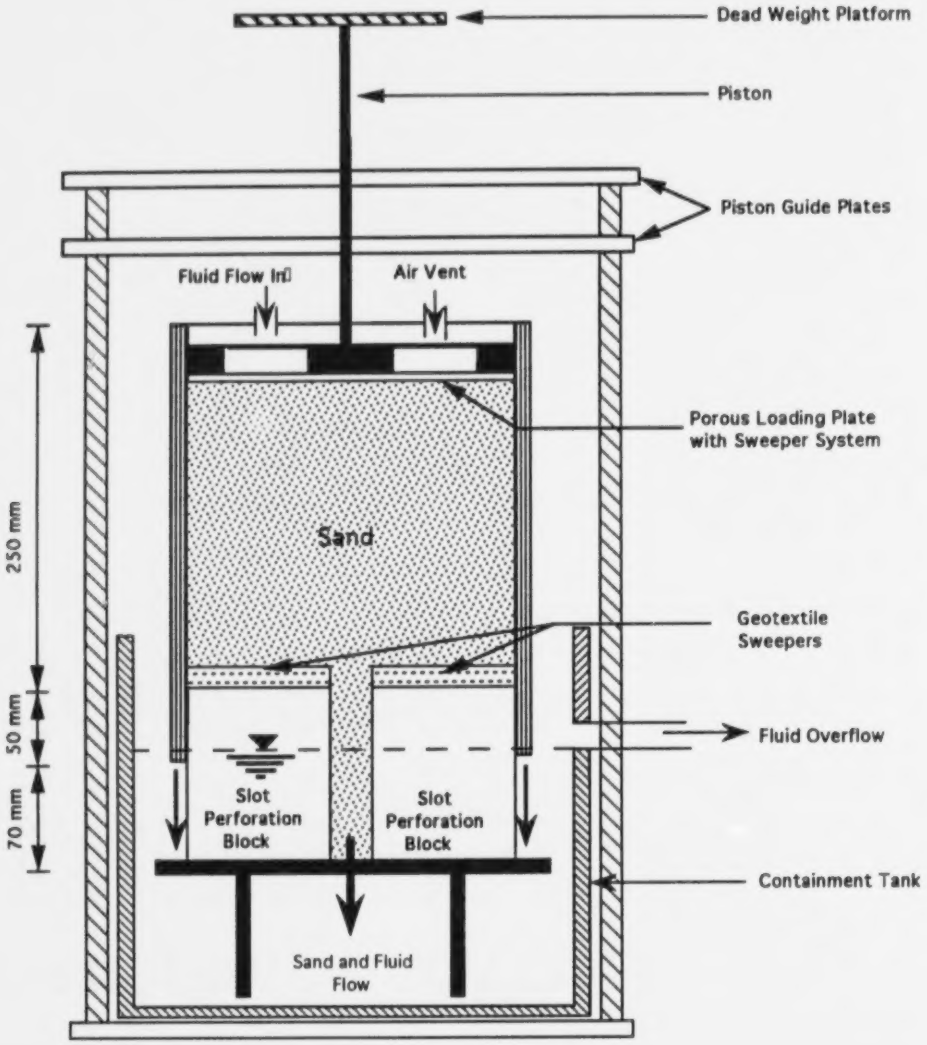
Dead Weight Platform
Piston
Piston Guide Plates
Fluid Flow In
Air Vent
Porous Loading Plate with Sweeper System
250 mm
Sand
Geotextile Sweepers
50 mm
Fluid Overflow
70 mm
Slot Perforation Block
Slot Perforation Block
Containment Tank
Sand and Fluid Flow

* Not To Scale

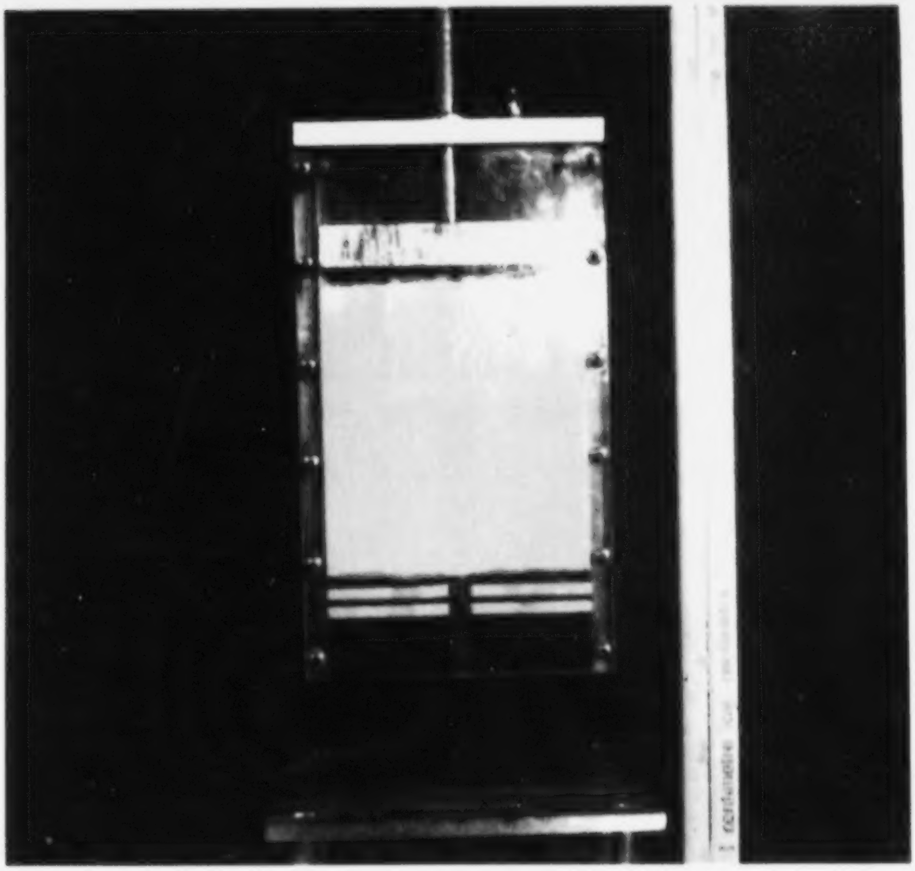

Plate 3-1: Third Visualization Model

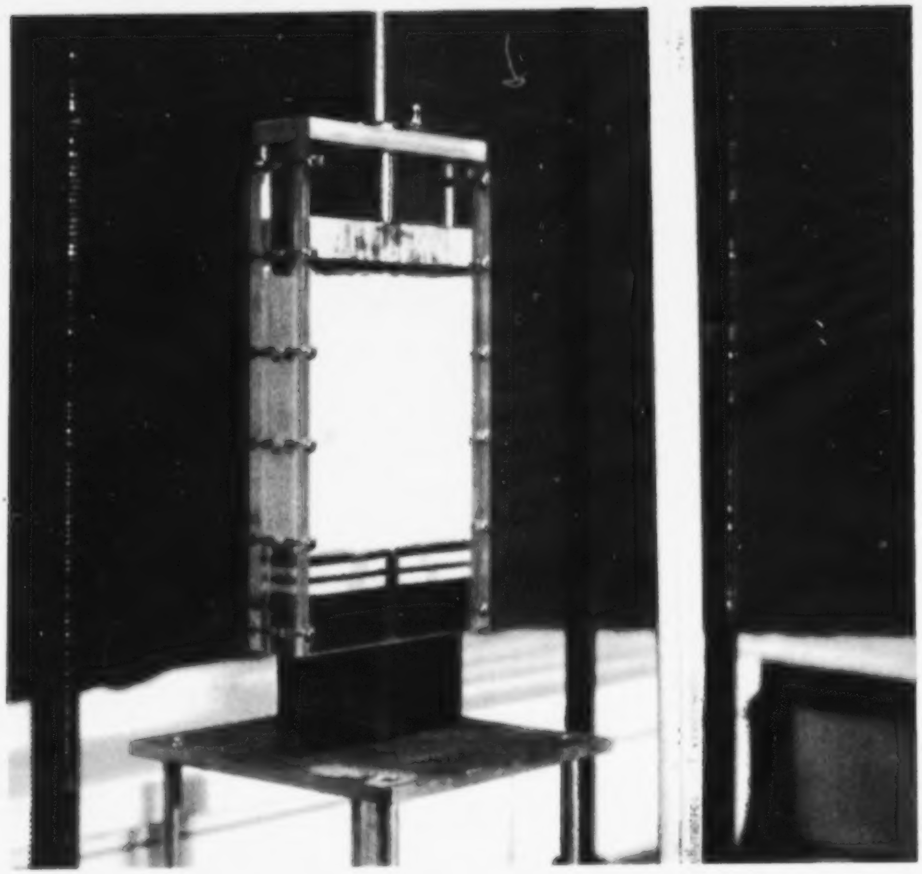

Plate 3-2: Side View of Third Visualization Model

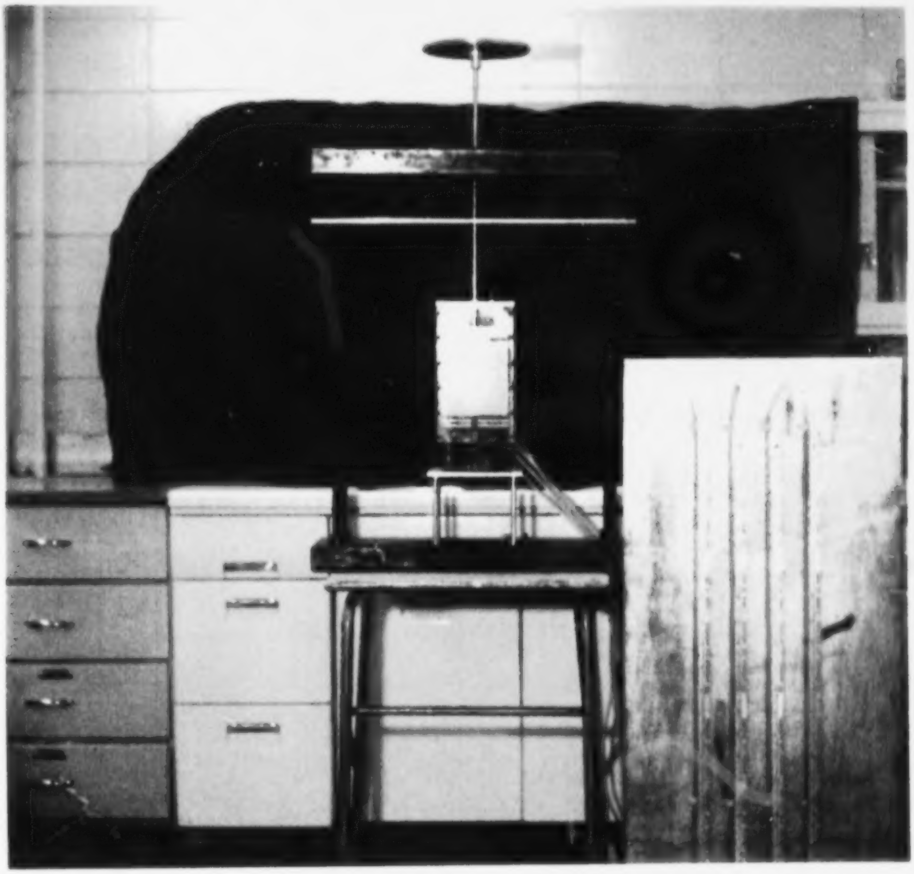

Plate 3-3: Overall Setup of Third Visualization Model

4. Experimental Results

4.1 Scope of Experimental Program

The experimental program can be broken down into five major components: tests with the first visualization model, tests with the second visualization model, tests with the third visualization model, index capillary cohesion tests and capillary cohesion direct shear tests. The first visualization model was originally used in a horizontal orientation to simulate conditions at a wellbore perforation. The sand would be subjected to horizontal flow conditions and a horizontal confining stress in this orientation. However, initial testing with the first visualization model indicated that this orientation did not allow the optimum conditions to examine sand behavior during fluid flow. The first visualization model was then used in a vertical orientation with the sand under dry and water saturated conditions. The vertical orientation tests allowed the effects of sand particle size and perforation diameter and the shape and roughness of the perforation opening to be examined. Based on the results of the first visualization model, it was decided to construct a second, more refined, visualization model to be used in a vertical orientation only.

The second visualization model was first used with dry sand without confining stress applied in order to check the results obtained using the first visualization model. The next set of tests involved dry sand with a confining stress applied. However, it was discovered that friction between the sand and the walls of the visualization model was impeding the transfer of confining stress to the sand just above the slot perforation. The second visualization model was modified into the third visualization model to correct this problem.

The third visualization model was first used to examine the effect of confining stress on dry sand. Next, the behavior of sand under fully water saturated flow conditions was investigated. Then upward flow of air through a slot perforation tests were performed to verify the results of Hall and Harrisberger (1970). The ability of fine sand to arch over a slot perforation at gas-water and oil-water saturations was then examined. Numerous gas-water and oil-water saturations were investigated in order to determine the degrees of saturations required to allow a stable arch to form. As well, the effect of saline water, typical of field conditions, on arch stability was observed. Also, attempts were made to flow water through an oil-water saturated sand arched over a slot perforation, which proved unsuccessful.

At this point, it was apparent that capillary cohesion due to interfacial tension between two fluids in a sand was playing a significant role in the stability of sand arches. A relative measure of capillary cohesion in the fine sand, designated the index capillary cohesion, was made using a fall-cone at varying gas-water, gas-heavy oil, gas-medium oil and heavy oil-water saturations.

It was noted that the fall-cone would provide only a relative measure of capillary cohesion. In order to obtain actual capillary cohesion values, direct shear tests of sand under varying saturations were performed. These were compared to earlier results of direct shear tests performed on dry sand to ascertain how capillarity affected the shear stress-strain and volume change behavior of the sand.

4.2 First Visualization Model Tests

The purpose of the first visualization model design was to examine the effect of the boundary conditions on the visualization model concept and give direction towards designing a more refined visualization model. To that end, the first visualization model was used in preliminary tests in both horizontal and vertical orientations and under dry and fully water saturated conditions. The results of these tests using the first visualization model were used to set up a design for and a testing program for the second and third visualization models. The inside dimensions of the first visualization model were 24 mm thick by 150 mm wide by 700 mm high. The walls of the model were 10 mm thick. A slot perforation 5 mm wide and 10 mm high was initially used with the first visualization model. The slot perforation had the same thickness, 24 mm, as the visualization model. The slot height was later increased to 50 mm. The dimension designation conventions used when describing the visualization models, regardless of orientation, are presented in Figure 3-7.

4.2.1 Horizontal Orientation

Only the fine and medium sands were tested using the first visualization model in a horizontal orientation. These tests examined sand behavior when the sand was under a condition of complete water saturation and subjected to a constant water flow. Two tests were performed using fine sand and three tests were conducted using medium sand. The procedure followed during these tests is described in Section 3.3.3.1 First Visualization Model. A picture of the first visualization model set up in the horizontal orientation is presented in Plate 4-1.

Tests #1d and #2 utilized the fine sand. The purpose of these tests was to examine the behavior of water saturated fine sand in a horizontal orientation subjected to water flow over a range of hydraulic gradients. In Test #2, the slot perforation was 5 mm wide and 10 mm high. This resulted in a grain diameter to width of opening ratio of 1:16.7. The fine sand was compacted in the visualization model at a void ratio of 0.74 and an associated dry density of 1.56 g/cm^3. The calculated relative density was equal to 2.6%. Low relative densities were used during tests with the first visualization model in order to compare the behavior of the sand under similar conditions but at higher relative densities using the second visualization model. The height of the sand in the visualization model was 66 cm. The hydraulic gradient through the sand was initially set at 0.10 and increased in stages to 0.20, 0.40 and 0.80. As water flows through the sand, it loses energy through friction with the sand grains. This loss of energy is called head loss. Hydraulic gradient is defined as the head loss due to liquid flowing through the soil divided by the length of the soil. At the initial hydraulic gradient of 0.10, removal of the plug resulted in an initial flow of a sand-water mixture out of the slot perforation. No mechanism of sand arching, bridging or plugging was observed as the sand sloughed forming a semispherical cavity adjacent to the slot perforation. The semispherical cavity was 2 cm high and 4 cm wide. A sketch of the semispherical cavity is provided in Figure 4-1. Once water flow through the slot perforation had commenced, the quantity of water flow was not sufficient to maintain water flow along the full thickness of the slot perforation. Only the bottom quarter of the slot perforation was required to carry the water flow out of the visualization model. Thus, the top three quarters of the slot perforation was open to the atmosphere. This allowed air to move into the visualization model and occupy the space vacated by the sand during the creation of the semispherical cavity. Once the cavity had stopped enlarging, only water continued to flow out of the slot perforation. The entire length of the slot perforation remained clear of sand particles except for a small number of sand particles resting on the bottom of the slot perforation.

Once movement of sand particles ceased and steady state water flow was achieved, the hydraulic gradient was increased to 0.20. The increase in hydraulic gradient resulted in a repetition of the events observed when the plug was removed at a hydraulic gradient of 0.10. An initial discharge of the sand-water mixture was accompanied by an enlargement of the semispherical cavity adjacent to the slot perforation. The semispherical cavity attained a height of 4 cm and a width of 6 cm. Once the semispherical cavity reached this size, only water continued to flow out of the slot perforation. When the hydraulic gradient was increased to 0.40, the semispherical cavity enlarged substantially to a height of 8 cm and a width of 8 cm. Shortly after the cavity reached these dimensions, more sand broke loose forming meandering, preferred channels of water flow next to the top plexiglass face of the visualization model. During the formation of the preferred channels of water flow, a sand-water mixture flowed out of the slot perforation. Once the channels were established, only water continued to flow out of the slot perforation. A flow rate equal to 66 cm^3/min was measured at this hydraulic gradient. The hydraulic gradient was finally increased to 0.80 which resulted in the discharge of the remaining sand adjoining the meandering preferred channels of water flow in contact with the top plexiglass face, as a single large preferred channel of water flow was formed. The total time elapsed during Test #2 was equal to 45 minutes.

During each stage of this test, the slot perforation remained clear of sand particles except for a small number of sand grains resting on the bottom of the slot perforation. As well, once the semispherical cavity had quit enlarging, sand movement ceased and only water continued to flow out the slot perforation. The sand remained immobile until a higher hydraulic gradient was applied. The sand did not appear to form any type of arch structure at the top of the slot perforation or within the perforation. No mechanism of sand arching, bridging or plugging was observed during any stage of Test #2. Another test, Test #1d, using the fine sand and an initial hydraulic gradient of 1.0 resulted in the immediate formation of a preferred channel of water flow similar to what was described above. A summary of Tests #2 and #1d is provided in Table 4-1.

Three similar tests, Tests #4, #12 and #11, were conducted with the medium sand. These tests provided results very similar to the results previously described using fine sand, even though the grain diameter to width of opening ratio was 1:4.2 when the medium sand was used. Increased slot perforation height and extended water flow periods also had no effect on the sand behavior described above. A summary of Tests #4, #12 and #11 is provided in Table 4-1.

4.2.2 Vertical Orientation

All three sands were tested using the first visualization model in a vertical orientation. These tests examined the behavior of the sand in a vertical flow orientation under two different sets of conditions. One set of conditions saw the sand placed in the visualization model in a completely dry state. The sand was not subjected to confining stress or fluid flow conditions. Observations were made regarding sand behavior after the plug was removed and the sand was free to flow through the slot perforation. The procedure followed during these tests is described in Section 3.3.1.1 First Visualization Model. The other type of test consisted of the same conditions outlined above with the exception that the sand was fully water saturated. Water flow was applied to the visualization model to maintain full water saturation with a constant water flow. The procedure for this type of test is also outlined in Section 3.3.3.1 First Visualization Model. Low relative densities were used during tests with the first visualization model in order to compare the behavior of the sand under similar conditions but at higher relative densities using the second visualization model. This would allow the effect of relative density on sand behavior to be evaluated.

Three tests were performed using the fine sand, five tests were performed using the medium sand and three tests were conducted using the coarse sand. Tests involving fine sand were identified as #1a, #10 and #3. Tests involving medium sand were identified as Tests #1b, #9, #8, #5 and #7. Tests involving coarse sand were identified as Tests #14 and #19. The results of tests conducted using dry sand will be summarized first, followed by tests utilizing fully water saturated sand.

4.2.2.1 Dry Conditions

During tests using the first visualization model under dry conditions, the slot perforation thickness was equal to the inside dimension of thickness of the visualization model, 24 mm, for all tests.

4.2.2.1.1 Fine Sand

The purpose of Test #1a was to examine the behavior of the dry fine sand at a slot perforation with no confining stress or flow conditions applied. The slot perforation was 5 mm wide and 10 mm high. This resulted in a grain diameter to width of opening ratio of 1:16.7. No measurements of mass or volume were taken in Test #1a and thus void ratio, dry density and relative density values are not available. When the plug was removed, the dry fine sand immediately flowed out of the slot perforation. A "V" shape formed at the top of the sand as the sand flowed out the slot perforation. All the sand mass flowed out of the visualization model except for sand remaining in the bottom corners of the model. The time required for the sand to flow out of the model was not measured during this test so rate of sand flow is not available. No mechanism of sand arching, bridging or plugging was observed as sand flowed through the slot perforation. The slot perforation remained clear of obstructions created by sand particles throughout the test.

The purpose of Test #10 was to determine if increasing the height of the slot perforation to 50 mm would alter the sand behavior observed in Test #1a. The slot perforation was 5 mm wide and 50 mm high. The fine sand had a void ratio, dry density and relative density of 0.74, 1.58 g/cm^3 and 2.7%, respectively. The results of Test #10 were very similar to the results of Test #1a. When the plug was removed, the dry fine sand immediately flowed out the slot perforation. The same "V" shape described in Test #1a was observed to form at the top of the sand as the sand flowed out the slot perforation.

The fine sand flowed out of the visualization model in 4 minutes, resulting in a rate of sand flow of 15.5 g/sec. As the sand flowed through the slot perforation, no mechanisms of arching, bridging or plugging were observed . The slot perforation remained clear of sand particles obstructing the flow of sand throughout the test. Thus, the increase in height of the slot perforation proved to have no visible effect on sand behavior. The results of Tests #1a and #10 are summarized in Table 4-2.

4.2.2.1.2 Medium Sand

The purpose of Test #1b was to determine if the dry medium sand would behave in the same manner as the dry fine sand under the same conditions of no confining stress or flow conditions applied. A 5 mm wide and 10 mm high slot perforation was used resulting in a grain diameter to width of opening ratio of 1:4.2. No measurements of mass or volume were taken in Test #1b and thus void ratio, dry density and relative density values are not available. The results of Test #1b were essentially the same as the results observed when dry fine sand was used. When the plug was removed, the dry medium sand immediately flowed out the slot perforation. All sand flowed out of the model and the characteristic "V" shape was observed at the top of the sand. No rate of sand flow was recorded for this test. The dry medium sand did not display arching or plugging characteristics as the sand flowed smoothly through the slot perforation. The results of this test using dry medium sand corresponded to the results obtained in the same type of test using dry fine sand.

The purpose of Test #9 was to determine if increasing the height of the slot perforation would alter the medium sand behavior observed in Test #1b. A slot perforation height of 50 mm was used and a slot perforation width of 5 mm was maintained. The compacted sand had a void ratio, dry density and relative density of 0.64, 1.64 g/cm^3 and 12.5, respectively. The results of Test #9 were very similar to the results of Test #1b.

When the plug was removed, the dry medium sand immediately flowed out the slot perforation. The characteristic "V" shape was observed at the top of the sand as the sand flowed out of the visualization model in 5.5 minutes, resulting in a rate of sand flow of 11.8 g/sec. No mechanism of sand arching, bridging or plugging was observed as sand flowed through the slot perforation. Hence, the increase in height of the slot perforation proved to have no visible effect on sand behavior.

Test #8 was intended to be identical to Test #9; however, a small amount of moisture was inadvertently present in the visualization model during compaction of the medium sand. The slot perforation was 5 mm wide and 50 mm high resulting in a grain diameter to width of opening ratio of 1:4.2. The medium sand was compacted in the visualization model at a void ratio, dry density and relative density of 0.66, 1.63 g/cm^3 and 4.5%, respectively. When the plug was removed from the slot perforation, only a few sand grains flowed out. There was no initial flow of sand and no plugging or arching was present along the length of the slot perforation. Therefore, it was concluded that the sand blockage was located above the top of the slot perforation. Tapping the sides of the visualization model resulted in the expulsion of only a few sand grains. In an attempt to dislodge the sand blockage that had formed above the slot perforation, a wire brush was inserted into the slot perforation. Contact of the wire brush with the sand caused the initiation of sand flow that continued in the same manner observed in Test #9. At the completion of the test, sand grains were observed to be sticking to the walls of the visualization model. This was taken as an indication that the visualization model had not been adequately dried prior to testing. The events witnessed in this test suggest that capillary forces present in partially saturated sand may have a significant influence on sand behavior under these conditions. The results of Tests #1b, #9 and #8 are summarized in Table 4-2.

4.2.2.1.3 Coarse Sand

The purpose of Test #14 was to determine if the dry coarse sand would behave in the same manner as the dry fine sand and dry medium sand under the same conditions of no confining stress or flow conditions applied. A 5 mm wide and 50 mm high slot perforation was used. This resulted in a grain diameter to width of opening ratio of 1:3.1. The coarse sand was compacted in the visualization model at a void ratio of 0.73 and an associated dry density of 1.57 g/cm^3. The calculated relative density was equal to 5.7%. When the plug was removed, no sand movement occurred except for a small number of grains passing through the slot perforation. The slot perforation was carefully examined and it was determined that the sand had formed an arch structure located above the slot perforation and not in the slot. Tapping the face of the visualization model with a rubber hammer resulted in destruction of the arch and resumed flow of sand until another arch would form. This cycle of arch destruction due to vibration, limited sand flow and reformation of an arch was repeated by continued tapping with the rubber hammer. At the completion of the test, all the sand had flowed out of the visualization model except for sand remaining in the bottom corners of the model. Based on the results of Test #14 and previous tests, it appears that sand in a dry state, subjected to no confining stress or flow conditions will not exhibit arching behavior until the slot perforation width is less than approximately four times the sand grain diameter. The results of Test #14 are summarized in Table 4-2.

4.2.2.2 Water Saturated Conditions

During tests using the first visualization model under water saturated conditions, no measurements were made of the time required for the sand to flow out of the visualization model. Thus, no rate of sand flow values were available for the following tests. The slot perforation had a thickness of 24 mm for all the tests performed under these conditions using the first visualization model.

4.2.2.2.1 Fine Sand

The purpose of Test #3 was to examine the behavior of fully water saturated fine sand with a constant water flow applied and compare this behavior to what was observed when the sand was tested under dry conditions. The slot perforation was 5 mm wide and 10 mm high which resulted in a grain diameter to width of opening ratio of 1:16.7. The compacted fine sand had a void ratio, dry density and relative density of 0.72, 1.58 g/cm^3 and 10.1%, respectively. A hydraulic gradient of 1.1 was applied and the height of sand was 66 cm. When the plug was removed, sand immediately flowed out the slot perforation in a sand-water mixture. The same "V" shape observed in Tests #1a and #10 under dry conditions was observed at the top of the water saturated sand as the sand-water mixture flowed out the slot perforation. All the sand mass flowed out of the visualization model except for sand remaining in the bottom corners of the model. The results of Test #3 are summarized in Table 4-3.

4.2.2.2.2 Medium Sand

The purpose of Test #5 was to determine if the medium sand would behave in the same manner as the fine sand under the same conditions of full water saturation and constant water flow. A 5 mm wide and 10 mm high slot perforation with a grain diameter to width of opening ratio of 1:4.2 was used. The medium sand was compacted in the visualization model at a void ratio, dry density and relative density of 0.66, 1.63 g/cm^3 and 5.8%, respectively. A hydraulic gradient of 1.1 was applied and the height of sand was 66 cm. When the plug was removed, sand immediately flowed out the slot perforation in a sand-water mixture. It should be noted that once the plug was removed and the sand had begun to flow out of the visualization model, the flow of water was insufficient to keep the model completely full of water. Thus, as the sand level dropped in the model, the water level also dropped. However, the water level never dropped below the sand level. The same "V" shape observed in Test #3 was observed at the top of the water saturated sand as the sand-water mixture flowed out the slot perforation. All the sand mass flowed out of the visualization model except for sand remaining in the bottom corners of the model. The results of Test #5 were identical to Test #3 with no arching or plugging of sand and the slot perforation remaining clear of obstructions throughout the test.

The purpose of Test #7 was to determine if increasing the height of the slot perforation would alter the sand behavior observed in Test #5. The slot perforation height was increased to 50 mm. The grain diameter to width of opening ratio remained at 1:4.2 and the void ratio, dry density and relative density of the compacted sand was 0.66, 1.63 g/cm^3 and 4.4%, respectively. A hydraulic gradient of 1.1 was applied and the height of sand was 66 cm. The results of Test #7 were very similar to the results of Test #5 with no sand arching or plugging and the slot perforation remaining clear of obstructions throughout the test. Again, the increased slot perforation height had no visible effect on the sand behavior. The results of Tests #5 and #7 are summarized in Table 4-3.

4.2.2.2.3 Coarse Sand

The purpose of Test #19 was to determine how the coarse sand would behave under conditions of full water saturation and a constant water flow. The slot perforation was 5 mm wide and 50 mm high resulting in a grain diameter to width of opening ratio of 1:3.1. The compacted coarse sand had a void ratio, dry density and relative density of 0.74, 1.56 g/cm^3 and 0.0%, respectively. Test #19 was performed with the slot perforation submerged beneath approximately 40 mm of water in order to prevent air from entering the visualization model through the slot perforation. The test was initially started at a hydraulic gradient of 1.3 and the sand had a height of 66 cm. When the slot perforation was opened, a small discharge of sand was observed followed by the formation of an arch structure over the slot perforation that prevented further sand flow. Unfortunately, the constant head device was not able to supply enough water flow to keep the visualization model completely full of water. A short period of time after the test had begun, a layer of air approximately 2 cm high was present at the top of the visualization model. The hydraulic gradient was increased to 1.4. The increased hydraulic gradient had no effect on the arch structure over the slot perforation. Finally, the hydraulic gradient was increased to 1.7 and again no effect on the arch structure was observed. It should be noted that due to the presence of the layer of air at the top of the visualization model, setting the constant head tank to higher gradients may not have actually increased the hydraulic gradient within the visualization model. Tapping the face of the visualization model caused the same cycle of arch destruction due to vibration, limited sand flow and reformation of an arch seen in the tests using dry coarse sand. The results of Test #19 are summarized in Table 4-3.

4.3 Second Visualization Model Tests

The second visualization model was designed based on results and experience gained using the first visualization model. The second visualization model was used mainly to examine the behavior of dry sand under no confining stress. These tests allowed a more extensive observation of sand behavior under these conditions and also allowed for a comparison with similar tests performed using the first visualization model. The second visualization model was approximately half the height of the first visualization model and had the ability to use three different slot perforation widths. As well, the second visualization model had attachments for flowing fluids through the sand and applying a confining stress to the sand. The inside dimensions of the second visualization model were 20 mm thick by 150 mm wide by 300 mm high. The walls of the model were 12.7 mm thick. The slot perforation was 50 mm high, 20 mm thick and slot perforation widths of 5 mm, 12.7 mm and 19.1 mm could be used. In all of the following tests, the slot perforation height was 50 mm and the slot perforation thickness was 20 mm.

4.3.1 Dry Sand Without Confining Stress Applied

The fine, medium and coarse sands were tested in a dry state without confining stress applied in order to confirm the results obtained from similar tests using the first visualization model in a vertical orientation. The tests performed with the second visualization model were performed at higher relative densities in order to determine the effect of relative density on the behavior of dry sand without confining stress applied. It was necessary to confirm that the design of the second visualization model would yield similar results to those obtained using the first visualization model and not alter the behavior of the sand. The procedure followed during these tests is outlined in Section 3.3.1.2 Second Visualization Model.

4.3.1.1 Fine Sand

The purpose of Test #2 was to examine the behavior of the dry fine sand at a 5 mm wide slot perforation without confining stress applied and compare this behavior to what was observed when the fine sand was tested under the same conditions in the first visualization model. The resulting grain diameter to width of opening ratio was 1:16.7. The fine sand was compacted in the visualization model at a void ratio, dry density and relative density of 0.62, 1.68 g/cm^3 and 54%, respectively. When the plug was removed, the dry fine sand immediately flowed out the slot perforation. The sand flowing out of the visualization model formed a flow pattern that extended from the top of the slot perforation to the top of the sand in a parabolic shape. A sketch of the flow pattern is provided in Figure 4-2. A "V" shape formed at the top of the sand as sand flowed out the slot perforation. Plate 4-2 provides a view of the "V" shape formed in the dry fine sand in the second visualization model under the conditions described above. The sand flowed out of the model in 30 seconds which corresponds to a rate of sand flow of 34.5 g/sec. All the sand flowed out of the visualization model except for sand remaining in the bottom corners of the model. No mechanism of arching, bridging or plugging was observed as sand flowed through the slot perforation. The slot perforation remained clear of obstructions created by sand particles throughout the test. The behavior of the sand during this test was very similar to that of Test #10. Test #10 was essentially the same as this test, except the first visualization model was used. However, Test #2 using the second visualization model had a sand flow rate of 34.5 g/sec while Test #10 had a rate of sand flow of 15.5 g/sec. This indicates that under similar conditions of no confining stress applied, dry sand compacted to higher relative densities exhibits higher sand flow rates. The results of Test #10 are described in detail in Section 4.1.2.1.1 Fine Sand. Thus, the fine sand behaved in the same manner in both the first and second visualization models showing no signs of arching or plugging. The results of Test #2 are summarized in Table 4-4.

4.3.1.2 Medium Sand

The purpose of Test #3 was to examine the behavior of the dry medium sand at a slot perforation without confining stress applied using the second visualization model design and compare it to the behavior observed under the same conditions using the first visualization model. A 5 mm wide slot perforation was used resulting in a grain diameter to width of opening ratio of 1:4.2. The medium sand had a void ratio, dry density and relative density of 0.58, 1.70 g/cm^3 and 39%, respectively. Similar to Test #2, when the plug was removed, the dry medium sand immediately flowed out the slot perforation. Again, a parabolic flow pattern, presented in Figure 4-2, was observed as the sand flowed out of the model. The typical "V" shape was observed at the top of the sand as the sand flowed out of the model in 45 seconds. This resulted in a rate of sand flow of 23.1 g/sec. No sand arching or plugging was observed as sand flowed out the slot perforation. With regard to sand behavior, the results of this test were very similar to the results of Test #9 using the first visualization model. However, the rate of sand flow for Tests #3 and #9 were 23.1 g/sec and 11.8 g/sec, respectively. This supports the earlier conclusion that dry sands compacted to higher relative densities exhibit higher sand flow rates under conditions of no confining stress. The results of Test #9 are described in detail in Section 4.1.2.1.2 Medium Sand. Thus, the medium sand behaved in the same manner in both the first and second visualization models showing no signs of arching or plugging. The results of Test #3 are summarized in Table 4-4.

4.3.1.3 Coarse Sand

The purpose of Test #4 was to examine the behavior of the dry coarse sand at a slot perforation without confining stress applied using the second visualization model design and compare it to the behavior observed under the same conditions using the first visualization model. The slot perforation was 5 mm wide and the resulting grain diameter to width of opening ratio was 1:3.1. The coarse sand was compacted in the visualization model at a void ratio of 0.63 and an associated dry density of 1.66 g/cm^3. The calculated relative density was equal to 53%. When the plug was removed, a small quantity of sand passed through the slot perforation followed by the formation of an arch over the slot perforation. No obstructions created by sand grains were present along the height of the slot perforation. A sketch of a typical arch formed by dry coarse sand over a 5 mm wide slot perforation is provided in Figure 4-3 and pictures of two typical arches are presented in

Plate 4-3. Sand flow resumed when the face of the visualization model was tapped with a rubber hammer. The sand flowed for a short period of time and ceased when another arch formed over the slot perforation. The cycle of destruction of the arch due to vibration, a short period of sand flow, followed by the reformation of an arch was repeated until all sand, except for what remained in the bottom corners, flowed out of the model. A "V" shape gradually formed at the top of the sand as more and more sand flowed out of the model. A parabolic flow pattern, presented in Figure 4-3, extending from the top of the slot perforation to the top of the sand was observed. Test #4 provided results that were essentially the same as the behavior that was observed in Test #14 using the first visualization model. The results of Test #14 are described in detail in Section 4.1.2.1.3 Coarse Sand. This further confirms the observation made using the first visualization model that sand in a dry state, subjected to no confining stress or flow conditions, will not exhibit arching behavior until the slot perforation is less than four times the sand grain diameter.

The purpose of Test #5 was to examine the behavior of the coarse sand under the same conditions described in Test #4 with the exception that the slot width was increased to 12.7 mm (1/2 inch). The resulting grain diameter to width of opening ratio was 1:7.9. The compacted coarse sand had a void ratio, dry density and relative density of 0.63, 1.66 g/cm^3 and 53%, respectively. When the plug was removed, the coarse dry sand immediately flowed out the slot perforation in a manner similar to the fine and medium sands in Tests #2 and #3, respectively. Only 13 seconds were required for the sand to flow out of the model, resulting in a rate of sand flow of 80.4 g/sec. The parabolic flow pattern extending from the top of the slot perforation to the top of the sand was observed, as well as the characteristic "V" shape at the top of the sand. This supports the observation that a slot perforation width of less than four times the sand grain diameter is required for uniform dry sand under no confining stress to exhibit arching behavior. The results of Test #4 and #5 are summarized in Table 4-4.

In order to examine the influence of relative density on sand behavior under conditions of dry sand without confining stress applied, similar tests at different relative densities were performed using the first and second visualization models. Tests using the first visualization model were performed at low relative densities in the range of 2% to 13%. These low relative densities were used to observe sand behavior near its loosest state. The behavior of loose sand was determined because under field conditions, once movement of sand occurs at well casing perforations, the sand may be in a loose state. The second visualization model was used to repeat the tests performed using the first visualization model with the exception that higher relative densities were used. Relative densities of approximately 40% to 55% were used with tests using the second visualization model. This range of relative densities was chosen because it would allow the sand behavior to be observed at moderately dense conditions. Thus, the behavior of loose and moderately dense dry sand under no confining stress could be compared.

The effect of relative density on the fine sand was not visible with regard to causing arching or plugging of the sand flow out of the model at relative densities of 2.7% and 54%. The same can be said for the medium sand at relative densities of 12.5% and 39%. The relative density may have had a slight effect that was visible on the coarse sand. Coarse sand at a relative density of 53% formed arches that qualitatively appeared to be slightly more stable than arches formed by coarse sand at a relative density of 5.7%. However, the effect is qualitative and exerts only a minor influence on overall sand behavior.

Relative density does have an effect on rate of sand flow. In cases where sand flowed continuously out of the visualization model, sand flow rates were higher for sand at higher relative densities. This indicates that under conditions of dry sand with no confining stress applied where sand will flow through a slot perforation, rate of sand flow will be higher for sand at higher relative densities. An increase in relative density means an increase in shear strength and dilation occurring during shearing. It was expected that an increase in relative density would result in a decrease in sand flow rate because more work would have to be done during shearing. However, the opposite behavior was observed and no explanation for this behavior could be ascertained.

4.3.2 Dry Sand With Confining Stress Applied

Tests were performed with the second visualization model and dry sand with confining stress applied. However, it was felt that friction between the sand and the plexiglass was preventing the applied stress from acting directly above the slot perforation. This was overcome by the third visualization model design which eliminated the problem of stress transfer from the sand to the plexiglass box. Thus, the results of tests performed using the second visualization model under these conditions will not be considered or discussed further.

4.4 Third Visualization Model Tests

The third visualization model was essentially the same as the second visualization model with the important modification mentioned earlier that allowed confining stress to be applied effectively. The third visualization model had inside dimensions identical to the second visualization model of 20 mm thick by 150 mm wide by 300 mm high. However, slot perforation height was 70 mm, slot thickness was 20 mm and slot perforation widths of 5 mm, 12.7 mm and 19.1 mm could be used. Several different types of tests were performed using the third visualization model providing a variety of results. Each type of test was designed to examine specific variables that will be discussed in the following sections. In all of the following tests, the slot perforation had a height of 70 mm and a thickness of 20 mm.

4.4.1 Dry Sand With Confining Stress Applied Results

The fine, medium and coarse sands were tested in a dry state with a confining stress up to a maximum of 300 kPa applied. No tests were conducted without confining stress because these tests had already been performed using the second visualization model. These tests using the third visualization model were performed in order to determine the influence of confining stress on the ability of dry sand to form an arch and investigate the effect of increased confining stress on arch stability. The procedure followed during these tests is outlined in Section 3.3.2 Dry Sand with Confining Stress Applied.

Relative densities in the range of 65-85% were intended to be used in tests performed using the third visualization model. This small range of relative densities was higher than any relative densities previously used during testing with the first and second visualization models and was chosen as it was closer to initial field conditions. This range of relative densities does not model all field conditions but the scope of this thesis did not include the entire range of densities possible. In future work the full density range of the sand should be examined and the effects of relative density investigated more thoroughly.

4.4.1.1 Fine Sand

The purpose of Test #57 was to determine if applying a confining stress of 200 kPa to dry fine sand would alter the behavior of the sand and induce arching over the slot perforation. The slot perforation was 5 mm wide which resulted in a grain diameter to width of opening ratio of 1:16.7. The compacted fine sand had a void ratio, dry density and relative density of 0.63, 1.67 g/cm^3 and 49%, respectively. When the plug was removed, the dry fine sand immediately flowed out the slot perforation. No mechanism of arching or plugging was observed as the sand flowed out of the model at a rate of sand flow of 28.9 g/sec. The slot perforation remained clear of obstructions throughout the test.

The behavior of the sand was very similar to the behavior of the sand in Test #2 when no confining stress was applied, with one exception. The flow pattern when no confining stress was applied was a parabolic shape extending from the top of the slot perforation to the top of the sand, as presented in Figure 4-2. The flow pattern in this test with a confining stress applied formed a dome shape over the slot perforation. Sand moved inward from the sides of the visualization model in a dome shape and then flowed out through the slot perforation. A sketch of this dome shaped sand flow pattern is presented in Figure 4-4. However, the presence of a confining stress of 200 kPa acting on the fine sand had no other appreciable effect on the behavior of the sand. The results of Test #57 are summarized in Table 4-5.

Test #64 was identical to Test #57 but the confining stress applied was increased to 300 kPa. The fine sand was compacted in the visualization model at a void ratio, dry density and relative density of 0.57, 1.73 g/cm^3 and 74%, respectively. The results of Test #64 were very similar to the results of Test #57 and therefore will not be repeated. However, the rate of sand flow in Test #64 was 7.4 g/sec, compared to a value of 28.9 g/sec in Test #57. Thus, the dry fine sand at a higher confining stress had a lower rate of sand flow. The increase to a confining stress of 300 kPa acting on the sand altered the rate of sand flow but did not effect the behavior of the sand with respect to flow or nonflow through the slot perforation. The results of Test #64 are summarized in Table 4-5.

4.4.1.2 Medium Sand

The purpose of Test #51 was to determine if applying a confining stress of 100 kPa to dry medium sand would alter the behavior of the sand and induce arching over the slot perforation. A 5 mm wide slot perforation resulting in a grain diameter to width of opening ratio of 1:4.2 was used. The fine sand was compacted in the visualization model at a void ratio, dry density and relative density of 0.52, 1.77 g/cm^3 and 71%, respectively. When the plug was removed, the dry medium sand immediately flowed out the slot perforation. The rate of sand flow was 20.3 g/sec. The behavior of the sand was very similar to the behavior of the sand in Test #3 when no confining stress was applied with the exception that Test #51 exhibited a dome shaped flow pattern presented in Figure 4-4. The change in sand flow pattern will be discussed later in this section. However, the presence of a confining stress of 100 kPa acting on the medium sand had no other appreciable effect on the behavior of the sand with regard to causing arching at the slot perforation.

Test #54 was identical to Test #51 but the confining stress applied was increased to 200 kPa. The compacted medium sand had a void ratio, dry density and relative density of 0.55, 1.75 g/cm^3 and 62%, respectively. The results of Test #54 were very similar to the results of Test #51 with the sand flowing out of the model at a rate of sand flow of 15.3 g/sec and therefore will not be repeated. Thus, as was the case with a confining stress of 100 kPa, the presence of a confining stress of 200 kPa acting on the medium sand had no appreciable effect on the behavior of the sand.

As with the fine sand, dry medium sand under higher confining stresses exhibited lower rates of sand flow. Test #51 at a confining stress of 100 kPa had a rate of sand flow of 20.3 g/sec while Test #54 at a confining stress of 200 kPa had a sand flow rate of only 15.3 g/sec.

Test #65 was identical to Tests #51 and #54 but the confining stress applied was increased to 300 kPa. The medium sand was compacted in the visualization model at a void ratio of 0.52 and an associated dry density of 1.78 g/cm^3. The calculated relative density was equal to 75%. The results of Test #65 were again very similar to the results of Tests #51 and #54 with the only difference being a change in rate of sand flow. The rate of sand flow in Test #65 was 15.5 g/sec. The presence of a confining stress of 300 kPa acting on the medium sand had no appreciable effect on the behavior of the sand with regard to causing arching at the slot perforation. The results of Tests #51, #54 and #65 are summarized in Table 4-5.

It is possible to compare the sand flow rates at different confining stresses for both the fine and medium sands. Tests #2, #57 and #56 utilizing the fine sand at confining stresses of 0, 200 and 300 kPa had sand flow rates of 34.5, 28.9 and 7.4 g/sec, respectively. As well, Tests #3, #51, #54 and #65 using the medium sand at confining stresses of 0, 100, 200 and 300 kPa, respectively had rates of sand flow of 23.1, 20.3, 15.3 and 15.5 g/sec, respectively. Due to the increased confining stress applied to the sand, increased interparticle stresses are present and the sand has a larger shear strength. When the slot perforation was opened and the sand began to flow through, sand at higher confining stresses flowed at a slower rate. It may be postulated that the confining stress could be increased to a large enough value that the intergranular shear strength could prevent sand flow. Such an action may not be true arching but a bridging phenomena.

When no confining stress was applied to the fine, medium and coarse sands under dry conditions, a parabolic sand flow pattern extending from the top of the slot perforation to the top of the sand was visible when sand flow occurred. A sketch of the parabolic sand flow pattern is presented in Figure 4-2. However, when a confining stress was applied to the sands under similar conditions, a dome shaped flow pattern was observed when sand flowed through the slot perforation. A sketch of the dome shaped flow pattern is provided in Figure 4-4. In the dome shaped flow pattern, sand moves inward from the sides of the visualization model in a dome shape and then flows out through the slot perforation.

When no confining stress is applied, the flow of sand out of the visualization model is accompanied by a shear failure along two surfaces of sliding as described by Terzaghi (1943). In his trap door experiment, Terzaghi describes the movement of sand particles as soon as the trap door yields sufficiently. He states that in the vicinity of the surface, all the sand grains moved vertically downward. As well, he describes the shape of the surfaces of sliding which are very similar to the boundaries of sand flow indicated on the sketch of the parabolic sand flow pattern (Figure 4-2).

Thus, the parabolic sand flow pattern described in the project is in agreement with the expected pattern of sand flow provided by Terzaghi's explanation of limited sand movement. It is reasonable to assume that this explanation extends to sand flows that are somewhat longer in duration, like those studied during this project.

The change from the parabolic to dome shaped sand flow pattern when a confining stress is applied may be analogous to sand behavior at shallow depth and sand behavior at deeper depths. When a confining stress is applied, it is done so by placing a piston on top of the sand. The piston is loaded with dead weights to achieve the desired confining stress. Once the test is begun by removing the plug from the slot perforation, the plexiglass box is free to slide down the slot perforation blocks. This is to allow the stress transferred by the sand under the piston to the plexiglass, to be returned and applied to the sand above the slot perforation blocks as the plexiglass box slides down. In this configuration, when no arch is formed, the sand directly above the slot perforation blocks is pushed inwards towards the slot perforation. This is due to the effects of wall friction acting on the sand particles. Sand beneath the piston and along the walls remains stationary because it is held in place by wall friction. As the plexiglass box slides down, the sand grains are prevented from traveling further with the plexiglass box by the slot perforation blocks. Thus the sand grains are forced to move in from the sides of the model and flow out through the slot perforation, as illustrated in Figure 4-4. This behavior may be representative of what is seen at depth in the field. The wall friction of the visualization model is similar to the friction generated in the field by stationary sand adjacent to the sand moving towards the perforation. As well, an increase in vertical stress results in an increase in horizontal stresses. The increased horizontal stresses acting on the sand results in greater interparticle stresses and higher shear strength. The higher shear strength may prevent sand grains from flowing in the parabolic shape seen under no confining stress. Instead, the sand grains experience no shearing and move down with the plexiglass box until sufficient stresses are applied to overcome the shear strength and force the sand to move in and flow through the slot perforation.

4.4.1.3 Coarse Sand

The purpose of Test #58 was to examine how the application of confining stresses up to 200 kPa would affect the behavior of the coarse sand. The slot perforation was 5 mm wide resulting in a grain diameter to width of opening ratio of 1:3.1. The compacted coarse sand had a void ratio of 0.62, a dry density of 1.68 g/cm^3 and a relative density of 63%. A confining stress of 100 kPa was initially applied to the coarse sand. When the plug was removed, a small quantity of sand passed through the slot perforation followed by the formation of an arch over the slot perforation. A sketch of a typical arch formed by dry coarse sand over a 5 mm wide slot perforation and the associated parabolic sand flow pattern is presented in Figure 4-3. Similar to tests conducted without confining stress applied, the arch could be destroyed by tapping the visualization model with a rubber hammer. However, more effort was required to destroy an arch with a confining stress of 100 kPa applied. Destruction of an arch was followed by sand flow until another arch was formed over the slot perforation.

After the flow had occurred and an arch had been formed at the 100 kPa confining stress stage, the confining stress was increased to 200 kPa. This had no detrimental effect on the stability of the arch, but may have increased arch stability. Sand flow could be initiated again by tapping with a rubber hammer. More effort was required to destroy an arch under a confining stress of 200 kPa than an arch with a confining stress of only 100 kPa applied to it.

In Test #66 a confining stress of 300 kPa was applied initially to the coarse sand. A 5 mm wide slot perforation was used. The coarse sand had a void ratio, dry density and relative density of 0.59, 1.70 g/cm^3 and 75%, respectively. When the plug was removed, a very small quantity of sand passed through the slot perforation followed by the formation of an arch over the slot perforation. The arch could be destroyed by tapping the visualization model with a rubber hammer. More effort was required to destroy an arch with a confining stress of 300 kPa than an arch with a confining stress of only 200 kPa applied. Destruction of an arch was followed by short sand flow until another arch was formed. Thus, for the stress range considered, increased confining stress resulted in increased arch stability. However, increasing confining stress did not affect the behavior of dry coarse sand with regard to flow or nonflow through the slot perforation. The results of Tests #58 and #66 are summarized in Table 4-5.

Higher confining stresses result in increased intergranular stresses which result in a better interlocking of sand grains and higher intergranular shear strength. The effects of increased intergranular shear strength is improved arch stability. As well, it is more difficult for the sand to dilate at higher confining stresses. Thus, sand grains have greater difficulty sliding and rolling over each other during shear. The dry sand direct shear tests discussed in Section 3.1.5 show this behavior. The volume change behavior results, provided in Appendix A, indicated that the amount of dilation decreased as confining stress increased for all sands. As well, peak and residual shear strength increased as confining stress increased. The inability of sand grains to slide and roll past each other prevents the arch from breaking down because the sand grains are trapped inside the arch structure. Thus, an increase in confining stress results in improved arch stability because a greater shear stress is required to cause dilation of the sand grains and overcome the intergranular stresses.

Relative density also has an effect on arch stability. At low relative densities, the sand grains would be packed more loosely. This would allow the sand grains to roll and slide around each other with greater ease. That is, sand grains would be able to move into the voids and spaces present between sand grains due to the loose packing. At higher relative densities, it would be more difficult for sand grains to move because of the tight packing and close contact of the sand grains. Thus, sand at higher relative densities should create more stable arches than sand at lower relative densities.

Grain size and shape also have an influence on arch stability. In order for the arch to break down, the sand grains must break free of the arch structure. In some cases the sand grains may simply fall out, but the majority of sand grains must first slide or roll over adjoining grains before they are free to leave the arch structure. The arch collapses after sufficient sand grains are removed. Larger sand grains would require greater degrees of dilation before the grains could break free. This is simply because the grains are larger, so they have to travel farther before the grains could escape from the arch structure. Thus, larger sand grains would experience a more difficult time moving in the arch structure than smaller grains and the stability of arches formed using larger grains would be better.

Angular sand grains form more stable arches than rounded grains because they are able to form a structure with better interlocking between sand grains. The rounded grains are smooth and have no way of lodging themselves with other sand grains, whereas the angular grains are irregular in shape and can form an interlocking structure which requires greater stress to break down the interlocked sand grains.

4.4.2 Fully Saturated Water Flow Test Results

In previous tests, dry coarse sand was observed to form an arch over a slot perforation 5 mm wide. The purpose of Test #73A was to determine how the behavior of the sand would change if the coarse sand was saturated with water and a constant water flow was applied to the sand. No confining stress was applied. The procedure followed during this test is described in detail in Section 3.3.3 Fully Saturated Water Flow Tests. The slot perforation was 5 mm wide and 50 mm long. This slot width resulted in a grain diameter to width of opening ratio of 1:3.1. No measurements of mass or volume were taken in Test #73A and thus void ratio, dry density and relative density values are not available.

When the plug was removed, an initial sand flow occurred followed by the formation of an arch. The water flow rate was set at 3.0 L/min. Similar to tests using dry sand, the arch could be destroyed by tapping with a hammer. The arch remained stable as the flow rate was gradually increased to a flow rate of 8.3 L/min in 0.4 L/min increments. However, a rapid increase from a flow rate of 8.3 L/min to 10.2 L/min caused the destruction of the arch and the continuous flow of all remaining sand out of the visualization model. Based on the results of this test, destruction of sand arches will take place with water flow.

During the fully saturated water flow test it was observed that the arch formed remained stable as the flow rate was gradually increased from 3.0 to 8.3 L/min. However, a rapid increase from 8.3 to 10.2 L/min caused the destruction of the arch. Tippie and Kohlhaas (1973) reported similar findings. That is, they found that gradual rate increases resulted in higher sand free production when compared to sudden increases to full rate. It is expected that a rapid increase of water flow during the initial stages of the fully saturated water flow test would have resulted in the destruction of the arch.

Durrett et al. (1976) provide an explanation regarding transport of sand grains due to drag forces. Once a stable arch has been formed, the arch will remain established until the forces tending to break down the arch exceed the forces tending to maintain the arch. The forces tending to break down the arch are the drag forces of the produced fluid. Fluid drag forces are made up of skin drag (friction) and form drag (inertia) forces. Skin drag predominates at low flow rates, while form drag forces are more significant at higher flow rates. Durrett et al. (1976) point out that as produced fluid flows through a porous body, a critical velocity is reached where unit pressure loss in hindered flow is sufficient to overcome the forces tending to maintain the arch. These forces tending to maintain the arch are identified as the holding forces and include intergranular friction forces and capillary cohesion forces. Capillary cohesion forces are present only when two fluids occupy the voids of the sand mass.

Durrett et al. performed tests which allowed them to apply pressure loss to a projected area of sand particle. This allowed the drag force acting on the particle to be determined. They state that critical fluidization velocity for a particle has been reached when the drag forces equal the holding force. They also calculated a critical transport velocity for sand transport in an open channel (i.e. unhindered flow) that is described by Stokes' law (settling of particles). Figure 2-6 shows these fluidization and critical transport velocities for water flow plotted against grain size.

The flow rates measured during the fully saturated water flow test were converted to apparent water velocity by dividing these values by the cross-sectional area of the slot perforation, 30 cm^2. These apparent water velocities were plotted (Figure 4-5) against a sand size of 1600 microns (the D_{50} of the coarse sand) on the fluidization and critical transport velocity plot presented by Durrett et al. (1976). The dashed lines in Figure 4-5 indicate the full grain size range of the coarse sand. Looking at the upper grain size of 2400 microns, apparent water velocities of 0.55 ft/sec and 1.51 ft/sec (which correspond to flow rates of 3.0 L/min and 8.3 L/min, respectively) are below the critical transport velocity for the coarse sand. At these apparent water velocities during the fully water saturated water flow tests, the arch created by the coarse sand was stable. However, an increase to an apparent water velocity of 1.86 ft/sec (which corresponds to a flow rate of 10.2 L/min) was beyond the critical velocity of the coarse sand. Consequently, this increase in apparent water velocity resulted in the destruction of the previously stable arch. Figure 4-5 indicates that the larger grain sizes in the coarse sand appear to have the greatest influence on arch resistance to water flow because it is this grain size which exhibits the boundary between flow and nonflow based on critical transport velocity.

Thus, the behavior of the sand observed during these tests with regard to stability and destruction of arches agrees well with the data presented by Durrett et al. (1976).

Stable arches are broken down when the apparent velocity of the producing fluid, in this case water, exceeds the critical transport velocity for the sand size.

The arch failure can also be explained in terms of changes in effective stress. An increased flow rate of water through the sand structure results in increased pore pressure. The increased pore pressure results in decreased effective stress as total stress remains constant. When the pore pressure equals the total stress, the effective frictional shear strength will be zero and the arch will fail. This approach which uses total stress and pore pressure to determine failure conditions and the previous explanation which utilized drag forces created by seepage forces will provide identical results. Seepage force does not appear in the effective stress approach but that does not mean that the effects of seepage are not cared for (Taylor, 1948). Taylor (op cit) provides a detailed discussion and analysis regarding the agreement between the two approaches.

Intergranular friction forces are included in the holding forces which tend to maintain the arch. The fully saturated water flow test was performed without a confining stress applied. It is expected that a higher water flow rate through the sand may have been attained if a confining stress had been applied to the sand mass. Confining stress has the effect of increasing the intergranular forces between sand grains, thereby tending to lock the sand grains in place. In geotechnical terms, a confining stress applies an effective stress to the sand which increases the shear strength of the sand. The stability of an arch is dependent on the shear strength of the sand. Such was the case during tests with dry sand and confining stress applied where arches formed at higher confining stresses were more stable. Thus, the higher intergranular frictional shear strength would have been able to withstand the higher drag forces of a faster flow rate.

4.4.3 Upward Air Flow Test Results

All upward air flow test results are provided in Appendix C along with analysis, discussion and conclusions related to these tests. It was concluded that the sand behavior observed during these tests was not an arching phenomena. Instead, it is believed that fluidization of the sand was being observed. For this reason, the discussion of the upward air flow tests was confined to Appendix C.

4.4.4 Partial Saturation Arching Test Results

4.4.4.1 Gas-Water Saturation Tests

All tests conducted to investigate air-water capillary action utilized only the fine sand under conditions of a 20 mm thick and a 12.7 mm (1/2 inch) wide slot perforation and no confining stress applied. Thus, all tests had a grain diameter to width of opening ratio of 1:42.3. However, the degree of saturation was varied for each test to determine the effect of interfacial tension forces on sand stability. In previous tests using 5 mm and 12.7 mm wide slot perforations, the fine sand flowed freely through the slot perforation when the sand was either completely dry or completely water saturated. The purpose of Tests #93 to #103 was to determine what degree of gas-water saturation would cause the sand to arch over the slot perforation. In Tests #93 to #96, an air hose was attached to the top of the visualization model in order to supply a flow of air down through the sand and out the slot perforation. The procedure followed during all the tests described below is detailed in Section 3.3.5.1 Gas-Water Saturation Tests.

The degree of water saturation in Test #93 was 30%. The compacted fine sand had a void ratio, dry density and relative density of 0.63, 1.66 g/cm^3 and 45%, respectively. The fine sand showed no flow or movement of sand when the plug was removed from the slot perforation. When the downward air flow was applied, water originally located around sand at the top of the model was pushed down towards the bottom of the model and the water began to saturate the sand over the slot perforation. The sand directly over the slot perforation dropped out of the slot perforation when it visually appeared that the sand was almost fully saturated. The falling sand created a dome shaped cavity in the sand over the slot perforation. As the downward air flow was increased, more sand dropped out of the slot perforation and the cavity size increased accordingly. When downward air flow was increased even further, the top of the cavity failed and the sand above, which had been dried by the downward air flow, flowed into the cavity and out the slot perforation. The walls of the cavity remained stable after the top of the cavity had failed.

Test #94 utilized a degree of water saturation of 18%. The fine sand was compacted in the visualization model at a void ratio, dry density and relative density of 0.62, 1.68 g/cm^3 and 54%, respectively. The fine sand at this saturation showed behavior similar to the sand in Test #93 when the plug was removed and when subjected to the same conditions of downward air flow.

The degree of water saturation in Test #95 was 9.0%. The compacted fine sand had a void ratio, dry density and relative density of 0.64, 1.66 g/cm^3 and 45%, respectively. The fine sand at this saturation showed behavior similar to the sand in Tests #93 and #94 when the plug was removed and subjected to the same conditions of downward air flow. After the downward air flow had caused a small amount of sand to fall out and a dome shaped cavity to form over the slot perforation, the visualization model was tapped with a rubber hammer. This caused sand to fall out of the slot perforation forming a much larger cavity. Further tapping created larger cavities to a maximum of 4 cm high and 2.5 cm wide. When the model was tapped with the hammer, the sand inside the cavity failed but the failed sand formed a loose bridge over the slot instead of flowing out. This resulted in additional failed material from the cavity walls building up over the bridge formed by previously failed sand. This was the only test in which failed sand from the walls of a cavity formed a blockage over the slot perforation instead of flowing out.

Test #96 had a degree of water saturation of 3.8% and a void ratio , dry density and relative density of 0.61, 1.69 g/cm^3 and 58%, respectively. This test showed the same behavior of initially bridging over the slot perforation after the plug was removed. A downward air flow was applied and the results were similar to previous tests at higher saturations.

The degree of water saturation in Test #97 was 1.2%. The fine sand was compacted in the visualization model resulting in a void ratio, dry density and relative density of 0.63, 1.67g/cm^3 and 49%, respectively. This test showed the same behavior of initially bridging over the slot perforation after the plug was removed. This test did not have a downward air flow applied, but the model was tapped with a hammer. This resulted in the same behavior observed during tests at higher saturations of causing sand to fall out of the slot perforation forming a larger arch. The arch would grow in width and height with successive tapping. Figure 4-6 provides sketches of the typical growth of an arch formed by partially gas-water saturated fine sand at low gas saturations due to vibration and Plate 4-4 provides a picture of the arch after a moderate amount of vibration.

The degree of water saturation in Test #98 was 0.56%. The fine sand was placed in the visualization model at a void ratio of 0.57 and an associated dry density of 1.73 g/cm^3. The calculated relative density was equal to 74%. This test showed the same behavior of initially bridging over the slot perforation after the plug was removed. This test did not have a downward air flow applied, but the model was tapped with a hammer. Tapping the model resulted in behavior similar to tests using higher saturations.

Test #100 was performed to confirm the results observed in Test #98. The degree of water saturation in Test #100 was 0.64% and the void ratio, dry density and relative density of the compacted fine sand were 0.57, 1.66 g/cm^3 and 46%, respectively. This test confirmed the findings of Test #98 by provided identical results with the sand forming an arch over the slot perforation.

Test #99 was performed at a degree of water saturation of 0.29%. The fine sand was compacted in the visualization model at a void ratio, dry density and relative density of 0.60, 1.70 g/cm^3 and 62%, respectively. The fine sand flowed out of the model in a manner similar to dry sand when the plug was removed. There were small areas of sand exhibiting cohesion visible in the sand remaining in the model.

Test #101 was performed to confirm the results observed in Test #99. The degree of water saturation in Test #101 was 0.25%. The compacted fine sand had a void ratio, dry density and relative density of 0.59, 1.71 g/cm^3 and 66%, respectively. This test confirmed the findings of Test #99 by provided identical results with the sand flowing out of the model.

Test #103 was performed at a degree of water saturation of 0.45%. This degree of water saturation was chosen because it was positioned approximately at the midpoint between the degrees of water saturation that showed two distinct behaviors of either flow or non-flow of sand. The fine sand was compacted in the visualization model at a void ratio of 0.61 and an associated dry density of 1.69 g/cm^3. The calculated relative density was equal to 56%. Initially, this test showed behavior similar to the tests using higher degrees of water saturation by forming an arch over the slot perforation. However, a slight vibration caused the test to follow the behavior of the tests with lower degrees of water saturation by flowing out of the model. Thus, the degree of water saturation equal to 0.45% may lie on the boundary between flow or non-flow behavior. The results of Tests #93 through #101 and #103 are summarized in Table 4-6.

4.4.4.2 Oil-Water Saturation Tests

All tests conducted to investigate water-oil capillary action utilized only the fine sand under conditions of a 20 mm thick and a 12.7 mm (1/2 inch) wide slot perforation and no confining stress applied. A gear oil with a viscosity of 3600 mPa*s at 25°C was used. In these tests, water was the wetting fluid and oil was the non-wetting fluid. All tests had a grain diameter to width of opening ratio of 1:42.3. However, the degree of oil saturation was varied for each test to determine the effect of interfacial tension forces on sand stability. In previous tests using a 12.7 mm wide slot perforation, the fine sand flowed freely through the slot perforation when the sand was either completely dry or completely water saturated. However, sand with a degree of water saturation of 0.45% exhibited arching behavior while sand with a degree of water saturation of 0.25% flowed freely through the slot perforation. Tests investigating oil-water interfacial tension were performed using both non-saline and saline water. The saline water was used to duplicate reservoir conditions and determine if the presence of saline water would affect sand behavior. Finally, tests which attempted to achieve a constant water flow rate of 17 mL/min in order to model a standard field production rate were performed. The procedure followed during these tests is described in detail in Section 3.3.5.2 Oil-Water Saturation Tests. Difficulties were encountered in preparing oil/water/sand mixtures that were completely saturated with oil and water only, due to air entrainment in the mixing process. This resulted in some gas remaining in the oil/water/sand mixture during testing. Extraction tests performed at the end of each test allowed the degrees of oil, water and gas saturation to be calculated.

4.4.4.2.1 Water-Oil Capillary Results (Nonsaline Water, No Flow)

Test #110 was conducted using only water saturated sand. No oil was present. Fresh water was used for the nonsaline water tests. The purpose of Test #110 was to provide a baseline behavior by which the following tests with varying degrees of oil saturation could be compared. The fine sand was compacted in the visualization model at a void ratio, dry density and relative density of 0.55, 1.75 g/cm^3 and 81%, respectively. When the plug was removed, the fine sand flowed out the slot perforation in the same manner observed in previous tests conducted using fully water saturated fine sand. The fully water saturated fine sand did not form any type of arch structure over the slot perforation.

The purpose of Tests #112, #113, #114 and #116 was to determine what degree of oil saturation would cause the sand to arch over the slot perforation. The degree of oil saturation in Test #112 was 17.1% and the degrees of water and gas saturation were 68.2% and 14.7%, respectively. The compacted fine sand had a void ratio, dry density and relative density of 0.57, 1.71 g/cm^3 and 66%, respectively. When the plug was removed, the sand immediately arched over the slot perforation. The arch that formed was very stable and tapping the model with a hammer had no effect on arch stability. A sketch of the typical arch formed by partially oil-water saturated fine sand is presented in Figure 4-7.

The degree of oil saturation in Test #113 was 5.5%. The degrees of water and gas saturation were 84.7% and 9.8%, respectively The compacted fine sand had a void ratio, dry density and relative density of 0.55, 1.75 g/cm^3 and 81%, respectively. The fine sand at this oil saturation showed behavior similar to the sand in Test #112. A small amount of sand fell out the slot perforation when the plug was removed, followed by the formation of an arch over the slot perforation. Tapping the model with a hammer did not affect the stability of the arch. The sand that did pass through the slot perforation fell out in small clumps, 2 to 3 mm in diameter. This was unlike dry or completely water saturated sand flows that consisted of a flow of individual sand grains.

The degree of oil saturation in Test #116 was 3.1% and the degrees of water and gas satuartion were 94.2% and 2.6%, respectively. The fine sand was compacted in the visualization model at a void ratio, dry density and relative density of 0.57, 1.73 g/cm^3 and 71%, respectively. The results of this test were very similar to the results of Test #113. A small amount of sand fell out the slot perforation when the plug was removed, followed by the formation of an arch over the slot perforation. Tapping the model with a hammer did not affect the stability of the arch. The visualization model was filled with water in order to determine if a small head of water acting on the sand could destroy the arch. When the water was added to the visualization model, the arch was destroyed and sand began to flow out of the slot perforation when the head difference was approximately 2.5 cm.. The flow of sand through the slot perforation fell out in small clumps, 2 to 3 mm in diameter. This was unlike dry or completely water saturated sand flows that were a continuous flow of sand grains.

The degree of oil saturation in Test #114 was 1.0%. The degree of water saturation was calcualted to be 99.0% indicating that no gas was present in this sample. The compacted fine sand was placed in the visualization model at a void ratio, dry density and relative density of 0.57, 1.73 g/cm^3 and 74%, respectively. When the plug was removed, the fine sand flowed out of the slot perforation. The flow of sand out of the model was similar to what was described in Test #116 but the effect was not as pronounced as the sand appeared to flow in a more continuous fashion. The results of Tests #110, #112, #113, #116 and #114 are summarized in Table 4-7.

4.4.4.2.2 Water-Oil Capillary Results (Saline Water, No Flow)

The purpose of Tests #122B, #124 and #123 was to determine if using water with a saline concentration similar to reservoir conditions would alter the behavior observed in Tests #110 to #114 and #116. A saline concentration of 7.2 g/L was used to represent general reservoir conditions.

Test #122B was essentially the same as Test #110 except saline water was used. Test #122B was conducted using only water saturated sand. No oil was present. The fine sand was placed in the visualization model at a void ratio of 0.51 and an associated dry density of 1.79 g/cm^3. The calculated relative density was equal to 96%. The presence of saline water had no effect as the sand flowed out the slot perforation in the same manner observed when non-saline water was used.

Test #124 was essentially the same as Test #116 except saline water was used. The degree of oil saturation in Test #124 was 3.3% and the degrees of water and gas saturation were 95.8% and 0.9%. The compacted fine sand had a void ratio, dry density and relative density of 0.55, 1.75 g/cm^3 and 81%, respectively. Again, the saline water had no effect on sand behavior. A small amount of sand fell out the slot perforation when the plug was removed, followed by the formation of an arch over the slot perforation. Tapping the model with a hammer did not affect the stability of the arch. The visualization model was filled with water in order to determine if a small head of water acting on the sand could destroy the arch. The arch was destroyed and sand began to flow out of the slot perforation when the head difference was approximately 1.0 cm.. The flow of sand through the slot perforation fell out in small clumps, 2 to 3 mm in diameter.

Test #123 was essentially the same as Test #114 except saline water was used. The degree of oil saturation in Test #123 was 1.4%. The degree of water saturation was 98.6% indicating no gas was present within the sample. The fine sand was compacted in the visualization model at a void ratio, dry density and relative density of 0.53, 1.77 g/cm^3 and

89%, respectively. Again, the saline water had no effect. When the plug was removed, the fine sand immediately flowed out of the slot perforation. The flow of sand out of the model was similar to the results described in Test #114. The results of Tests #122B, #124, and #123 are summarized in Table 4-7.

4.4.4.2.3 Water-Oil Capillary Results (Nonsaline Water, Flow Applied)

The purpose of Tests #118, #119, #121 and #122 was to place fine sand in the visualization model at a specific degree of oil saturation and apply a flow of water to the model, such that a flow rate of 17 mL/min was passing through the sand. A flow rate of 17 mL/min corresponds to a production rate of 5 m^3/day from a casing interval 5 metres high, perforated at 39 shots per metre. Tests #118 and #119 used a water flow system controlled by a flow meter connected directly to a tap. Tests #121 and #122 had manometers attached during the test and used a constant head tank as a water flow system. Fresh water was used during these tests.

The degree of oil saturation used in Test #118 was 3.8% and the degrees of water and gas saturation were 93.9% and 2.3%, respectively. The fine sand was placed in the visualization model at a void ratio of 0.55 and an associated dry density of 1.75 g/cm^3. The calculated relative density was equal to 81%. As the plug was removed, a low water flow was applied to the visualization model. The sand flowed out of the model as soon as the plug was removed. In earlier tests without water flow, the sand formed an arch over the slot perforation. The sand that flowed out of the model created a failure void with a parabolic shape that extended from the top of the slot perforation to the top of the sand. The failure void was approximately 3 cm wide at mid-height and at the top of the sand. The sand flowed out of the visualization model in clumps rather than in a continuous flow.

The degree of oil saturation in Test #119 was 41.2%. The degrees of water and gas saturation were 38.6% and 20.2%, respectively. The fine sand was compacted in the visualization model at a void ratio, dry density and relative density of 0.63, 1.66 g/cm^3 and 45%, respectively. When the plug was removed, a small quantity of sand moved through the slot perforation. A low water flow was initiated, causing clumps of sand to fall through the slot perforation. The flow rate was immeasurable at this time. Eventually, the water forced a failure void to form through the sand. The failure void had the same general shape described in the results of Test #118.

The degree of oil saturation in Test #121 was 4.9% and the degrees of water and gas saturation were 92.0% and 3.1%, respectively. The compacted fine sand had a void ratio, dry density and relative density of 0.55, 1.75 g/cm^3 and 81%, respectively. The manometers showed a quick response when the constant head tank was adjusted indicating reliable readings could be attained from the manometers. The flow system was set at a hydraulic gradient of 6.0 and the plug was removed. The sand flowed out the slot perforation leaving a failure void similar to what was described in Test #118. Since the sand immediately flowed out of the visualization model, no manometer readings were noted.

The degree of oil saturation in Test #122 was 14.2%. The degree of water saturation was calculated to be 85.8% indicating that no air was present in the sample. The fine sand was compacted in the visualization model at a void ratio, dry density and relative density of 0.53, 1.77 g/cm^3 and 89%, respectively. The manometers did not show a quick or accurate response when the constant head tank was adjusted. The set-up was left overnight at a hydraulic gradient of 5.2 in order to allow the manometers to equalize. However, the manometers failed to equalize indicating they would not provide useful measurements during the test and no further manometer measurements were taken. With the flow system set at a gradient of 5.2, the plug was removed. The sand flowed out the slot perforation leaving a failure void similar to what was described in Test #118.

The attempt to maintain a constant water flow through oil-water saturated sand proved unsuccessful in all four trials. It was felt that due to high oil viscosity and other limiting factors, a constant water flow through oil-water saturated sand would be very difficult to achieve and therefore, no further trials were performed.

These tests indicate that at degrees of oil saturation ranging from approximately 4% to 46%, the arches formed over the 12.7 mm wide slot perforation are unable to withstand water flow through the oil/water/sand mixture. Flow rates proved to be immeasurable during these tests due to varying circumstances. It should be noted that not only could the oil/water/sand mixture not sustain the water flow, but also the water flow resulted in the flow of the oil/water/sand mixture through the slot perforation. These flows of the oil/water/sand mixture occurred at oil saturations where previously stable arches had been formed. This would indicate that under field conditions, previously stable arches formed over perforations by an oil/water/sand mixture may be destroyed by a water flow. The flow of water would result in the flow of the oil/water/sand mixture through the perforation and into the borehole.

It was expected that the water would be able to flow through the oil/water/sand mixture. However, this was not the case and the forces created by the water flow resulted in the destruction of the arch. A possible explanation for the ability of the water flow to destroy the arch is that the flow of water reduced the degree of oil saturation by displacing the oil from the sand voids, thus resulting in a decrease in the capillary cohesion required to cause arching. However, the oil has a very high viscosity and it is unlikely the water could displace enough oil to sufficiently reduce the capillary cohesion.

A second more likely explanation is that the presence of the highly viscous oil in the voids of the sand results in the water having a more difficult time flowing through the sand mass. The paths for the water to flow through have been decreased or are no longer continuous due to the presence of the oil. This results in the water not being able to flow through the sand voids and it then applys pressure on the sand mass. This increase in pressure results in the destruction of the arch, flow of the oil/water/sand mixture out of the visualization model and the creation of a large failure void to allow the flow of water through the model.

4.5 Index Capillary Cohesion Between Two Fluids in a Sand

In this study, the fall-cone test was used as a strength index test to provide an estimate of capillary cohesion of the fine sand at varying degrees of gas-water, gas-oil and oil-water saturations. It was felt that the results of the fall-cone tests could be used as a relative measure of capillary cohesion. The strength measured by the fall-cone test has been designated the index capillary cohesion. Due to a variation in sample porosities, all index capillary cohesions were corrected to a porosity of 35%. A porosity of 35% is equivalent to a relative density of 85% for the fine sand. It was felt that this porosity would reflect actual formation conditions near the wellbore and perforations reasonably well.

4.5.1 Index Capillary Cohesion Between Gas and Water in Fine Sand

Gas-water tests used air as the non-wetting fluid and water as the wetting fluid. The results of these tests are presented in Figure 4-8. It was observed that the index capillary cohesion increases from 0% to 40% to a maximum of 8.4 kPa and then decreases gradually as gas saturation increases to 100%. The dry densities and relative densities of the gas-water index capillary cohesion tests are summarized in Table 4-8.

4.5.2 Index Capillary Cohesion Between Gas and Heavy Oil in Fine Sand

Gas-heavy oil tests utilized air as the non-wetting fluid and oil with a viscosity of 3600 mPa*s as the wetting fluid. The results of these tests are presented in Figure 4-9. Values of index capillary cohesion at gas saturations below approximately 25% were not attainable due to difficulties associated with air entrainment in the gas/heavy oil/sand mixture. Index capillary cohesion increases from 25% to 45% to a maximum of 6.3 kPa and then decreases gradually as gas saturation increases to 100%. The dry densities and relative densities of the gas-heavy oil index capillary cohesion tests are summarized in Table 4-9.

4.5.3 Index Capillary Cohesion Between Gas and Medium Oil in Fine Sand

Gas-medium oil tests utilized air as the non-wetting fluid and oil with a viscosity of 1300 mPa*s as the wetting fluid. The purpose of using the medium oil was to have a fluid with a viscosity midway between the very low viscosity of water and the high viscosity of the 3600 mPa*s oil in order to determine if fluid viscosity was influencing the fall-cone measurements. The results of these tests are presented in Figure 4-10. Values of index capillary cohesion at gas saturations below approximately 30% were not attainable due to difficulties associated with air entrainment in the gas/medium oil/sand mixture. Index capillary cohesion increases from 30% to 50% to a maximum of 5.5 kPa and then decreases gradually as gas saturation increases to 100%. The dry densities and relative densities of the gas-medium oil index capillary cohesion tests are summarized in Table 4-10.

4.5.4 Index Capillary Cohesion Between Heavy Oil and Water in Fine Sand

Heavy oil-water tests utilized oil with a viscosity of 3600 mPa*s as the non-wetting fluid and water as the wetting fluid. The results are presented in Figure 4-11. Values of index capillary cohesion at water saturations below approximately 40% were not attainable due to difficulties with air entrainment in the water/heavy oil/sand mixture. It was observed that the index capillary cohesion at approximately 40% water saturation was 3.0 kPa. Index capillary cohesion decreased gradually as water saturation was increased to 100%.

The difficulties regarding air entrainment resulted in some gas remaining in the water/heavy oil/sand mixture. Extraction tests performed at the end of each test allowed the degrees of water, oil and gas saturation to be calculated. The 82% water saturation cone test had a degree of oil saturation of 16% and a degree of gas saturation of 2%. This test was performed at a dry density of 1.76 g/cm^3 and an associated relative density of 85%. The 65% water saturation cone test had a degree of oil saturation of 28% and a degree of gas saturation of 7%. This test was performed at a dry density of 1.74 g/cm^3 and an associated relative density of 78%. The 59% water saturation cone test had a degree of oil saturation of 31% and a degree of gas saturation of 10%. This test was performed at a dry density of 1.76 g/cm^3 and an associated relative density of 85%. The 43% water saturation cone test had a degree of oil saturation of 43% and a degree of gas saturation of 14%. This test was performed at a dry density of 1.78 g/cm^3 and an associated relative density of 93%. The 38% water saturation cone test had a degree of oil saturation of 45% and a degree of gas saturation of 18%. This test was performed at a dry density of 1.73 g/cm^3 and an associated relative density of 74%. The dry densities and relative densities of the heavy oil-water index capillary cohesion tests are summarized in Table 4-11.

The results in Figures 4-8, 4-9, 4-10 and 4-11 are for four different sets of saturation fluids. In order to compare these curves, it should be noted that magnitudes of capillary pressures are proportional to the product of the surface tension of the liquid being used and the cosine of its angle of contact against the solid (Purcell, 1949). The ratio between the magnitude of capillary pressures for two liquids would then be:

$$X = \frac{\text{surface tension liquid 1} * \text{cosine contact angle of liquid 1 against solid}}{\text{surface tension liquid 2} * \text{cosine contact angle of liquid 2 against solid}}$$

That is, the magnitude of capillary pressure of liquid 1 should be approximately X times greater than the magnitude of capillary pressure of liquid 2.

The surface tensions and contact angles were measured for water, heavy oil and medium oil. The surface tension of the water was found to be 0.072 N/m and a contact angle of 37° was determined. Distilled water should have a contact angle of 0°. Our measured contact angle of 37° indicates some impurities were present in the water. The heavy oil and medium oil had surface tensions of 0.034 N/m and 0.033 N/m, respectively and contact angles of 39° and 47°, respectively.

These surface tensions, contact angles and the theoretical ratio presented earlier were used to compare the index capillary cohesion curves of gas-water, gas-heavy oil and gas-medium oil saturations found in Figures 4-8, 4-9 and 4-10. Comparisons of gas-heavy oil index capillary cohesion values and gas-medium oil index capillary cohesion values showed good agreement with the theoretical ratio. Comparisons of gas-water index capillary cohesion values with gas-heavy oil and gas-medium oil index capillary cohesion values were not as close to the theoretical ratio but still appeared reasonable. These results indicate that the high viscosity of the heavy and medium oils may have an effect on fall-cone measurements. The comparisons between fluid saturations and theoretical ratios are presented in Table 4-12.

4.6 Capillary Cohesion Direct Shear Tests

Direct shear tests were used to provide a direct measurement of capillary cohesion at varying gas-water saturations. Fine sand was subjected to direct shear tests and the peak and residual shear stresses were measured under confining stresses of 0, 5, 10 and 15 kPa at gas saturations of 100, 40 and 20%. A dry density of 1.76 g/cm^3 (which corresponds to a relative density, D_r, of 85% for the fine sand) was used during all the capillary cohesion direct shear tests with four exceptions. At 100% gas saturation, the 5 kPa confining stress test was at a dry density of 1.74 g/cm^3 (D_r = 78%) and the 10 kPa and 15 kPa confining stress tests were both at a dry density of 1.77 g/cm^3 (D_r = 89%). At the 40% gas saturation, the 12.5 kPa confining stress test was at a dry density of 1.78 g/cm^3 (D_r = 93%). All capillary cohesion direct shear tests were performed at a shear rate of 0.24 mm/min. The procedure followed during these tests is detailed in Section 3.3.7 Capillary Cohesion Direct Shear Tests.

All 100% gas saturation capillary cohesion direct shear tests were at a gas saturation of exactly 100%. The 40% gas saturation capillary cohesion direct shear tests had a slight variation in degree of gas saturation. Tests at 0,5, again at 5, 10, 12.5 and 15 kPa were at gas saturations of 41.5, 40.5, 42.4, 41.6, 41.3 and 41.0%, respectively. The 20% gas saturation capillary cohesion direct shear tests also had a slight variation in degree of gas saturation. Tests at 0, again at 0, 5, 10 and 15 kPa were at gas saturations of 21.7, 21.4, 21.3, 21.7 and 21.4%, respectively.

The results of these direct shear tests are summarized in Table 4-13. The peak and residual angles of internal friction for the fine sand at 100% gas saturation was 40° and 35°, respectively. Both the peak and residual capillary cohesion was zero. The peak and residual angles of internal friction for the fine sand at 40% gas saturation was 38° and 29°, respectively. The peak and residual capillary cohesions (y-intercept) were 3.5 kPa and 1.5 kPa, respectively. The associated peak and residual negative pore pressures (x-intercept) were 4.5 kPa and 2.7 kPa, respectively. The peak and residual angles of internal friction for the fine sand at 20% gas saturation was also 38° and 29°, respectively. The peak and residual capillary cohesions (y-intercept) were 3.0 kPa and 1.9 kPa, respectively. The associated peak and residual negative pore pressures (x-intercept) were 3.8 kPa and 3.4 kPa, respectively. Peak shear strength versus normal stress is plotted in Figure 4-12 and the residual shear strength versus normal stress is provided in Figure 4-13. It should be noted when examining Table 4-13 and Figures 4-12 and 4-13 that the results of the 100% gas saturation tests are in terms of effective stress, while the results of the 40% and 20% gas saturation tests are in terms of total stress as pore pressure was not measured. Plots of shear stress versus shear displacement and specimen thickness changes versus shear displacement for the fine sand under gas saturations of 100, 40 and 20% are presented in Appendix B.

The direct shear test results presented in Appendix B merit discussion. In all three cases, 100, 40 and 20% gas saturations, only a small horizontal displacement was required to reach the peak shear stress. The horizontal displacement required to reach peak shear stress was in the range of 0.5 mm to 1.0 mm for all gas saturations and confining stresses. The total horizontal displacement was sufficient to reach the residual shear strength in all cases. It should be noted that these direct shear test results are not in agreement with conventional shear strength characteristics.

Normally, the point of inflection on a specimen thickness change versus horizontal displacement plot will occur at a horizontal displacement corresponding to the position of the peak shear stress on the shear stress versus horizontal displacement plot. In all the direct shear test results provided in Appendix B, the point of inflection of the specimen thickness change versus horizontal displacement occurs at very small horizontal displacements (generally in the range of 0.1 mm to 0.3 mm). However, peak shear stress occurred in the range of 0.5 mm to 1.0 mm.

The capillary cohesion direct shear tests also differ from conventional results in another aspect. Generally, once the sample has reached residual shear stress, the sample will be shearing at a constant volume. That is, there will be no change in sample height once the residual shear stress is reached. In the capillary cohesion direct shear tests, once the residual shear stress was reached, most samples still indicated a continuing increase in sample height. These variations from conventional shear strength characteristics may be a function of the direct shear tests. Stress concentrations at sample boundaries leading to nonuniform stress concentrations within the test specimen and uncontrolled rotation of principal planes and stresses are just some of the problematic issues inherit in the direct shear tests which may lead to the discrepancies observed in the capillary cohesion direct shear tests compared to conventional shear strength characteristics.

In all cases, except the dry fine sand under a 5 kPa confining stress, the increase in height during shearing is quite small. The increase in height ranges from 0.5 mm to 1.22 mm. This is a small increase in height when compared to the initial height of the samples of 38 mm and 39 mm. Since all tests exhibit an increase in height, this indicates that the shear band may be growing in thickness. The fine sand was compacted to high relative densities (78% to 89%) which would result in sand grains dilating when shearing. That is, sand grains are forced to roll up and over each other, resulting in sand moving upwards and a small increase in sample height being observed. Only the dry fine sand under a 5 kPa confining stress showed a somewhat greater increase in height of 2.5 mm. While this is a larger increase it is still relatively small with respect to the initial sample height of 39 mm. Thus, an increase in the shear band thickness may still account for this behavior.

During shearing of the gas-water saturated fine sand, there may be a loss of capillary cohesion. The fine sand dilates during shearing resulting in sand grains in the shear band moving farther apart as they roll up and over each other during shear. The greater separation of the sand grains would result in a larger radius of curvature of the gas-water interface between sand grains, resulting in lower capillary cohesion. Thus, loss of capillary cohesion may cause the sample to lose shear strength and approach residual strength while the sample is still increasing in height.

As well, water may migrate into the shear surface during shearing. The migration of water may cause some of the voids between the sand grains to become fully water saturated. This would result in an overall decrease in capillary cohesion. If there was no increase in shear band thickness or migration of water into the shear band, it is expected that, similar to the 100% gas saturation tests (with the exception of the 5 kPa confining stress test), the sample would shear at a constant volume once the residual stress was reached.

Direct shear tests on dry fine sand at confining stresses of 50, 150 and 250 kPa and relative densities of 62, 70 and 81%, respectively, resulted in peak and residual angles of internal friction of 35° and 33° (Figures 3-3 and 3-4, respectively). However, direct shear tests on dry fine sand performed during the capillary cohesion direct shear tests at confining stresses of 5, 10 and 15 kPa and relative densities of 78, 89 and 89%, respectively, provided peak and residual angles of internal friction of 40° and 35°, respectively (Figures 4-5 and 4-6, respectively). Comparing peak angles of internal friction, it is known that sand sheared at higher relative densities results in increased angles of peak internal friction. All of the tests mentioned above exhibited dilative behavior during shearing.

Once the sands have reached a state of residual stress, the sand in the shear band deforms at constant volume. Thus, the effects of the initial relative density are small, as seen in the similar residual angles of internal friction obtained from the two sets of tests at varying relative densities, 35° and 33° (high and low initial relative densities, respectively.)

Most of the above direct shear tests performed on dry fine sand resulted in dilative behavior of approximately 0.4 mm to 0.5 mm (Figures A-2 and B-2), the exception being the test at 5 kPa which resulted in an increase in height of 2.5 mm. Figures A-2 and B-2 indicate that dry fine sand at relative densities in the range of 62% to 89% will exhibit dilative behavior. This is reasonable, since the sands were compacted to a fairly high degree of relative density and the sand grains would have to dilate during shear.

The stress-horizontal displacement plots of the dry fine sand performed at lower relative densities show that peak shear stress is reached at 1.0 mm to 3.0 mm of horizontal displacement. However, at higher relative densities, the peak shear strength was attained after only 0.5 mm to 1.0 mm of horizontal displacement. Under higher relative densities, the sand grains are more tightly packed together. Thus, once the direct shear test is initiated, less horizontal displacement is required for the sand grains to dilate.

Table 4-1: Summary of Results From First Visualization Model: Horizontal Orientation

Test No.	Sand Type	Void Ratio	Dry Density	Relative Density	Slot Width	Slot Height	Total Elapsed Time	Hydraulic Gradient	Elapsed Time at Gradient	Flow Rate	Cavity Height	Cavity Width
			(g/cm^3)	(%)	(mm)	(mm)	(min)		(min)	(mL/min)	(cm)	(cm)
2	Fine	0.74	1.56	2.6	5	10	45	0.1	-	-	2.0	4.0
								0.2	-	-	4.0	6.0
								0.4	-	66	8.0	8.0
								0.8	-	-	channel	channel
1d	Fine	0.74	1.56	0.0	5	10	-	1.0	-	-	-	-
4	Medium	0.66	1.63	5.8	5	10	52	0.1	8	104	1.0	2.0
								0.2	8	158	2.1	4.1
								0.4	8	300	4.7	6.0
								0.6	8	476	9.5	6.5
								0.8	10	1131	channel	channel
								1.0	10	1280	channel	channel
12	Medium	0.66	1.63	3.8	5	50	48	0.1	8	133	1.5	2.7
								0.2	8	186	2.5	4.1
								0.4	8	340	6.5	5.5
								0.6	8	500	7.7	5.8
								0.8	8	620	channel	channel
								1.0	8	1460	channel	channel
11	Medium	0.65	1.64	10.6	5	50	340	0.1	60	84	1.3	2.4
								0.2	60	123	1.7	3.0
								0.4	60	237	4.1	5.5
								0.6	60	337	6.0	6.4
								0.8	40	451	channel	channel
								1.0	60	514	channel	channel

Table 4-2: Summary of Results From First Visualization Model: Vertical Orientation - Dry Conditions

Test No.	Sand Type	Void Ratio	Dry Density	Relative Density	Slot Width	Slot Height	Sand Behavior
			(g/cm^3)	(%)	(mm)	(mm)	
1a	Fine	-	-	-	5	10	sand flow through slot perforation
10	Fine	0.74	1.58	2.7	5	50	sand flow through slot perforation
1b	Medium	-	-	-	5	10	sand flow through slot perforation
9	Medium	0.64	1.64	12.5	5	50	sand flow through slot perforation
8	Medium	0.66	1.63	4.5	5	50	sand blockage over slot perforation (due to capillary cohesion forces)
14	Coarse	0.73	1.57	5.7	5	50	arches form over slot perforation

Table 4-3: Summary of Results From First Visualization Model: Vertical Orientation - Water Saturated Conditions

Test No.	Sand Type	Void Ratio	Dry Density	Relative Density	Slot Width	Slot Height	Hydraulic Gradient	Sand Behavior
			(g/cm^3)	(%)	(mm)	(mm)		
3	Fine	0.72	1.58	10.1	5	10	1.1	sand flow through slot perforation
5	Medium	0.66	1.63	5.8	5	10	1.1	sand flow through slot perforation
7	Medium	0.66	1.63	4.4	5	50	1.1	sand flow through slot perforation
19	Coarse	0.74	1.56	0.0	5	50	1.3 1.4 1.7	arches form over slot perforation arches form over slot perforation arches form over slot perforation

Table 4-4: Summary of Results From Second Visualization Model - Dry Sand Without Confining Stress Applied

Test No.	Sand Type	Void Ratio	Dry Density	Relative Density	Slot Width	Sand Behavior
			(g/cm^3)	(%)	(mm)	
2	Fine	0.62	1.68	54	5	sand flow through slot perforation
3	Medium	0.58	1.70	39	5	sand flow through slot perforation
4	Coarse	0.63	1.66	53	5	arches form over slot perforation
5	Coarse	0.63	1.66	53	12.7	sand flow through slot perforation

Table 4-5: Summary of Results From Third Visualization Model: Dry Sand With Confining Stress Applied

Test No.	Sand Type	Void Ratio	Dry Density	Relative Density	Slot Width	Confining Stress	Sand Behavior
			(g/cm^3)	(%)	(mm)	(kPa)	
57	Fine	0.63	1.67	49	5	200	sand flow through slot perforation
64	Fine	0.57	1.73	74	5	300	sand flow through slot perforation
51	Medium	0.52	1.77	71	5	100	sand flow through slot perforation
54	Medium	0.55	1.75	62	5	200	sand flow through slot perforation
65	Medium	0.52	1.78	75	5	300	sand flow through slot perforation
58	Coarse	0.62	1.68	63	5	100 200	arches form over slot perforation increased arch stability to vibration
66	Coarse	0.59	1.70	75	5	300	arches form over slot perforation increased arch stability to vibration

Table 4-6: Summary of Gas-Water Low Saturation Tests Results

Test No.	Sand Type	Void Ratio	Dry Density	Relative Density	Slot Width	Gas Saturation	Sand Behavior
			(g/cm^3)	(%)	(mm)	(%)	
93	Fine	0.63	1.66	45	12.7	70	arching over slot perforation
94	Fine	0.62	1.68	54	12.7	82	arching over slot perforation
95	Fine	0.64	1.66	45	12.7	91	arching over slot perforation
96	Fine	0.61	1.69	58	12.7	96.2	arching over slot perforation
97	Fine	0.63	1.67	49	12.7	98.8	arching over slot perforation
98	Fine	0.57	1.73	74	12.7	99.4	arching over slot perforation
100	Fine	0.57	1.73	74	12.7	99.4	arching over slot perforation
103	Fine	0.61	1.69	56	12.7	99.5	arching over slot perforation
99	Fine	0.60	1.70	62	12.7	99.7	sand flow through perforation
101	Fine	0.59	1.71	66	12.7	99.7	sand flow through perforation

Table 4-7: Summary of Heavy Oil-Water Low Saturation Tests Results

Test No.	Void Ratio	Dry Density	Relative Density	Slot Width	Oil Saturation	Water Saturation	Nonsaline /Saline Water	Sand Behavior
		(g/cm^3)	(%)	(mm)	(%)	(%)		
110	0.55	1.75	81	12.7	0	100	nonsaline	sand flow through slot perforation
112	0.57	1.71	66	12.7	17.1	68.2	nonsaline	arching over slot perforation
113	0.55	1.75	81	12.7	5.5	84.7	nonsaline	arching over slot perforation
116	0.57	1.73	71	12.7	3.1	94.2	nonsaline	arching over slot perforation
114	0.57	1.73	74	12.7	1.0	99.0	nonsaline	sand flow through slot perforation
122B	0.51	1.79	96	12.7	0	100	saline	sand flow through slot perforation
124	0.55	1.75	81	12.7	3.3	95.8	saline	arching over slot perforation
123	0.53	1.77	89	12.7	1.4	98.6	saline	sand flow through slot perforation
118	0.55	1.75	81	12.7	3.8	93.9	nonsaline	water flow causes oil/water/sand mixture to flow through perforation
119	0.63	1.66	45	12.7	41.2	38.6	nonsaline	water flow causes oil/water/sand mixture to flow through perforation
121	0.55	1.75	81	12.7	4.9	92.0	nonsaline	water flow causes oil/water/sand mixture to flow through perforation
122	0.53	1.77	89	12.7	14.2	85.8	nonsaline	water flow causes oil/water/sand mixture to flow through perforation

Table 4-8: Dry Densities and Relative Densities of Gas-Water Index Capillary Cohesion Tests

Gas Saturation (%)	Dry Density (g/cm^3)	Relative Density (g/cm^3)
100	1.68	54
90	1.77	89
78	1.76	85
68	1.75	81
67	1.76	85
55	1.77	89
42	1.79	96
35	1.79	96
32	1.77	89
23	1.76	85
18	1.71	66
0	1.75	81

Table 4-9: Dry Densities and Relative Densities of Gas-Heavy Oil Index Capillary Cohesion Tests

Gas Saturation (%)	Dry Density (g/cm^3)	Relative Density (g/cm^3)
100	1.68	54
88	1.69	58
76	1.72	70
67	1.73	74
56	1.73	74
51	1.74	78
43	1.76	85
40	1.73	74
39	1.74	78
33	1.75	81
24	1.74	78

Table 4-10: Dry Densities and Relative Densities of Gas-Medium Oil Index Capillary Cohesion Tests

Gas Saturation (%)	Dry Density (g/cm^3)	Relative Density (g/cm^3)
100	1.68	54
89	1.72	70
77	1.74	78
66	1.75	81
52	1.73	74
48	1.76	85
44	1.74	78
40	1.73	74
36	1.81	100
34	1.73	74
33	1.74	78

Table 4-11: Dry Densities and Relative Densities of Heavy Oil-Water Index Capillary Cohesion Tests

Water Saturation (%)	Oil Saturation (%)	Gas Saturation (%)	Dry Density (g/cm^3)	Relative Density (g/cm^3)
100	0	0	1.68	54
82	16	2	1.69	58
65	28	7	1.72	70
59	31	10	1.73	74
43	43	14	1.73	74
38	45	18	1.74	78

Table 4-12: Index Capillary Cohesion Magnitude Comparison

Gas Sauration (%)	Fluid Saturation Comparison		
	Gas-Water/ Gas-Heavy Oil	Gas-Water/ Gas-Medium Oil	Gas-Heavy Oil/ Gas-Medium Oil
30	1.9	2.3	1.2
40	1.5	1.8	1.2
50	1.3	1.5	1.2
60	1.3	1.4	1.1
70	1.3	1.4	1.1
80	1.4	1.6	1.2
Theoretical Ratio	2.2	2.6	1.2

Table 4-13: Capillary Cohesion Direct Shear Tests

(Fine Sand - Gas/Water Saturation)

Gas Sauration	Peak Angle of Internal Friction	Peak Capillary Cohesion	Residual Angle of Internal Friction	Residual Capillary Cohesion
(%)	(°)	(kPa)	(°)	(kPa)
100	40	0	35	0
40	38	3.5	29	1.5
20	38	3.0	29	1.9

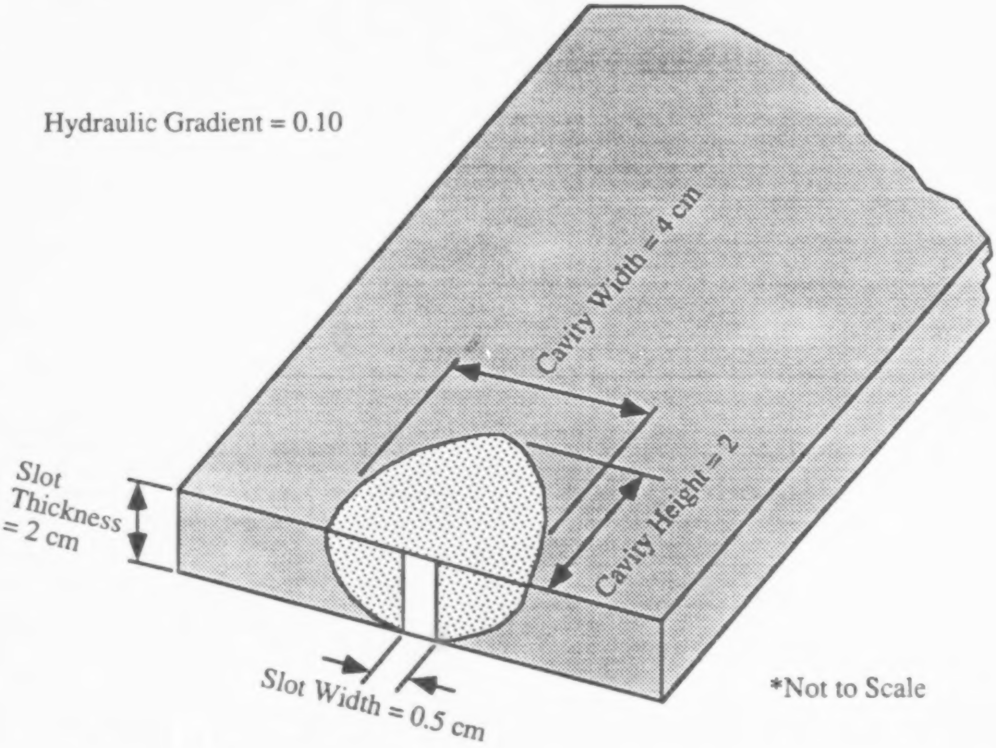
Hydraulic Gradient = 0.10
Cavity Width = 4 cm
Cavity Height = 2
Slot Thickness = 2 cm
Slot Width = 0.5 cm
*Not to Scale

Figure 4-1: Sketch of Semispherical Cavity Formed in Fine Sand During Water Flow With First Visualization Model in Horizontal Orientation

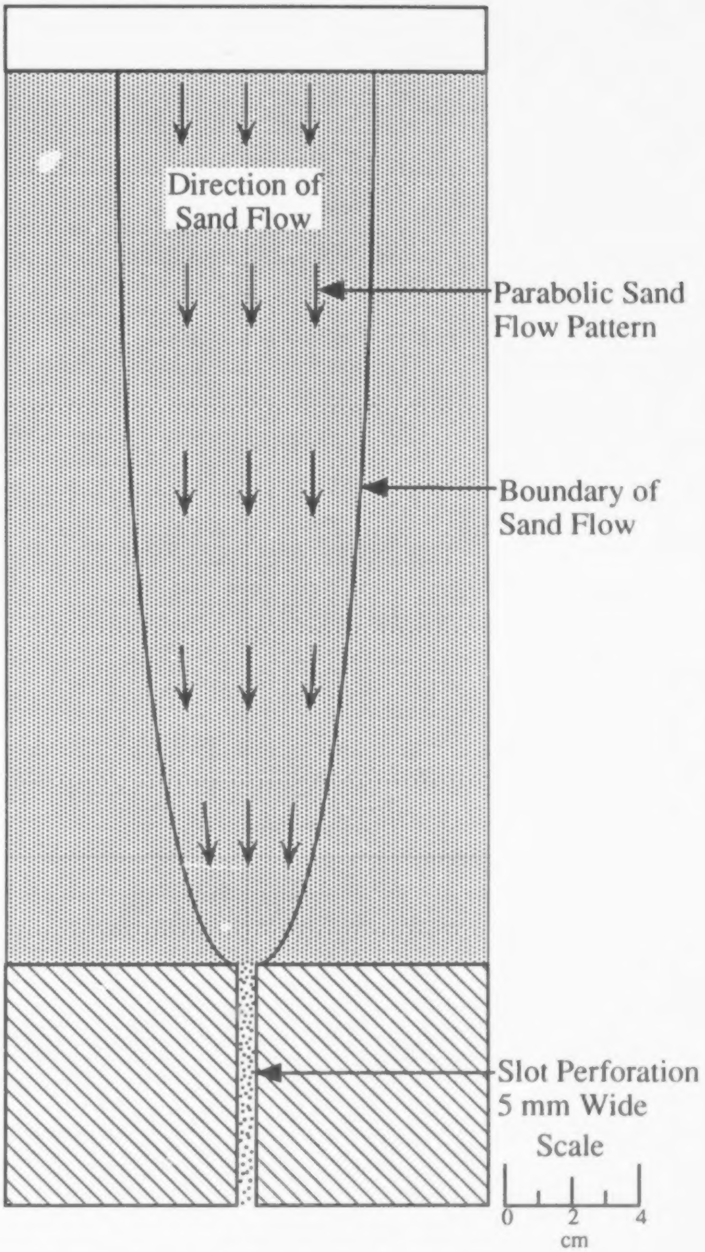
Direction of Sand Flow
Parabolic Sand Flow Pattern
Boundary of Sand Flow
Slot Perforation 5 mm Wide
Scale
0
2
4
cm

Figure 4-2: Typical Parabolic Sand Flow Pattern in Fine and Medium Sand

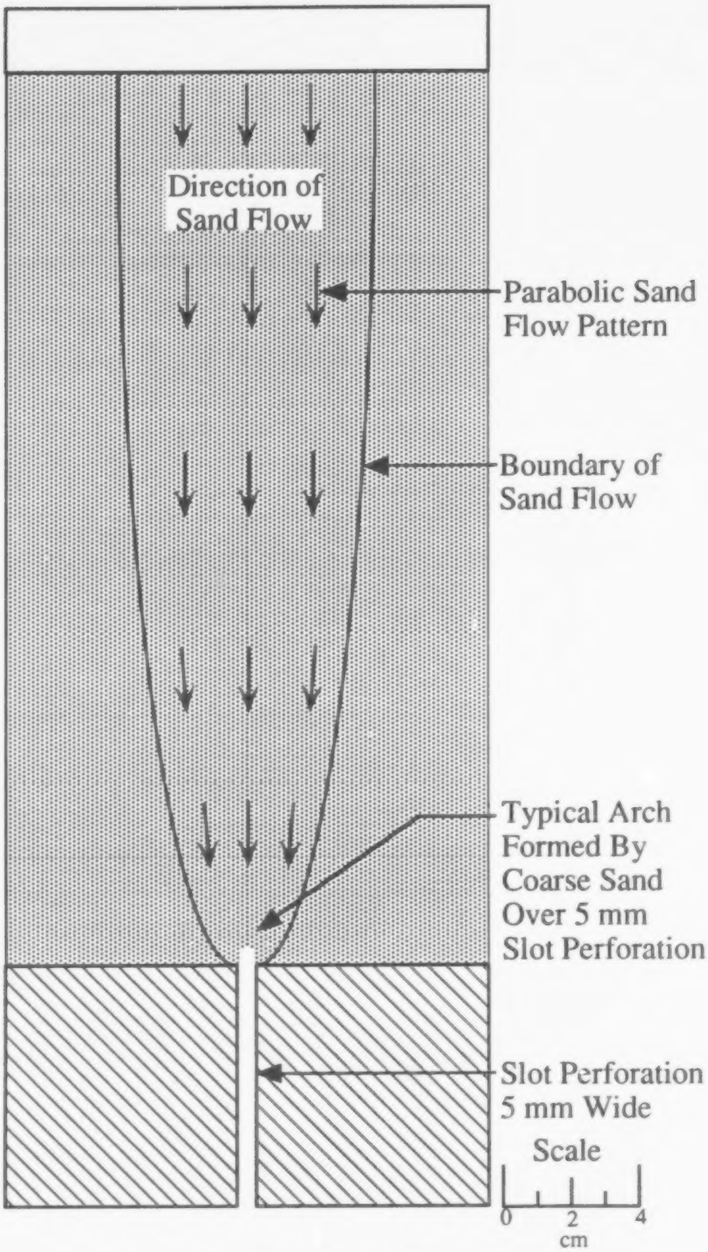
Direction of Sand Flow
Parabolic Sand Flow Pattern
Boundary of Sand Flow
Typical Arch Formed By Coarse Sand Over 5 mm Slot Perforation
Slot Perforation 5 mm Wide
Scale
0
2
4
cm

Figure 4-3: Typical Arch Formed By Dry Coarse Sand Over a 5 mm Wide Slot Perforation

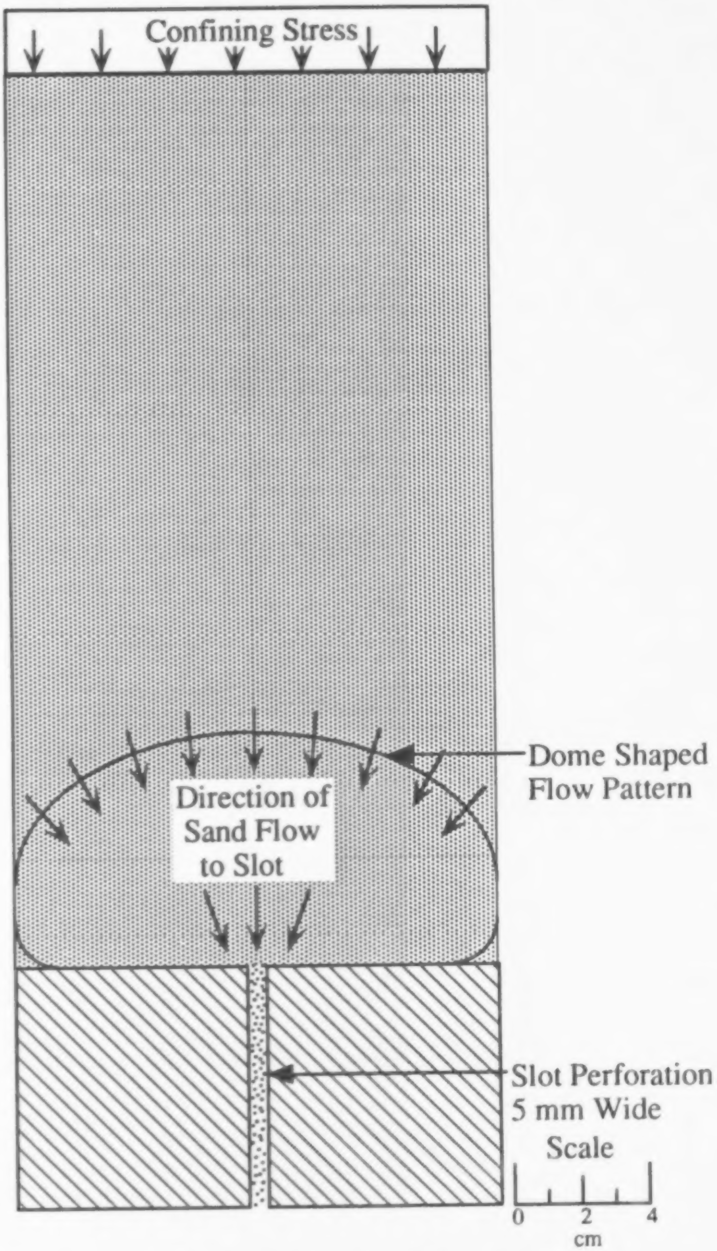
Confining Stress
Dome Shaped Flow Pattern
Direction of Sand Flow to Slot
Slot Perforation 5 mm Wide
Scale
0
2
4
cm

Figure 4-4: Typical Dome Shaped Sand Flow Pattern in Fine and Medium Sand

Figure 4-5: Apparent Water Velocities of Fully Saturated Water Flow Test and Durrett et al. (1976) Fluidization and Critical Transport Velocities

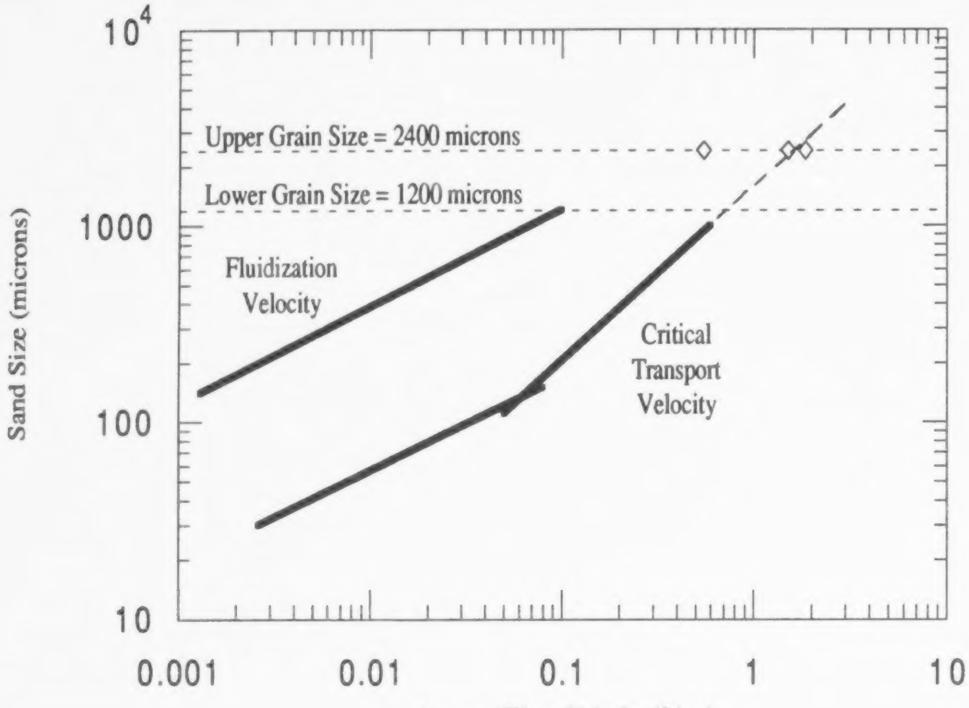

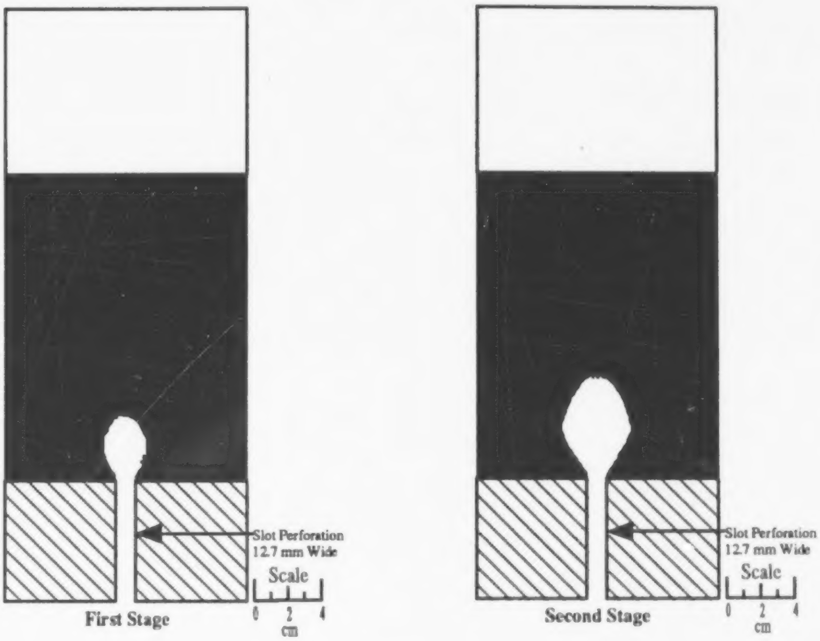
Slot Perforation
12.7 mm Wide
Scale
0 2 4
cm
Slot Perforation
12.7 mm Wide
Scale
0 2 4
cm

First Stage

Second Stage

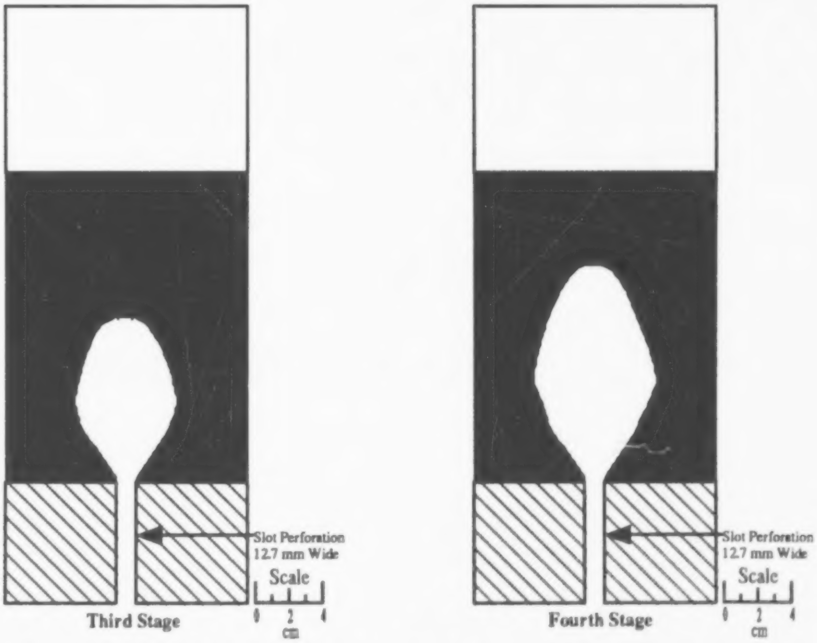
Slot Perforation
12.7 mm Wide
Scale
0 2 4
cm
Slot Perforation
12.7 mm Wide
Scale
0 2 4
cm

Third Stage

Fourth Stage

Figure 4-6: Typical Growth of an Arch Formed By Partially Gas-Water Saturated Fine Sand at Low Gas Saturations Due to Vibration

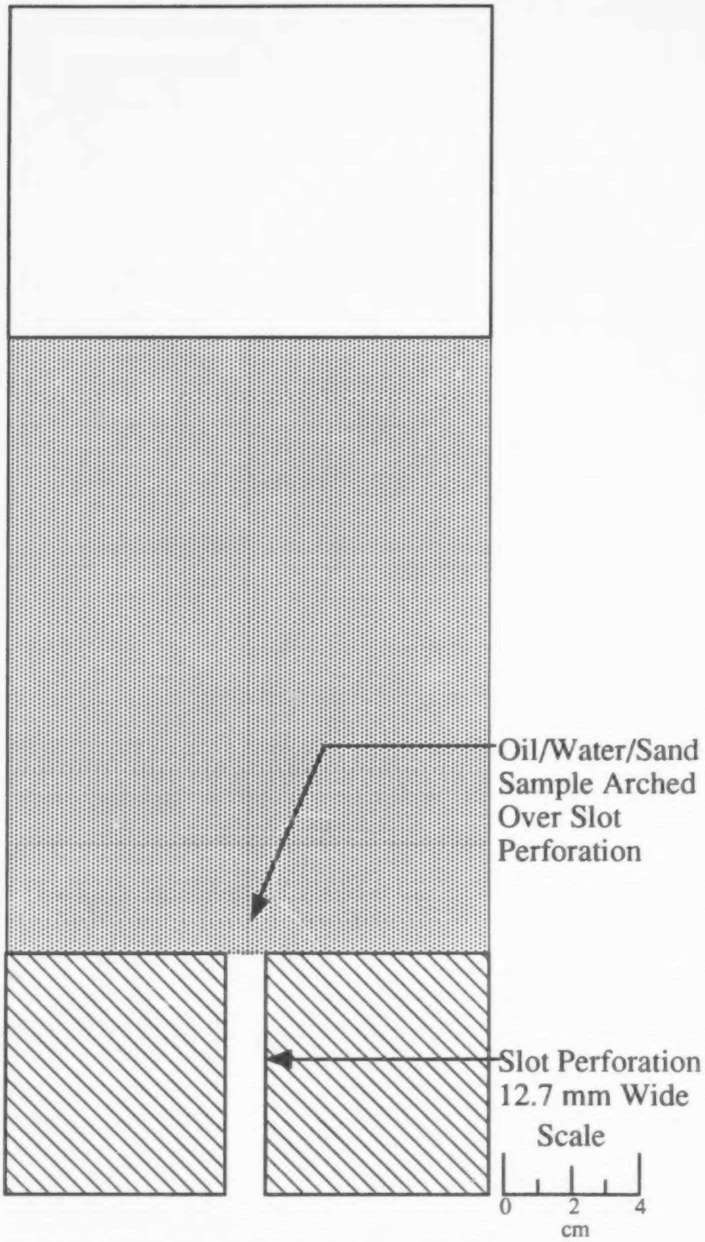
Oil/Water/Sand Sample Arched Over Slot Perforation
Slot Perforation 12.7 mm Wide
Scale
0
2
4
cm

Figure 4-7: Typical Arch Formed By Partially Oil-Water Saturated Fine Sand at Low Water Saturations

Figure 4-8: Gas-Water Index Capillary Cohesion

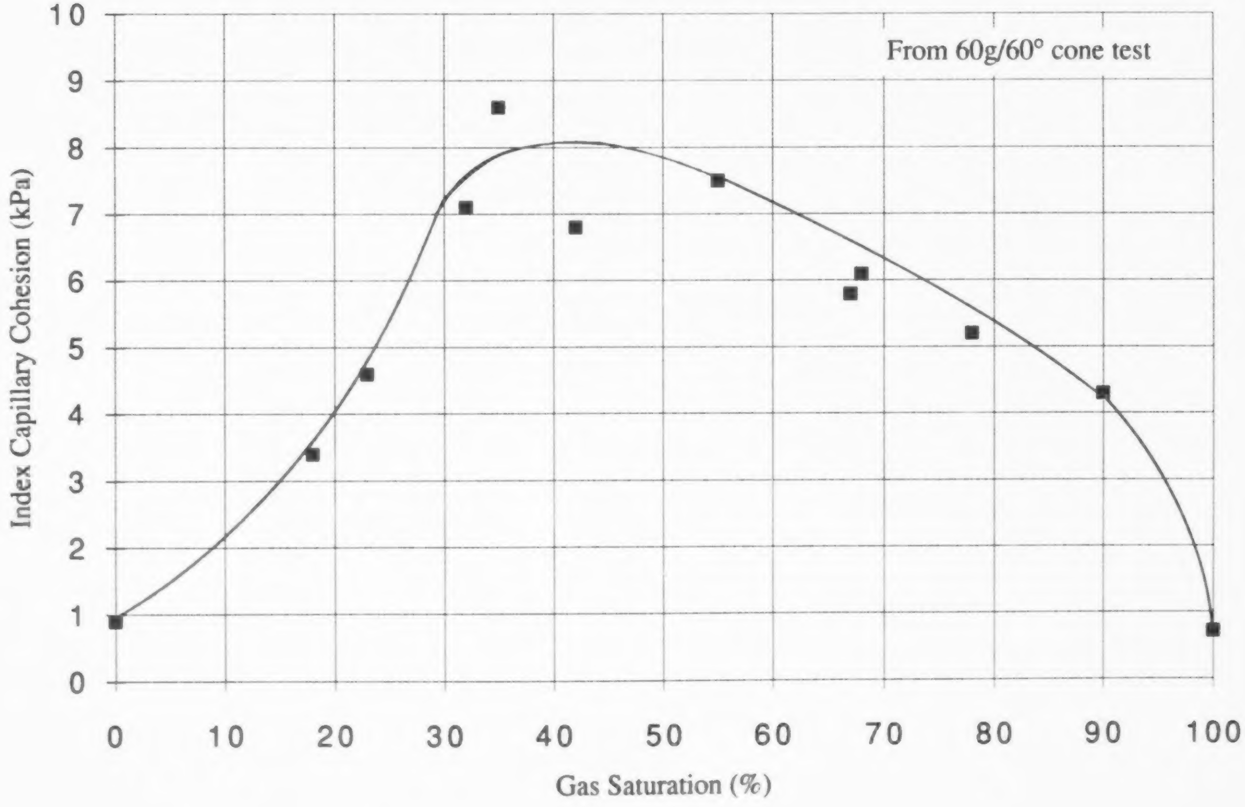

Figure 4-9: Gas-Heavy Oil Index Capillary Cohesion

(Oil Viscosity = 3600 mPa*s)

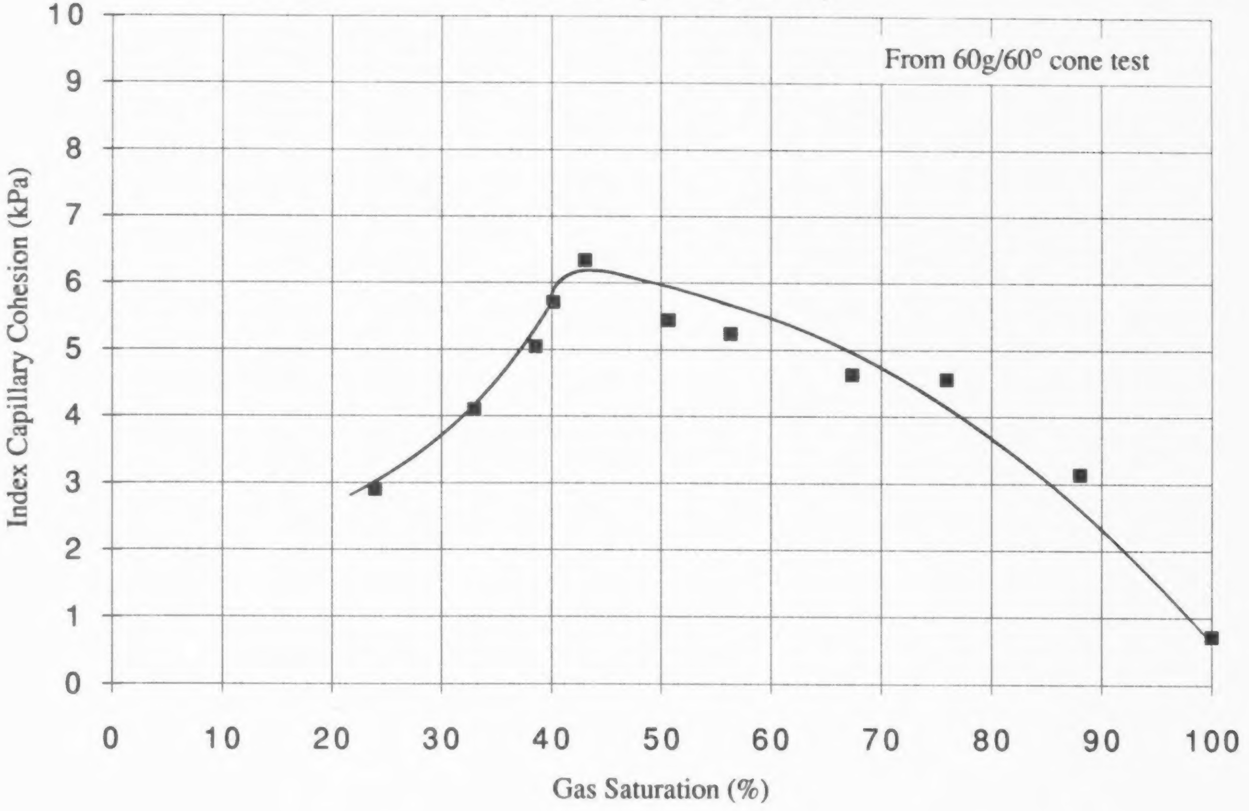

Figure 4-10: Gas-Medium Oil Index Capillary Cohesion

(Oil Viscosity = 1300 mPa*s)

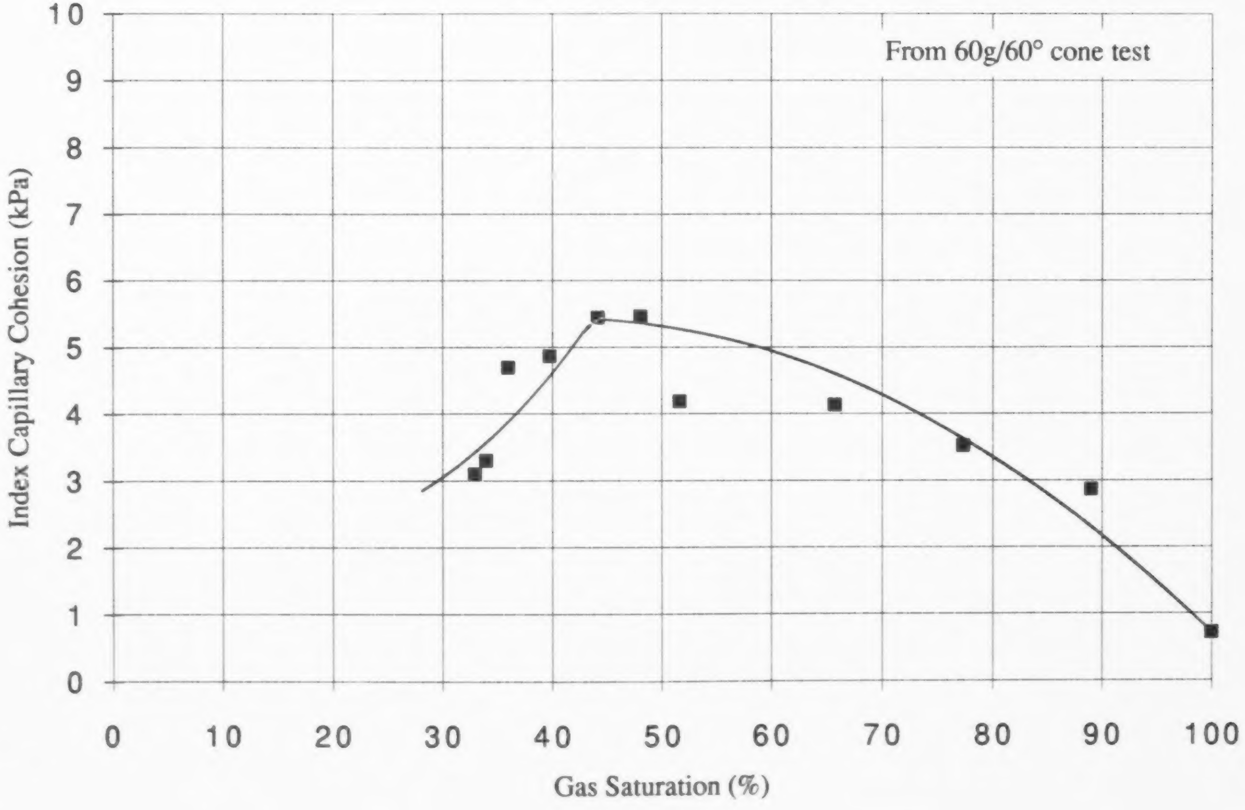

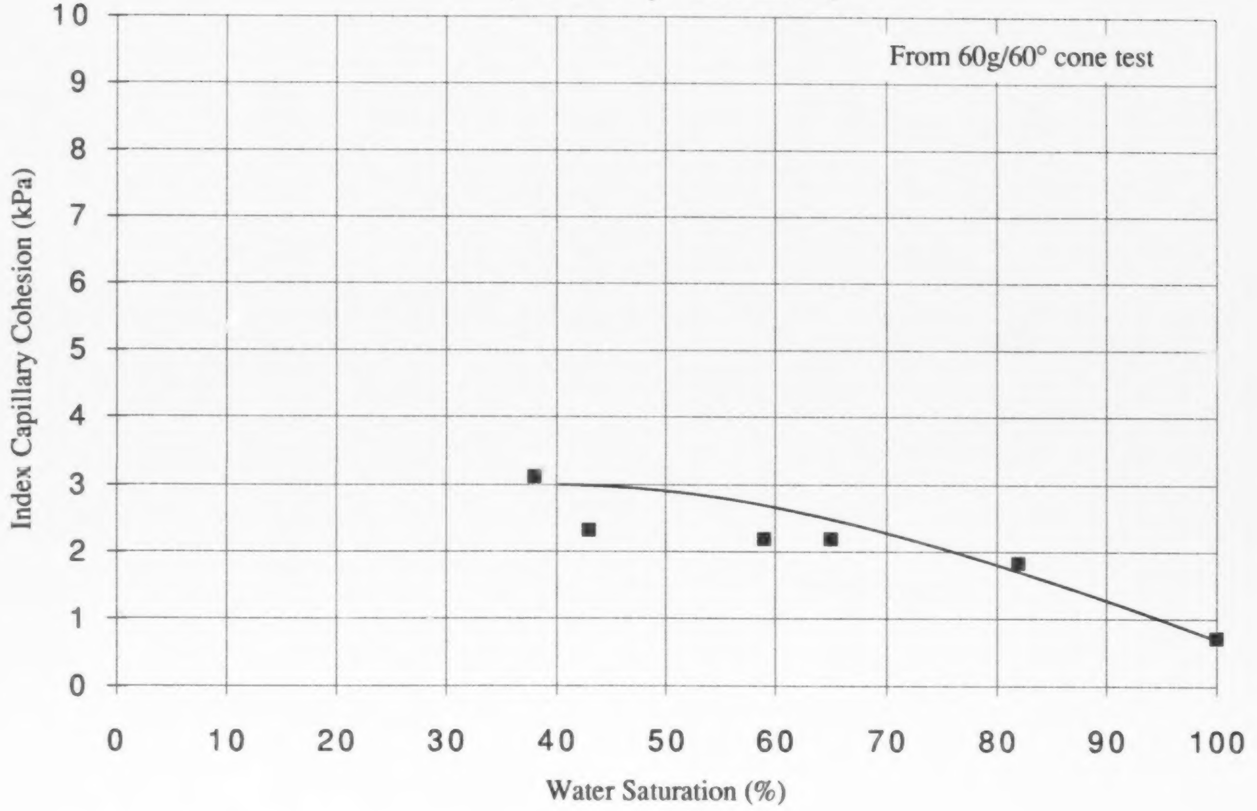

Figure 4-11: Heavy Oil-Water Index Capillary Cohesion

(Oil Viscosity = 3600 mPa*s)

Figure 4-12: Peak Shear Stress vs. Normal Stress - Direct Shear Tests

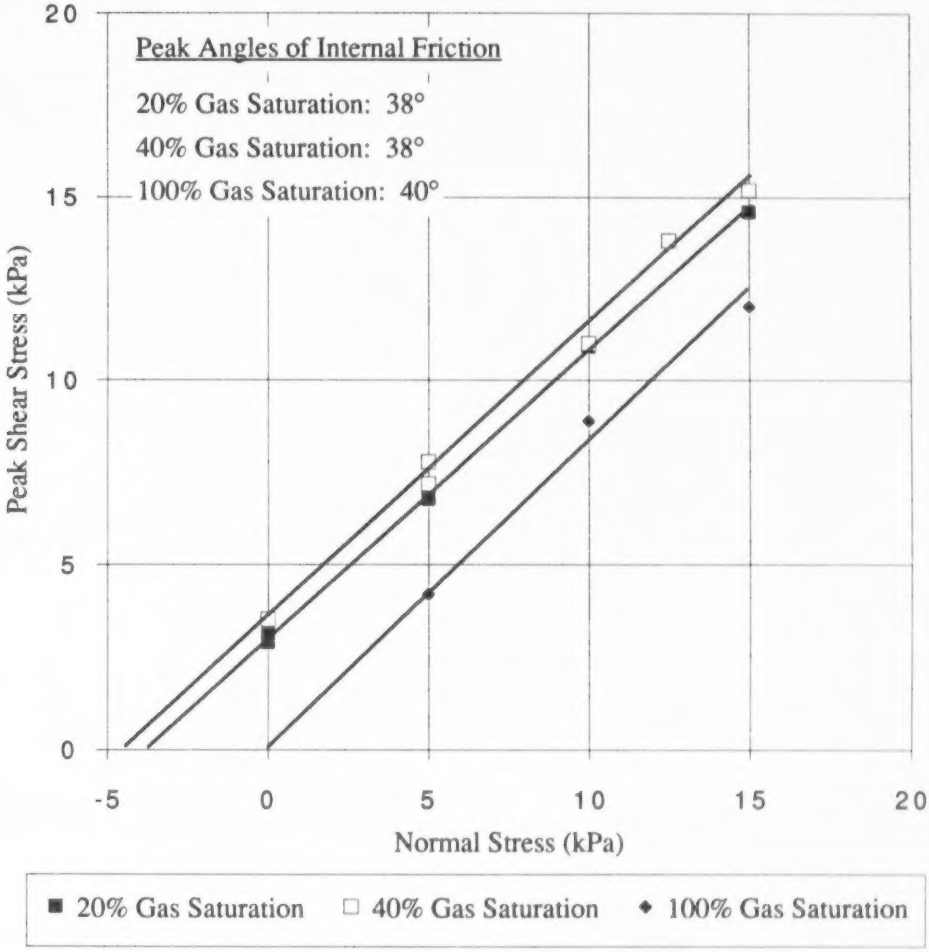

Figure 4-13: Residual Shear Stress vs. Normal Stress - Direct Shear Tests

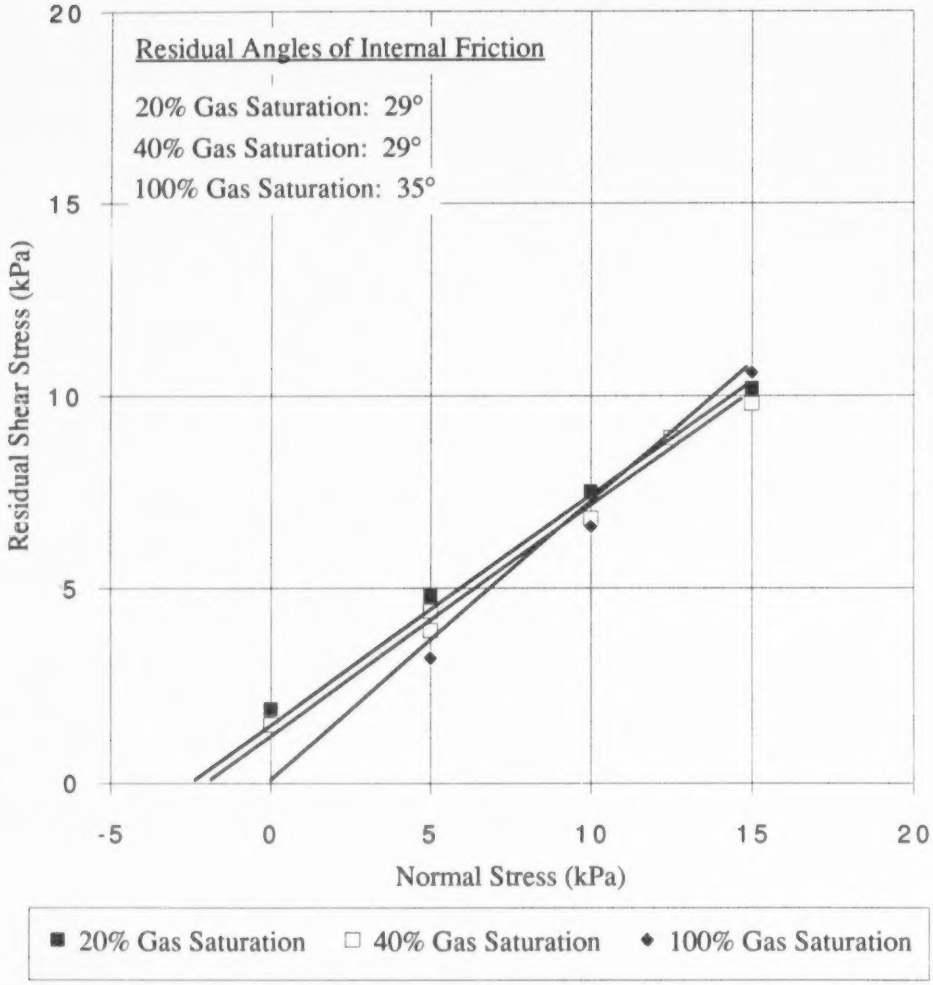

Plate 4-1: First Visualization Model - Horizontal Orientation

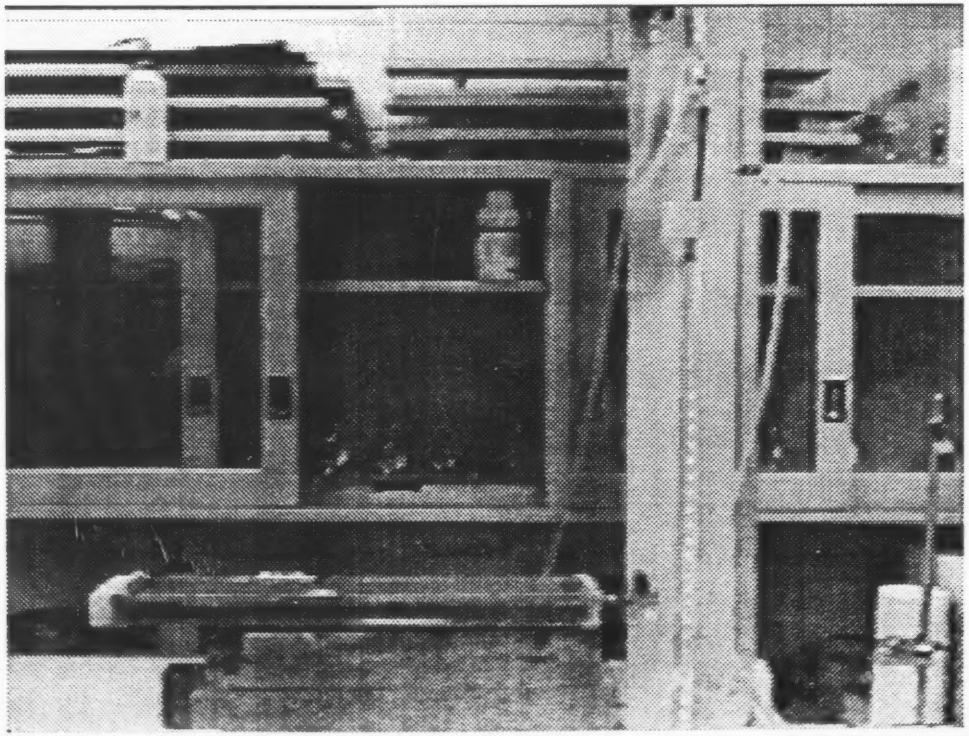

Plate 4-2: Dry Fine Sand Without Confining Stress Applied
Flowing Through 5 mm Wide Slot Perforation

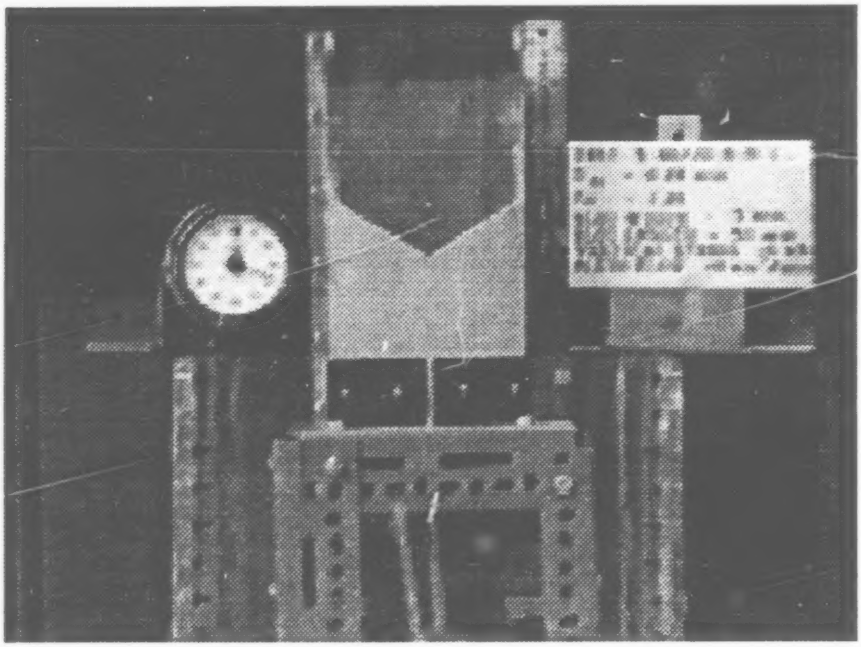

Plate 4-3: Stable Arches Formed By Dry Coarse Sand Over 5 mm Wide Slot Perforation

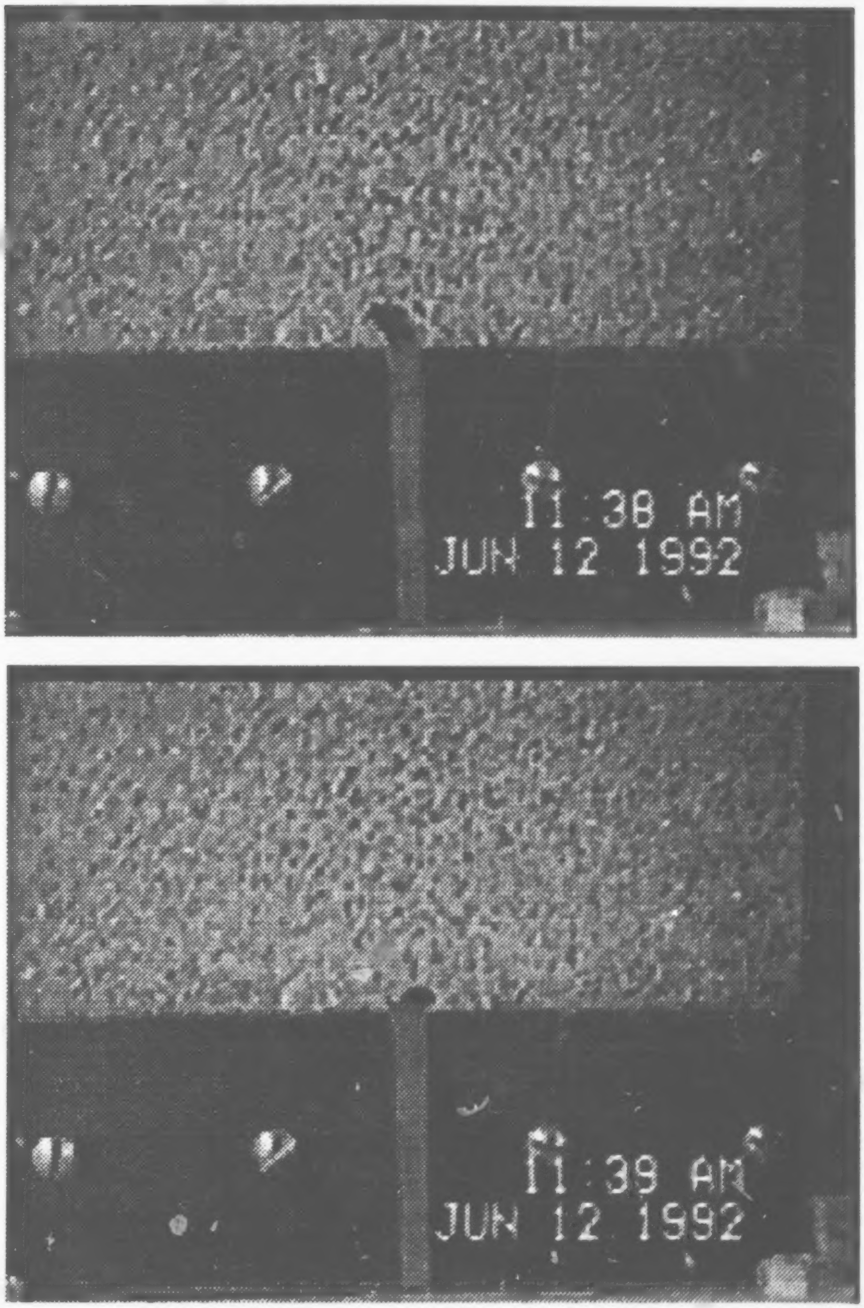
11:38 AM
JUN 12 1992
11:39 AM
JUN 12 1992

Plate 4-4: Stable Arch Formed By Partially Gas/Water Saturated Fine Sand at a Gas Saturation of 98.8% Over 12.7 mm Wide Slot Perforation

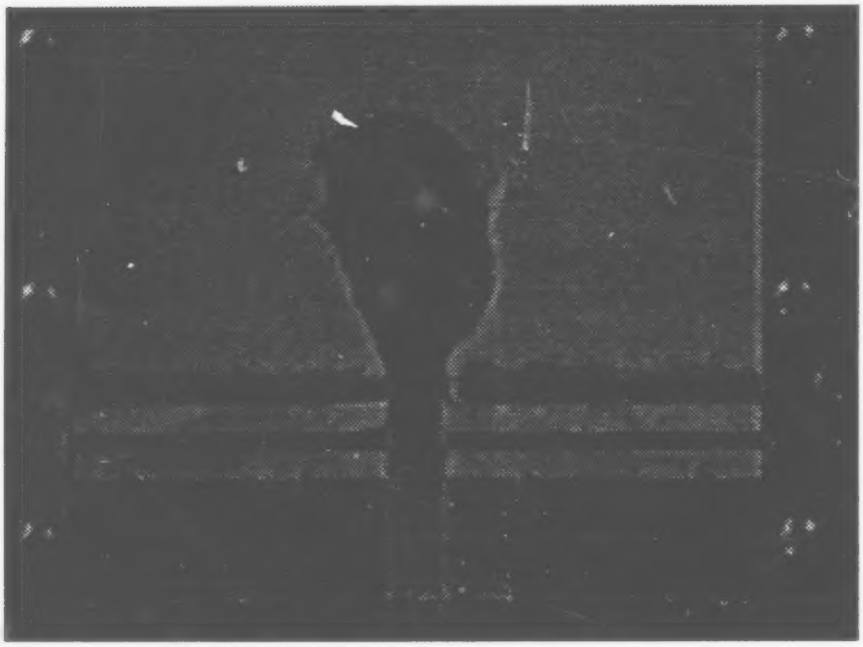

5. Analysis of Experimental Results

The results from the visualization model tests, index capillary cohesion tests and capillary cohesion direct shear tests discussed in the previous chapter were analyzed in terms of assessing the influence of each of the following variables on sand flow through well casing perforations: sand particle size and perforation diameter, shape and roughness of perforation opening, sand porosity, confining stress, flow conditions through sand and perforations and capillary cohesion between two fluids in a sand. The influence of each variable on sand arching will be discussed in the following sections.

5.1 Sand Particle Size and Perforation Diameter

One of the first conclusions reached based on tests using the first and second visualization models was that uniform dry sand, under no confining stress, will exhibit no arching behavior until the slot perforation width is less than four times the sand grain diameter. The fine sand and 5 mm wide slot perforation used in Test #1a with the first visualization model had a grain diameter to width of opening ratio of 1:16.7. The fine sand did not exhibit arching behavior at this ratio. These results were confirmed using the fine sand and the second visualization model at the same grain diameter to width of opening ratio in Test #2.

The medium sand and 5 mm wide slot perforation used in Test #1b with the first visualization model had a grain diameter to width of opening ratio of 1:4.2. Similar to the behavior of the fine sand, the medium sand did not display arching behavior at this ratio. These results were verified by the results of Test #3, employing the medium sand and the second visualization model at the same grain diameter to width of opening ratio.

The coarse sand and 5 mm wide slot perforation used in Test #14 with the first visualization model had a grain diameter to width of opening ratio of 1:3.1. Unlike the fine and medium sands at higher ratios, the coarse sand exhibited arching behavior. These results were confirmed using the coarse sand and the second visualization model in Test #4. Test #5 was conducted using coarse sand and a 12.7 mm (1/2 inch) wide slot perforation with the second visualization model. The grain diameter to width of opening ratio was 1:7.9. Similar to results using fine and medium sand, when the slot perforation width was greater than four times the sand grain diameter, the coarse sand did not exhibit arching behavior. It should be noted in the evaluation of test data that the fine sand is representative of sand found in the field and therefore of the most interest. The medium and coarse sands were used only to determine the effect of sand particle size on arching behavior.

Using a 11.1 mm diameter perforation, Hall and Harrisberger (1970) observed that a 10-20 mesh (D_{50} = 1.4 mm) angular sand, under no confining stress, formed arches of slight stability or not at all at a grain diameter to width of opening ratio of 1:9.4. They also observed that rounded, 20-40 mesh (D_{50} = 0.63 mm) and 80-100 mesh (D_{50} = 0.17 mm) sand, under no confining stress, would not arch at grain diameter to width of opening ratios of 1:20 and 1:68, respectively. This supports the conclusion that uniform, rounded, dry fine sand, under no confining stress, will only exhibit arching behavior when the grain diameter to width of opening ratio is less than four. However, increased angularity and coarseness of sand grains increases the shear strength of sand. This allows angular and coarse sand to form arches at larger grain diameter to width of opening ratios than rounded and fine sand.

Fully water saturated fine and medium sand at grain diameter to width of opening ratios of 1:16.7 and 1:4.2, respectively, under hydraulic gradients of 1.1 but no confining stress, did not exhibit arching behavior. However, coarse sand under identical conditions, except for a grain diameter to width of opening ratio of 1:3.1, exhibited arching behavior. The behavior of the sand in these tests is comparable to tests using dry sand even though a hydraulic gradient was applied to the fully water saturated tests.

As discussed above, several tests were performed to evaluate the ability of dry and fully water saturated fine, medium and coarse sands under no confining stress to form arches over a slot perforation. The results of these tests indicated that only the coarse sand would form an arch over a 5 mm wide slot and no sands formed arches over a 12.7 mm wide slot. Results of these tests are summarized in Table 5-1. The observation that uniform sand, under no confining stress, will exhibit no arching behavior until the slot width is less than four times the sand grain diameter led to the conclusion that for the formation sand and typical perforation diameters, arching will not occur if there is only one fluid in the sand.

5.2 Shape and Roughness of Perforation Opening

It was found that varying the slot perforation height from 10 mm to 50 mm had no influence on dry sand behavior. Increasing the height of the slot perforation provided a greater opportunity for the sand grains to form an obstruction along the height of the slot perforation. Tests #1a and #10 utilizing fine sand and the first visualization model were identical with the exception of slot perforation heights of 10 mm and 50 mm, respectively. In both tests, the fine sand did not display arching behavior. An influence of the increased slot perforation height was not observable in the behavior of the fine sand.

The influence of increased slot perforation height was checked again in Tests #1b and #9 employing medium sand and the first visualization model. These tests were identical except for the use of slot perforation heights of 10 mm and 50 mm, respectively. Similar to the behavior of the fine sand, no arching behavior was exhibited in either test and no influence of the increased slot perforation was observed. The coarse sand showed similar results with increased slot perforation height having no effect.

In summary, the shape of the perforation used in this study was a rectangular slot. Slot heights from 10 mm to 50 mm high were used to provide a greater opportunity for the sand grains to form an obstruction within the slot. The inside of the slot was also varied from a smooth surface to a rough surface. Regardless of the slot height or surface characteristics, under test conditions where sand was found to flow through the slot, the variation of the above variables had no effect on impeding the flow of sand. Arch structures that did form always did so above the slot and never along the height of the slot. Results of tests using a 5 mm wide slot are summarized in Table 5-2. It was concluded that the shape and roughness of the perforation opening had no effect on sand arching.

5.3 Sand Porosity

Porosity (relative density) has an effect on rate of sand flow. Under conditions of dry sand with no confining stress applied where sand will flow through a slot perforation, rate of sand flow increases with increased relative density of the sand. It was observed during tests using the first and second visualization models that in cases where dry sand flowed continuously out of the visualization model, sand flow rates were higher for sand at higher relative densities. Fine sand flowing through a 5 mm wide slot perforation at relative densities of 2.7% and 54% had sand flow rates of 15.5 g/sec and 34.5 g/sec, respectively. Flowing through the same slot perforation width, medium sand at relative densities of 13% and 39% exhibited sand flow rates of 11.8 g/sec and 23.1 g/sec, respectively. An increase in relative density means an increase in shear strength and dilation occurring during shearing. It was expected that an increase in relative density would result in a decrease in sand flow rate because more work would have to be done during shearing. However, the opposite behavior was observed and no explanation for this behavior could be ascertained. An increase in relative density from a very low range of 0 to 15% to a high range of 65 to 85% did not alter the sand behavior with regard to the occurrence of arching.

Relative density also has an effect on arch stability. Shear strength is made up of the grain-to-grain frictional resistance and the work required to make particles move up and over one another. An increase in the relative density of a sand results in increased interparticle resistance and more work required to cause dilation of particles. That is, an increase in relative density means an increase in shear strength. Due to the increased shear strength, sand at higher relative densities should create more stable arches than sand at lower relative densities.

The influence of porosity on fully gas saturated (dry) sand was studied by performing laboratory fall-cone tests on dry fine sand. These fall-cone tests provide a clear indication concerning the influence of porosity on shear strength of the dry fine sand. The dry fine sand was tested at porosities ranging from 43% to 35% (relative densities of 0% and 85%, respectively) using both the 10g/60° cone and 60g/60° cone. These results are presented in Figure 5-1. A decrease in porosity from 43% to 35% resulted in increases in shear strength index of only 0.18 kPa and 0.36 kPa, using the 10g/60° cone and 60g/60° cone, respectively. The results of these tests indicate that the porosity of the dry sand mass has little effect on frictional shear strength measured by the fall-cone test of the fully gas saturated fine sand, compared to the magnitude of index capillary cohesion measurements that will be discussed later. However, the influence of porosity on the index capillary cohesion of partially saturated sand is significant and will also be discussed later.

5.4 Confining Stress

Dry fine sand was subjected to confining stresses up to 300 kPa using the third visualization model in Tests #57 and #64. The grain diameter to width of opening ratio was 1:16.7 for both tests. It had been concluded earlier that uniform dry sand, under no confining stress, would not exhibit arching behavior until the slot width was less than four times the sand grain diameter. The behavior of the dry fine sand, under confining stresses up to 300 kPa, was similar to the behavior of the dry fine sand under no confining stress. The only exception was a change in sand flow pattern from a parabolic shape, when no confining stress was applied, to a dome shaped flow pattern when a confining stress was applied. The fine sand did not exhibit arching behavior at this grain diameter to width of opening ratio and range of confining stresses.

Tests #51, #54 and #65 were conducted using the medium sand subjected to confining stresses of 100, 200 and 300 kPa, respectively. The grain diameter to width of opening ratio was 1:4.2 in all tests. This ratio did not meet the condition required to cause dry sand to display arching behavior under no confining stress. The behavior of the dry medium sand, under confining stresses up to 300 kPa, was comparable to the behavior of the dry medium sand under no confining stress. The medium sand did not exhibit arching behavior at this grain diameter to width of opening ratio and confining stresses. The only effect was the change in sand flow pattern mentioned earlier.

The coarse sand was subjected to confining stresses up to 300 kPa using the third visualization model in Tests #58 and #66. The grain diameter to width of opening ratio was 1:3.1. It was stated earlier that uniform dry sand under no confining stress would not exhibit arching until the slot width was less than four times the sand grain diameter. These tests using the coarse sand met this condition for arching behavior. Similar to behavior in tests with no confining stress, the dry coarse sand exhibited arching behavior at confining stresses up to 300 kPa. However, it appears to be more difficult to destroy arches formed under the influence of a confining stress.

Destruction of sand arches can be attained by vibration. In tests involving dry sand, only the coarse sand formed arches over the slot perforation. The sand arches could be destroyed by tapping the face of the visualization model with a hammer. The destruction of the sand arch was followed by a short flow of sand out of the visualization model and the formation of an new sand arch. This process of sand arch destruction due to vibration and reformation was present under conditions of no confining stress and confining stresses up to 300 kPa. However, arches formed under the influence of a confining stress appeared more difficult to destroy.

Hall and Harrisberger (1970) observed that a confining stress of 3500 kPa applied to fully gas saturated, 10-20 mesh angular sand improved arch stability at a grain diameter to width of opening ratio of 1:9.4. They presumed the increase in arch stability was due to higher shear strength. Cleary et al. (1979) supports this conclusion stating that arch stability increases with increasing horizontal and vertical stress. However, a confining stress of 13.8 MPa caused failure of the angular sand due to grain crushing. They also observed confining stresses of up to 13.8 MPa could not induce arching in fully gas saturated, rounded 20-40 mesh and 80-100 mesh sand at grain diameter to width of opening ratios of 1:20 and 1:68, respectively. The average size of formation sand is 0.2 mm and perforations typically have widths of 12.7 mm (1/2 inch) and 19.1 mm (3/4 inch). This results in grain diameter to width of opening ratios of 1:64 and 1:96, respectively.

Several other researchers have noted a relationship between arch stability and high confining stress. Suman (1975) proposed four qualitative stress ranges that describe arch behavior as a function of load based on the work of Hall and Harrisberger (1970). Range I is a range of low load acting on the arch. No arch or tenuous arches form and sand flows in a rolling, sliding motion through perforation openings in this dilatant failure region. All of the tests where sand flowed through the slot perforation and arches that were formed by coarse sand under no confining stress would fall into this range. Fluid flow rate sensitive arches form in Range II under greater arch loads. The arch is in the dilatant failure region and is sensitive to interfacial tension and sand grain angularity. The greater loads applied to the arch, create higher interparticle stresses resulting in greater shear strength. Thus, the arch has greater stability and can withstand certain levels of fluid flow. Tests using coarse sand under a confining stress which formed arches would fall into Range II. In Range III, shear strength is sufficient to prevent interlocked sand grains from dilation sufficient to cause a rolling or sliding failure. This is described as a stable arch region. Arch loads that will cause arch failure due to grain crushing are in Range IV. Hall and Harrisberger (1970) found that dry and water moistened 8-12 mesh angular sand formed arches that failed due to grain crushing at confining stresses of 13.5 MPa and 14.5 MPa, respectively. As well, a 30-250 mesh angular sand having a much wider grain size range, formed arches that failed due to grain crushing under dry and water moistened conditions at confining stresses of 11.7 MPa and 23.8 MPa, respectively. These results indicate that arch failure due to confining stress occurs at lower stresses for angular sands than rounded sands and grain crushing usually accompanies the failure of the angular sand. The failure of these sands due to grain crushing would fall into Range IV. These stress ranges can be used to describe arch load as a function of depth. Range I would apply to perforations at shallow depths and Range IV would correspond to very deep depths with Ranges II and III reflecting intermediate depths. Based on these ranges, the tests performed in this project would fall into Ranges I and II. Durrett et al. (1976), Selby and Farouq Ali (1988) and Islam and George (1991) also point out that interlocking of grains under confining stress has an effect on shear strength of formation sands.

To summarize, the influence of confining stress on arching behavior was investigated. In earlier tests, the fine and medium sands exhibited no arching behavior. Similar to the behavior observed under no confining stress, the medium and fine sands under dry conditions and confining stresses up to 300 kPa did not form arches over the slot perforation. The results of tests using a 5 mm wide slot are summarized in Table 5-3.

There was a change in the sand flow pattern from a parabolic shape when no confining stress was applied to a dome shaped flow pattern when a confining stress was applied. The parabolic sand flow pattern was observed when no confining stress was applied to the sand. The shapes of the surfaces of sliding described by Terzaghi (1943) are very similar to the boundaries of the sand flow indicated on the sketch of the parabolic sand flow pattern presented in Figure 4-2. The parabolic sand flow pattern described above was found to be in agreement with Terzaghi's explanation of limited sand movement. The change from a parabolic to dome shaped sand flow pattern when a confining stress is applied may be analogous to sand behavior at shallow depth and sand behavior at deeper depths. The friction between the sand grains and the walls of the visualization model is similar to the friction generated in the field by stationary sand adjacent to the sand moving towards the perforation. As well, an increase in vertical stress results in an increase in horizontal stresses. The increased horizontal stresses acting on the sand results in greater interparticle stresses and higher shear strength. The higher shear strength may prevent sand grains from flowing in the parabolic shape seen under no confining stress. Instead, the sand grains experience no shearing and move down with the visualization model until sufficient stresses are applied to overcome the shear strength and force the sand to move in and flow through the slot perforation.

Similar to tests performed with no confining stress, the dry coarse sand exhibited arching behavior at confining stresses up to 300 kPa when the grain diameter to width of opening ratio was less than four. Arches may be destroyed by vibration; however, it appears to be more difficult to destroy arches formed under the influence of a confining stress. Other related published works indicate that a high confining stress (>3 MPa) can initiate arching and increase arch stability in angular sand, but confining stresses up to 14 MPa could not induce arching in rounded sand.

Higher confining stresses result in increased shear strength which results in a high frictional resistance between sand grains and more work required to cause movement of sand grains. The effect of increased shear strength is improved arch stability. As well, it is more difficult for the sand to dilate at higher confining stresses. Thus, sand grains have greater difficulty sliding and rolling over each other during shear. The dry sand direct shear tests discussed in Section 3.1.5 support this concept. The volume change behavior results provided in Appendix A, indicates that the amount of dilation decreased as confining stress increased for all sands. Dilation decreases because as confining stress increases, interlocking of particles decreases. Particles become flattened at contact points, sharp corners are crushed and particles break resulting in decreased dilation during shearing. As well, peak and residual shear strength increased as confining stress increased.

Grain size and shape also have an influence on arch stability. In order for the arch to fail, the sand grains must dilate. In some cases the sand grains may simply fall out, but the majority of sand grains must first slide or roll over adjoining grains. Larger sand grains would require greater degrees of dilation during shearing than smaller grains. Thus, the stability of arches formed using larger grains would be better. Angular sand grains form more stable arches than rounded grains because the shear strength of angular grains is greater. Angular grains can interlock more thoroughly than rounded grains. This results in higher shear strength and the formation of arches with increased stability.

Confining stress has an influence on rate of sand flow. During tests using the third visualization model and dry sand with a confining stress applied, it was observed that rate of sand flow decreased with increasing confining stress. Sand flow rates of 34.5, 28.9 and 7.4 g/sec were measured using dry fine sand flowing through a 5 mm wide slot perforation at confining stresses of 0, 200 and 300 kPa, respectively. Tests using dry medium sand at confining stresses of 0, 100, 200 and 300 kPa had sand flow rates of 23.1, 20.3, 15.3 and 15.5 g/sec, respectively. Due to the increased confining stress applied to the sand, increased interparticle stresses are present and the sand has a greater shear strength. It may be postulated that the confining stress could be increased to a large enough value that the intergranular shear strength could prevent sand flow. It is believed that a confining stress of 7000 kPa would be sufficient to cause the dry fine sand used in this project to arch over a 12.7 mm (1/2 inch) wide slot perforation. This value of confining stress was determined by evaluating the behavior of similar sands under high confining stress presented by other researchers. The dry round sand used by Hall and Harrisberger (1970) did not exhibit arching at a confining stress of 13.8 MPa. However, the fine sand used in this project was subrounded and is expected to be able to form arches if the confining stress is high enough, similar to the angular sand used by Hall and

Harrisberger which was able to form stable arches at high confining stresses. The ability of the fine sand to form an arch would also be influenced by the relative density of the sand with denser sand being able to form an arch with greater ease.

5.5 Flow Conditions Through Sand and Perforations

5.5.1 Fully Water Saturated Flow Conditions

A test using saturated coarse sand, a 5 mm slot, no confining stress and water as a test fluid was performed. It was found that at a water flow rate of 3.0 L/min, the coarse sand would form an arch after an initial sand flow. Similar to tests using dry sand, the arch could be destroyed by tapping with a hammer. The arch was stable as the flow rate was gradually increased to a flow rate of 8.3 L/min in 0.4 L/min increments. However, a rapid increase from a flow rate of 8.3 L/min to 10.2 L/min caused the destruction of the arch and the continuous flow of all remaining sand out of the visualization model. Although these results did not involve the fine sand, they indicate that a high water flow rate can break down a sand arch structure.

Hall and Harrisberger (1970) found that 10-20 mesh dry angular sand under a load of 3500 kPa formed an arch over a 11.1 mm diameter perforation. The arch remained stable when a slow outward air flow was applied, but failed when a faster flow as used. These results support the conclusion that high fluid flow rates can destroy a sand arch.

During the fully water saturated water flow test it was observed that the arch remained stable as the flow rate was gradually increased from 3.0 to 8.3 L/min. However, a rapid increase from 8.3 to 10.2 L/min caused the destruction of the arch. Tippie and Kohlhaas (1973) reported similar findings. They flowed fluid radially through a sand pack which was loaded vertically to simulate overburden pressure. Flow rates were increased gradually until sand flowed. The flow was restarted at a low rate and gradually increased until sand production occurred. Thus, gradual increases in flow rate result in higher sand free production when compared to sudden increases to full rate. It is expected that a rapid increase of water flow during the initial stages of the fully saturated water flow tests would have resulted in the destruction of the arch. Tippie and Kohlhaas (op cit) also state that flow rate influences arch size and stability. Larger arches resulted from higher flow rates. As well, they observed that smaller sand arches are more stable and allow a high fluid viscosity to be reached before failure.

Bratli and Risnes (1981) analyzed the stress due to fluid flow in the sand arches formed behind perforation openings. They used air as the flowing fluid through a sand pack near irreducible water content. In an arching experiment, the flow rate was increased steadily until a small amount of sand was produced suddenly. Further increase of the flow rate could be made without incident before a new lump of sand blew out. This repeated itself several times until the rest of the sand in the cylinder suddenly flowed out. The arches formed were stable in the sense that the flow rate could be reduced to zero and increased to its former value several times without affecting the arch stability. The flow rate used during the fully water saturated flow test was never reduced to zero. However, it is expected that the flow rate could be reduced to a very low value and increased to its previous level without causing arch destruction, if the changes in flow rate were performed gradually.

Bratli and Risnes also found that the flow rate could be held constant for hours without causing significant changes. The arch formed during the fully water saturated test remained stable when subjected to a constant flow rate for extended periods of time. These results indicate that if a flow rate applied to a stable arch is unable to destroy the arch, sand free production is possible for prolonged periods of time without affecting arch stability.

Selby and Farouq Ali (1988) observed that when no confining stress was applied, sand formed arches regardless of different flow rates of 2, 8 and 13.3 mL/min. Sand arched rapidly at higher flow rates and initial sand production was higher at higher flow rates. At high confining stress, arching occurred at a low flow rate of 2 mL/min but not at higher flow rates. As well, sand production increased at higher flow rates. They concluded that sand production increases as fluid flow rate is increased. As well, arching of the sand occurs at low and high flow rates under low confining stress and only at low flow rates under high confining stress.

Durrett et al. (1976) provide an explanation regarding transport of sand grains due to drag forces. Once a stable arch has been formed, the arch will remain established until the forces tending to break down the arch exceed the forces tending to maintain the arch. The forces tending to break down the arch are the drag forces of the produced fluid. Fluid drag forces are made up of skin drag (friction) and form drag (inertia) forces. Skin drag predominates at low flow rates, while form drag forces are more significant at higher flow rates. Durrett et al. (1976) point out that as produced fluid flows through a porous body, a critical velocity is reached where unit pressure loss in hindered flow is sufficient to overcome the forces tending to maintain the arch. These forces tending to maintain the arch are identified as the holding forces and include intergranular friction forces and capillary cohesion forces. Capillary cohesion forces are present only when two fluids occupy the voids of the sand mass.

Durrett et al. performed tests which allowed them to apply pressure loss to a projected area of sand particle. This allowed the drag force acting on the particle to be determined. They state that critical fluidization velocity for a particle has been reached when the drag forces equal the holding force. They also calculated a critical transport velocity for sand transport in an open channel (i.e. unhindered flow) that is described by Stokes' law (settling of particles). Figure 2-6 shows these fluidization and critical transport velocities for water flow plotted against grain size.

The flow rates measured during the fully saturated water flow test were converted to apparent water velocity by dividing these values by the cross-sectional area of the slot perforation, 30 cm^2. These apparent water velocities were plotted (Figure 4-5) against a sand size of 1600 microns (the D_{50} of the coarse sand) on the fluidization and critical transport velocity plot presented by Durrett et al. (1976). The dashed lines in Figure 4-5 indicate the full grain size range of the coarse sand. Looking at the upper grain size of 2400 microns, apparent water velocities of 0.55 ft/sec and 1.51 ft/sec (which correspond to flow rates of 3.0 L/min and 8.3 L/min, respectively) are below the critical transport velocity for the coarse sand. At these apparent water velocities during the fully water saturated water flow tests, the arch created by the coarse sand was stable. However, an increase to an apparent water velocity of 1.86 ft/sec (which corresponds to a flow rate of 10.2 L/min) was beyond the critical velocity of the coarse sand. Consequently, this increase in apparent water velocity resulted in the destruction of the previously stable arch. Figure 4-5 indicates that the larger grain sizes in the coarse sand appear to have the greatest influence on arch stability to water flow because it is this grain size which exhibits the boundary between flow and nonflow based on critical transport velocity.

Thus, the behavior of the sand observed during these tests with regard to stability and destruction of arches agrees well with the data presented by Durrett et al. (1976). Stable arches are broken down when the apparent velocity of the producing fluid, in this case water, exceeds the critical transport velocity for the sand size.

Intergranular friction forces are included in the holding forces which tend to maintain the arch. The fully saturated water flow test was performed without a confining stress applied. It is expected that a higher water flow rate through the sand may have been attained if a confining stress had been applied to the sand mass. Confining stress has the effect of increasing the intergranular forces between sand grains, thereby tending to lock the sand grains in place. Such was the case during tests with dry sand and confining stress applied where arches formed at higher confining stresses were more stable. Thus, the higher intergranular friction forces would have been able to withstand the higher drag forces of a faster flow rate.

5.5.2 Upward Air Flow Conditions

The complete analysis of the upward air flow tests performed during this study is presented in Appendix C.

5.6 Capillary Cohesion Between Two Fluids in a Sand

In this study, the fall-cone test was used as a strength index test to provide an estimate of capillary cohesion of the fine sand at varying degrees of gas-water, gas-oil and oil-water saturations. It was felt that the results of the fall-cone tests could be used as a relative measure of capillary cohesion. The strength measured by the fall-cone test has been designated the index capillary cohesion. Due to a variation in sample porosities, all index capillary cohesions were corrected to a porosity of 35%. A porosity of 35% is equivalent to a relative density of 85% for the fine sand. It was felt that this porosity would reflect initial formation conditions near the wellbore and perforations reasonably well.

5.6.1 Capillary Cohesion Between Gas and Water in Fine Sand

Gas-water tests used air as the non-wetting fluid and water as the wetting fluid. The results of these tests are presented in Figure 4-8. It was observed that the index capillary cohesion increases with an increase in air saturation from 0% to 40% to a maximum of 8.4 kPa and then decreases gradually as air saturation increases to 100%.

The ability of the fine sand to arch over a 12.7 mm wide slot perforation under low gas-water saturations was studied using the visualization model. The results of these tests showed that fine sand with gas saturations as high as 99.4% exhibit arching at a slot width/grain diameter ratio of 42. The results of these tests are summarized in Table 5-4. Thus, with regard to Figure 4-8 and Table 5-4, an index capillary cohesion of approximately 1 kPa is sufficient to cause sand arching. This magnitude of cohesion occurs over a range of gas saturation from 1% to 99%.

When the fine sand exhibited arching behavior in the visualization model, an air flow was passed from the top of the visualization model through the sand and out the slot. When the downward air flow was applied, water originally located around the top of the model was pushed down towards the bottom of the model and water began to saturate the sand over the slot. It was concluded that flow of water into partially saturated sand can cause arch failure by decreasing gas saturation. Hall and Harrisberger (1970) examined the effects of the flow of the wetting and nonwetting fluids through a sand pack. Arches remained stable to the outward flow of the nonwetting fluid with the wetting fluid at residual saturation. However, arches failed when subjected to outward flow of the wetting fluid. They point out that the outward flow of the wetting fluid fills the pores of the sand leaving the nonwetting phase as separated globules existing in the voids. The arch fails as the cohesion created by the interfacial tension between the two fluids is decreased, because there are fewer nonwetting fluid-wetting fluid-sand contacts. It may be concluded that flow of the wetting fluid into a partially saturated sand can cause sand arch failure by decreasing the nonwetting fluid saturation and thereby decreasing the capillary cohesion present in the sand.

Direct shear tests were used to provide a direct measurement of capillary cohesion of fine sand at varying gas-water saturations. Fine sand was subjected to direct shear tests and the peak and residual shear stresses were measured under confining stresses of 0, 5, 10 and 15 kPa at gas saturations of 100, 40 and 20%. A porosity of 35% (relative density of 85% for the fine sand) was used for all the direct shear tests.

The results of these direct shear tests are summarized in Table 4-13. Peak shear strength versus normal stress is plotted in Figure 4-12 and the residual shear strength versus normal stress is provided in Figure 4-13. It should be noted when examining Table 4-13 and Figures 4-12 and 4-13 that the results of the 100% gas saturation tests are in terms of effective stress, while the results of the 40% and 20% gas saturation tests are in terms of total stress as the negative (below atmospheric) pore pressure was not measured.

Figure 4-12 indicates peak angles of internal friction for gas saturations of 100, 40 and 20% of 40°, 38° and 38°, respectively. As well, the fine sand at gas saturations of 100, 40 and 20% had peak capillary cohesions of 0, 3.5 and 3.0 kPa, respectively and negative pore pressures of 0, 4.5 and 3.8 kPa, respectively. Since the lines of failure in Figure 4-12 for the three different gas saturations are essentially parallel, changes in strength are due to cohesion effects and not frictional effects. The change in saturation causes the shift in the lines and is reflected in the negative pore pressures observed at the different gas saturations. Thus, numerous values of capillary cohesion may be obtained by varying gas-water saturations of the fine sand.

Figure 4-13 indicates residual angles of internal friction for gas saturations of 100, 40 and 20% of 35°, 29° and 29°, respectively. As well, the fine sand at gas saturations of 100, 40 and 20% had peak capillary cohesions of 0, 1.5 and 1.9 kPa, respectively and negative pore pressures of 0, 2.7 and 3.4 kPa, respectively. The residual capillary cohesions measured are less than the peak capillary cohesions for the 40% and 20% gas saturation tests. It may be postulated that due to the dilation of the samples during shearing (as seen in Appendix B), the voids in the sample become larger. This increase in void size leads to an increased radius of meniscus resulting in lower capillary cohesion. A simple analogy to the voids between sand grains is the capillarity observed in small glass tubes. In glass tubes, the height of rise of a liquid is inversely proportional to the diameter of the tubing; the smaller the inside of the tube, the greater the height of capillary rise (Holtz and Kovacs, 1981).

The peak capillary cohesion for the fine sand at a gas saturations of 20% and 40% measured using the direct shear tests were 3.0 kPa and 3.5 kPa, respectively. The fall cone test provided index capillary cohesions of 3.7 kPa and 8.3 kPa at gas saturations of 20% and 40%, respectively. The different values of capillary cohesion obtained from the two test methods indicates that the fall-cone tests provide a relative measure of capillary cohesion and not an absolute value. However, the fall-cone index capillary cohesion values can be used to predict relative magnitudes of capillary cohesion at varying saturations.

5.6.2 Capillary Cohesion Between Gas and Heavy Oil in Fine Sand

Gas-heavy oil tests utilized air as the non-wetting fluid and oil with a viscosity of 3600 mPa*s as the wetting fluid. The results of these tests are presented in Figure 4-9. Values of index capillary cohesion at gas saturations below approximately 25% were not attainable due to difficulties associated with air entrainment in the gas/heavy oil/sand mixture. Index capillary cohesion increases with an increase in air saturation from 25% to 45% to a maximum of 6.3 kPa and then decreases gradually as air saturation increases to 100%. The index capillary cohesion required to form an arch (approximately 1 kPa) was discussed in the previous section. An index capillary cohesion sufficient to cause sand arching occurs over the full range of gas saturation from above 0% to almost 100%.

5.6.3 Capillary Cohesion Between Gas and Medium Oil in Fine Sand

Gas-medium oil tests utilized air as the non-wetting fluid and oil with a viscosity of 1300 mPa*s as the wetting fluid. The results of these tests are presented in Figure 4-10. Values of index capillary cohesion at gas saturations below approximately 30% were not attainable due to difficulties associated with air entrainment in the gas/medium oil/sand mixture. Index capillary cohesion increases with an increase in air saturation from 30% to 50% to a maximum of 5.5 kPa and then decreases gradually as air saturation increases to 100%. As seen in Figure 4-1, the index capillary cohesion required to form an arch (approximately 1 kPa) occurs over the full range of gas saturation from above 0% to almost 100%.

By comparing Figures 4-9 and 4-10, the effect of the viscosity of the heavy and medium oils on index capillary cohesion may be determined. The heavy oil has a viscosity twice as large as the viscosity of the medium oil. Both oils have similar index capillary curves reaching a peak strength in the range of about 5.5 kPa to 6.5 kPa at gas saturations of 40% to 50%. Thus, the viscosity of the oil used to measure index capillary cohesion does not appear to have a large effect on the strength measured. The similarity of the results is due to the fact that regardless of viscosity, all oils have similar surface tension values. The results of the gas-heavy oil and gas-medium oil index capillary cohesion tests confirm this explanation. In light of this conclusion, future tests involving oil as one of the saturation fluids could be performed with oils having much lower viscosity in order to avoid the difficulties of using highly viscous oils that were experienced in this study.

5.6.4 Capillary Cohesion Between Heavy Oil and Water in Fine Sand

Heavy oil-water tests utilized oil with a viscosity of 3600 mPa*s as the non-wetting fluid and water as the wetting fluid. The results are presented in Figure 4-11. Values of index capillary cohesion at water saturations below approximately 40% were not attainable due to difficulties with air entrainment in the water/heavy oil/sand mixture. It was observed that the index capillary cohesion at approximately 40% water saturation was 3.0 kPa. Index capillary cohesion decreased gradually as water saturation was increased to 100%.

The ability of the fine sand to arch over a 12.7 mm wide slot with low heavy oil saturations was studied using the visualization model. These test results indicated that fine sand will arch at water saturations as high as 99.0% over a slot width/grain diameter ratio of 42. The results of these tests are summarized in Table 5-5. Thus, considering Figure 4-11 and Table 5-5, sand arching occurs over a range of water saturation from at least 55% to

99%. It is uncertain whether sand arching would occur at low water saturations. However, the magnitude of the index capillary cohesion is small and stability of the sand arch would be low. Therefore, at low water saturations, stable sand arches may not develop.

In order to examine more thoroughly the effect of porosity on index capillary cohesion, a plot of index capillary cohesion versus porosity for the fine sand under three conditions is presented in Figure 5-2. These conditions were 40% gas saturation using the heavy oil as the wetting fluid, 45% gas saturation using the medium oil as the wetting fluid and 100% gas saturation (dry sand). It may be clearly seen that under 100% gas saturation (dry sand), changes in intergranular frictional strength due to porosity variations are negligible when compared to the cohesion values measured in Figures 4-8, 4-9, 4-10 and 4-11. When the sand is partially saturated, the change in index capillary cohesion caused by a variation of porosity is significant. Increased porosity results in lower frictional strengths and decreased capillary cohesion strength. However, the change in capillary cohesion strength is much larger relative to the change in frictional strength, as seen in Figure 5-2. Thus, the capillary cohesion strength is more significant in partially saturated sands than the frictional strength.

The results plotted in Figures 4-8, 4-9, 4-10 and 4-11 are for four different sets of saturation fluids. The magnitudes of these curves have been verified theoretically as well as experimentally. Capillary cohesion is proportional to the product of the interfacial tension of the liquid being used and the contact angle against the solid. Using laboratory measured interfacial tensions and contact angles, the theoretical ratios in strength between fluid sets were calculated. These ratios agree reasonably well with the experimental strength ratios for the fall-cone tests and are summarized in Table 4-12. The gas-water/gas-heavy oil ratios have an average of 1.5 compared to a theoretical ratio of 2.2. Likewise, the gas-water/gas-medium oil and gas-heavy oil/gas-medium oil have average ratios of 1.7 and 1.2, respectively, compared to theoretical ratios of 2.6 and 1.2, respectively. The variation between the measured ratios and the theoretical ratios may be due to inaccuracies in either the surface tension of the liquid or the contact angle of the liquid against a solid. Surface tensions of liquid may be determined with a fair degree of accuracy. However, measurements of the contact angle of a liquid against a solid are considerably more difficult. It is expected that inaccuracies in the measurement of the contact angle of the liquid is responsible for the variation between measured and theoretical ratios seen in Table 4-12.

Hall and Harrisberger (1970) observed under stress conditions where arches were unstable in dry or saturated sand, arches were stable if immiscible liquid phases were present and the wetting phase saturation was less than funicular (Islam and George, 1991). When the wetting-phase saturation reaches a funicular state, arches will fail. This agrees well with the failure of arches due to water migration (caused by an air flow) to sand just above the slot perforation observed in this study. Stein and Hilchie (1972), Durrett et al. (1972), Cleary et al. (1979), Veeken et al. (1991) and Islam and George (1991) have also stated that cohesive strength derived from two fluids in a sand plays an important role in arch stability.

Durrett et al. (1976) performed static tensile tests on a simulated formation sand (D_{50} = 0.07 mm) at various levels of air-water saturation to determine cohesive strength. Their measured cohesive strengths are presented in Figure 2-3. Durrett et al. found that cohesive strength increased from 0 kPa at 0% water saturation as the saturation of the wetting phase increased to a maximum of 4.8 kPa (0.70 psi) at a water saturation of 80%. The cohesive strength then decreased to zero as water saturation was increased to 100%. The direct shear capillary cohesion tests performed during this study also measured capillary cohesion at various gas-water saturations. Direct shear tests were performed at water saturations of 0, 60 and 80% and resulted in measured peak capillary cohesions of 0, 3.5 and 3.0 kPa, respectively. Figure 5-3 is a plot of the results of this study and the results of Durrett et al. (1976) for the cohesive strength of a gas-water saturated sand.

Figure 5-3 reveals that the two sets of results agree reasonably well. This indicates that the static tensile tests conducted by Durrett et al. provide similar results to the direct shear capillary cohesion tests performed on gas-water saturated sand.

Durrett et al. used the cohesive strength measured on the air-water system to calculate the cohesive strength for a similar oil-water system having 0.035 N/m interfacial tension. The cohesive strength of the oil-water system is presented in Figure 2-4. The curve has a shape similar to the air-water system with a maximum cohesive strength of 2.4 kPa at 80% water saturation. To calculate the cohesive strength of the oil-water system, Durrett et al. (1976) used a ratio provided by Purcell (1949) based on the magnitudes of cohesive strength being proportional to the product of the surface tension of the liquid being used and the cosine of its angle of contact against the solid. The ratio between the magnitude of capillary pressures for two liquids would then be:

$$X = \frac{\text{surface tension liquid 1 * cosine contact angle of liquid 1 against solid}}{\text{surface tension liquid 2 * cosine contact angle of liquid 2 against solid}}$$

That is, the magnitude of capillary pressure of liquid 1 should be approximately X times greater than the magnitude of capillary pressure of liquid 2. Durrett et al. assumed a surface tension of water of 0.070 N/m and a contact angle of zero and a interfacial tension of oil of 0.035 N/m and a contact angle of zero. This resulted in a ratio of 2.0. That is, the calculated oil-water cohesive strengths were half as large as the air-water cohesive strengths. In this study, the surface tension and contact angle of the water used during the capillary cohesion direct shear tests were measured as 0.072 N/m and 37°, respectively. The heavy oil had a interfacial tension and contact angle of 0.034 N/m and 39°, respectively. These values result in a ratio of 2.18. The calculated peak capillary cohesions of the oil-water system at water saturations of 0, 60 and 80% are 0, 1.6 and 1.4 kPa, respectively. The calculated cohesive strengths for the respective oil-water systems of Durrett et al. and this study are plotted in Figure 5-4. Due to the different ratios used to calculate the oil-water systems' cohesive strengths there is a slightly increased difference between the two sets of results. However, the results are still quite similar.

The laboratory testing program undertaken by Golder Associates Ltd. (Weaver, 1994) measured apparent cohesion induced by multi-phase pore fluid capillary in a sand matrix. As well, the influence of porosity and oil-water ratio on the magnitude of apparent cohesion was investigated. They chose direct shear tests at normal stresses from 0 to 20 kPa to measure the apparent cohesion. A clean tailings sand with a D_{50} of approximately 0.2 mm was used along with a mineral oil having a viscosity similar to water for the test specimens. Reagent grade deionized water (pH=7) was used in the testing program. Specimens were water-wet, oil saturated and compacted to a desired porosity.

The first set of tests was on specimens at a dry density of 15.3 kN/m^3 (porosity = 43%) and at 70% oil saturation and 30% water saturation. These tests resulted in an apparent cohesion of 4.5 kPa and a curved peak shear strength envelope with a peak secant friction angle of 46°. The slope of the peak shear strength envelope decreased with increasing normal effective stress. The constant volume (residual) shear strength envelope had a friction angle of 43° and zero cohesion. The details of the first set of tests are summarized in Table 2-3 and Figure 2-8 presents the peak and residual strength envelopes.

The second set of tests at dry densities of 16.0 kN/m^3 (porosity = 40%) and an oil/water ratio of 70:30 were sheared at normal stresses of 0, 5 and 10 kPa. Similar to the first set of tests, a curved peak shear strength envelope was obtained with a peak secant friction angle of 55° and the peak apparent cohesion was measured as 4.5 kPa. The residual shear strength had a friction angle of 39° and zero cohesion. These results led Golder Associates Ltd. to conclude that porosity of the sand appeared to not have a major influence on apparent cohesion, in the porosity range used in their testing program. The details of the second set of tests are summarized in Table 2-3 and Figure 2-9 presents the peak and residual strength envelopes.

The third set of tests investigated the influence of the oil/water ratio. Samples had an oil/water ratio of 50:50 and a dry density of 15.3 kN/m^3 (porosity = 43%) and were sheared at normal effective stresses of 0, 5 and 10 kPa. As in the other sets of tests, a curved peak shear strength envelope was measured with a peak secant friction angle of 55°. However, the peak apparent cohesion had a value of 2.7 kPa. The residual shear strength had a friction angle of 42° and cohesion of zero. Thus, the reduced oil saturation resulted in a decrease in the apparent cohesion. The details of the third set of tests are summarized in Table 2-3 and Figure 2-10 presents the peak and residual strength envelopes.

The peak friction angles for the tests performed at oil/water ratios of 70:30 and porosities of 43% and 40% were 46° and 55°, respectively. As expected, decreased porosity results in higher peak friction angles. The denser the sand, the greater the expansion which tends to take place during shear and more energy must be used to shear the soil resulting in a higher friction angle. The residual friction angles of the first, second and third sets of tests were 43°, 39° and 42°, respectively. It was expected that the residual friction angles for the three tests be similar since after considerable straining of any soil, initial porosity has no effect on the residual strength of a sand.

The peak friction angles for the tests performed at porosities of 43% and oil/water ratios of 70:30 and 50:50 were 46° and 55°, respectively. If the changes in strength are due only to cohesion effects and not frictional effects, the peak friction angles should be approximately the same and only a change in cohesion should be observed. Peak friction angles of 40°, 38° and 38° were obtained when direct shear tests were performed on gas-water sand packs at gas saturations of 100, 40 and 20%, respectively, indicating that the change in strength was due to cohesion effects. As reported above, Weaver's tests do not follow this trend.

To summarize, they found apparent cohesions of the oil-water saturated sand of 4.5 kPa and 2.7 kPa at water saturations of 30% and 50%, respectively. They performed two sets of tests at 30% water saturation at two different porosities that resulted in the same apparent cohesion leading to the conclusion that porosity (in the range tested) had no major influence on apparent cohesion. The results of the Golder Associates Ltd. direct shear tests are also plotted on Figure 5-4.

Weaver's results measured using an oil-water sand pack are somewhat higher than the results obtained during this study and those obtained by Durrett et al. (1976) which were converted from a gas-water sand pack using Purcell's equation. Capillary cohesion values for oil-water-sand packs were calculated from the direct shear tests performed during this study on the gas-water-sand packs. Similar calculations were used to convert the capillary cohesion strengths found by Durrett et al. (1976) using gas-water-sand packs. Both this study and Durrett et al. gave cohesive strengths up to 2 kPa depending on water saturation. Actual direct shear measurements performed by Weaver (1994) gave cohesive strengths up to 4.5 kPa. Conversion of gas-water capillary cohesion measurements to oil-water capillary cohesion values using Purcell's equation appears to underestimate the oil-water capillary cohesion. The equation is only an approximation and, if important, the capillary cohesion should be measured using the appropriate oil-water saturations.

Table 5-1

Effect of Sand Particle Size and Perforation Diameter

Sand Type	Average Grain Size (mm)	Slot Width (mm)	Slot Width/Grain Diameter Ratio	Sand Flow /Arching
Fine	0.3	5	16.7	Sand Flow
Fine	0.3	12.7	42.3	Sand Flow
Fine	0.3	19.1	63.7	Sand Flow
Medium	1.2	5	4.2	Sand Flow
Medium	1.2	12.7	10.6	Sand Flow
Medium	1.2	19.1	15.9	Sand Flow
Coarse	1.6	5	3.1	Arching
Coarse	1.6	12.7	7.9	Sand Flow
Coarse	1.6	19.1	11.9	Sand Flow

Table 5-2

Effect of Shape & Roughness of Perforation

(For a 5 mm Wide Slot)

Sand Type	Average Grain Size (mm)	Slot Width (mm)	Slot Width/Grain Diameter Ratio	Slot Length (mm)	Slot Surface	Sand Flow /Arching
Fine	0.3	5	16.7	10	Smooth	Sand Flow
Fine	0.3	5	16.7	50	Smooth	Sand Flow
Fine	0.3	5	16.7	10	Rough	Sand Flow
Fine	0.3	5	16.7	50	Rough	Sand Flow
Medium	1.2	5	4.2	10	Smooth	Sand Flow
Medium	1.2	5	4.2	50	Smooth	Sand Flow
Medium	1.2	5	4.2	10	Rough	Sand Flow
Medium	1.2	5	4.2	50	Rough	Sand Flow
Coarse	1.6	5	3.1	10	Smooth	Arching
Coarse	1.6	5	3.1	50	Smooth	Arching
Coarse	1.6	5	3.1	10	Rough	Arching
Coarse	1.6	5	3.1	50	Rough	Arching

Table 5-3

Effect of Confining Stress

(For a 5 mm Wide Slot)

Sand Type	Average Grain Size (mm)	Slot Width (mm)	Slot Width/Grain Diameter Ratio	Confining Stress (kPa)	Sand Flow /Arching
Fine	0.3	5	16.7	0	Sand Flow
Fine	0.3	5	16.7	145	Sand Flow
Fine	0.3	5	16.7	300	Sand Flow
Medium	1.2	5	4.2	0	Sand Flow
Medium	1.2	5	4.2	145	Sand Flow
Medium	1.2	5	4.2	300	Sand Flow
Coarse	1.6	5	3.1	0	Arching
Coarse	1.6	5	3.1	145	Arching
Coarse	1.6	5	3.1	300	Arching

Table 5-4

Gas-Water Low Saturation Tests

Sand Type	Gas Saturation (%)	Average Grain Size (mm)	Slot Width (mm)	Sand Flow /Arching
Fine	70	0.3	12.7	Arching
Fine	82	0.3	12.7	Arching
Fine	91	0.3	12.7	Arching
Fine	96.2	0.3	12.7	Arching
Fine	98.8	0.3	12.7	Arching
Fine	99.4	0.3	12.7	Arching
Fine	99.7	0.3	12.7	Sand Flow

Table 5-5

Heavy Oil-Water Low Saturation Tests

Sand Type	Water Saturation (%)	Average Grain Size (mm)	Slot Width (mm)	Sand Flow /Arching
Fine	83.0	0.3	12.7	Arching
Fine	94.6	0.3	12.7	Arching
Fine	97.0	0.3	12.7	Arching
Fine	99.0	0.3	12.7	Sand Flow

Figure 5-1: Effect of Sand Porosity on Dry Fine Sand

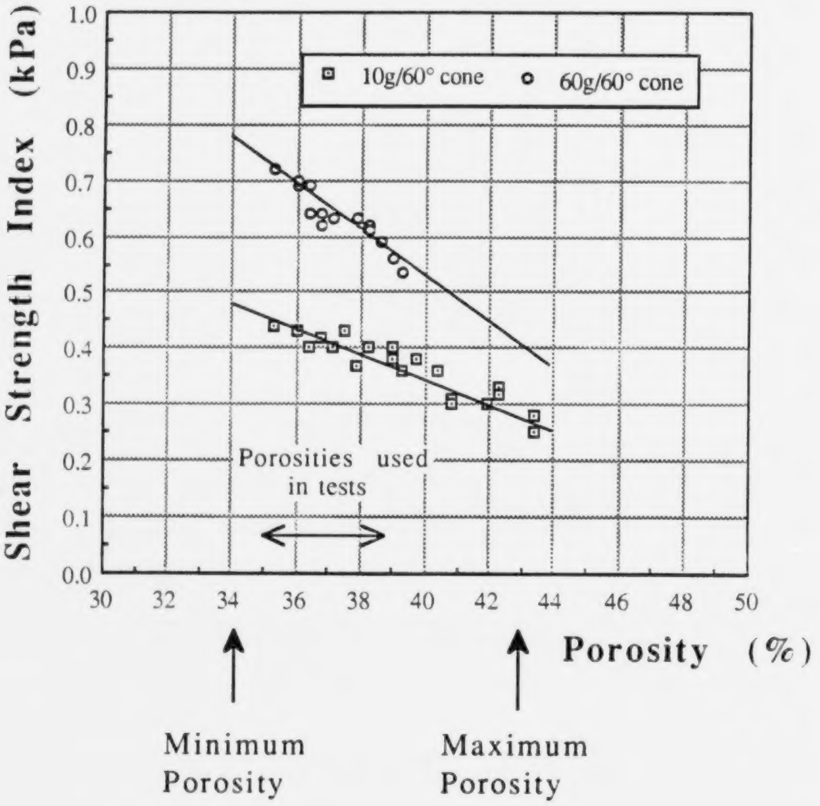

Figure 5-2: Effect of Sand Porosity on Partially Saturated Fine Sand

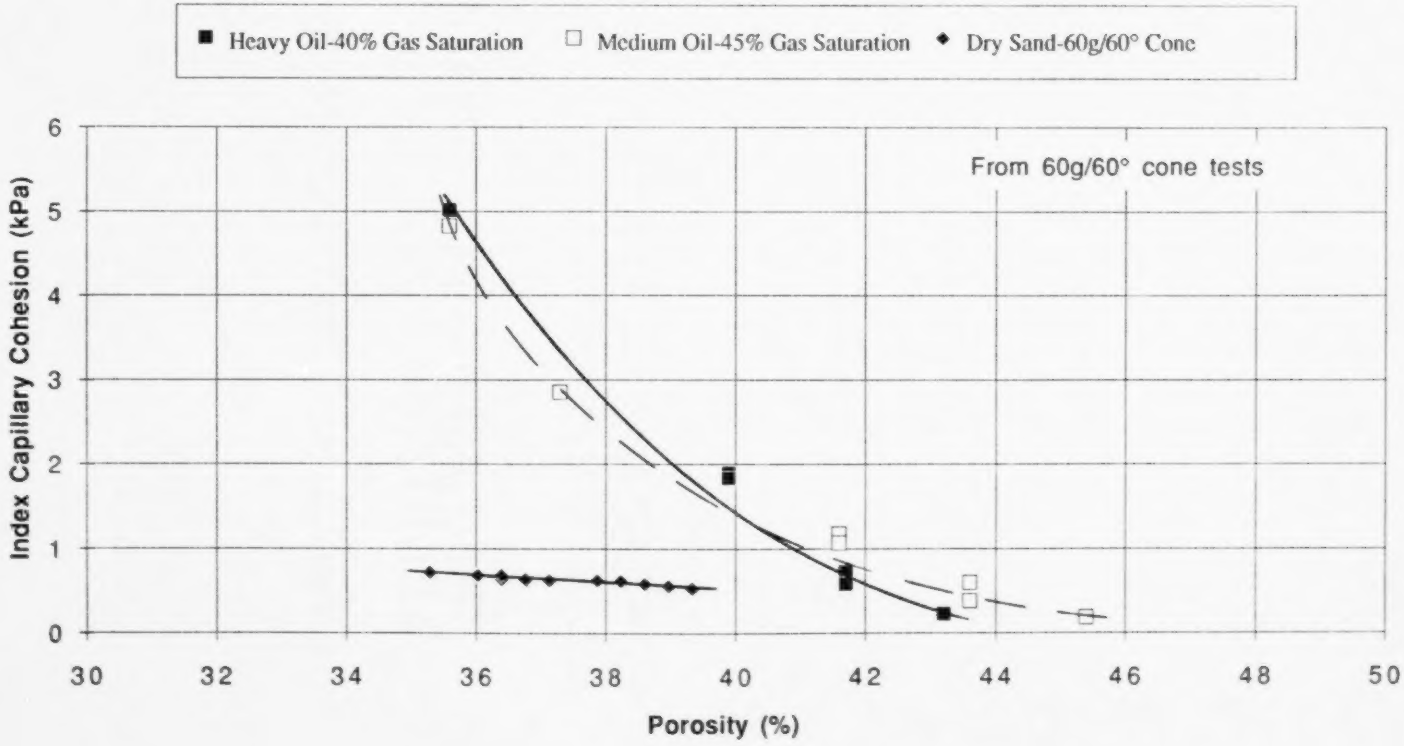

Figure 5-3: Comparison of Capillary Cohesions Measured on Gas-Water Systems

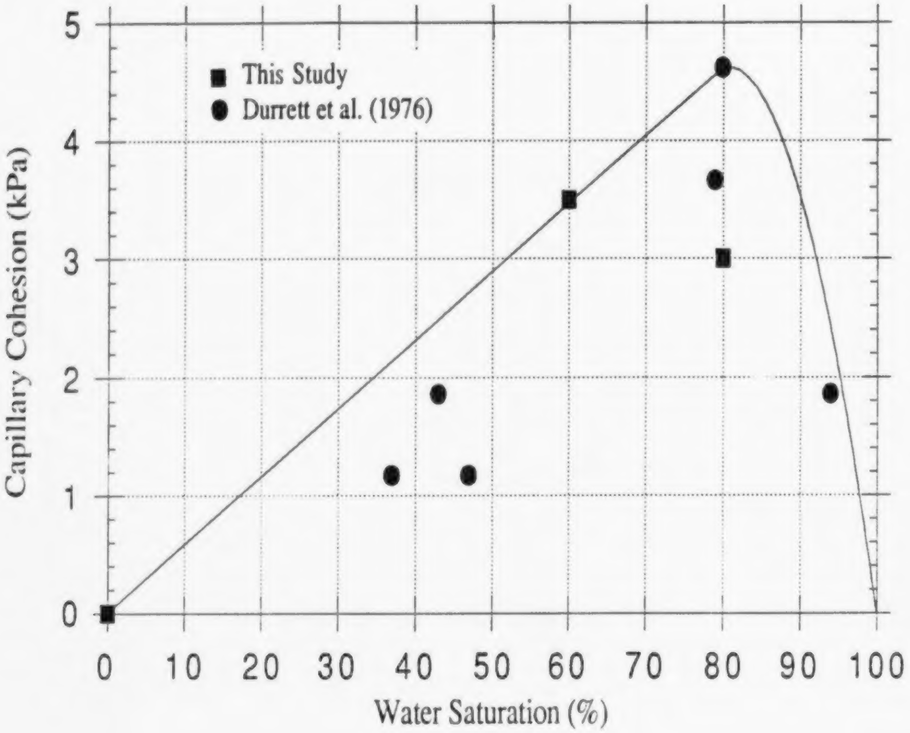

Figure 5-4: Comparison of Capillary Cohesions Measured on Oil-Water Systems

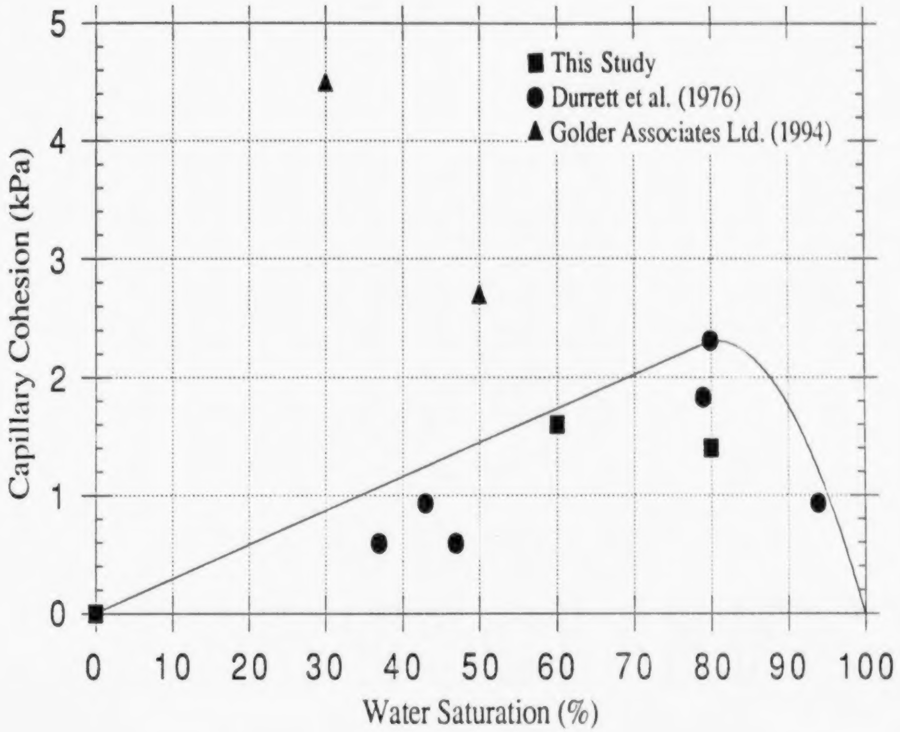

6. Conclusions and Recommendations

6.1 Summary

Results of tests using the fine, medium and coarse sand indicate that uniform, dry, subrounded sand, under no confining stress, will exhibit no arching behavior until the slot width is less than four times the sand grain diameter. As well, uniform, fully water saturated, subrounded sand, under no confining stress, follows the same arching criteria stated above. However, increased angularity, grain size distribution and coarseness of sand grains increases the shear strength of sand. This allows angular, well graded and coarse sand to form arches at larger grain diameter to width of opening ratios than round, uniform, fine sand. A test in the literature indicated that for a uniform, coarser, angular sand, the sand arches when the perforation diameter was about nine times larger than the sand. Therefore, for the formation sand subjected to low or no confining stress and typical perforation diameters where the perforation is 85 times larger than the sand, arching will not occur if there is only one fluid in the sand pores.

The shape of the perforation used in this study was a rectangular slot. Slot lengths from 10 mm to 50 mm long were used to provide a greater opportunity for the sand grains to form an obstruction within the length of the slot. The inside of the slot was also varied from a smooth surface to a rough surface. Regardless of the slot length or surface characteristics, under test conditions where sand was found to flow through the slot, the variation of the above variables had no effect on impeding the flow of sand. Arch structures that did form always did so above the slot and never along the length of the slot. It was concluded that the shape and roughness of the perforation have no effect on sand arching when subjected to low or no confining stress.

Porosity variations in dry fine sand have little effect on frictional shear strength measured by the fall-cone tests when compared to the magnitude of index capillary cohesion measurements. Capillary cohesion is created by the presence of two immiscible fluids in a sand. The influence of porosity on the index capillary cohesion of partially saturated sand, however, is significant.

The influence of confining stress on arching behavior was investigated. In earlier tests, the fine and medium sands exhibited no arching behavior Similar to the behavior observed under no confining stress, the medium and fine sands under dry conditions and confining stresses up to 300 kPa exhibited no arching behavior.

However, increased confining stress resulted in decreased sand flow rates through the perforation. Due to the increased confining stress applied to the sand, increased interparticle stresses are present and the sand has a larger shear strength. It may be postulated that the confining stress could be increased to a large enough value that the intergranular shear strength could prevent sand flow. Such an action may not be true arching but a bridging phenomena. Other related published works indicate that a high confining stress (>3 MPa) can initiate arching and increase arch stability in dry angular sand, but confining stresses up to 14 MPa could not induce arching in dry rounded sand. It is believed that a confining stress of approximately 7000 kPa would be sufficient to cause the subrounded, dry, fine sand used in this project to arch over a 12.7 mm (1/2 inch) slot perforation. This value of confining stress was determined by evaluating the behavior of similar sands under high confining stress presented by other researchers. As well, a change in the sand flow pattern from a parabolic shape when no confining stress was applied to a dome shaped flow pattern when a confining stress was applied occurred.

Similar to tests performed with no confining stress, the dry coarse sand exhibited arching behavior at confining stresses up to 300 kPa when the grain diameter to width of opening ratio was less than four. Arches may be destroyed by vibration; however, it appears to be more difficult to destroy arches formed under the influence of a confining stress.

A stable arch subjected to gradually increased fluid flow rates remained stable until a high fluid flow rate was applied. Thus, a high fluid flow rate can break down a sand arch. As well, gradual rate increases result in higher sand free fluid production when compared to sudden increases to full rate. Work by Tippie and Kohlhaas (1973) support this conclusion. Other related published works indicate that a low fluid flow rate results in smaller arches that are more stable and a high fluid flow rate results in larger arches that are less stable.

Hall and Harrisberger (1970) stated that air drawn into dry, rounded sand allowed the formation of arches at grain diameter to width of opening ratios that previously failed to induce arching. They concluded that the drag force on the surface grains gave enough restraint to initiate an arch. The same types of tests performed with the visualization model indicated that when sufficient upward air flow was applied, sand flow through the slot perforation stopped. However, it has been concluded that this stoppage of sand flow is not an arching phenomena. Instead, it is believed that fluidization of the sand grains above the slot perforation due to upward air velocities exceeding the minimum fluidization velocities is responsible for stopping the sand flow out of the model. Pressure measurements taken during these tests support this conclusion.

The capillary cohesion between gas and water in fine sand was investigated. The index capillary cohesion increases with an increase in gas saturation from 0% to 40% to a maximum of 8.4 kPa and then decreases gradually as gas saturation increases to 100%. An index capillary cohesion of approximately 1 kPa is sufficient to cause sand arching at slot width/grain diameter ratios greater than four. This magnitude of cohesion occurs over a range of gas saturation from 1% to 99%.

Flow of the wetting fluid into a partially saturated sand can cause sand arch failure by decreasing the nonwetting fluid saturation and thereby decreasing the capillary cohesion present in the sand. It was found in this study that flow of water into partially saturated sand can cause sand arch failure by decreasing gas saturation. Other researchers have found that arches remain stable when subjected to flow of the nonwetting fluid, but failed when the wetting fluid was flowed through the sand.

Direct measurements of capillary cohesion at varying gas saturations were obtained from direct shear tests. At a gas saturation of 100%, peak and residual capillary cohesions are both 0 kPa. At a gas saturation of 40%, peak and residual capillary cohesion are 3.5 kPa and 1.5 kPa, respectively. Finally, at a gas saturation of 20%, the peak capillary cohesion was 3.0 kPa, while the residual capillary cohesion was 1.9 kPa.

The capillary cohesion between gas and heavy oil in fine sand was examined. Index capillary cohesion increases with an increase in gas saturation from 25% to 45% to a maximum of 6.3 kPa and then decreases gradually as gas saturation increases to 100%. An index capillary cohesion sufficient to cause sand arching occurs over the full range of gas saturation from above 0% to almost 100%.

The capillary cohesion between gas and medium oil in fine sand was investigated. Index capillary cohesion increases with an increase in gas saturation from 30% to 50% to a maximum of 5.5 kPa and then decreases gradually as gas saturation increases to 100%. An index capillary cohesion sufficient to cause sand arching occurs over the full range of gas saturation from above 0% to almost 100%.

The capillary cohesion between heavy oil and water in fine sand was examined by fall cone tests. Index capillary cohesion at 40% water saturation has a value of 3.0 kPa and then decreases gradually as water saturation increases to 100%. It is uncertain whether sand arching would occur at low water saturations. However, the magnitude of the index capillary cohesion is small and stability of the sand arch would be low. Therefore, at low water saturations, stable sand arches may not develop.

Capillary cohesion values for oil-water-sand packs were calculated from the direct shear tests on the gas-water-sand packs. These values and other published values gave cohesive strengths up to 2 kPa depending on water saturation. Actual direct shear measurements in the literature gave cohesive strengths up to 4.5 kPa. Conversion of gas-water capillary cohesion measurements to oil-water capillary cohesion values using Purcell's equation appears to underestimate the oil-water capillary cohesion. The equation is only an approximation and, if important, the capillary cohesion should be measured using the appropriate oil-water saturations.

6.2 Conclusions

The following variables were investigated to determine their effect on sand flow into and through well casing perforations.

1. Sand Particle Size and Perforation Diameter

- For the formation sand and typical perforation diameters of 12.7 to 19.1 mm, arching will not occur if there is only one fluid in the sand pores under conditions of low confining stress.

2. Shape and Roughness of Perforation Opening

- Shape and roughness of perforation opening has no effect on sand arching at low confining stress.

3. Sand Porosity

- Porosity variations have little effect on frictional shear strength of dry, fine sand relative to the magnitude of index capillary cohesions.
- However, the influence of porosity on partially saturated sand is significant.

4. Confining Stress

- No arching is exhibited with fine and medium sands at confining stresses up to 300 kPa.
- Increased confining stress results in decreased sand flow rates.
- Other related published works indicate that a high confining stress (>3 MPa) can initiate arching.
- Arch stability increases with increasing confining stress.

5. Flow Conditions Through Sand and Perforations

- A high fluid flow rate can break down an arch.
- Gradual fluid flow rate increases result in higher sand free production compared to sudden increases.

6. Index Capillary Cohesion Between Gas and Water in Fine Sand

- Index capillary cohesion increases with gas saturation from 0% to 40% reaching a maximum of 8.4 kPa, then gradually decreases as gas saturation increases to 100%.
- An index capillary cohesion of ≈1 kPa is sufficient to cause arching and this magnitude of index capillary cohesion occurs over a gas saturation range of 1% to 99%.
- Flow of the wetting fluid into partially saturated sand can cause arch failure by decreasing the nonwetting fluid saturation and thereby decreasing the capillary cohesion present in the sand.

7. Index Capillary Cohesion Between Gas and Heavy Oil in Fine Sand

- Index capillary cohesion increases with gas saturation from 25% to 45% reaching a maximum of 6.3 kPa, then gradually decreases as gas saturation increases to 100%.
- An index capillary cohesion sufficient to cause arching occurs over a gas saturation range from above 0% to almost 100%.

8. Index Capillary Cohesion Between Gas and Medium Oil in Fine Sand

- Index capillary cohesion increases with gas saturation from 30% to 50% reaching a maximum of 5.5 kPa, then gradually decreases as gas saturation increases to 100%.
- An index capillary cohesion sufficient to cause arching occurs over a gas saturation range from above 0% to almost 100%.

9. Index Capillary Cohesion Between Heavy Oil and Water in Fine Sand

- Index capillary cohesion at 40% water saturation is 3.0 kPa, then gradually decreases as water saturation increases to 100%.
- It is uncertain whether arching would occur at low water saturations, however, the magnitude of index capillary cohesion is small and stability of the arch would be low.

10. Capillary Cohesion From Direct Shear Tests

- Capillary cohesion values for oil-water-sand packs were calculated from tests on gas-water-sand packs.
- This resulted in cohesive strengths up to 2 kPa depending on water saturation.
- Actual direct shear tests on oil-water-sand packs gave cohesive strengths of up to 4.5 kPa.

6.2 Recommendations For Further Research

The complexity of the mechanisms of sand production creates a large area suitable for further research. With regard to laboratory visualization modeling, it is recommended that a visualization model capable of withstanding very high confining stresses, in the range of 15 to 20 MPa, but still allowing for the visual observation of sand flow mechanisms at the perforation, be constructed. This would allow the very high stress ranges cited in work by other researchers to be analyzed using the visualization model technique. The ability to visually examine the sand grains at the perforation would be essential to the model, so a unique design using transparent material, able to withstand high confining stresses, would be necessary.

With regard to capillary cohesion testing, air entrainment in two oil-water-sand pack mixtures proved to create difficulties in obtaining low saturations of the wetting fluid, water. It is recommended that an improved method of mixing of oil and water in sand be developed so that air entrainment will be avoided and low saturations of the wetting fluid can be tested.

As well, it is recommended that further capillary cohesion direct shear tests be performed. Further tests should focus on different degrees of fluid saturations, the use of fluids of different viscosities and different levels of confining stress.

References

American Society For Testing and Materials, "Standard Test Method for Direct Shear Test of Soil Under Consolidated Drained Conditions," Designation D 3080-90, 1993, pp 417-422.

American Society For Testing and Materials, "Standard Test Method for Maximum Index Density of Soils Using a Vibratory Table," Designation D 4253-93, 1993, pp 661-673.

American Society For Testing and Materials, "Standard Test Method for Minimum Index Density of Soils and Calculation of Relative Density," Designation D 4254-91, 1993, pp 674-681.

American Society For Testing and Materials, "Standard Test Method for Particle -Size Analysis of Soils," Designation D 422-63 (Reapproved 1990), 1993, pp 93-99.

American Society For Testing and Materials, "Standard Test Method for Permeability of Granular Soils (Constant Head)," Designation D 2434-68 (Reapproved 1974), 1993, pp 308-312.

American Society For Testing and Materials, "Standard Test Method for Specific Gravity of Soils," Designation D 854-92, 1993, pp 176-179.

Amyx, J.W., Bass, D.M. and Whiting, R.L., Petroleum Reservoir Engineering, Vol. 1, New York, McGraw-Hill Book Company, Inc., 1960, 610 p.

Bratli, R.K. and Risnes, R., "Stability and Failure of Sand Arches," paper SPE 8427, Presented at the SPE 54th Annual Technical Conference and Exhibition, Las Vegas, Sept. 23-26, 1979, pp 236-248.

Brown, R.L. and Richards, Principles of Powder Mechanics, New York, Pergamon Press, 1970, p. 221.

Chalaturnyk, R.J., Wagg, B.T. and Dusseault, M.B., "The Mechanisms of Solids Production in Unconsolidated Heavy-Oil Reservoirs," paper SPE 23780 presented at the Society of Petroleum Engineers International Symposium on Formation Damage Control, Lafayette, 1992, pp 137-149.

Cleary, M.P., Melvan, J.J. and Kohlhaas, C.A., "The Effect of Confining Stress and Fluid Properties on Arch Stability in Unconsolidated Sands," paper SPE 8426 presented at the SPE 54th Annual Technical Conference and Exhibition, Las Vegas, Sept. 23-26, 1979, 7 p.

Durrett, J.L., Golbin, W.T., Murray, J.W. and Tighe, R.E., "Seeking a Solution to Sand Control," paper SPE 6210 presented at the 51st Annual Fall Technical Conference and Exhibition, SPE of AIME, New Orleans, Oct. 3-6, 1976, pp 1664-1672.

Hall, C.D., Jr. and Harrisberger, W.H., "Stability of Sand Arches: A Key to Sand Control," Journal of Petroleum Technology, July, 1970, pp 821-829.

Hansbo, S., "A New Approach to the Determination of the Shear Strength of Clay by the Fall-Cone Test," Proceedings No. 14, Swedish Geotechnical Institute, 1957, 47 p.

Holtz, R.D. and Kovacs, W.D., An Introduction to Geotechnical Engineering, Englewood Cliffs, New Jersey, Prentice-Hall, Inc., 1981, 733 p.

Islam, M.R. and George, A.E., "Sand Control in Horizontal Wells in Heavy-Oil Reservoirs," Journal of Petroleum Technology, July, 1991, pp 844-853.

Jardine, D., "Cretaceous Oil Sands of Western Canada," In: Hills, L.V. (Ed.), Oil Sands Fuel of the Future, Canadian Society of Petroleum Geologists memoir 3, pp 50-67.

Klinkenberg, L.J., The Permeability of Porous Media to Liquids and Gases, Drilling and Production Practices, American Petroleum Institute, 1941, pp 200-213.

Kunni, D. and Levenspiel, O., Fluidization Engineering, New York, John Wiley and Sons, 1969, 534 p.

Lambe, T.W. and Whitman, R.V.: Soil Mechanics SI Version, New York, John Wiley and Sons, 1979, 553 p.

McCaffrey, B., "Recent Success in Primary Bitumen Production, " paper presented at the 7th Annual Heavy Oil and Oil Sands Technical Symposium, Calgary,.1990.

Purcell, W.R., "Capillary Pressures - Their Measurements Using Mercury and the Calculation of Permeability Therefrom," Trans., AIME, 1949, Vol. 186, 39, pp 39-48.

Risnes, R., Bratli, R.K. and Horsrud, P., "Sand Arching - A Case Study," EVR 310, Presented at the European Petroleum Conference, London, England, Oct. 25-28, 1982, pp 313-317.

Rumpf, H.: Agglomeration, W.A. Knepper, Ed., New York, Interscience Publishers (1961).

Selby, R.W. and Farouq Ali, S.M.: "Mechanics of Sand Production and the Flow of Fines in Porous Media," Journal of Canadian Petroleum Technology, Vol. 27, No. 3, May-June 1988,.pp 55-63.

Stein, N. and Hilchie, D.W., "Estimating the Maximum Producing Rate Possible from Friable Sandstones Without Using Sand Control," Journal of Petroleum Technology, Sept., 1972, pp 1157-1160.

Stein, N., Odeh, A.S. and Jones, L.G. "Estimating Maximum Sand-Free Production Rates From Friable Sands for Different Well Completion Geometries," Journal of Petroleum Technology, Oct., 1974, pp 1156-1158.

Suman, G.O., Jr., "Unconsolidated Sand Stabilization Through Wellbore Stress State Control," paper SPE 8427 presented at the 54th Annual Technical Conference and Exhibition SPE of AIME, Las Vegas, Sept. 23-26, 1979, 6 p.

Taylor, D.W., Fundamentals of Soil Mechanics, New York, John Wiley and Sons, Inc., 1948, p. 700.

Terzaghi, K., Theoretical Soil Mechanics, New York, John Wiley and Sons, Inc., 1943, pp 66-76.

Tippie, D.B. and Kohlhaas, C.A., "Effect of Flow Rate on Stability of Unconsolidated Producing Sands," paper SPE 4533 presented at the 48th Annual Fall Meeting SPE of AIME, Las Vegas, Sept., 30 to Oct. 3, 1973, 11 p.

Tippie, D.B. and Kohlhaas, C.A., "Variation of Skin Damage with Flowrate Associated with Sand Flow or Unstability in Unconsolidated Sand Reservoirs," paper SPE 4886 presented at the SPE 44th Annual California Meeting, San Francisco, April 4-5, 1974, 6 p.

Veeken, C.A.M., Davies, D.R., Kenter, C.J. and Kooijman, A.P., "Sand Production Prediction Review: Developing an Integrated Approach," paper SPE 22792 presented at the 66th Annual Technical Conference and Exhibition of the Society of Petroleum Engineers, Dallas,1991, pp 335-346.

Weaver, J., Imperial Oil Research, Calgary, Alberta., Personnel Communication, 1994.

Appendix A

Dry Sand Direct Shear Tests

Shear Stress vs. Horizontal Displacement Plots

Increase in Height vs. Horizontal Displacement Plots

Wall Friction Direct Shear Tests

Shear Stress vs. Horizontal Displacement Plots

Increase in Height vs. Horizontal Displacement Plots

Figure A-1: Shear Stress vs. Horizontal Displacement - Dry Fine Sand

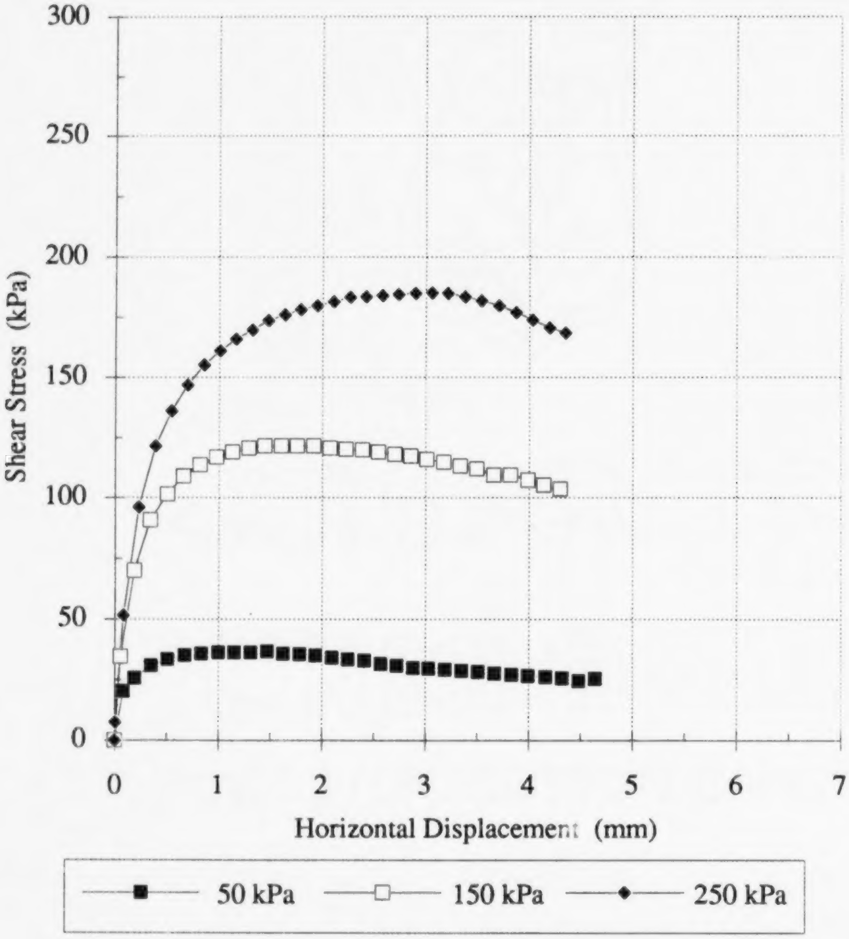

Figure A-2: Vertical Displacement vs. Horizontal Displacement - Dry Fine Sand

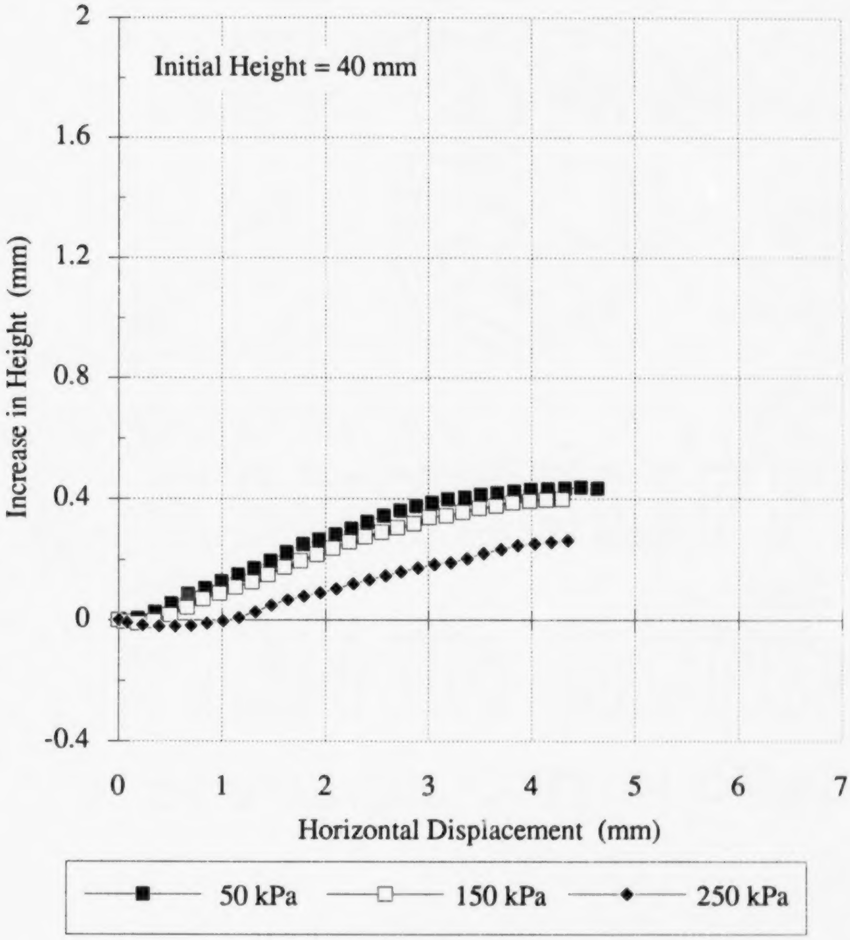

Figure A-3: Shear Stress vs. Horizontal Displacement - Dry Medium Sand

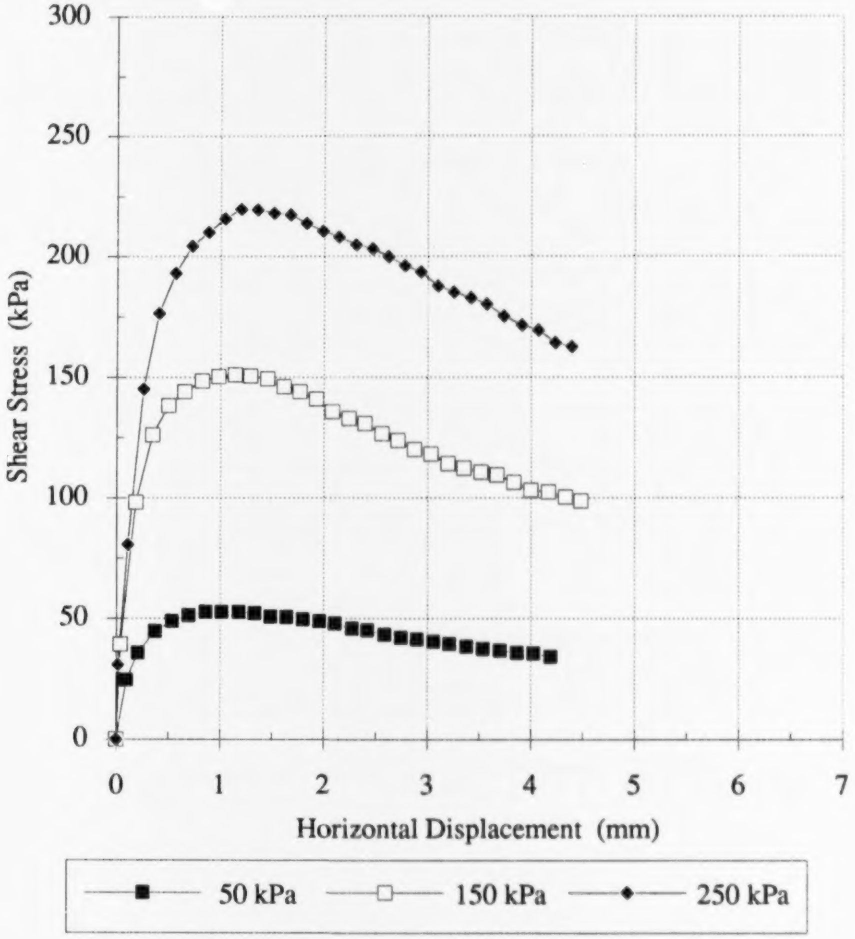

Figure A-4: Vertical Displacement vs. Horizontal Displacement - Dry Medium Sand

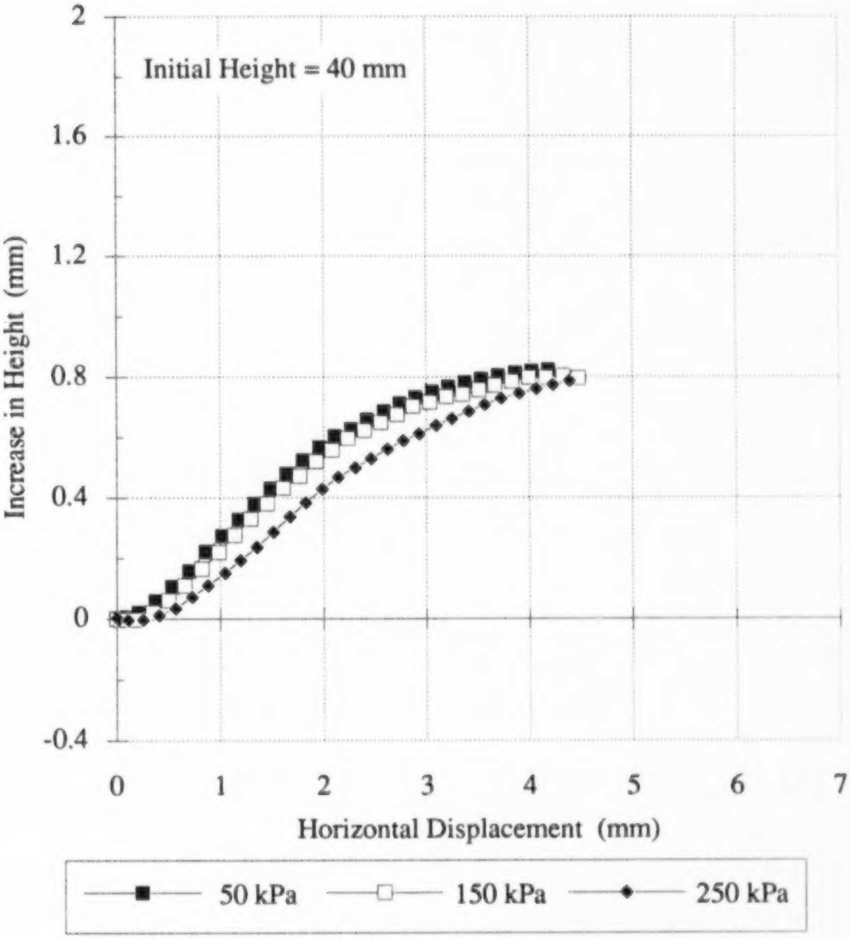

Figure A-5: Shear Stress vs. Horizontal Displacement - Dry Coarse Sand

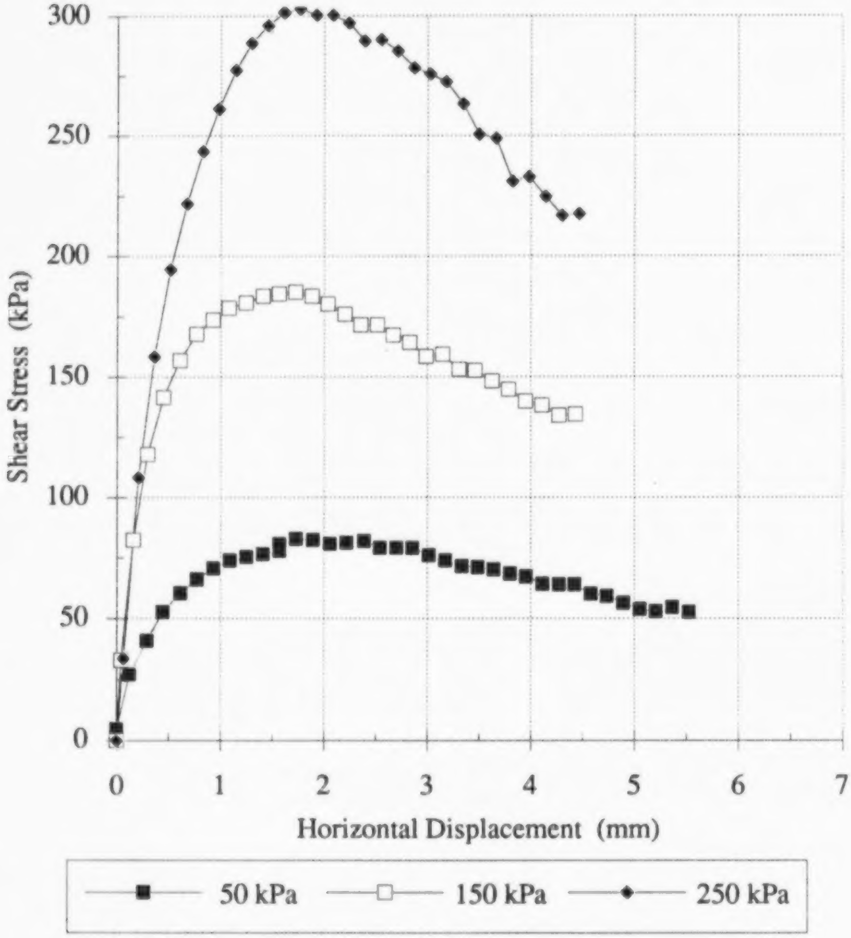

Figure A-6: Vertical Displacement vs. Horizontal Displacement - Dry Coarse Sand

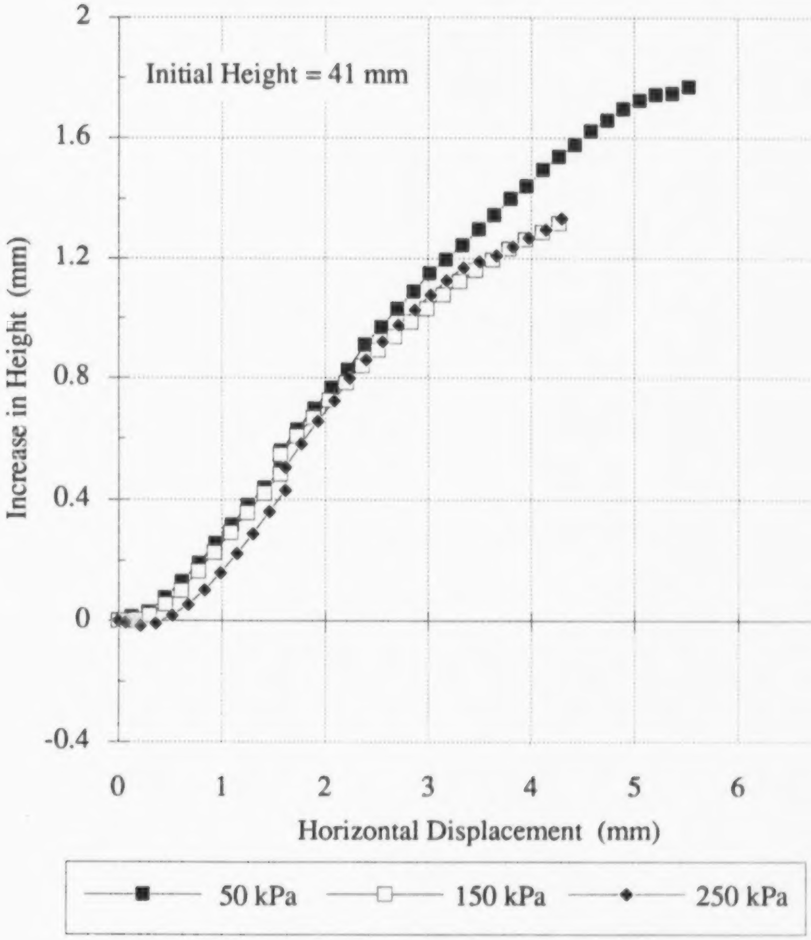

Figure A-7: Shear Stress vs. Horizontal Displacement - Dry Fine Sand/Plexiglass Interface

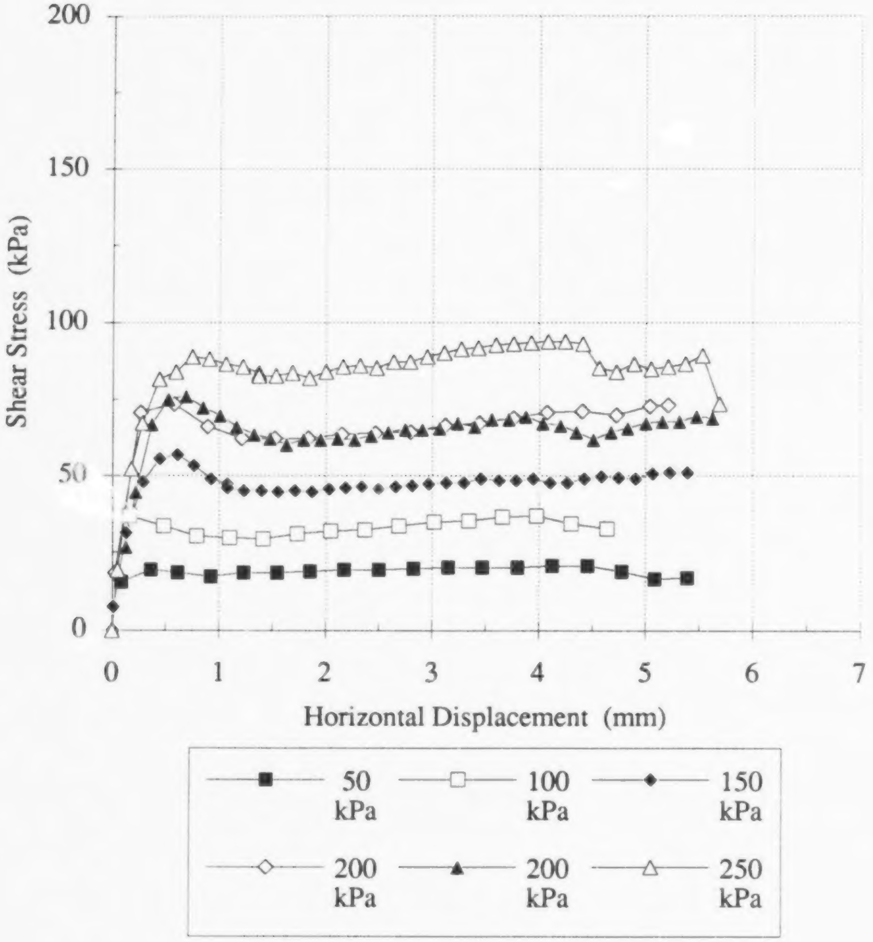

Figure A-8: Vertical Displacement vs. Horizontal Displacement - Dry Fine Sand/Plexiglass Interface

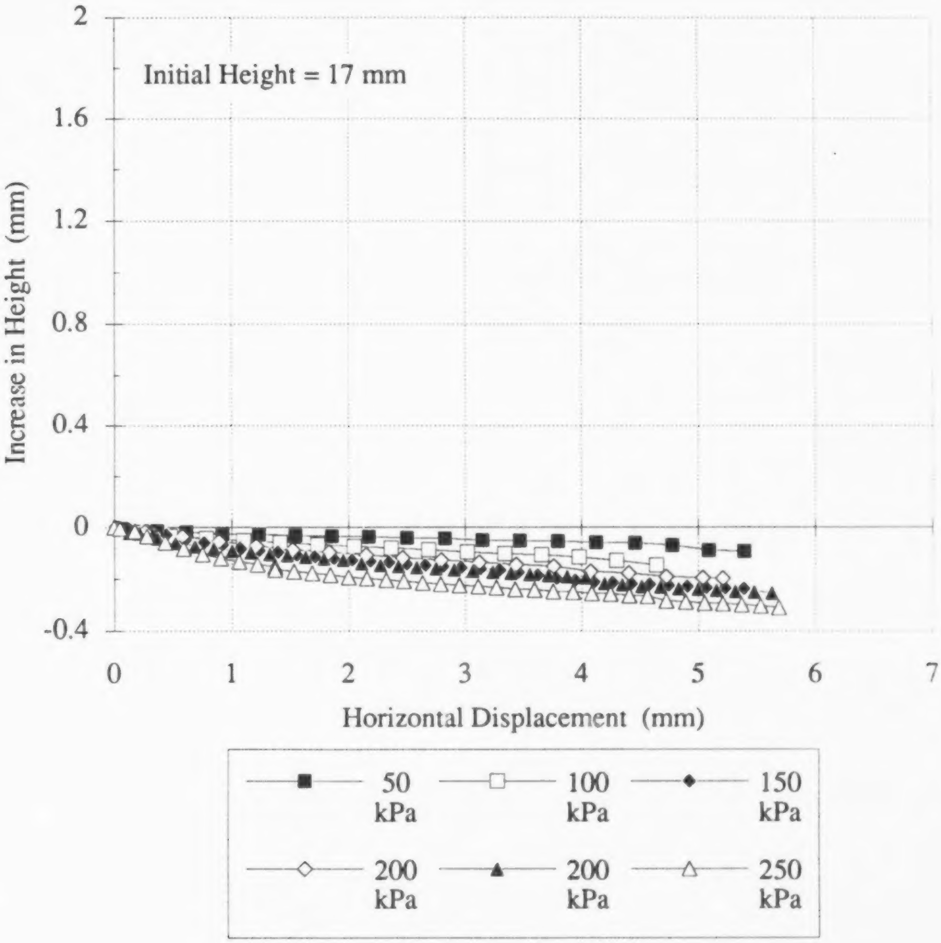

Figure A-9: Shear Stress vs. Horizontal Displacement - Dry Medium Sand/Plexiglass Interface

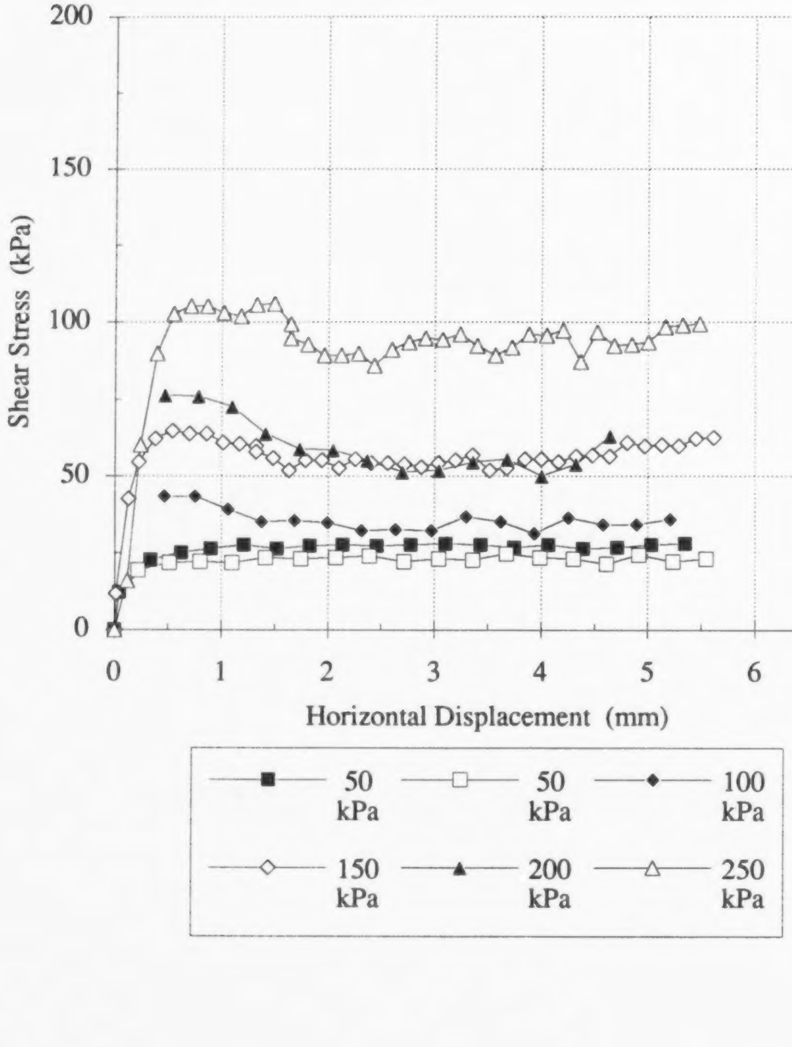

Figure A-10: Vertical Displacement vs. Horizontal Displacement - Dry Medium Sand/Plexiglass Interface

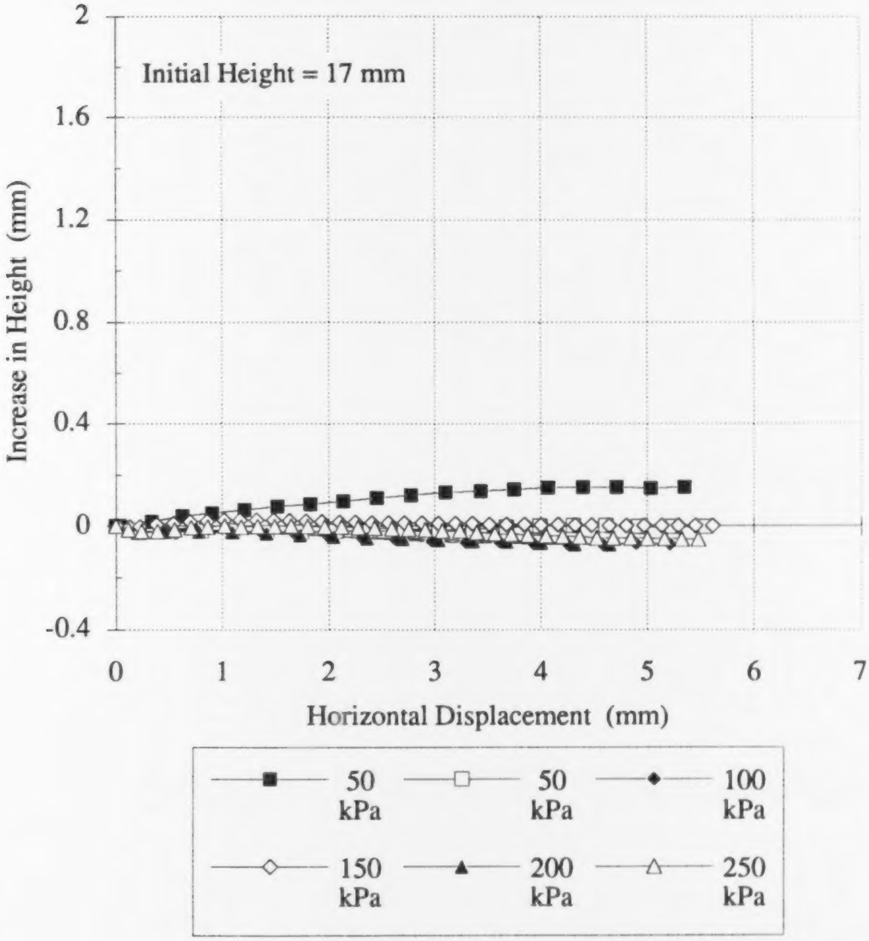

Figure A-11: Shear Stress vs. Horizontal Displacement - Dry Coarse Sand/Plexiglass Interface

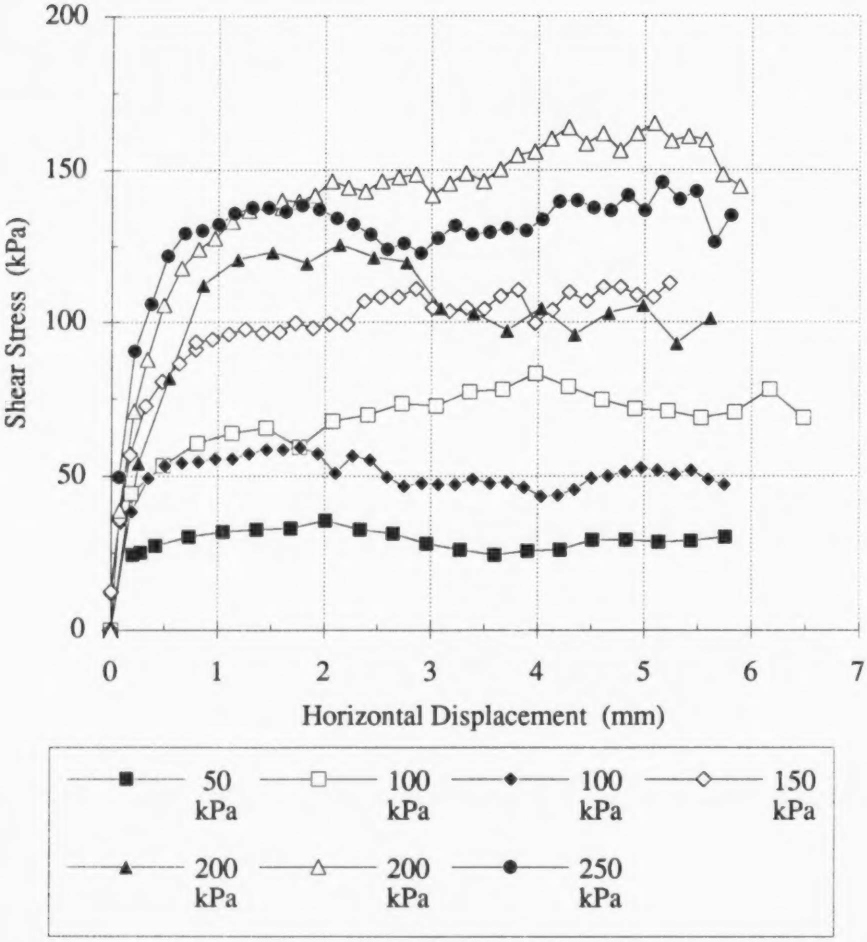

Figure A-12: Vertical Displacement vs. Horizontal Displacement - Dry Coarse Sand/Plexiglass Interface

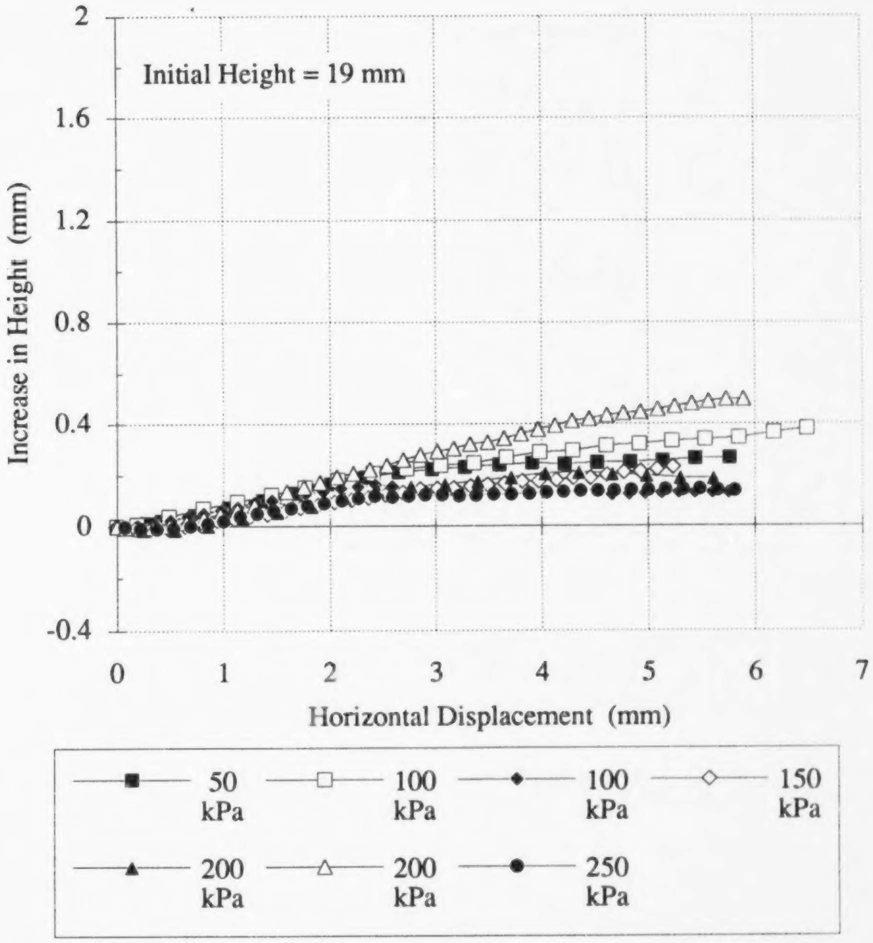

Appendix B

Capillary Cohesion Direct Shear Tests

Shear Stress vs. Horizontal Displacement Plots

Increase in Height vs. Horizontal Displacement Plots

Figure B-1: Shear Stress vs. Horizontal Displacement - Dry Fine Sand

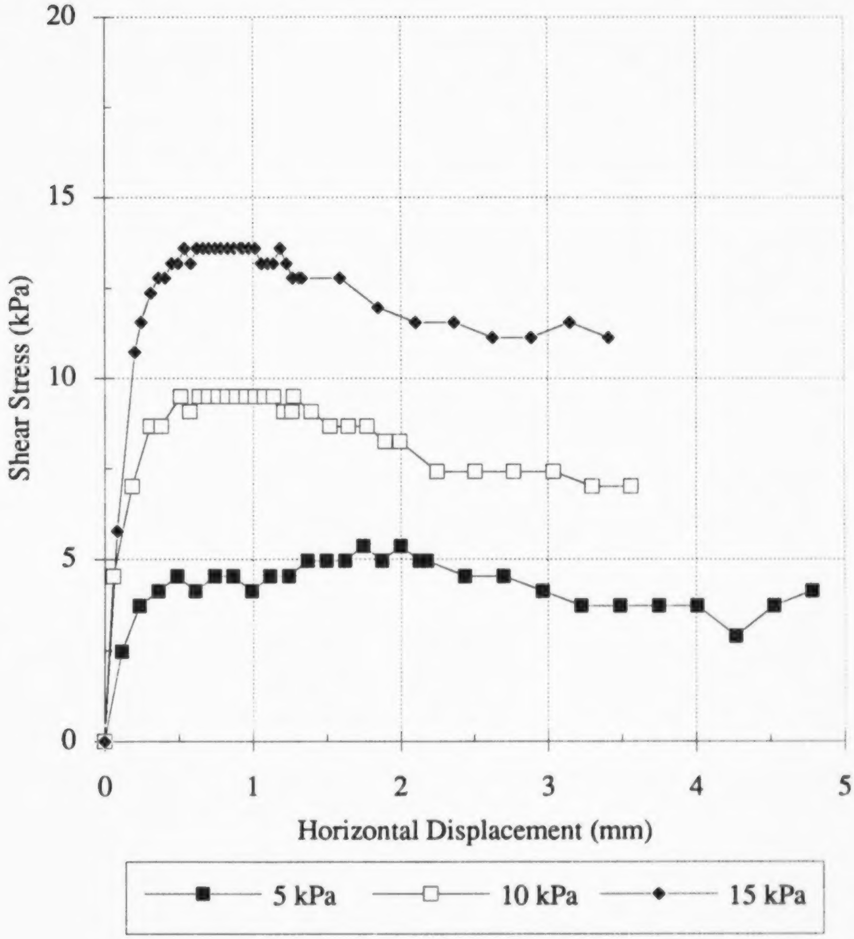

Figure B-2: Vertical Displacement vs. Horizontal Displacement - Dry Fine Sand

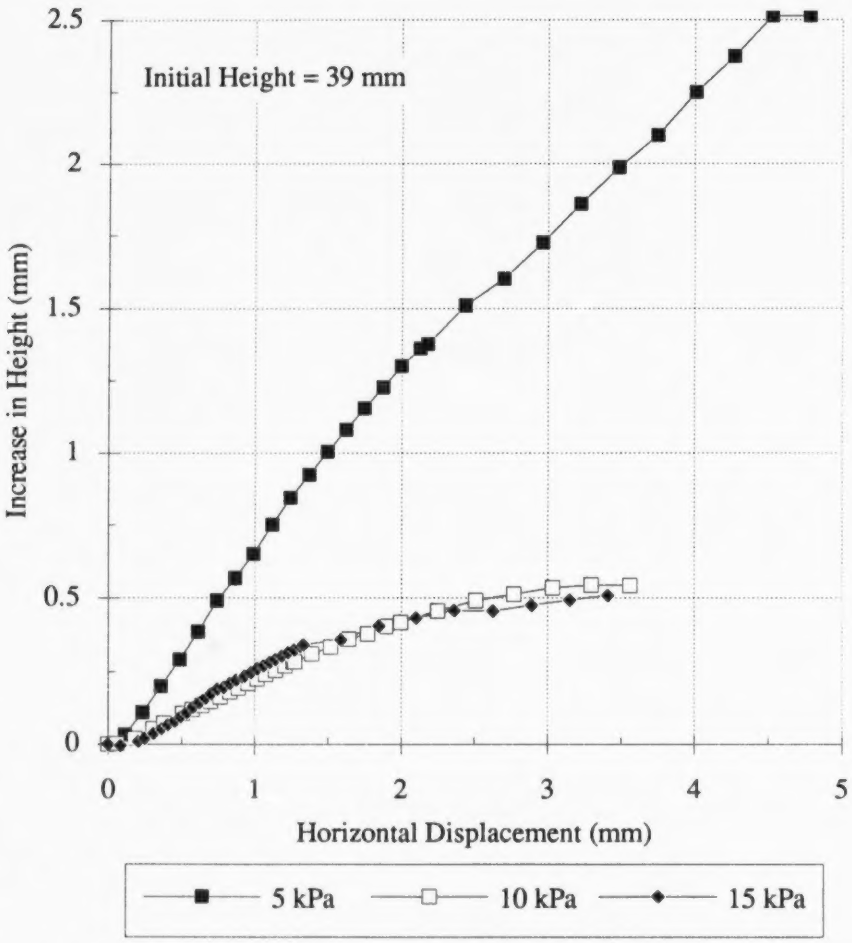

Figure B-3: Shear Stress vs. Horizontal Displacement - 40% Gas/60% Water Saturated Fine Sand

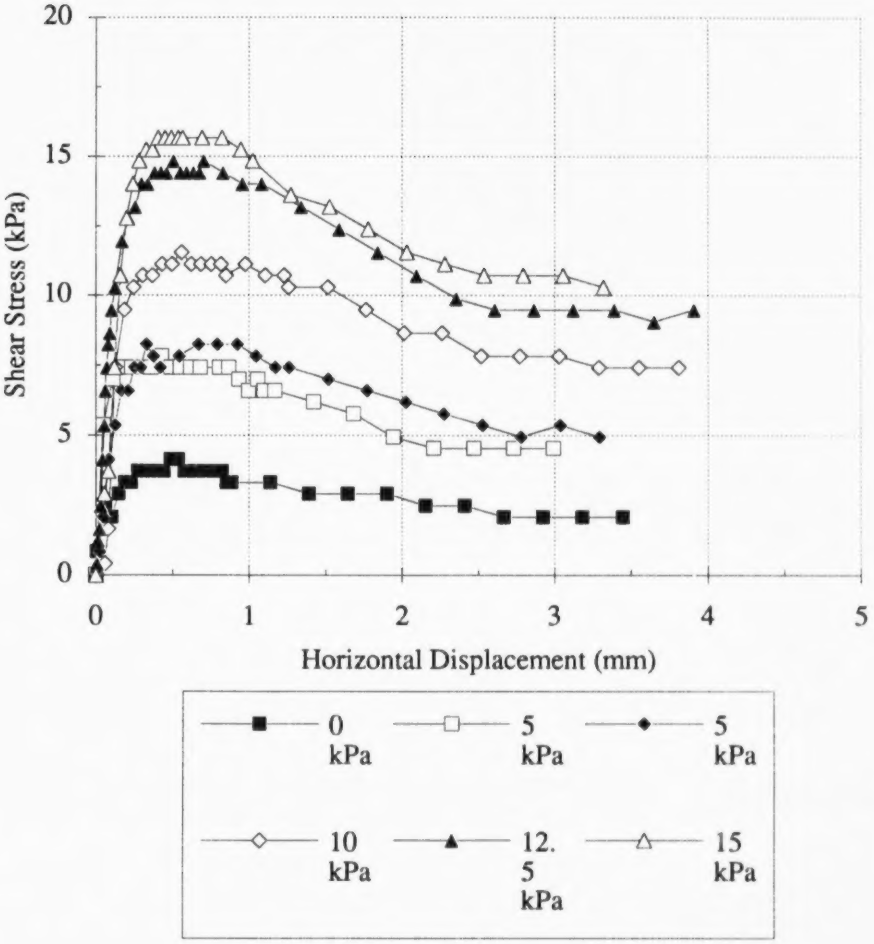

Figure B-4: Vertical Displacement vs. Horizontal Displacement - 40% Gas/60% Water Saturated Fine Sand

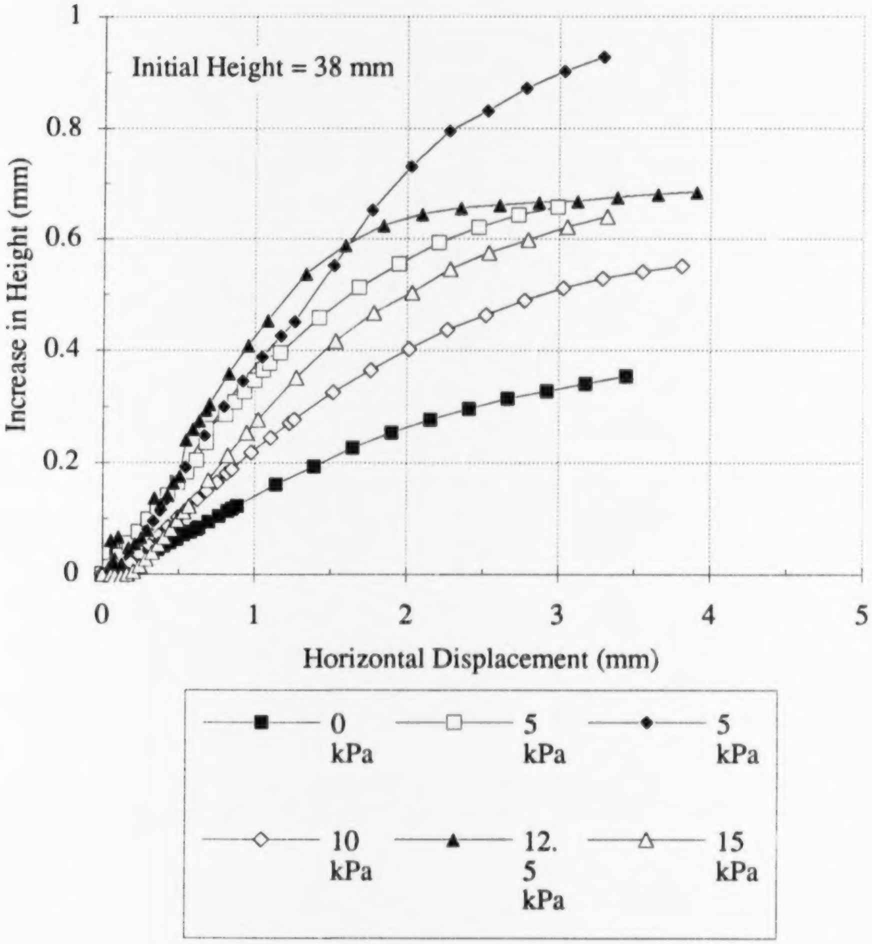

Figure B-5: Shear Stress vs. Horizontal Displacement - 20% Gas/80% Water Saturated Fine Sand

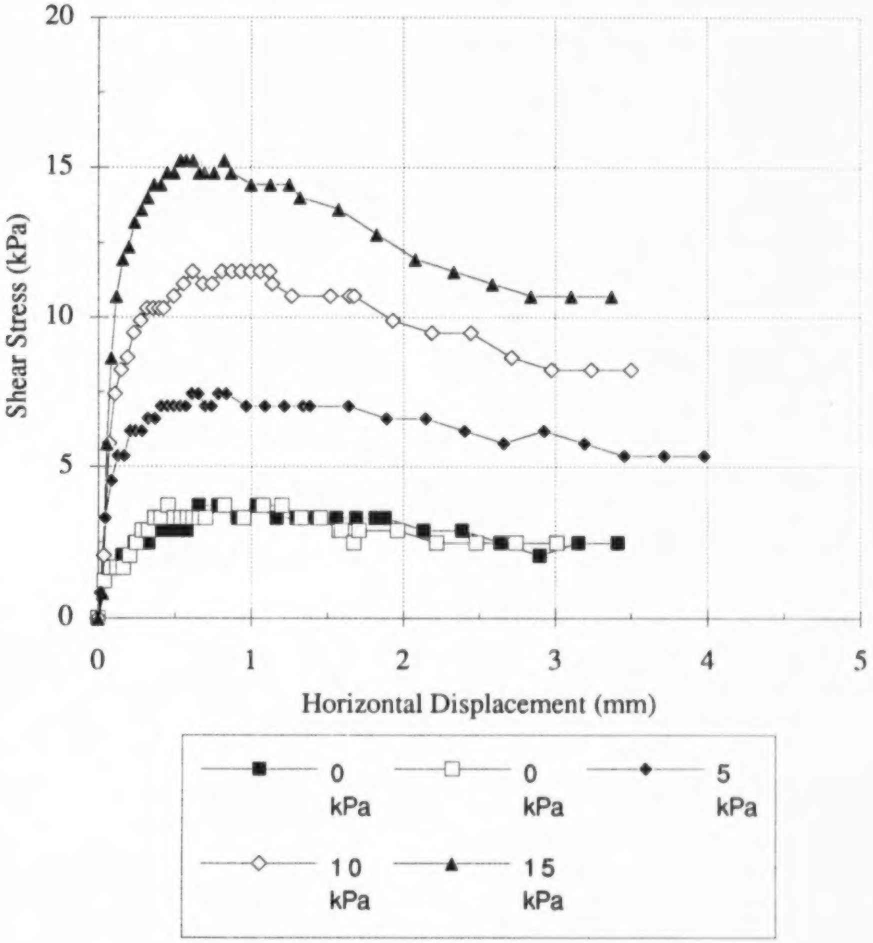

Figure B-6: Vertical Displacement vs. Horizontal Displacement-20% Gas/80% Water Saturated Fine Sand

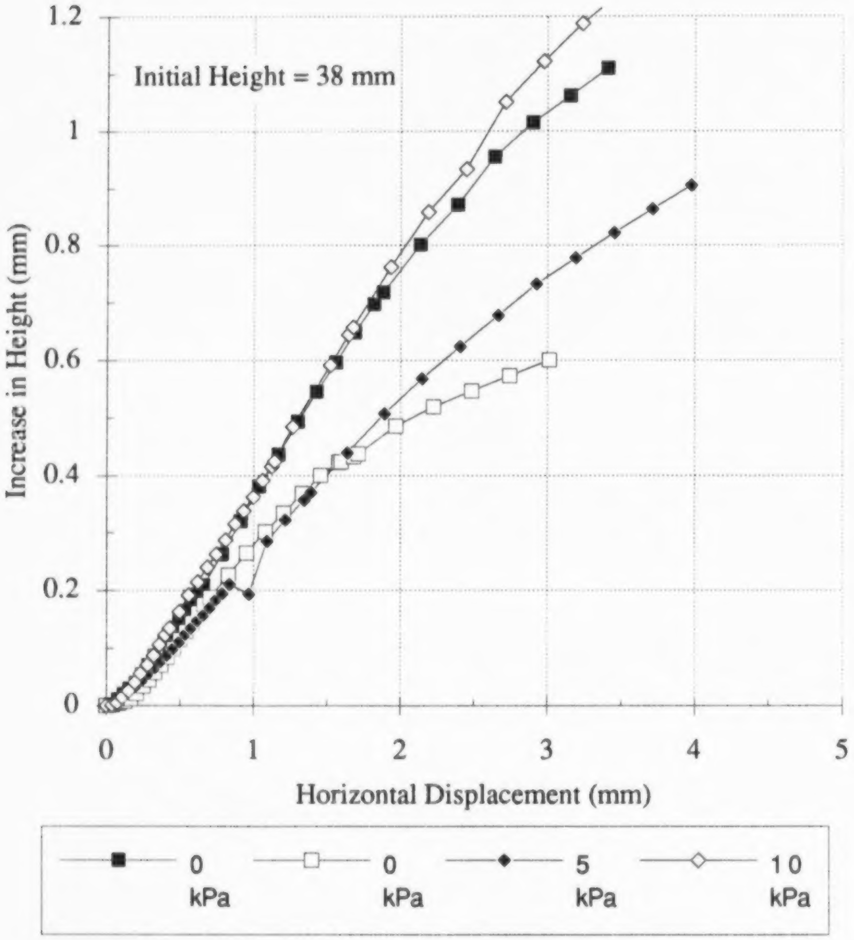

Appendix C

Upward Air Flow Tests

Background

Laboratory Procedure

Experimental Results

Analysis of Experimental Results

Conclusions

C.1 Background of Upward Air Flow Tests

The test results of Hall and Harrisberger (1970) that showed that an upward air flow could cause arching indicated that this procedure could be used to measure the increase in intergranular stress and therefore shear strength that was necessary to create stable arches. A test program was initiated to investigate this phenomena and to determine how stable arches could be established. Hall and Harrisberger reported that air drawn into dry, rounded sand allowed the formation of arches at grain diameter to width of opening ratios that previously failed to induce arching. They found this was the case for 20-40 mesh and 80-100 mesh rounded sand at a range of confining stresses from 0 to 14 MPa. They concluded that the drag force on the surface grains gave enough restraint to initiate an arch.

The same type of tests were performed using the third visualization model. Air was used as the test fluid and its direction of flow was upward through the slot perforation and sand, and out the top of the visualization model. When sufficient upward air flow was applied, sand flow through the slot stopped. Stoppages in the flow of sand were observed using the fine and medium sands at slot width/grain diameter ratios greater than four, when previously at these ratios, sand flowed freely through the slot perforation.

C.2 Laboratory Procedure

In order to investigate the results of Hall and Harrisberger (1970), a vacuum pump was connected to a fitting on the top plate of the visualization model. With this experimental arrangement, air was used as the test fluid and its direction of flow was upward through the slot perforation, through the dry sand and out the top of the visualization model. All sands tested in upward air flow tests were completely dry during testing. The procedure followed regarding visualization model preparation, sand placement and model setup when performing tests with upward air flow was the same as the procedure outlined in Section 3.3.2 Dry Sand With Confining Stress Applied with two exceptions. The first was that the fitting located in the top plate of the visualization model was connected to a vacuum pump. The second exception was that the manometer ports located on the back face of the visualization model were connected to a water manometer board designed to measure air pressure.

To start the test, the plug was removed from the slot perforation by applying a sharp pull on a string attached to the plug. Immediately after the plug was removed from the slot perforation, the vacuum was applied. The magnitude of the vacuum was adjusted in an attempt to cause a stoppage in sand flow out of the slot perforation. If it was possible to prevent sand flow by adjusting the vacuum magnitude, the following procedure was followed. The vacuum magnitude was decreased to a critical rate of upward air flow. The critical upward air flow rate is defined as the upward air flow at which the sand bridge is just about to break down and the sand about to start flowing again. This critical flow was determined visually by observing movement of sand grains at the slot opening as the vacuum magnitude was reduced. Once the critical upward flow rate had been established, manometer readings were taken. At this point the confining stress acting on the sand was increased. After increasing the confining stress, the stability of the sand bridge was observed. If the sand bridge remained stable, the vacuum magnitude was decreased again to find the new critical upward flow rate. Once this new critical flow had been established another set of manometer readings was taken. The sand bridge was then subjected to a vibration by striking the face of the plexiglass box with a rubber hammer and the stability of the sand bridge was observed.

C.3 Experimental Results

Tests were performed on the fine, medium and coarse sands in order to observe the effect of upward air flow on sand flow or nonflow. As well, slot perforation widths of 5 mm and 12.7 mm were used. The slot perforation was 50 mm high for all of the following tests.

C.3.1 Fine Sand

Test #77 was the first test conducted using dry fine sand and upward air flow. The purpose of Test #77 was to investigate how the dry fine sand would alter its behavior when an upward air flow was applied by the vacuum pump. In previous tests without an upward air flow applied, the fine dry sand flowed through the slot perforation immediately after the plug was removed. The slot perforation was 5 mm wide resulting in a grain diameter to width of opening ratio of 1:16.7. The fine sand was compacted in the visualization model at a void ratio of 0.62 and an associated dry density of 1.67 g/cm^3. The calculated relative density was equal to 49%. No confining stress was applied. When the plug was removed, the sand flowed continuously through the slot perforation. When the vacuum pump was activated, sand flow through the slot perforation stopped and a sand bridge formed over the slot perforation. Turning the vacuum pump off resulted in resumed sand flow until the vacuum pump was reactivated. At higher air flows, air could be seen bubbling through the sand bed towards the top of the sand and a cavity in the shape of an semicircle would form above the slot perforation. It was also observed that a small fluctuation in upward air flow could control sand flow or nonflow.

The purpose of Test #78 was to examine the effect of confining stress on the formation and stability of sand bridges created when an upward air flow was applied. Again, a 5 mm wide slot perforation was used. The fine sand was compacted in the visualization model at a void ratio, dry density and relative density of 0.64, 1.66 g/cm^3 and 45%, respectively. A confining stress of 145 kPa was initially applied. The confining stress reduced the ability of the upward air flow to stop sand flow as it took a higher air velocity to cause sand bridging (Table C-2). That is, application of an upward air flow resulted in no further sand flow, similar to what was observed when no confining stress was applied. When the sand had formed a bridge over the slot, the confining stress was increased to 300 kPa. Again, the higher confining stress reduced the ability of the air flow to stop sand flow.

In Tests #77 and #78 described above, pressure drops were read from a gauge attached to the vacuum pump. This was not an accurate assessment of the air pressure within the visualization model. The visualization model was modified by installing manometers to allow measurement of air pressures within the model at different points. Manometers were installed into the back of the visualization model directly above the slot perforation at a spacing of 0, 2.5, 8 and 16 cm above the top of the slot perforation.

After the manometers were in place, Test #87 was performed under the same conditions described in Test #78. The compacted fine sand had a void ratio, dry density and relative density of 0.56, 1.75 g/cm^3 and 81%, respectively. The results of Test #87 were very similar to the results of Test #78 with respect to air flow stopping sand flow and confining stress reducing the ability of the upward air flow to stop sand flow. Air pressure measurements were taken using the manometers throughout Test #87. An analysis of the air pressures measured during this test will be discussed in a later section.

The purpose of Test #90 was to determine if the upward air flow could continue to stop sand flow if a wider slot perforation was used. The slot perforation used was 12.7 mm (1/2 inch) wide. This resulted in a grain diameter to width of opening ratio of 1:42.3. The fine sand was placed in the visualization model at a void ratio of 0.56 and an associated dry density of 1.75 g/cm^3. The calculated relative density was equal to 81%. The results of Test #90 were very similar to the results of Tests #78 and #87, with respect to air flow stopping sand flow and confining stress reducing the ability of the upward air flow to stop air flow. The slot perforation used in Test #90 was 2.5 times wider than the slot perforation used in Test #87 but the air's ability to stop sand flow was unaffected. Air pressure measurements were taken using the manometers during Test #90 and will be discussed in a later section. The results of Tests #77, #78, #87 and #90 are summarized in Table C-1.

C.3.2 Medium Sand

The purpose of Test #75 was to determine if the presence of an upward air flow would have the same affect of causing a stoppage in medium sand flow that was observed in a similar test using fine sand. The slot perforation was 5 mm wide resulting in a grain diameter to width of opening ratio of 1:4.2. The medium sand was compacted in the visualization model at a void ratio, dry density and relative density of 0.55, 1.74 g/cm^3 and 58%, respectively. No confining stress was applied. When the plug was removed, the sand flowed continuously through the slot perforation. When the vacuum pump was activated, sand flow stopped and the sand formed an arch-like structure over the slot perforation. Turning the vacuum pump off resulted in resumed sand flow until the vacuum pump was reactivated. Small fluctuations in upward air flow could control sand flow or non-flow. The results of this test were very similar to results obtained in Test #77 which was essentially the same, except fine sand was used.

The purpose of Test #76 was to examine the effect of confining stress on the formation and stability of arches created when an upward air flow was applied. The same slot perforation width was as in Test #75. The compacted medium sand had a void ratio, dry density and relative density of 0.55, 1.74 g/cm^3 and 58%, respectively. A confining stress of 145 kPa was initially applied. The application of the upward air flow resulted in a stoppage of sand flow. The confining stress reduced the ability of the upward air flow to stop sand flow. When the sand had formed a bridge over the slot, the confining stress was increased to 300 kPa. Again, the higher confining stress reduced the ability of the air flow to stop sand flow.

In Tests #75 and #76 described above, pressure drops were read from a gauge attached to the vacuum pump. This was not an accurate assessment of the air pressure within the visualization model. As mentioned earlier, the visualization model was modified by installing manometers to allow measurement of air pressures within the model at different points.

After the manometers were in place, Test #91 was performed under the same conditions described in Test #76. The medium sand was compacted in the visualization model at a void ratio, dry density and relative density of 0.51, 1.79 g/cm^3 and 79%, respectively. The results of Test #91 were very similar to the results of Test #76 with respect to air flow stopping sand flow and confining stress reducing the ability of the upward air flow to stop sand flow. However, air pressure measurements taken using the manometers throughout Test #91 indicated that the manometers were not operating properly for this test. Thus, no pressure measurements are available for this test.

The purpose of Test #88 was to determine if the upward air flow could continue to stop sand flow if a wider slot was used. The slot perforation was 12.7 mm (1/2 inch) wide and 50 mm high. This resulted in a grain diameter to width of opening ratio of 1:10.6. The compacted medium sand had a void ratio, dry density and relative density of 0.51, 1.79 g/cm^3 and 79%, respectively. A confining stress of 145 kPa was applied. When the plug was removed, the sand flowed freely out the slot perforation. The upward air flow was not able to stop the flow of the medium sand when a 12.7 mm (1/2 inch) wide slot perforation was used. The slot perforation used in Test #88 was 2.5 times wider than the slot perforation used in test #91. This increase in slot width rendered the upward air flow incapable of stopping the free flow of sand out of the model. The results of Tests #75, #76, #91 and #88 are summarized in Table C-1.

C.3.3 Coarse Sand

The purpose of Test #79 was to examine how the application of an upward air flow would effect the behavior of the coarse sand. In previous tests, the coarse sand arched over a slot perforation 5 mm wide but flowed through a slot perforation 12.7 mm (1/2 inch) wide. Test #79 was performed with a slot perforation 5 mm wide resulting in a grain diameter to width of opening ratio of 1:3.1. The coarse sand was compacted in the visualization model at a void ratio of 0.62 and an associated dry density of 1.68 g/cm^3. The calculated relative density was equal to 63%. The confining stress was initially set at 145 kPa and was later increased to 300 kPa. No differences in behavior of the coarse sand or in the formation and destruction of arches were observed from Test #58, which was conducted earlier without upward air flow applied. The results of Test #58 are described in detail in Section 4.8.1.3 Coarse Sand.

The purpose of Test #89 was to determine if the application of an upward air flow could induce arching in the coarse sand over a 12.7 mm (1/2 inch) wide slot perforation. The resulting grain diameter to width of opening ratio was 1:7.9. The compacted coarse sand had a void ratio of 0.58 and an associated dry density of 1.72 g/cm^3. The calculated relative density was equal to 80%. The confining stress was set at 145 kPa. When the plug was removed, the sand flowed freely out the slot perforation. The upward air flow was not able to stop the flow of the coarse sand when a 12.7 mm (1/2 inch) wide slot perforation was used. The behavior of the coarse sand was very similar to a previous test which did not employ upward air flow. Thus, the upward air flow had no effect on the behavior of the coarse sand. The results of Tests #79 and #89 are summarized in Table C-1.

C.4 Analysis of Experimental Results

In this study, tests were performed to investigate the results of Hall and Harrisberger (1970). It should be pointed out that the upward air flow tests performed during this study had some significant shortcomings. A suitable method of measuring flow rate was not used and a smoke tracer did not provide an effective means of measuring the flow path and cross-sectional area of air flow through the sand bed. Despite these shortcomings, several important observations were obtained during these tests. It was theorized that instead of the upward air flow providing enough restraint to cause sand arching over the slot perforation as suggested by Hall and Harrisberger (1970), the sand above the slot perforation was being fluidized. An indication as to which phenomena was occurring is if there is upward movement of sand particles just prior to the formation of an arch. If an upward movement of sand particles can be observed, it can be concluded that the bed is being fluidized. This is because the velocity of air flow must be greater than the minimum fluidization velocity for this to occur. This was observed in Test #77, as air bubbles formed above the slot perforation and flowed upward through the sand to the top of the sand at flow rates just above the minimum flow rate required to form the arch. A possible explanation for the arch shape observed above the slot perforation is that the increased pressure due to the high air velocity at the slot perforation pushes (fluidizes) the sand grains against the rest of the sand bed forming an arch shape. However, the entire sand bed does not move upwards because it is confined by the piston resting on top of the sand. In other words, the sand above the slot perforation is being fluidized and the arch shape is the top half of an air bubble that would move upward through the sand if the piston resting on top of the sand was not present.

Fluidization of the bed occurs when the drag force caused by the upward flow of a liquid or gas equals the weight of the particles in the bed. The velocity of flow at which this occurs is called the minimum fluidization velocity and is given as a superficial velocity.

The superficial velocity is the fictitious velocity of flow considered over the entire cross-section of the bed (the porosity of the sand is not used to determine flow area). The minimum fluidization velocity is given by Kunni and Levenspiel (1969) as:

$$u_{mf} = \frac{(\phi d)^2}{150} \frac{g(\rho_s - \rho)}{\mu} \left[\frac{e^3}{1-e}\right]$$

where:
u_{mf} = minimum fluidization velocity
ϕ = sphericity of the particle (0.86 for a round sand)
d = average sand grain diameter
ρ_s = density of the solid particle
ρ = density of the fluid
μ = dynamic viscosity of the fluid
e = void ratio

For the upward air flow tests where manometer readings were taken, the velocity of the air at the slot perforation may be calculated. If the calculated air velocity is greater than the minimum fluidization velocity provided by the above equation, fluidization of the sand is occurring. Unfortunately, reliable manometer readings were only available for Tests #87 and #90 using the fine sand. Thus, the possibility of fluidization occurring will only be investigated for the fine sand.

Regrettably, the air conductivity of the test sands, which is required to calculate the air velocity at the slot perforation, was not measured during the upward air flow tests. However, a measurement of the hydraulic conductivity of the fine sand to water was available. This water conductivity can be converted to an air conductivity. Amyx (1960) states that the constant of proportionality of Darcy's Law, k, could be written as K/μ, where μ is the viscosity of the fluid and K is the permeability of the medium and is a property of the medium only. That is:

$$k = \frac{K}{\mu}$$

Thus, using a ratio of k_{air}/k_{water}, it may be stated that:

$$k_{air} = k_{water} \frac{(\frac{K_{air}}{\mu_{air}})}{(\frac{K_{water}}{\mu_{water}})}$$

Permeability is a property of the medium only and not of the fluids. However, as described by Klinkenberg (1941) when gas is used as a fluid to measure permeability, the phenomenon of gas slippage is important. That is, the permeability determined with gases is dependent upon the type of gas used. The apparent permeability obtained from permeability tests using gas at different pressures may be extrapolated to infinite pressure which provides a permeability which is characteristic of the porous medium alone. The permeability at this infinite pressure is equal to the equivalent liquid permeability.

Ideally, measures of permeability using air at varying pressures should have been performed on the test sands in order to obtain air and equivalent liquid permeabilities. However, these values are not available. Instead, the results of Klinkenberg's core sample L at a reciprocal mean pressure of 1.0 atm^{-1} and using nitrogen as a gas were used to determine K_{air} and K_{water} (Amyx, 1960). The resulting values of K_{air}=4.4 millidarcies and K_{water}=2.8 millidarcies were obtained. Substituting these values into the conductivity of air equation mentioned earlier using viscosities of air and water of 1.8x10^{-5} Pa*s and 1.0x10^{-3} Pa*s, respectively, results in a k_{air} value which is 87 times greater than k_{water}. That is:

$$k_{air} = k_{water} \frac{(\frac{4.4 \text{ millidarcies}}{1.8\text{x}10^{-5} \text{ Pa*s}})}{(\frac{2.8 \text{ millidarcies}}{1.0\text{x}10^{-3} \text{ Pa*s}})}$$

$$k_{air} = 87^{*}k_{water}$$

Test #87 utilized the fine sand and a 5 mm wide slot perforation. The minimum fluidization velocity for Test #87 was 0.26 m/sec. The velocity of the air flow at the slot perforation was calculated using the manometer readings recorded during the test at critical upward air flows at different confining stresses. The water conductivity of the fine sand was measured to be 0.045 cm/sec. The equivalent air conductivity is 3.93 cm/sec. The flow rate of the air, Q, may be determined using the following relationship:

$$Q = kiA = k\frac{\Delta h}{\Delta l}A$$

The cross-sectional area of the air flow through the visualization model, A, is unknown because the flow path of the air through the sand matrix was not visible. Therefore, a cross-sectional area of air flow must be assumed. Originally, it was assumed that the air flow covered the entire cross-sectional area of the visualization model (30 cm^2). Velocity of the air at the slot perforation, associated Reynold's numbers and values used to calculate air flow velocities at critical upward air flows for Test #87 based on this area assumption are presented in Table C-2. Velocity of the air flow at the slot, V_{slot}, is determined as follows:

$$V_{slot} = \frac{Q}{A_{slot}}$$

where: Q = air flow rate

A_{slot} = the cross-sectional area of the slot perforation

All of the calculated air velocities at the slot perforation are greater than the minimum fluidization velocity indicating that fluidization of the sand is occurring. However, the Reynold's numbers (R_e) for these air flow velocities are outside the Stoke's regime of flow (laminar flow) and lies in the intermediate regime of flow of $1<R_e<1000$. If the air is not in a laminar flow regime, it may not follow a flow path that will expand to the full cross-sectional area of the visualization model as originally assumed. Back calculating the minimum cross-sectional area required to cause fluidization and assuming air will flow across the entire thickness of the visualization model results in a flow width of 36 mm. This is a reasonable flow width and results in an assumed cross-sectional area of air flow of 7.2 cm^2. In light of this, the assumption of the width of the air flow pattern was modified to be equal to 7.2 cm^2. The new air flow velocities calculated using this new area assumption are presented in Table C-3. The air flow velocities at the slot perforation remain greater than the minimum fluidization velocity indicating that based on these assumptions, fluidization of the sand is occurring.

Similar calculations were performed for Test #90 which utilized the fine sand and a 12.7 mm wide slot perforation. The minimum fluidization velocity for Test #90 was also 0.26 m/sec. The velocity of the air flow at the slot perforation was calculated using the manometer readings recorded during the test at critical upward air flows at different confining stresses. The required cross-sectional area to achieve the fluidization at the 12.7 mm wide slot perforation was back calculated to be 16.5 cm^2. This results in a 81 mm wide air flow which again is reasonable considering the width of the slot perforation. The velocity of the air at the slot perforation, associated Reynold's numbers and values used to calculate air flow velocities at critical upward air flows for Test #90 based on the above area assumption are presented in Table C-4. Again, the air flow velocities at the slot perforation were greater than the minimum fluidization velocity indicating that based on these assumptions, fluidization of the sand is occurring in this test as well.

The results of Tests #87 and #90 indicate that the upward air flow results in the fluidization of the fine sand above the slot perforation which is responsible for causing the nonflow of sand and it is not an arching phenomenon. However, some of the assumptions used in the above analysis have a significant influence on the calculated velocity of air flow at the slot perforation. The first of these assumptions is the value of k_{air} used in the calculations. In order to properly analyze the effects of upward air flow on sand behavior, the air conductivity of the fine sand under test conditions should be measured. Permeability tests performed using air at pressures that would be used under tests conditions would be essential. This would allow the actual air permeability of the fine sand to be known and would remove the need for a conversion from water to air conductivities. It is realized that the permeabilities of the air and water assumed from Klinkenberg (1940) in this study, are not exactly representative of the fine sand under test conditions. However, for most of Klinkenberg's data, the k_{air} reported is in the range of 1.1 to 1.6 times larger than k_{water}. It is felt that the k_{air} and k_{water} values for the fine sand would also be in this range of values so the assumption of the values provides a reasonable approximation since the viscosities of water and air have the greatest effect on the air/water conductivity ratio.

The assumption of the cross-sectional area covered by the air flow as it flowed through the sand is the second significant assumption. Since the slot perforation is the same thickness as the inside of the visualization model, it is reasonable to assume that the air flowed across the entire thickness of the visualization model. Thus, only an assumption of the width of air flow is necessary. Ideally, a visible smoke tracer or other techniques which could be placed in the air flow in order to indicate the boundaries of the air flow should be used. However, this procedure did not work during these tests and a width of air flow had to be assumed. Originally, calculations were based on the assumption that if the air flow velocity was low enough, air flow would cover the entire cross-sectional area of the visualization model. However, the calculated Reynold's numbers based on this assumption indicate air flow was not laminar and that air flow across the entire cross-sectional area was not likely. The area of air flow required to cause fluidization was back calculated for both tests. In both cases, the areas appeared to be reasonable given slot perforation widths and air flow velocities.

In order to fully understand the effects of upward air flow on sand behavior, it is recommended that tests similar to those described above be repeated following the additional recommendations discussed. This would allow the removal of the troublesome assumptions present in this discussion and remove any doubt of actual effects of upward air flow on sand behavior.

Unfortunately, no pressure measurements were available for upward air flow tests utilizing the medium sand. However, a qualitative assessment of sand behavior based on minimum fluidization velocity and slot perforation area is possible. The minimum fluidization velocities for Tests #75, #76 and #91 were 3.9 m/sec, 3.9 m/sec and 2.8 m/sec, respectively. All of these tests were performed with a 5 mm wide slot perforation. In all cases, the application of an upward air flow was able to stop sand flow. Presumably, by fluidizing the sand above the slot perforation. However, even the maximum upward air flow rate possible was not capable of stopping the flow of medium sand in Test #88 which utilized a 12.7 mm wide slot perforation. The minimum fluidization velocity for Test #88 was 2.8 m/sec. It may be theorized that since a larger slot perforation area was used in Test #88, the upward air flow was not able to achieve a sufficient velocity at the slot perforation to fluidize the sand. Thus, the sand flowed out of the visualization model. It is expected that if a source could be found that could apply a larger upward air flow through the visualization model, the medium sand could be observed to cease flowing through a 12.7 mm wide slot perforation due to fluidization, similar to Tests #75, #76 and #91.

C.5 Conclusions

Hall and Harrisberger (1970) stated that air drawn into dry, rounded sand allowed the formation of arches at grain diameter to width of opening ratios that previously failed to induce arching. They concluded that the drag force on the surface grains gave enough restraint to initiate an arch. The same types of tests performed with the visualization model indicated that when sufficient upward air flow was applied, sand flow through the slot perforation stopped. However, it has been concluded that this stoppage of sand flow is not an arching phenomena. Instead, it is believed that fluidization of the sand grains above the slot perforation due to upward air velocities exceeding the minimum fluidization velocities is responsible for stopping the sand flow out of the model. Pressure measurements taken during these tests support this conclusion. However, it is recommended that these tests be repeated following the procedures outlined in the previous section in order to remove any ambiguity created by the use of assumptions regarding conductivity of the sands to air and cross-sectional area of air flow.

Table C-1: Summary of Results From Third Visualization Model: Upward Air Flow Tests

Test No.	Sand Type	Void Ratio	Dry Density	Relative Density	Slot Width	Confining Stress	Sand Behavior
			(g/cm^3)	(%)	(mm)	(kPa)	
77	Fine	0.62	1.67	49	5	0	stoppage of sand flow
78	Fine	0.64	1.66	45	5	145 300	stoppage of sand flow stoppage of sand flow
87	Fine	0.56	1.75	81	5	145 300	stoppage of sand flow stoppage of sand flow
90	Fine	0.56	1.75	81	12.7	145 300	stoppage of sand flow stoppage of sand flow
75	Medium	0.55	1.74	58	5	0	stoppage of sand flow
76	Medium	0.55	1.74	58	5	145 300	stoppage of sand flow stoppage of sand flow
91	Medium	0.51	1.79	79	5	145 300	stoppage of sand flow stoppage of sand flow
88	Medium	0.51	1.79	79	12.7	145	sand flow through slot perforation
79	Coarse	0.62	1.68	63	5	145 300	no effect of upward air flow no effect of upward air flow
89	Coarse	0.58	1.72	80	12.7	145	sand flow through slot perforation

Table C-2: Upward Air Flow Velocity and Minimum Fluidization Velocity of Test #87

Slot Perforation Width = 5 mm

Air flow assumed to cover entire cross-sectional area of visualization model (15 cm x 2 cm = 30 cm^2)

Manometer No.	Confining Stress (kPa)	k_{air} (m/sec)	Δh (m)	Δl (m)	A (cm^2)	Q (m^3/sec)	V_{slot} (m/sec)	R_e	$V_{fluidization}$ (m/sec)
3	145	3.93×10^{-2}	0.051	0.055	30	1.09×10^{-4}	1.09	18.9	0.26
3	300	3.93×10^{-2}	0.066	0.052	30	1.50×10^{-4}	1.50	26.1	0.26
4	145	3.93×10^{-2}	0.130	0.135	30	1.14×10^{-4}	1.14	19.8	0.26
4	300	3.93×10^{-2}	0.171	0.132	30	1.53×10^{-4}	1.53	26.5	0.26

Table C-3: Upward Air Flow Velocity and Minimum Fluidization Velocity of Test #87

Slot Perforation Width = 5 mm

Air flow assumed to have a width of 3.6 cm and thickness of 2 cm (3.6 cm x 2 cm = 7.2 cm^2)

Manometer No.	Confining Stress (kPa)	k_{air} (m/sec)	Δh (m)	Δl (m)	A (cm^2)	Q (m^3/sec)	V_{slot} (m/sec)	R_e	$V_{fluidization}$ (m/sec)
3	145	3.93x10^{-2}	0.051	0.055	7.2	2.62x10^{-5}	0.26	4.55	0.26
3	300	3.93x10^{-2}	0.066	0.052	7.2	3.61x10^{-5}	0.36	6.25	0.26
4	145	3.93x10^{-2}	0.130	0.135	7.2	2.73x10^{-5}	0.27	4.74	0.26
4	300	3.93x10^{-2}	0.171	0.132	7.2	3.67x10^{-5}	0.37	6.37	0.26

Table C-4: Upward Air Flow Velocity and Minimum Fluidization Velocity of Test #90

Slot Perforation Width = 12.7 mm

Air flow assumed to have a width of 8.1 cm and thickness of 2 cm (8.1 cm x 2 cm = 16.2 cm^2)

Manometer No.	Confining Stress (kPa)	k_{air} (m/sec)	Δh (m)	Δl (m)	A (cm^2)	Q (m^3/sec)	V_{slot} (m/sec)	R_e	$V_{fluidization}$ (m/sec)
3	145	3.93×10^{-2}	0.053	0.038	16.2	8.88×10^{-5}	0.36	6.16	0.26
3	300	3.93×10^{-2}	0.051	0.026	16.2	1.25×10^{-4}	0.50	8.66	0.26
4	145	3.93×10^{-2}	0.122	0.118	16.2	6.60×10^{-5}	0.26	4.57	0.26
4	300	3.93×10^{-2}	0.127	0.106	16.2	7.65×10^{-5}	0.31	5.31	0.26